

Paleoceanographic significance of the Neoproterozoic Polanco Limestones Formation  
(Uruguay): stratigraphy, isotopic geochemistry and age

by

Natalie Aubet

A thesis submitted in partial fulfillment of the requirements for the degree of

Doctor of Philosophy

Department of Earth and Atmospheric Sciences

University of Alberta

© Natalie Aubet , 2016

## ABSTRACT

Carbon and Strontium isotope data for marine carbonates can provide a detailed record of isotopic variations in seawater through time and have proven to be a valuable tool for interpreting biogeochemical events and correlating Neoproterozoic sedimentary successions worldwide. The Neoproterozoic of Uruguay has been regarded as containing a significant geological and palaeontological record, which would make these successions critical to unraveling diverse aspects regarding the assembly of southwestern Gondwana and to understanding the conditions surrounding the rise of animal life in a period punctuated by drastic palaeoenvironmental changes. Particularly, the Polanco Limestones Formation is the only carbonate unit of the entire record, and therefore offers a unique opportunity to explore the palaeoenvironmental conditions during sedimentation. This thesis is built on previous chemostratigraphic studies reporting a negative carbon ( $\delta^{13}\text{C}_{\text{carb}}$ ) isotope excursion to values as low as -4.5‰ and interpreted as recording the aftermath of a post-Gaskiers glacial event occurred elsewhere on southwest Gondwana and correlated with the Shuram-Wonoka-Johnnie carbon isotope anomaly (~551 Ma). In the following dissertation, a multi-proxy approach combining extensive fieldwork, geochronology and isotope geochemistry on the Polanco carbonates is presented with the aim of better constraining the environmental changes and their implications during this critical period of time.

The stratigraphy and age of the Neoproterozoic record in Uruguay, including the Polanco Limestones Formation, is proved to be equivocal. The same is true for existing basin models and tectonic evolution, which show different and sometimes contradicting supporting evidence. From a tectonic perspective, the sequence of events begins with a period of tectonic quiescence and

deposition of extensive mixed siliciclastic-carbonate sedimentary successions. This is followed by the development of small fault-bounded siliciclastic and volcanoclastic basins and the emplacement of voluminous granites associated with episodic terrane accretion. The deposition of mixed siliciclastic-carbonate sedimentary successions, which encompasses the Arroyo del Soldado Group -including the Polanco Limestones Formation- and the Arroyo de la Pedrera Group occurred between 650 and 1000 Ma. In contrast, the Ediacaran record consists of the volcano-sedimentary Maldonado Group, and the Tacuarí, Barriga Negra, Rocha and Sierra de Aguirre formations. The best available radiometric age constraints indicate that intense magmatic-tectonic activity occurred during the deposition of these units, between 600 and 560 Ma, incompatible with previous models suggesting a stable, Atlantic-type passive margin on this portion of southwestern Gondwana. By combining new U-Pb ages in limestones and detrital zircons as well as K-Ar ages in shales along with chemostratigraphic data, the Polanco Limestones Formation is constrained between ~680 and 650 Ma implying that the unit was deposited during the Cryogenian interglacial period, between the Sturtian and Marinoan glaciations.

Carbon isotopic profiles from deep- to shallow-water facies of the Polanco Limestones Formation show a dominance of negative values in deep-water facies and a progressive rise towards positive values in shallow-water settings. This previously unrecognized trend suggests that deposition of Polanco carbonates occurred in a stratified marine basin where degradation of organic matter below the redox boundary led to lower  $\delta^{13}\text{C}$  values at greater depths. Carbonates were analyzed for paired  $\delta^{13}\text{C}_{\text{org}}$  and  $\delta^{13}\text{C}_{\text{carb}}$ . Their records reveal local changes in nutrient input and phytoplankton growth rates. This is supported by simultaneous changes in the concentrations of nutrients (P), lithophile elements (e.g., Al, Zr) and  $^{87}\text{Sr}/^{86}\text{Sr}$  ratios, which also indicate a

terrestrial source. However, the dominant control on the  $\delta^{13}\text{C}_{\text{org}}$  and  $\delta^{13}\text{C}_{\text{carb}}$  curves is interpreted to reflect changing  $[\text{CO}_2]_{\text{aq}}$ , and possibly in global  $p\text{CO}_2$ . The consistently small  $\Delta^{13}\text{C}$  values suggest low atmospheric  $p\text{CO}_2$  wherein, under  $\text{CO}_2$ -limiting conditions, the utilization of  $\text{HCO}_3^-$  by planktic cyanobacteria lowered  $\Delta^{13}\text{C}$  and produced the precipitation of biogenic whittings. This study challenges the idea by which in a hard-snowball scenario subsequent rapid deglaciation resulted from the buildup of volcanic carbon dioxide during glaciation reaching high partial pressures of atmospheric  $\text{CO}_2$  (50-250 PAL). Alternatively, it accounts for independent evidence and supports recent studies on cap carbonates arguing for a rather low atmospheric  $p\text{CO}_2$  possibly as low as the current value even during deglaciation periods.

## PREFACE

Chapter 2 of this thesis has been published as: Natalie R. Aubet, Ernesto Pecoits, Larry M. Heaman, Gerardo Veroslavsky, Murray K. Gingras, Kurt O. Konhauser. 2014. Ediacaran in Uruguay: Facts and controversies. 2014. *Journal of South American Earth Sciences* 55, 43-57. I was responsible for the data collection and analysis as well as the manuscript composition. E Pecoits, L. Heaman, G. Veroslavsky, M. Gingras and K. Konhauser assisted with the data collection and contributed to manuscript edits.

Chapter 4 of this thesis has been published as: Natalie R. Aubet, Ernesto Pecoits, Andrey Bekker, Murray K. Gingras, Horst Zwingmann, Gerardo Veroslavsky, Héctor de Santa Ana, Kurt O. Konhauser. 2012. Chemostratigraphic constraints on early Ediacaran carbonate ramp dynamics, Río de la Plata craton, Uruguay. *Gondwana Research* 22, 1073-1090. I was responsible for the data collection and analysis as well as the manuscript composition. E Pecoits, A. Bekker, M. Gingras, H. Zwingmann G. Veroslavsky, H. de Santa Ana and K. Konhauser assisted with the data collection and contributed to manuscript edits.

*“What is really good is to fight with determination, embrace life and live it with passion. Lose your battles with class and dare to win because the world belongs to those who dare to live. Life is worth too much to be insignificant.”*

Charles Chaplin

## ACKNOWLEDGEMENTS

I wish to express my warmest gratitude to all those persons whose comments, questions, criticism, support and encouragement, personal and academic, have left a mark on this work.

First of all, I am extremely grateful to my research guide Kurt Konhauser for his valuable guidance, scholarly inputs, and consistent encouragement I received throughout my work.

I would like to extend great thanks to my Thesis Committee members who offered their time, support and commitment: this piece of research looks very different because of their input, influence and expert knowledge.

I wish to thank those institutions that have supported me during the work on this thesis: I gratefully acknowledge the funding received towards my PhD from the Alberta Ingenuity Program, the Society of Economic Geologists, and the Canadian Circumpolar Institute. Some faculty members of the Department of Earth and Atmospheric Sciences have been kind enough to extend their help at various phases of my research, whenever I approached them. I thank Dr. Larry Heaman, for his valuable suggestions, input and concise comments on the research papers of the thesis and other research topics we are currently developing. Thanks to Dr. Tom Chacko for his constant academic and personal support. To Dr. Karlis Muehlenbachs for his support during my stable isotope research and to Dr. Murray Gingras for his comments on the different work we have done together.

Many thanks to Dr. Pieter Visscher for his comments and for the good moments we had together. I acknowledge Dr. Gerardo Veroslavsky for his suggestions and encouragement and for being a constant support since early stages of my career.

I want to thank present and past members of the Geomicrobiology lab for the good times we had during all these years: Stefan Lalonde, Daniel Petrash, Jamie “Jaime” Robbins, Set Castro, Aleksandra Mloszewska, and Rasmus Haugaard. I am also indebted to all my friends in Canada who opened their homes to me during my time at UofA and who were always very helpful in numerous ways. Special thanks to Set, Saulo, Marga, Alice, Ana, and Ossie, and to all the amazing colleagues, friends and people I met and I will never forget. A mis grandes amigos, quienes a pesar de la distancia física han estado cerca en todo momento celebrando alegrías y apoyando en reveses. Thanks to my parents Jota and Fernando to whom my gratitude is always beyond words.

To Ernesto, who has been by my side throughout the past 15 years and without whom I would not have had the courage to embark on this journey.... and finally to our lovely Zoé for being such a good “*alien*” during the past months, and for helping us to understand that “*Life is worth too much to be insignificant*”...

Inevitably, this list of names has been incomplete so I hope that those who are missing will still accept my sincere appreciation of their influence on my work and life.

## TABLE OF CONTENTS

<b>CHAPTER 1: INTRODUCTION</b>	<b>1</b>
1.1. Rationale.....	1
1.2. Thesis organization.....	3
1.3. References .....	4
<b>CHAPTER 2: EDIACARAN IN URUGUAY: FACTS AND CONTROVERSIES</b>	<b>7</b>
2.1. Introduction .....	7
2.2. Previous work.....	9
2.2.1. Arroyo del Soldado Group .....	9
2.2.2. Maldonado Group .....	10
2.2.3. Rocha Formation .....	13
2.2.4. Sierra de Aguirre Formation.....	13
2.2.5. Tacuarí Formation .....	14
2.3. Stratigraphy of the Ediacaran in Uruguay .....	14
2.3.1. Arroyo del Soldado Group .....	14
2.3.1.1. Lithostratigraphy .....	14
2.3.1.1.a. Barriga Negra Formation .....	15
2.3.1.2. Age .....	16
2.3.1.2.a. Geochronology .....	16
2.3.1.2.b. Biostratigraphy .....	24
2.3.1.3. C-and Sr-chemostratigraphy.....	25
2.3.1.4. Geological setting.....	27
2.3.2. Maldonado Group .....	28
2.3.2.1. Lithostratigraphy .....	28
2.3.2.2. Age .....	29
2.3.2.2.a. Geochronology .....	30
2.3.2.2.b. The problem of the volcanic rocks and metamorphism.....	31
2.3.2.2.c. Biostratigraphy .....	33
2.3.2.3. Geological setting.....	33
2.4. Final remarks .....	34
2.5. References .....	36
<b>CHAPTER 3: U-Pb DETRITAL ZIRCON AGES FROM SOME NEOPROTEROZOIC SUCCESSIONS OF URUGUAY: PROVENANCE, STRATIGRAPHY AND TECTONIC EVOLUTION</b>	<b>48</b>
3.1. Introduction .....	48
3.2. Geological setting .....	50
3.3. Methodology .....	54
3.4. Results .....	55
3.4.1. U-Pb detrital zircon geochronology .....	55
3.4.1.1. Yermal Formation .....	55

3.4.1.2. Playa Hermosa Formation .....	58
3.4.1.3. Las Ventanas Formation.....	58
3.4.1.4. San Carlos Formation .....	58
3.4.1.5. Barriga Negra Formation.....	59
3.5. Discussion .....	59
3.5.1. Possible source areas .....	59
3.5.2. Chronostratigraphy and geological setting .....	68
3.5.3. Accretion of the Piedra Alta and Nico Pérez Terranes .....	74
3.5.4. Paleogeographic and Paleotectonic Implications .....	81
3.6. Conclusions .....	90
3.7. References .....	91

**CHAPTER 4: CHEMOSTRATIGRAPHIC CONSTRAINTS ON EARLY EDIACARAN CARBONATE RAMP DYNAMICS, RIO DE LA PLATA CRATON (URUGUAY) 103**

4.1. Introduction .....	103
4.2. Geologic setting and stratigraphy .....	104
4.3. Analytical methods .....	107
4.4. Results .....	109
4.4.1. Facies Associations .....	109
4.4.1.1. Medium- to coarse-grained calcarenites with occasional sandstone beds .....	109
4.4.1.2. Parallel laminated or thinly interbedded limestone and dolostone calcisiltites .....	110
4.4.1.3. Laminated to bedded limestones and dolostones .....	112
4.4.2. Petrography.....	114
4.4.3. Carbonate geochemistry.....	117
4.4.3.1. Oxygen and carbon isotopes.....	117
4.4.3.2. Trace elements.....	117
4.4.3.3. Strontium isotopes.....	122
4.4.4. Clay mineralogy.....	122
4.4.5. K-Ar dating.....	122
4.5. Discussion .....	122
4.5.1. Effect of diagenetic alteration on carbonate carbon, oxygen and strontium isotope compositions .....	122
4.5.2. C- and Sr-isotope chemostratigraphy .....	126
4.5.3. <sup>40</sup> K- <sup>40</sup> Ar geochronology .....	129
4.5.4. Palaeo-oceanographic significance of the C- and Sr-isotope records .....	132
4.5.3.1. Non-steady state conditions .....	133
4.5.3.2. Steady-state conditions .....	134
4.6. Conclusions .....	135
4.7. References .....	137

**CHAPTER 5: A LOW PCO<sub>2</sub> INTERGLACIAL PERIOD? INSIGHTS FROM PAIRED  $\delta^{13}\text{C}_{\text{ORG}}$  AND  $\delta^{13}\text{C}_{\text{CARB}}$  RECORDS OF CRYOGENIAN CARBONATES 149**

5.1. Introduction .....	149
5.2. Geological setting.....	150
5.3. Methods .....	150
5.4. Results .....	155
5.4.1. C, O, Sr and preliminary N isotopes.....	155

5.4.2. Geochronology .....	159
5.4.2.1. U-Pb (Pb-Pb) dating .....	159
5.4.2.2. K-Ar dating .....	164
5.5. Discussion .....	165
5.5.1. Assessment of post-depositional alteration on primary C, O and Sr isotope signatures .....	165
5.5.2. $\delta^{13}\text{C}_{\text{carb}}$ record of the Polanco Limestones Formation .....	172
5.5.3. Fractionation between inorganic and organic carbon .....	175
5.5.4. Implications for atmospheric $\text{pCO}_2$ .....	179
5.5.5. Age of the Polanco Limestones Formation and correlation with other units.....	181
5.6. Conclusions .....	185
5.7. References .....	186
<b>CHAPTER 6: CONCLUSIONS</b> .....	<b>203</b>
6.1. Neoproterozoic of Uruguay .....	203
6.1.1. Litho- and chronostratigraphy .....	203
6.1.2. Geochronology .....	204
6.1.3. Palaeogeography and Tectonic Evolution .....	204
6.2. Polanco Limestones Formation .....	204
6.2.1. Sedimentology and diagenesis .....	204
6.2.2. Carbon and strontium isotope records .....	205
6.2.3. Age .....	206
6.3. Future work .....	206
<b>REFERENCES</b> .....	<b>209</b>
<b>APPENDIX 1: SUPPLEMENTARY INFORMATION FOR CHAPTER 2</b> .....	<b>249</b>
<b>APPENDIX 2. SUPPLEMENTARY MATERIAL OF CHAPTER 3</b> .....	<b>250</b>
<b>APPENDIX 3. SUPPLEMENTARY MATERIAL OF CHAPTER 4</b> .....	<b>259</b>

## LIST OF TABLES

### Chapter 3

Table 3.1. Compilation of published U-Pb zircon (unless otherwise indicated) geochronology data.....	60
--	----

### Chapter 4

Table 4.1. Oxygen, C, and Sr isotope values as well as trace element concentrations of carbonates from the Polanco Limestones and Cerro Espuelitas formations.....	119
--	-----

### Chapter 5

Table 5.1. Oxygen, C, Sr and N isotope values as well as trace element concentrations (in ppm) of carbonates from the Polanco Limestones Formation data.....	157
Table 5.2. U-Th-Pb isotopic data for Polanco Limestones Formation whole rock.....	159

### Appendix 2

Table A.2.1. U-Pb Zircon LA-MC-ICP-MS results from the Yermal Formation (sample 101115/1).....	251
Table A.2.2. U-Pb Zircon LA-MC-ICP-MS results from the Playa Hermosa Formation (sample 101026/2).....	252
Table A.2.3. U-Pb Zircon LA-MC-ICP-MS results from the Las Ventanas Formation (sample 101012/2).....	253
Table A.2.4. U-Pb Zircon LA-MC-ICP-MS results from the Las Ventanas Formation (sample 101026/1).....	254
Table A.2.5. U-Pb Zircon LA-MC-ICP-MS results from the San Carlos Formation (sample San Carlos).....	255
Table A.2.6. U-Pb Zircon LA-MC-ICP-MS results from the Barriga Negra Formation (sample 101116/3).....	256
Table A.2.7. Summary of U-Pb results for GJ1-32 and OG-1 standard zircons analyzed during this study.....	257
Table A.2.8. Sample locations.....	258

## LIST OF FIGURES

Chapter 1	
Figure 1.1. Major biogeochemical changes during the Proterozoic Eon.....	1
Chapter 2	
Figure 2.1. Simplified geologic map of Uruguay and southern Brazil .....	8
Figure 2.2. Lithostratigraphic columns of the Arroyo del Soldado, Arroyo de la Pedrera and Maldonado groups, showing a comparison between the stratigraphy reported in previous studies and in this work.....	10
Figure 2.3. Geologic map of southeastern Uruguay showing published geochronological data and distribution of Ediacaran volcano-sedimentary units: Arroyo del Soldado and Maldonado groups, and San Carlos, Sierra de Aguirre and Rocha formations.....	12
Figure 2.4. Field photographs showing some features of the angular, erosional unconformity between the Polanco Limestones Formation and the overlying Barriga Negra Formation.....	17
Figure 2.5. Compilation of radiometric ages and their error bars measured for intrusive and volcanic rocks from Uruguay and southernmost Brazil .....	22
Chapter 3	
Figure 3.1. Simplified geologic map of Uruguay and southern Brazil .....	49
Figure 3.2. Geologic map of southeastern Uruguay showing published U-Pb geochronological data and sample locations .....	52
Figure 3.3. Simplified geologic map of the type area of the Barriga Negra Formation .....	53
Figure 3.4. Stratigraphic profiles at sample locations. ....	56
Figure 3.5. Combined relative probability density and histogram plots.....	57
Figure 3.6. Stratigraphic columns for tectono-stratigraphic terranes of Uruguay.....	71
Figure 3.7. Diagrams of $\epsilon\text{Nd}(t)$ vs. time (Ma).....	79
Figure 3.8. Palaeogeographic reconstructions of Rodinia at a) ca. 850-750Ma and Rodinia to Gondwana at 750-650 Ma (b).....	82
Figure 3.9. Schematic reconstruction showing a possible scenario of episodic oblique terrane collisions during the Neoproterozoic .....	88
Chapter 4	
Figure 4.1. Location map of Uruguay and tectonostratigraphic subdivision of the crystalline basement.....	105
Figure 4.2. Simplified stratigraphical column of the Arroyo del Soldado Group .....	106
Figure 4.3. Inner and middle ramp facies at the Recalde and South Isla Patrulla sections .....	111
Figure 4.4. Outer ramp facies at the Los Tapes section.....	113
Figure 4.5. Thin section microphotographs of carbonate rocks of the Polanco Limestones Formation .....	116
Figure 4.6. Schematic stratigraphic profile of the Polanco Limestones Formation at the Los Tapes section and corresponding vertical variations in $\delta^{13}\text{C}$ , $\delta^{18}\text{O}$ , and Mn/Sr values .....	120
Figure 4.7. Schematic stratigraphic profile of the Polanco Limestones Formation at the South Isla Patrulla section and corresponding vertical variations in $\delta^{13}\text{C}$ and $\delta^{18}\text{O}$ values .....	120
Figure 4.8. Scatter diagrams for the Polanco Limestones Formation and the overlying Cerro Espuelitas Formation at the Los Tapes and South Isla Patrulla sections .....	124

Figure 4.9. $\delta^{18}\text{O}$ vs. $\delta^{13}\text{C}_{\text{carb}}$ cross plot for carbonates from the Polanco Limestones Formation and the overlying Cerro Espuelitas Formation at the Los Tapes and South Isla Patrulla sections.....	125
Figure 4.10. Scatter diagrams for limestones from the Los Tapes, South Isla Patrulla and Recalde sections. ....	126
Figure 4.11. Comparison of carbon isotope profiles from the deep- and shallow-water sections.	130
Figure 4.12. Summary of the illite age data from the uppermost Yermal Formation.....	132

Chapter 5

Figure 5.1. (A) Simplified stratigraphic column of the Arroyo del Soldado Group and (B) Schematic geological map of the Recalde Syncline area showing the location of the sections ...	151
Figure 5.2. Photographs of the Polanco Limestones Formation showing typical features of inner, middle and outer ramp facies .....	152
Figure 5.3. Profiles of the Polanco Limestones Formation at the Recalde Syncline area with corresponding vertical variations in $\delta^{13}\text{C}_{\text{carb}}$ , $\delta^{13}\text{C}_{\text{org}}$ , $\Delta^{13}\text{C}$ and $^{87}\text{Sr}/^{86}\text{Sr}$ . locations .....	156
Figure 5.4. U-Pb isochron diagram for carbonates of the Polanco Limestones Formation. ....	160
Figure 5.5. Pb-Pb diagrams for carbonates of the Polanco Limestones Formation. ....	163
Figure 5.6. Summary of the illite age data from the uppermost Yermal Formation .....	164
Figure 5.7. Scatter diagrams for profiles 1, 2 and 3.....	168
Figure 5.8. Profiles of the Polanco Limestones Formation at the Recalde Syncline area with corresponding vertical variations in $\delta^{13}\text{C}_{\text{carb}}$ , $\delta^{13}\text{C}_{\text{org}}$ , $\Delta^{13}\text{C}$ , $^{87}\text{Sr}/^{86}\text{Sr}$ , P, Al and Zr.....	177

**Appendix 1**

Figure A.1.1. U-Pb zircon results for sample 060517/2.....	249
--	-----

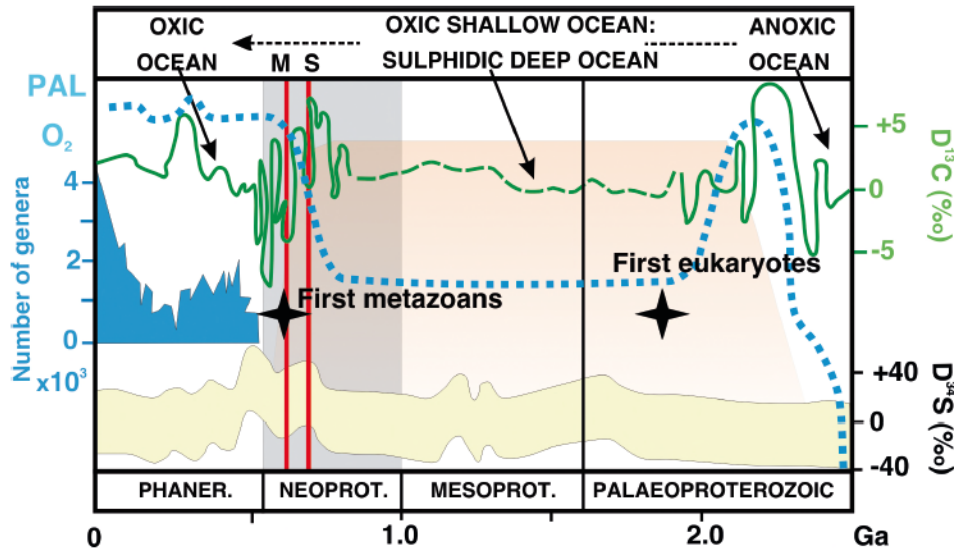
**Appendix 2**

Figure A.2.1. A selection of representative detrital zircon grains from each sample analyzed in this study.....	250
---	-----

# CHAPTER 1: INTRODUCTION

## 1.1. RATIONALE

The Neoproterozoic Era (1000-541 Ma) stands out as one of the greatest turning points in Earth history. The irreversible environmental changes of that time have been linked to tectonic upheavals that presumably provoked a cascade of global-scale geochemical, climatic and biotic events. Significantly, large perturbations in the carbon cycle, two of which are associated with global (Snowball) glaciations, are temporally related to changes in the deep-water redox state and metazoan radiation (Figure 1.1; Narbonne et al., 2012; Shields-Zhou et al., 2012). Interpreting these chemical signals, in concert with sedimentological and geochronological data, is therefore crucial to better understand their origin within the context of contemporaneous tectonic, biological and climatic changes.



**Figure 1.1.** Major biogeochemical changes during the Proterozoic Eon. Neoproterozoic Era is indicated by the shaded area. M-S: Marinoan and Sturtian glaciations. Source: International Continental Scientific Drilling Program-Neoproterozoic Research Group (Modified from [http://www-icdp.icdp-online.org/front\\_content.php?idcat=1816](http://www-icdp.icdp-online.org/front_content.php?idcat=1816) and Lyons et al., 2014).

The Neoproterozoic in Uruguay has emerged as a new promising site to the study of this period of time as it records global climatic, biogeochemical and biotic events (Frei et al., 2009; 2011; Pecoits et al., 2012). Of particular interest is the Arroyo del Soldado

Group, whose record has been regarded as crucial for unraveling critical aspects of the Ediacaran Period (635-541 Ma). The Arroyo del Soldado Group is a ~2,200 m-thick mixed carbonate-siliciclastic succession and includes, from the base to top, the Yerbal, Polanco Limestones and Cerro Espuelitas formations. The presence of iron formations, thick limestone-dolostone strata and organic matter-rich shales interbedded with cherts are the main features that characterize these three lithostratigraphic units, respectively (Pecoits et al., 2008).

Previous chemostratigraphic studies on the Polanco Limestones Formation, which constitutes the main goal of this study, have identified a significant negative  $\delta^{13}\text{C}$  excursion in shallow-water facies (down to -4.5‰) and a connection to glaciation has been suggested as the most likely explanation (Gaucher et al., 2004; 2009). According to the same authors, this negative anomaly would reflect seawater composition in the aftermath of a non-global post-Gaskiers glaciation (<581 Ma) that occurred elsewhere and correlatable with the Shuram-Wonoka-Johnnie carbon isotope anomaly (~551 Ma). Crucially, the apparent synchronicity between this excursion, correlated with the Shuram-Wonoka-Johnnie carbon isotope anomaly, and glacial conditions carries important implications for the palaeo-oceanographic and palaeo-climatic evolution in the Ediacaran and ultimately, for the rise of animal life.

In order to assess the fidelity, extent, context and environmental significance of this negative shift, this study aims to: (1) reconstruct lateral variations of  $\delta^{13}\text{C}_{\text{org}}$ ,  $\delta^{13}\text{C}_{\text{carb}}$  and  $\Delta^{13}\text{C}_{\text{carb-org}}$  across the Polanco platform, (2) constrain the age of the Polanco Limestones Formation by means of new chemostratigraphic (Sr and C) and radiometric data, (3) incorporate these new age constraints into our understanding of the geologic history of the Arroyo del Soldado Group, (4) discuss the mechanisms, either syn- or post depositional, controlling the isotopic fractionation and secular variations of  $\delta^{13}\text{C}_{\text{carb}}$  and  $\delta^{13}\text{C}_{\text{org}}$ , (5) evaluate the relative contributions of local versus global carbon cycles, and (6) correlate the C isotope curves of the Polanco Limestones Formation with those of successions of similar age with the aim to better constraining the Neoproterozoic carbon isotope reference curve.

## 1.2. THESIS ORGANIZATION

The main part of the presented work consists of two published manuscripts (Chapters 2-4) and two manuscripts presently in review in international journals (Chapters 3-5), which are based on my own sampling, analyses, data evaluation and interpretation. Finally, a conclusion (Chapter 6) sums up the most important findings and gives a brief outlook and recommendations for future work.

Chapter 2 deals with a re-evaluation of the stratigraphy and age of the Arroyo del Soldado Group and other Neoproterozoic units. After extensive field work and review of available data it was concluded that, although variable, the stratigraphy, distribution and age of these units (including the Polanco Formation) remained ambiguous. The same is true for existing basin models and tectonic evolution, which show different and sometimes contradicting supporting evidence. Here, it is proposed that the Arroyo del Soldado Group (Yerbal, Polanco Limestones and Cerro Espuelitas formations) was likely deposited between 650 and 1000 Ma (Aubet et al., 2014).

Chapter 3 presents new U-Pb detrital zircon ages, combined with previously published geochronologic and stratigraphic data in order to provide more precise temporal constraints on their depositional age and to establish a more solid framework for the stratigraphic and tectonic evolution of Neoproterozoic units. Based on these new radiometric constrains, it was concluded that deposition of the Arroyo del Soldado Group took place between ~1,000 and 650 Ma, which fully supports our previous estimates. This manuscript established a new chronostratigraphic and tectonic evolution framework for the Neoproterozoic volcano-sedimentary successions of Uruguay (Aubet et al., a, *in review*).

Chapter 4 provides high-resolution  $\delta^{13}\text{C}_{\text{carb}}$ -chemostratigraphy and Sr-isotope data from deep-water sections of the Polanco Limestones Formation. Although carbon isotopic values are negative in deep-water facies they progressively rise towards positive values in shallow-water settings, which suggests that deposition of Polanco carbonates occurred in a stratified marine basin. The previously recognized negative  $\delta^{13}\text{C}_{\text{carb}}$  excursion is therefore, restricted to specific horizons in shallow-water facies and hypothesized as being originated due to local processes (oxidation of organic matter).  $^{87}\text{Sr}/^{86}\text{Sr}$  and  $\delta^{13}\text{C}_{\text{carb}}$  chemostratigraphy coupled with new radiometric data allowed us to

revise the previously proposed age for the unit. This new data support an age between 590 and 560 Ma for the deposition of the Polanco Limestones Formation (Aubet et al., 2012).

In Chapter 5, carbonates of the Polanco Limestones Formation were analyzed for paired  $\delta^{13}\text{C}_{\text{org}}$  and  $\delta^{13}\text{C}_{\text{carb}}$ . Their records reveal local changes in nutrient input and phytoplankton growth rates. This is supported by simultaneous changes in the concentrations of nutrients (P), lithophile elements (e.g., Al, Zr) and  $^{87}\text{Sr}/^{86}\text{Sr}$  ratios, which also indicate a terrestrial source. However, the dominant control on the  $\delta^{13}\text{C}_{\text{org}}$  and  $\delta^{13}\text{C}_{\text{carb}}$  curves is interpreted to reflect changing  $[\text{CO}_2]_{\text{aq}}$ , and possibly in global  $p\text{CO}_2$ . The consistently small  $\Delta^{13}\text{C}$  values suggest low atmospheric  $p\text{CO}_2$  wherein, under  $\text{CO}_2$ -limiting conditions, the utilization of  $\text{HCO}_3^-$  by planktic cyanobacteria lowered  $\Delta^{13}\text{C}$  and produced the precipitation of biogenic whittings. New geochronologic and chemostratigraphic data permit to constrain the age of the unit to the Cryogenian interglacial period (Aubet et al., b, *in review*).

Finally, in Chapter 6 the main findings and conclusions of previous chapters are brought together and categorized into (1) litho- and chronostratigraphy, geochronology and palaeogeography, and tectonic evolution of the Neoproterozoic of Uruguay, and (2) sedimentology and diagenesis, carbon and strontium isotope records, and age of the Polanco Limestones Formation. This type of integrated analysis has proven to be useful to constrain the depositional environment and the age of the Polanco Limestones Formation and to understand the platform dynamics. Furthermore, by comparing chemostratigraphic profiles across the basin (i.e., shallow- vs. deep-water settings), we show that this approach can help to interpret Precambrian carbonate systems, especially those associated with major palaeo-climatic and palaeo-environmental events. This chapter concludes by listing specific future work that is needed to better constrain the palaeo-environmental significance of the Polanco Limestones Formation within the context of contemporaneous global changes during the Neoproterozoic.

### **1.3. REFERENCES**

Aubet, N., Pecoits, E., Bekker, A., Gingras, M.K., Zwingmann, H., Veroslavsky, G., de Santa Ana, H., Konhauser, K.O., 2012. Chemostratigraphic constraints on early Ediacaran

- carbonate ramp dynamics, Rio de la Plata craton, Uruguay. *Gondwana Research* 22, 1073-1090.
- Aubet, N., Pecoits, E., Heaman, L., Veroslavsky, G., Gingras, M., Konhauser, K. 2014. Ediacaran in Uruguay: facts and controversies. *Journal of South American Earth Sciences* 55, 43-57.
- Aubet, N., Pecoits, E., Heaman, L., Veroslavsky, G., Konhauser, K.O., a, *In review*. U-Pb detrital zircon ages from some Neoproterozoic successions of Uruguay: provenance, stratigraphy and tectonic evolution. *Precambrian Research*.
- Aubet, N., Pecoits, Bekker, A., Heaman, L., Veroslavsky, G., Konhauser, K.O., b, *In review*. A low  $p\text{CO}_2$  interglacial period? Insights from paired  $\delta^{13}\text{C}_{\text{org}}$  and  $\delta^{13}\text{C}_{\text{carb}}$  records of Cryogenian carbonates. *Gondwana Research*.
- Frei, R., Gaucher, C., Canfield, D.E., Poulton, S.W. 2009. Fluctuations in Precambrian atmospheric oxygenation recorded by chromium isotopes. *Nature* 461, 250-253.
- Frei, R., Gaucher, C., Døssing, L.N., Sial, A.N., 2011. Chromium isotopes in carbonates -a tracer for climate change and for reconstructing the redox state of ancient seawater. *Earth and Planetary Science Letters* 312, 114-125.
- Gaucher, C., Sial, A.N., Blanco, G., Sprechmann, P., 2004. Chemostratigraphy of the lower Arroyo del Soldado Group (Vendian, Uruguay) and paleoclimatic implications. *Gondwana Research* 7, 715-730.
- Gaucher, C., Sial, A.N., Poire, D., Gomez-Peral, L., Ferreira, V.P., Pimentel, M.M., 2009. Chemostratigraphy. In: Gaucher, C., Sial, A.N., Halverson, G.P., Frimmel, H.E. (Eds.), *Neoproterozoic-Cambrian Tectonics, Global Change and Evolution: a Focus on Southwestern Gondwana*, vol. 16, pp. 115-122. *Developments in Precambrian Geology*.
- Lyons, T., Reinhard, C., Planavsky, N., 2014. The rise of oxygen in Earth's early ocean and atmosphere. *Nature*, 506, 307-315.
- Narbonne, G.M., Xiao, S., Gehling, J.G., Shields-Zhou, G.A., 2012. The Ediacaran Period. In: Gradstein, F.M., Ogg, J.G., Schmitz, M., Ogg, G. (Eds.), *Geological Time Scale 2012*. Cambridge University Press, Cambridge, pp. 413-435.
- Pecoits, E., Gingras, M.K., Aubet, N.R., Konhauser, K.O., 2008. Ediacaran in Uruguay; palaeoclimatic and palaeobiologic implications. *Sedimentology* 55, 689-719.

Pecoits, E., Konhauser, K.O., Auet, N.R., Heaman, L.M., Veroslavsky, G., Stern, R.A., Gingras, M.K., 2012a. Bilaterian burrows and grazing behavior at >585 Million years ago. *Science* 336, 1693-1696.

Shields-Zhou, G.A., Hill, A.C., Macgabhann, B.A., The Cryogenian Period. In: Gradstein, F.M., Ogg, J.G., Schmitz, M., Ogg, G. (Eds.), *Geological Time Scale 2012*. Cambridge University Press, Cambridge, pp. 393-411.

## CHAPTER 2: EDIACARAN IN URUGUAY: FACTS AND CONTROVERSIES

### 2.1. Introduction

The Ediacaran Period (635-541 Ma) witnessed significant environmental and biological transformations. Ediacaran sedimentary rocks contain information on atmospheric and oceanic composition (e.g., C- and Sr-isotopic excursions), as well as on the appearance and diversification of metazoans (Narbonne et al., 2012). Besides the well-known Ediacaran successions, such as those located in South Australia, Namibia, Russia, China and the Avalon Peninsula in Canada (e.g., Geyer, 2005; O'Brien and King, 2005; Knoll et al., 2006; Grey and Calver, 2007; Jiang et al., 2011; Johnston et al., 2012), new promising areas have emerged in the last few years (McCall, 2006), including those in Uruguay which have been suggested to record global climatic, biogeochemical and biotic events (Gaucher et al., 2009; Frei et al., 2011; Pecoits et al., 2012).

According to previous interpretations, the Ediacaran Period in Uruguay is represented by the Arroyo del Soldado and Maldonado groups, the Sierra de Aguirre, Rocha and Tacuarí formations, and part of the Arroyo de la Pedrera Group (Figure 2.1). These units have been the focus of numerous sedimentary, stratigraphic, paleontological and geochemical studies. As a result, a range of divergent chrono-stratigraphic, depositional and tectonic interpretations has been proposed to explain the origin and evolution of these volcano-sedimentary units. Unfortunately, most of these models are supported by limited and, in some cases, questionable evidence (see for example Sánchez Bettucci et al., 2010; Zimmermann, 2011). This has resulted in controversial associations with important Ediacaran events and correlations with other successions worldwide.

In this article, we review and summarize tectonostratigraphic schemes of Uruguayan Ediacaran strata focusing on lithostratigraphy, age and geological setting: the purpose of this paper is to identify and analyze the strengths, limitations and misconceptions pertaining to the nature and age of units. Of particular interest are the Arroyo del Soldado and Maldonado groups because of their potential relevance to unravel several aspects of the Ediacaran Period. Therefore, the ultimate goal of this article is to present a constructive but critical review of key issues regarding the Ediacaran of Uruguay, with the aim of promoting further research that allows a better

understanding of the local geology and its implications for the Precambrian processes and events.

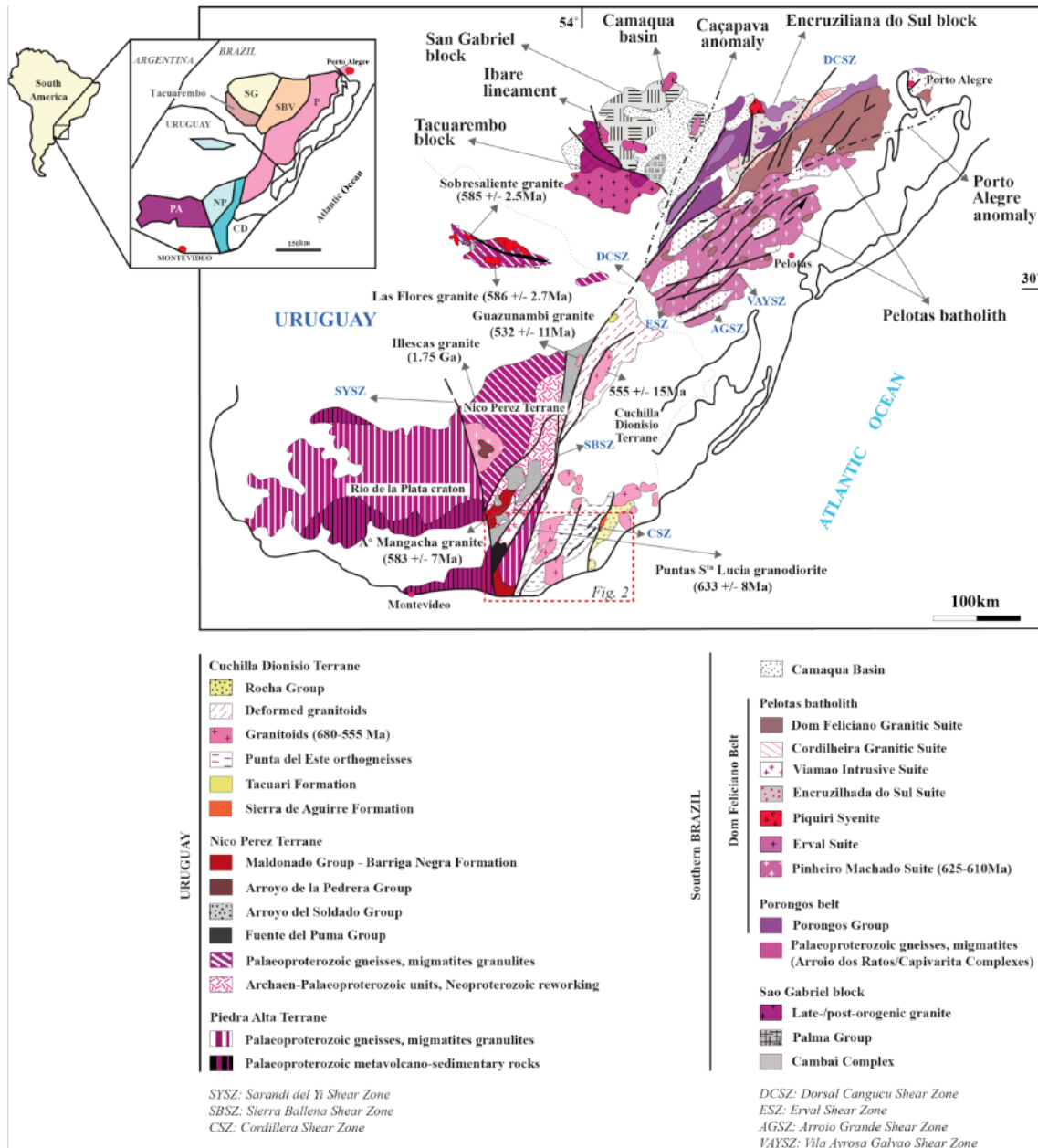


**Figure 2.1.** Simplified geologic map of Uruguay and southern Brazil (modified from Saalman et al., 2011 and references therein). Inset: PA-Piedra Alta, NP-Nico Pérez, and CD-Cuchilla Dionisio Terranes of Uruguay; SG-São Gabriel, SBV-Santana da Boa Vista, P-Pelotas and Tacuarembó Blocks of southern Brazil.

## 2.2. Previous work

### 2.2.1. Arroyo del Soldado Group

The conceptual stratigraphic framework of lithologies now included in the Arroyo del Soldado Group was first made by Preciozzi et al. (1988 and references therein; see also Preciozzi et al., 1993). However, this lithostratigraphic unit was formally defined by Gaucher et al. (1996) to include a marine shallowing-upward succession (~1500 m) comprising, from base to top, the Polanco Limestones Formation (Goñi and Hoffstetter, 1964), Cerro Espuelitas, Cerros San Francisco and Cerro Victoria formations (Montaña and Sprechmann, 1993). Later, Gaucher et al. (1998) included the basal Yermal Formation and the Barriga Negra Formation (Midot, 1984) resulting in more than 5000 m in thickness for the entire group (Figure 2.2). Subsequently, Pecoits et al. (2008) proposed a new lithostratigraphic scheme for the Arroyo del Soldado Group excluding the Cerros San Francisco and Cerro Victoria formations into the Arroyo de la Pedrera Group. This exclusion was based on the lack of continuity between the Cerro Espuelitas and the Cerros San Francisco formations.

The age of the Arroyo del Soldado Group is also controversial. Gaucher et al. (2009) concluded that the age of the group is geochronologically constrained by dates obtained from basement and intrusive granites with a maximum U-Pb SIMS zircon age of  $583 \pm 7$  Ma for the Arroyo Mangacha Granite in the basement, and a minimum Rb-Sr isochron age of  $532 \pm 11$  Ma for the intrusive De Los Guazunambí Granite ( $R_i = 0.70624$ ) (Figure 2.1). The youngest detrital zircon populations from the Yermal and Barriga Negra formations show ages between 664 Ma and  $566 \pm 8$  Ma (Blanco et al., 2009), respectively, and further supports an Ediacaran age for the whole group. According to Gaucher et al. (2009), biostratigraphic data also point to an upper Ediacaran age for the lower and middle Arroyo del Soldado Group, and a lowermost Cambrian age for the Cerro Victoria Formation. In this regard, the organic-walled microfossils identified and the occurrence of the upper Ediacaran index fossil *Cloudina* would appear to support an Ediacaran age (<550 Ma). The same authors also proposed that the presence of a low-diversity stromatolite community and a low-diversity trace fossil association (*Thalassinoides* - *Gyrolithes* - *Palaeophycus* assemblage) suggests a lowermost Cambrian age (541 to 535 Ma) for the Cerro Victoria Formation. Therefore, the Precambrian-Cambrian boundary

would be within the Cerro Victoria Formation or, alternatively, in the Cerros San Francisco Formation; both units still being part of the Arroyo del Soldado Group according to Gaucher et al. (2009). Recently, Aubet et al. (2012; 2013) provided new K-Ar ages from diagenetic illite and proposed a minimum age of 600-580 Ma for the uppermost Yerbal Formation. These authors also challenged some of the geochronological constraints presented by Gaucher et al. (2009) and suggested that the *Cloudina* material was so poorly preserved that their identification as fossil material remains uncertain.

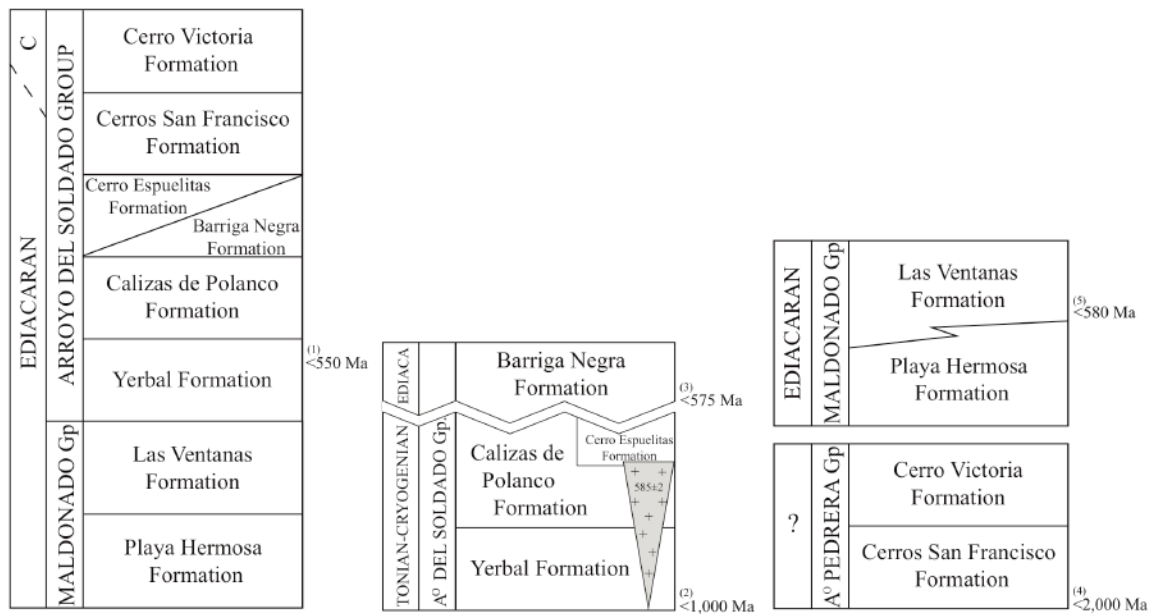


**Figure 2.2.** Lithostratigraphic columns of the Arroyo del Soldado, Arroyo de la Pedrera and Maldonado groups, showing a comparison between the stratigraphy reported in previous studies and in this work (see text for explanation). Chronostratigraphic constraints: (1) *Cloudina*; (2-4) Oldest detrital zircon populations (U-Pb LA-ICP-MS); (5) Volcaniclastic rocks (U-Pb SHRIMP).

### 2.2.2. Maldonado Group

The Maldonado Group was formally erected by Pecoits et al. (2004) to include the Playa Hermosa Formation (Elizalde, 1979; Preciozzi et al., 1989; Masquelin and Sánchez Bettucci, 1993) and Las Ventanas Formation (Midot, 1984). Given its structural, chronostratigraphic and lithologic attributes, the San Carlos Formation was informally included in the group (Pecoits et al., 2004; Pecoits et al., 2008). Masquelin and Sánchez

Bettucci (1993) described the main sedimentological features of the Playa Hermosa Formation. Pazos et al. (2003) characterized in detail the lower part of this unit and recognized two distinct facies associations: (i) medium- to coarse-grained facies (consisting of interbedded breccias, conglomerates, sandstones and minor mudstones), and (ii) fine-grained facies (composed mostly of mudstones but also diamictites, rhythmites and sandstones). The authors concluded that both facies associations accumulated in a sub-aqueous glacially influenced marine environment and represent a proximal to distal depositional trend. Pazos et al. (2003) further suggested that this glacially-influenced succession constitutes a record of the Varanger glaciation.

Midot (1984) erected the Las Ventanas Formation to include conglomerates, sandstones and pelites cropping out at Las Ventanas Hill and in the surrounding areas. This unit was considered to be an Ordovician sedimentary sequence (e.g., Midot, 1984; Masquelin and Sánchez Bettucci, 1993). Pecoits (2003) redefined the unit as a Neoproterozoic (ca. 580 Ma) volcano-sedimentary succession. These deposits were interpreted as a product of sheetflood-dominated fan deltas, which were intercalated with minor marine deposits. Pecoits (2003) and Pecoits et al. (2004) reported the presence of organic-walled microfossils and evidence for glacial influence in the lower part of the unit, respectively. Subsequent work showed that the unit continues to the north in the vicinity of Minas (Pecoits et al., 2004; 2008; Gaucher et al., 2008). Blanco and Gaucher (2005) proposed a different lithostratigraphic scheme from that proposed by Pecoits (2003) and reported seven additional species of organic-walled microfossils (acritarchs).

The San Carlos Formation (Masquelin, 1990) occurs to the east of the Sierra Ballena Shear Zone but shows characteristics similar to the Las Ventanas Formation. Field relationships suggest a similar geological setting and age for both units (Pecoits et al., 2008). At the stratotype, the succession consists of interbedded conglomerates, sandstones and pelites, with the latter dominating up-section. Palynological macerations carried out for the pelites (Pecoits et al., 2004) revealed the occurrence of microfossils similar to those described for the Las Ventanas Formation (Pecoits, 2003). Pecoits et al. (2004; 2008) indicated that further research was needed to resolve whether both units are the same or were deposited in the same basin that was subsequently dismantled by the displacement of the Sierra Ballena Shear Zone (Figure 2.3).

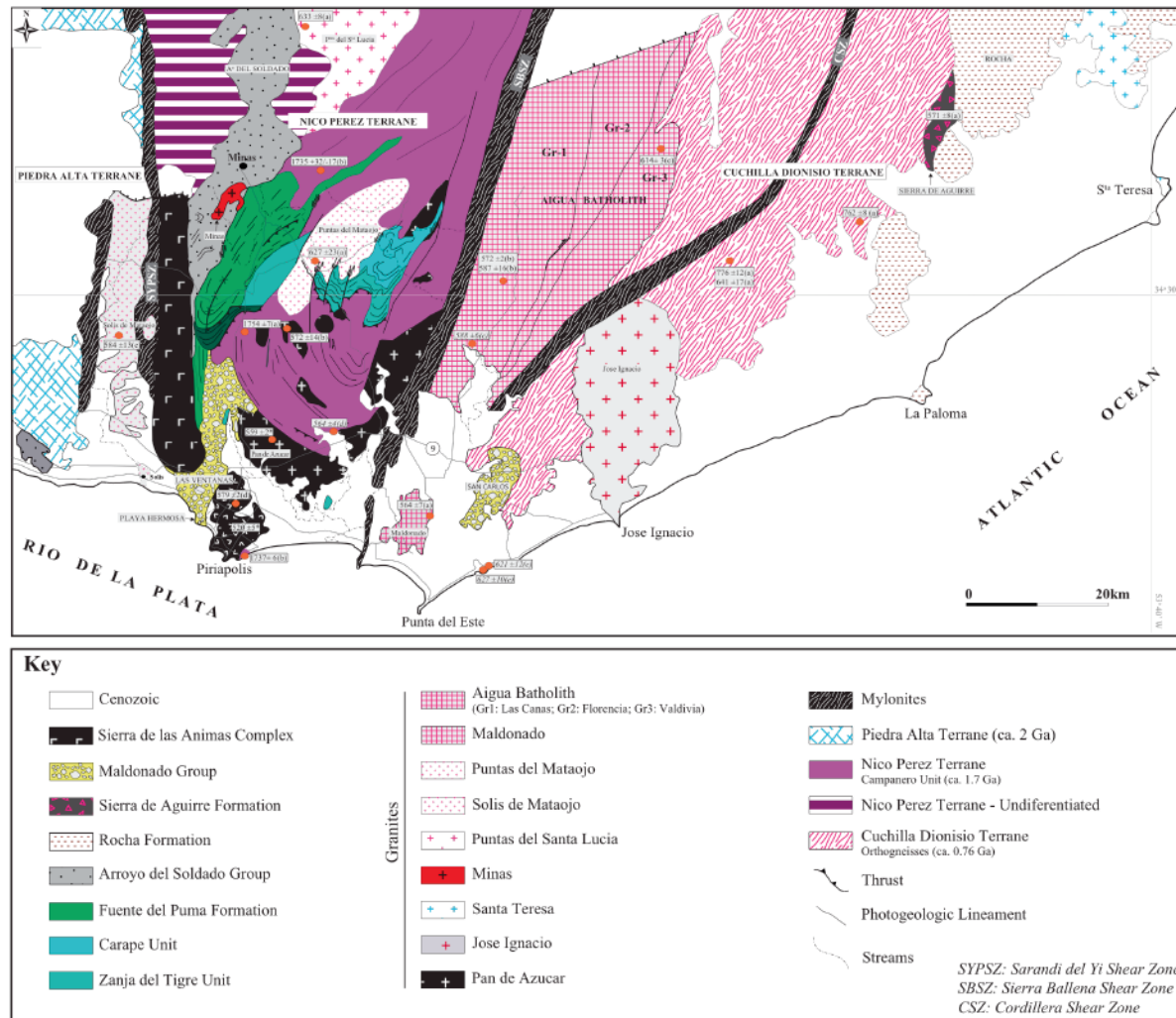


**Figure 2.3.** Geologic map of southeastern Uruguay showing published geochronological data and distribution of Ediacaran volcano-sedimentary units: Arroyo del Soldado and Maldonado groups, and San Carlos, Sierra de Aguirre and Rocha formations. Modified from Oyhantçabal (2005), Oyhantçabal et al. (2009) and Pecoits et al. (2011).

### **2.2.3. Rocha Formation**

This unit was originally defined as the Rocha Group by Hasui et al. (1975), but Sánchez Bettucci and Mezzano (1993) proposed a formation rank. The succession comprises a lower unit dominated by chlorite phyllite and minor graphitic phyllite, and an upper unit of bedded meta-sandstones with minor meta-siltstones. It has been inferred that the group formed in a platformal marine-shelf environment, with the basin deepening eastwards (Sánchez Bettucci and Mezzano, 1993).

Granites from the basement yielded a maximum age of  $762 \pm 8$  Ma (SHRIMP, U-Pb; Hartmann et al., 2002), while the minimum age was given by post-tectonic alkaline granite bodies in the region (e.g., Santa Teresa Granite; Figure 3.3). According to Basei et al. (2005), sedimentation took place between ca. 600 Ma, as indicated by the youngest detrital zircon grains, and ca. 550 Ma, the onset of post-tectonic alkaline magmatism. Based on their similar lithologies, comparable tectonic setting and the detrital zircon age patterns, Basei et al. (2005) further suggested that the Oranjemund Group (Namibia) and the Rocha Formation are time equivalents, and probably represent sediment fill of the same basin.

### **2.2.4. Sierra de Aguirre Formation**

Bossi (1966) first described this sedimentary succession dominated by sandstones and pelites. Masquelin and Tabó (1988) later defined it as the Sierra de Aguirre Formation and interpreted this unit as a marine sedimentary succession consisting of pelites, sandstones and pyroclastic rocks intruded by rhyolite dykes. By contrast, Campal and Schipilov (2005) described the unit as composed of volcanic and pyroclastic rocks, including rhyolite, trachyte, ignimbrite of rhyodacitic composition, and laminated tuff. Fantin (2003) reported 110 m thickness for the unit in the southern part of the type area and recognized volcanic, sub-volcanic and epiclastic rocks. In its lower part, the succession is dominated by volcanic deposits, whereas, in the upper part, sedimentary deposits are more common. Depositional environments correspond to shallow-marine and deltaic settings (Fantin, 2003) of a pull-apart basin (Campal and Schipilov, 2005). The contact with the basement (to the west) is unconformable and with the Rocha Formation (to the east) is tectonic (Figure 2.3). A dacite yielded a SHRIMP U-Pb concordia age of

571±8 Ma (Hartman et al., 2002). This age is similar to that obtained further to the north for acidic volcanic rocks of the Sierra de Ríos Formation at 575±14 Ma (Bossi et al., 1993), which indicates an extensive volcanic activity at that time.

### **2.2.5 Tacuarí Formation**

The Tacuarí Formation was erected by Veroslavsky et al. (2006). It comprises basal diamictites, sandstones and minor pelites that grade upwards into fine-grained rhythmites which contain abundant out-sized clasts. The latter, interpreted as dropstones, along with diamictites hosting faceted and striated clasts and associated varved sediments, provide definitive evidence for the glacial origin of these deposits. Although the Tacuarí Formation was long considered Carboniferous-Permian in age (formerly San Gregorio Formation), U-Pb zircon ages (LA-MC-ICP-MS and SHRIMP) obtained for a cross-cutting granitic dyke places a minimum age of the unit to 585±3 Ma (Pecoits et al., 2012). A maximum depositional age for the Tacuarí Formation is 600±9 Ma, based on the youngest detrital zircon age cluster reported (Pecoits et al., 2012). Significantly, metazoan trace fossils occur within the uppermost fine-grained rhythmites. This new discovery provides evidence for bilaterian burrows from shallow-water sediments that are at least 30 million years older than previously reported trace fossils (Pecoits et al., 2012). Although Gaucher et al. (2013) questioned the age of these trace fossils, Pecoits et al. (2013) presented new evidence further supporting an age between 585±3 and 600±9 Ma.

## **2.3. Stratigraphy of the Ediacaran in Uruguay**

For the units briefly described above, the following discussion will focus on the Arroyo del Soldado and Maldonado groups. Both are regarded as important for unraveling critical aspects of the Ediacaran Period and are the subject of controversy in terms of their lithostratigraphy, age and geological setting.

### **2.3.1. Arroyo del Soldado Group**

#### **2.3.1.1. Lithostratigraphy**

The Arroyo del Soldado Group (*sensu* Gaucher et al., 1998) includes, from base to top, Yerbal, Polanco Limestones, Cerro Espuelitas, Barriga Negra, Cerros San Francisco and

Cerro Victoria formations (Figure 2.2). In other lithostratigraphic schemes, the group would include all those units with the exception of the Cerros San Francisco and Cerro Victoria formations (Pecoits et al., 2008; Aubet et al., 2012). This redefinition is based on the absence of a conformable contact between the Cerro Espuelitas and the Cerros San Francisco formations (see discussion on the Arroyo Mangacha granite below). Therefore, following the original name proposed by Montaña and Sprechmann (1993), the Arroyo de la Pedrera Formation (composed of the Cerros San Francisco and the Cerro Victoria units) was elevated to group status and separated from the Arroyo del Soldado Group (Pecoits et al., 2008).

#### ***2.3.1.1.a. The Barriga Negra Formation***

Recently, Frei et al. (2013) suggested that the Barriga Negra Formation represents the base of the Arroyo del Soldado Group and not its middle part as was previously accepted. This change was challenged by Aubet et al. (2013) who questioned the rationale of relocating strata previously bracketed between two distinct units (Figure 2.2), the Polanco Limestones and Cerro Espuelitas formations with their respective upper and lower contacts exposed and described (Gaucher 2000, Gaucher et al. 1998; 2004; 2008; Gaucher and Poiré, 2009b; Blanco et al. 2009; Frei et al., 2011), to a lower stratigraphic position. The only argument presented by Frei et al. (2013) to justify this change in the lithostratigraphy is the apparent resetting (values were not shown) of the  $^{87}\text{Sr}/^{86}\text{Sr}$  ratios. Isotopic ratios, however, are not considered as a basis for lithostratigraphic subdivision (Murphy and Salvador, 1999; NACSN, 2005). Furthermore, the alteration of the  $^{87}\text{Sr}/^{86}\text{Sr}$  ratios in this unit is not rare. As shown by Aubet et al. (2012), even the stratotype of the Polanco Limestones Formation displays Sr isotopic values that have been heavily overprinted.

There is a number of compelling arguments that support that the Barriga Negra Formation overlies the Polanco Limestones Formation, namely: (i) clasts of the Polanco Limestones Formation have been described and illustrated within the Barriga Negra Formation (Preciozzi, 1988; Preciozzi et al., 1988; Fambrini et al., 2005); (ii) there are incised valleys in the Polanco Limestones Formation that are infilled with Barriga Negra breccias and conglomerates (Gaucher et al., 2004), and (iii) the contact between units is

traceable and observable for several kilometers in the field, mainly in the type area of the Polanco Limestones Formation (Fragoso-Cesar et al., 1987; Preciozzi, 1988; Preciozzi et al., 1988; Gaucher, 2000; Fambrini et al., 2005).

Recent geological mapping in the area support these observations and, more importantly, revealed an angular unconformity between these units (see Figure 2.4). Although this observation is not new (see references below), it has largely been ignored and inevitably led to a reevaluation of the lithostratigraphy of the Arroyo del Soldado Group. Fragoso-Cesar et al. (1987) originally suggested that the Barriga Negra Formation rests unconformably on marbles of the Polanco Limestones Formation and on the Polanco Granite. Preciozzi (1988) later indicated an angular discordance between these units while mapping the area, confirming previous observations by Fragoso-Cesar et al. (1987). It is worth noting that the lithological attributes and diagnostic features of the Polanco Limestones Formation are unique, which has permitted its separation since the original definition by Goñi and Hoffstetter (1964). This stratigraphic relationship has been accepted by all the researchers working in the area (e.g., Fragoso-Cesar et al., 1987; Preciozzi et al., 1988; Preciozzi, 1988; Bossi et al., 1998; Gaucher et al., 2000; Fambrini et al., 2005; Pecoits et al., 2008). Therefore, it is clear that the Polanco Limestones Formation underlies the Barriga Negra Formation. The existence of an unconformity is not only supported by field relationships (Figure 2.4), but also by detrital zircon geochronology for the Barriga Negra Formation (see below).

### **2.3.1.2. Age**

#### **2.3.1.2.a. Geochronology**

##### *Basement*

##### 1) Arroyo Mangacha Granite

The Arroyo Mangacha Granite is undeformed, porphyritic, and composed of quartz (40%), orthoclase (38%), oligoclase (17%) and biotite (5%), with accessory microcline, titanite, zircon and opaque minerals (Gaucher et al., 2008). This intrusion is part of the Barriga Negra batholith defined by Preciozzi et al. (1988), which is characterized by pink, leucocratic, fine to coarse-grained granites, and is considered to be part of a suite of late- to post-tectonic granites (Figure 3.1). Gaucher et al. (2008) reported a U-Pb SIMS

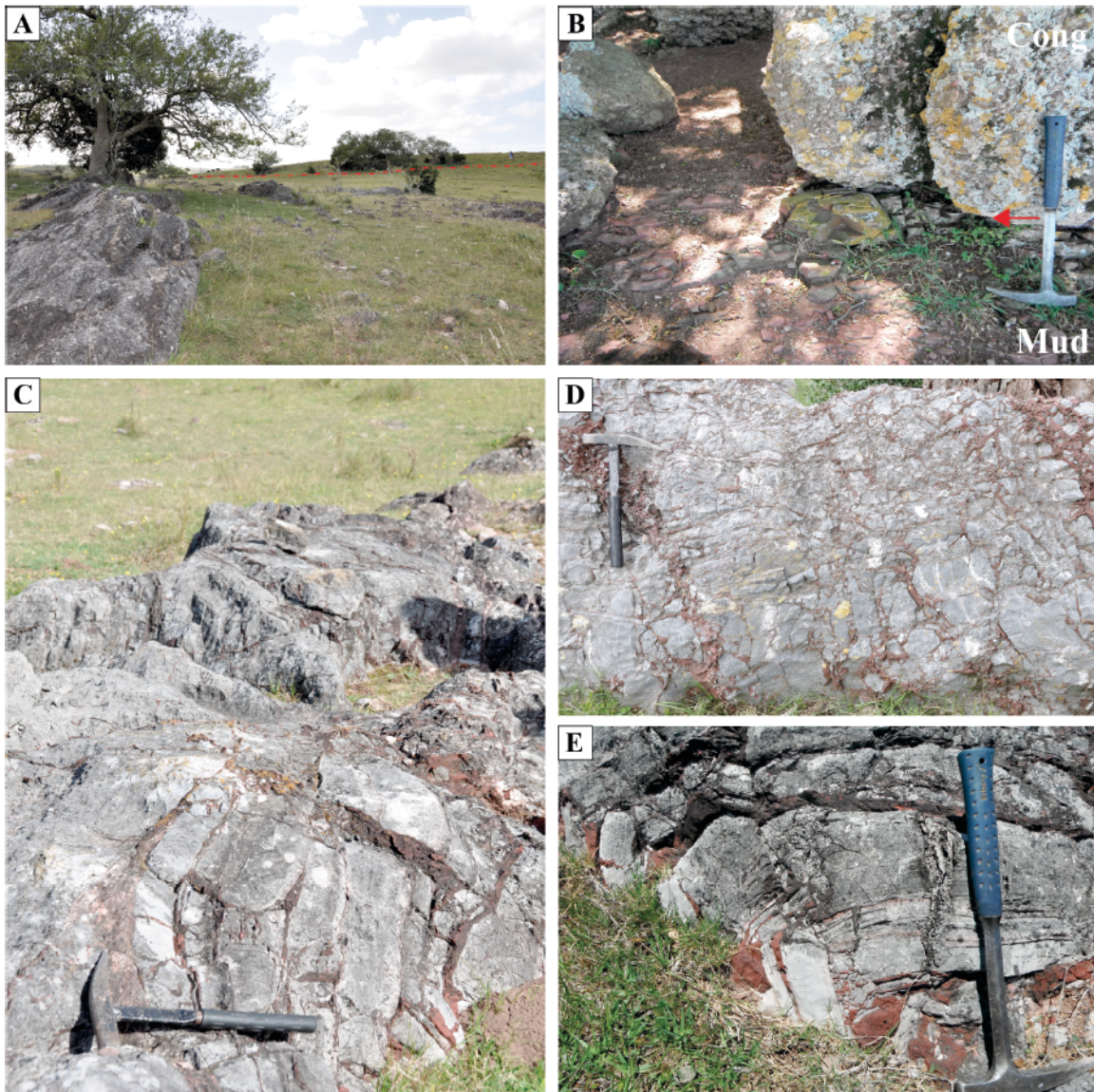


**Figure 2.4.** Field photographs showing some features of the angular, erosional unconformity between the Polanco Limestones Formation and the overlying Barriga Negra Formation (outcrop location: type area of the Polanco Limestones Formation, NE of Polanco village). **(A)** General view of the outcrop (looking east). The red dashed line indicates location of the unconformity between the underlying and folded (nearly vertical) sedimentary layers of the Polanco Formation and the overlying slightly tilted (nearly horizontal) strata of the Barriga Negra Formation. **(B)** Lowermost strata of the Barriga Negra Formation. Note the almost horizontal (dip about 5-10° to the east) bedding plane of the basal red mudstone (Mud) and its contact (red arrow) with heterolithic pebble conglomerate (Cong). **(C)** Upright beds of the Polanco Limestones Formation, dipping ca. 85° to the south, showing evidence of paleo-karst features near the unconformity surface. Paleo-karst cavities have been extensively infilled with red mudstones of the overlying Barriga Negra Formation. **(D-E)** Detailed views of outcrop surfaces with visible paleo-karst features, including solution features, breccias, collapse structures and extensive infill along bedding planes and fractures.

zircon age of  $583\pm 7$  Ma for this granite and concluded that this age represents the best maximum depositional age constraint available for the Arroyo del Soldado Group because the Cerros San Francisco Formation rests unconformably on this granite.

Although small, the area mapped by Gaucher et al. (2008; their Fig. 9) is crucial for two reasons. First, it potentially provides the maximum age constraint for the Arroyo del Soldado Group (i.e., the dated granite). Second, it shows the relationship between three different lithostratigraphic units, namely, (i) a carbonate-siliciclastic succession, (ii) sandstones of the Cerros San Francisco Formation, and (iii) the Arroyo Mangacha Granite. Although now considered part of the basement of the Arroyo del Soldado Group by Gaucher et al. (2008; 2009) and Frei et al. (2013), the carbonate-siliciclastic unit was previously thought to be part of the Cerro Espuelitas Formation (Arroyo del Soldado Group) and considered conformable with the overlying sandstones of the Cerros San Francisco Formation (Gaucher, 2000; his Fig. 27). Importantly, this is one of three outcrops where the Cerro Espuelitas Formation was considered to be conformable with the Cerros San Francisco Formation. The second outcrop is located at the stratotype of the Cerro Espuelitas Formation (Gaucher et al., 1996; their Fig. 4). However, as with the first area, it was later recognized that such continuity does not exist (Gaucher 2000; his Fig. 17). The third outcrop is located in the Cerro Carreras (Gaucher, 2000; his Fig. 24). At this location, the iron formation assigned to the Cerro Espuelitas Formation is interpreted to be conformable with sandstones of the Cerros San Francisco Formation (Gaucher, 2000). However, the iron formations at Cerro Carreras are discordant with the sandstones. In turn, the iron formations are conformable with pink marbles, tourmaline-bearing quartzites and micaceous quartzites. All these lithologies belong to the metamorphic (amphibolite facies) basement (Las Tetras Complex of Hartmann et al., 2001). The same conclusion was reached by Campal and Schipilov (1998; their Fig. 13). Furthermore, the Cerro Espuelitas Formation does not contain iron formations (Pecoits et al., 2008; Pecoits, 2010).

This stratigraphic issue was acknowledged by Pecoits et al. (2008) who proposed a new stratigraphic scheme whereby the Cerros San Francisco Formation and the overlying Cerros Victoria Formation were removed from the Arroyo del Soldado Group (Pecoits et al., 2008; their Fig. 2). Therefore, the relationship between the sandstones of

the Cerros San Francisco Formation and the Arroyo Mangacha granite cannot be used to constrain the age of the Arroyo del Soldado Group (see also Aubet et al. 2013). In addition, the unconformity between the granite and the sandstones is not observed in the field, which is not surprising given the lack of zircons younger than ~2.19 Ga in these sandstones (Gaucher et al., 2008).

## 2) Puntas del Santa Lucía Pluton

The leucocratic granodiorite is pale pink, medium- to coarse-grained, and composed of quartz (40%), plagioclase (45%) and orthoclase (14%), with accessory biotite, opaque minerals and apatite (Bossi et al., 1998). This batholith forms part of the late- to post-tectonic Arroyo del Soldado Granitic Complex defined by Preciozzi et al. (1988), which includes a number of calc-alkaline granites and granodiorites (Figures 3.1 and 3.3). The intrusion exhibits cataclastic and microgranular textures (Bossi et al., 1998; Preciozzi et al., 1988). Extensive field work did not reveal any unit of the Arroyo del Soldado Group resting unconformably on the granodiorite (Aubet et al., 2013). Only sandstones of the Cerros San Francisco Formation, which belongs to the Arroyo de la Pedrera Group (as explained above), are in contact with the granodiorite. Moreover, this contact is tectonic, as previously reported by Gaucher et al. (1996) and Bossi et al. (1998). Despite both of these observations, Gaucher et al. (2004) suggested that this batholith is part of the basement of the Arroyo del Soldado Group, and thus it can be used to constrain the maximum depositional age of the group. The dated sample is a medium-grained and equigranular monzogranite, composed of quartz (35%), plagioclase (34%), microcline (20%), hornblende (6%), biotite (3%), and accessory opaque minerals, zircon and apatite, and yielded a zircon SHRIMP U-Pb emplacement age of  $633 \pm 8$  Ma (Hartmann et al., 2002). Detrital zircon analysis of the Yermal and Cerros San Francisco formations did not yield any zircon population younger than ca. 1000 Ma (see discussion on detrital zircons and diagenetic clays below). Therefore, the Puntas del Santa Lucía Pluton shows neither field nor geochronological evidence of being older than the Arroyo del Soldado Group.

### *Intrusives*

There are several granites intruding the Arroyo del Soldado Group (Preciozzi et al., 1988 and references therein), including (i) Minas, (ii) de los Guazunambí, (iii) Polanco, (iv) Yermal, and (v) Sobresaliente (Figures 3.1 and 3.3). Some of them have been dated but using different, including Rb-Sr, geochronological methods. The Guazunambí and Polanco granites yield Rb-Sr isochron ages of  $532\pm 11$  and  $548\pm 11$  Ma, respectively (Kawashita et al., 1999; Umpierre and Halpern, 1971). SHRIMP U-Pb zircon dating of the Sobresaliente granite yielded an age of  $585\pm 2$  Ma (Oyhantçabal et al., 2012), and thus constitutes the minimum age constraint for the Arroyo del Soldado Group (Figure 3.2). This minimum age is further supported by K-Ar ages of diagenetic illites from the uppermost Yermal Formation (see below).

### *Detrital zircons and diagenetic clays*

#### 1) Detrital Zircons

A total of six samples for detrital zircon analysis were analyzed by Gaucher et al. (2008) and Blanco et al. (2009) using laser ablation inductively coupled plasma mass spectrometry (LA-ICP-MS). Detrital age spectra from the Barriga Negra Formation (one sample, 34 detrital zircons) revealed four major peaks: (a) Mesoarchaeon ( $2890\text{-}3155$  Ma), (b) Paleoproterozoic ( $2157\text{-}2284$  Ma and  $1795\text{-}1723$  Ma), and (c) Neoproterozoic ( $631\text{-}566$  Ma) (Blanco et al., 2009). Thus, the youngest detrital zircon age ( $566\pm 8$  Ma) has been used to constrain the maximum depositional age for the Barriga Negra Formation.

The Piedras de Afilar Formation (one sample, 91 detrital zircon grains) showed a polymodal age distribution with mainly Mesoproterozoic and Paleoproterozoic ages. They are as follows; (a) a dominant Mesoproterozoic population with four distinct peaks at 1009, 1242, 1347 and 1487 Ma; (b) a Paleoproterozoic population with peaks at 2005-2068 Ma and 1779-1876 Ma, and (c) a single zircon with an Archean age of 2890 Ma (Gaucher et al., 2008). Accordingly, the maximum age of this formation is 1009 Ma.

Two samples were analyzed from the Yermal Formation. One sample (92 detrital zircon grains) yielded an essentially unimodal age mode centered at 2450 Ma, two grains have an age of 2044 Ma, and five grains were dated between 2895 and 2662 Ma (Gaucher

et al., 2008). The second sample (28 zircon grains) showed a predominance of Paleoproterozoic ages ranging from 1898 to 2220 Ma, but also has a significant Late Mesoproterozoic cluster (1009-1063 Ma). The oldest zircon population is of Mesoarchean age (3027 Ma), the youngest, and the only Neoproterozoic-aged zircon, is dated at 664 Ma (Blanco et al., 2009). The latter age is statistically insignificant and was not observed in any other sample from the Yermal Formation, and thus it should be viewed with caution.

Two samples were analyzed from the Cerros San Francisco Formation. One sample (86 detrital zircon grains) showed a polymodal distribution, with mainly Archean and Paleoproterozoic ages. Two prominent Archean peaks were recognized, one double peak at 2778-2715 Ma and a minor one between 3225 and 3045 Ma. The younger Paleoproterozoic cluster occurs at 2188 Ma (Gaucher et al., 2008). The other sample (39 detrital zircon grains) displayed a predominance of Paleoproterozoic sources in the age range of 1990-2122 Ma, along with zircon grains derived from Archean rocks. One single zircon showed a Neoproterozoic age (605 Ma) (Blanco et al., 2009). Similar to the sample from the Yermal Formation with a single Neoproterozoic zircon, this youngest zircon age from the Cerros San Francisco Formation should be treated with caution.

When age spectra for both samples of the Cerros San Francisco are compared, they show a similar range of ages between 1990 and 3551 Ma, and only slight differences in the size of the peaks are observed. Crucially, the sample that does not show the Neoproterozoic zircon was taken proximal to the  $583 \pm 7$  Ma-old Arroyo Mangacha granite. As mentioned above (see Arroyo Mangacha section), this observation further supports the fact that this Ediacaran granite is not the basement for the sandstones and as such, the sandstones must be older than the granite. This is not surprising when considering that extensive magmatism (granite intrusions and felsic volcanism) is recorded in the entire region between ca. 570 and 640 Ma (see Figures 2.1, 2.3 and 2.5) and is not represented as a detrital zircon population either in the sandstones of the Cerros San Francisco and Piedras de Afilar formations or in the Yermal Formation (Arroyo del Soldado Group). Conversely, the Barriga Negra Formation records this magmatism, particularly between 570-600 Ma, which confirms its younger age than that for other units. Therefore, we suggest the following maximum age constraints for these units:

Barriga Negra Formation: 566±8 Ma; Yermal Formation: 1009 Ma; Cerros San Francisco Formation: 1990 Ma; and Piedras de Afilar Formation: 1009 Ma (Figure 2.5).

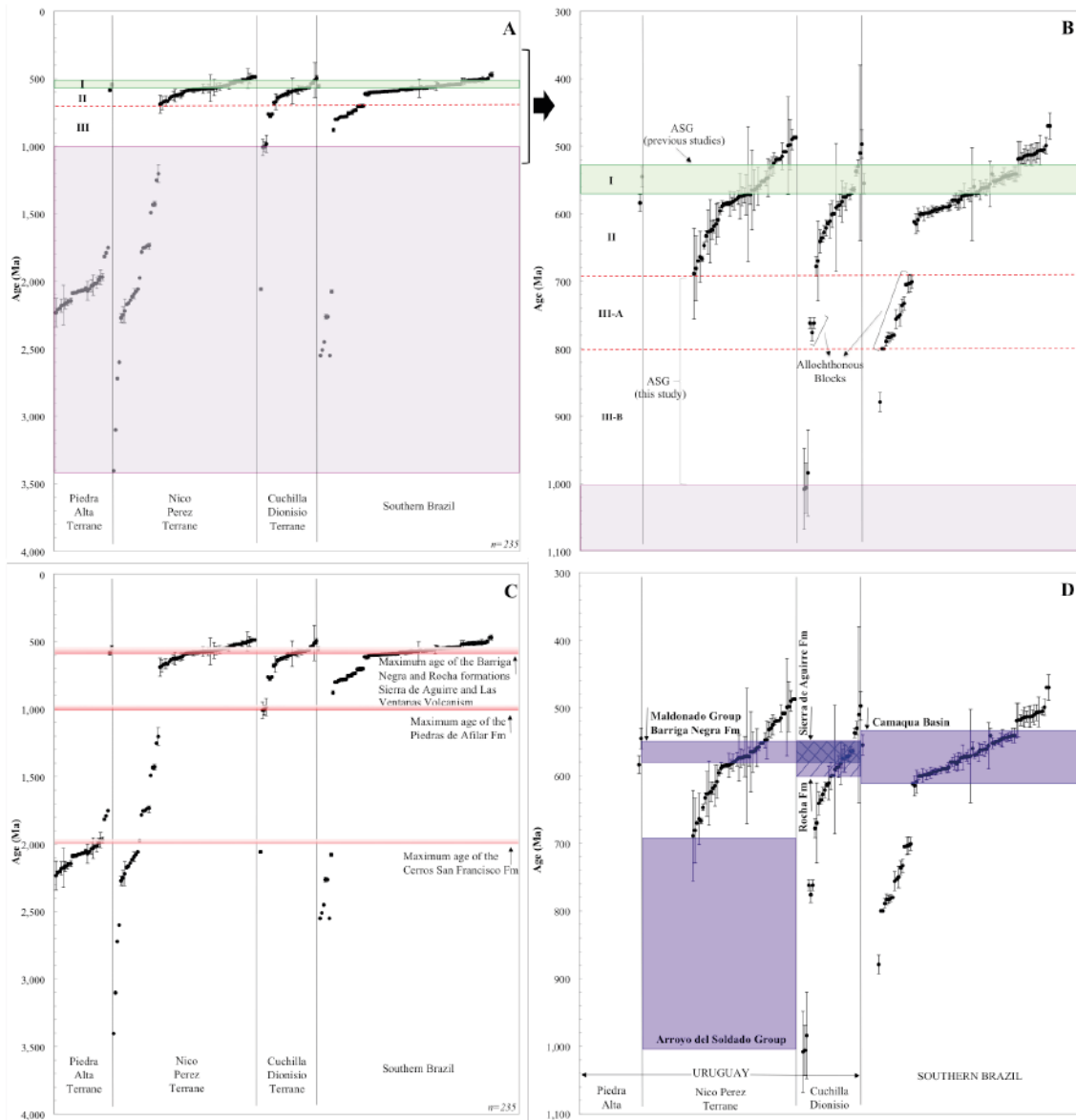


**Figure 2.5.** Compilation of radiometric ages and their error bars measured for intrusive and volcanic rocks from Uruguay and southernmost Brazil (n=sample size). The Uruguayan portion comprises three main units: Piedra Alta, Nico Pérez and Cuchilla Dionisio Terranes, while the Brazilian side comprises the Sul-Rio-Grandense Shield with its four main blocks: Taquarembó, São Gabriel, Santana da Boa Vista and Pelotas (see Figure 1). **(A-B)** There exist time periods during the evolution of these crustal blocks that are characterized by either intense magmatic activity or magmatic quiescence. Particularly important are the periods between approximately (1) 530 and 570 Ma, (2) 570 and 700 Ma, and (3) 700 and 1,000 Ma; identified in Figs. A and B with the symbols I, II and III, respectively. The first period (ca. 530-570 Ma) is defined by the deposition of the Arroyo del Soldado Group (ASG), as suggested by previous studies, but also by an important magmatic activity in all the tectonic blocks. The voluminous magmatism recorded within this interval (25% of the radiometric ages plotted) contradicts the idea of an Atlantic-type passive margin for the deposition of the unit. The second period (ca. 570-700 Ma) is also characterized by important magmatic activity. Although 27% of the data plotted correspond to this interval, no detrital zircons of this age are found within the Arroyo del Soldado Group. Therefore, it is very unlikely that the Arroyo del Soldado Group had been deposited during the Ediacaran, either during period I or II of Figures A and B (i.e., between 700 and 530 Ma). The third period (ca. 700-1,000 Ma) is characterized by magmatic quiescence in the Nico Pérez Terrane, where we propose the Arroyo del Soldado Group occurs. The beginning of this interval coincides with the youngest detrital zircon ages (i.e., maximum age) reported for the Arroyo del Soldado Group (1,000 Ma). The upper part of this period reflects: (i) the oldest Neoproterozoic magmatic ages recorded in the Nico Pérez Terrane (ca. 700 Ma; Period III-A of Fig. B), and (ii) the oldest magmatic Neoproterozoic ages recorded in the Cuchilla Dionisio “Terrane” and Southern Brazil (ca. 800 Ma; Period III-B of Fig. B). Therefore, the deposition of the Arroyo del Soldado Group took place sometime between 1,000 and 700 Ma. The absence of zircons sourced from the allochthonous blocks, with ages between 700 and 800 Ma, suggests that either these blocks were located far oceanward from the Arroyo del Soldado Basin or that the group is even older; i.e., deposited between ca. 800 and 1,000 Ma. **(C)** Maximum ages for the Cerros San Francisco and Piedras de Afilar formations (Arroyo de la Pedrera Group) and Barriga Negra Formation, which have been removed from the Arroyo del Soldado Group (see text for explanation). **(D)** Synthetic chronostratigraphic chart showing volcano-sedimentary Neoproterozoic units (shaded rectangles) from Uruguay and their correlatives in Southern Brazil. The Arroyo del Soldado Group, including the Yermal, Polanco Limestones and Cerro Espuelitas formations, was deposited between 1,000 and 700 Ma. The Maldonado Group *s.l.* (Playa Hermosa, Las Ventanas and San Carlos formations) was deposited between 590 and 550 Ma and overlaps with the Sierra de Aguirre Formation (590-550 Ma) and the Rocha Formation (ca. 600-550 Ma). The age of the Arroyo de la Pedrera Group cannot be firmly established, but the available data would suggest a similar age to the Arroyo del Soldado Group. Data sources: Borba and Mizusaki (2003), Oyhantçabal (2005), Saalman et al. (2011), Oyhantçabal et al. (2012), Janikian et al. (2012), and references therein.

## 2) Diagenetic clays

K-Ar ages of diagenetic illites from the uppermost Yerbal Formation were presented by Pecoits (2010) and Aubet et al. (2012), where the authors used the most conservative maximum age estimate for the Arroyo del Soldado Group as suggested by Gaucher et al. (2004); i.e.,  $633\pm 8$  Ma (Puntas del Santa Lucía pluton). Even in this case, the Ar diffusion calculations clearly indicate a minimum age of 600-580 Ma for the uppermost Yerbal Formation (see also Aubet et al., 2013).

### **2.3.1.2.b. Biostratigraphy**

Another age constraint is based on the purported presence of the index fossil *Cloudina* (Gaucher, 2000). The apparent discovery of *Cloudina* in the uppermost Yerbal Formation (Gaucher et al., 2000; 2003; 2004) deserves special attention because it is the only potential fossil that can provide precise stratigraphic constraint (for discussion see Pecoits et al., 2008; pp. 710). The wide geographic distribution and geochronologically calibrated stratigraphic occurrences, between  $549\pm 1$  and  $542\pm 1$  Ma, make *Cloudina* an excellent index fossil for the biostratigraphic subdivision of the Ediacaran System (Grotzinger et al., 1995; Saylor et al., 1998; Martin et al., 2000; Amthor et al., 2003; Knoll et al., 2004; Hua et al., 2005). Therefore, its occurrence would indicate a maximum age of 550 Ma for the overlying Polanco Limestones Formation. However, the occurrence of *Cloudina* in Uruguay poses some peculiarities (see for example Aubet et al., 2013). First, considering the radiometric data available (see below) the presence of *Cloudina* would be at least 40 Ma older than any *Cloudina* reported before (Hua et al., 2005) and its temporal span would be four times longer, which seems very unlikely for what is considered an index fossil of the late Ediacaran Period. Second, *Cloudina* was only reported unambiguously from one single small ( $5\text{ m}^2$ ) outcrop of the Yerbal Formation (Gaucher 2000; his Fig. 10) and repeated sampling of the *Cloudina*-hosting bed (4 cm thick) by other researchers never yielded any well-preserved and unambiguous *Cloudina* fossil (outcrop coordinates:  $32^{\circ}48'12''$  S,  $54^{\circ}26'16''$  W). Third, the same few specimens repeatedly illustrated by Gaucher (2000), Gaucher et al. (2003; 2004) and Gaucher and Poiré (2009) are poorly preserved, and even the original carbonate shell was apparently dissolved and replaced by iron-oxides or silica (Gaucher, 2000). This is an unusual mode of preservation for

*Cloudina*, which typically occurs in large population densities, and not as sparse individuals as reported above. Fourth, the stratigraphic range of *Cloudina* postdates the Shuram(-Wonoka-Johnnie)  $\delta^{13}\text{C}$  excursion worldwide (e.g., Hua et al., 2005; Verdel et al., 2011), and thus the occurrence of *Cloudina* in the upper Yermal Formation is inconsistent with an inferred Shuram excursion ( $> 551$  Ma) for the negative  $\delta^{13}\text{C}$  anomaly of Polanco Limestones Formation (cf. Gaucher et al., 2009). Therefore, in the absence of further confirmation for the presence of *Cloudina* in Uruguay, its ‘occurrence’ must be regarded as equivocal.

A further complication is that the acritarchs reported for the whole group have no stratigraphic significance. Some of them have been reported in strata ranging from Mesoproterozoic to Silurian and others were shown to be contaminants. As an example, one of the dominant species (*Leiosphaeridia*) reported in the Arroyo del Soldado Group is common even in Mesoproterozoic strata (Javaux et al., 2001; 2004). Other species (e.g., *Soldadophycus*) have only been described by the same authors (Gaucher et al., 2009). In fact, Gaucher et al. (1996) reported a list of more than 30 species of organic-walled microfossils, many of which the authors regarded as stratigraphically important. However, in Gaucher et al. (2000), 80% of these specimens turned out to be contaminants.

Finally, the occurrence of the *Thalassinoides* - *Gyrolithes* - *Palaeophycus* assemblage described by Sprechmann et al. (2004) has no stratigraphic implication for the Arroyo del Soldado Group because they occur in the Cerro Victoria Formation (Arroyo de la Pedrera Group). Based on these trace fossils the authors placed the Cerro Victoria Formation in the lowermost Cambrian (541 to 535 Ma). However, the illustrated structures resemble diagenetic concretions of inorganic origin (Pecoits et al., 2008).

### **2.3.1.3. C- and Sr-Chemostratigraphy**

As highlighted by Melezhik et al. (2001),  $\delta^{13}\text{C}_{\text{carb}}$  and  $^{87}\text{Sr}/^{86}\text{Sr}$  values cannot be used with confidence for ‘blind dating’ without independent geochronologic support. It is even more problematic when considering local  $\delta^{13}\text{C}_{\text{carb}}$  variations that may have nothing to do with global fluctuations. Both problems are applicable to the Polanco Limestones Formation and have added more inconsistencies with regard to the age of the entire

group. Although Gaucher (2000) assigned the entire Arroyo del Soldado Group to the Kotlin horizon (550-542 Ma) of the East European Platform (mainly based on the occurrence of *Cloudina* and the acritarch assemblage), a Valdai age (>570-542 Ma) was later suggested using C- and Sr-isotopic data (Gaucher et al., 2003). Subsequently, based on exactly the same Sr-isotopic data, Gaucher et al. (2004) assigned an age of 580 Ma for the base of the Polanco Limestones Formation. The latter two ages, however, are in clear contradiction with the presence of *Cloudina* in the underlying Yermal Formation (see above). This inconsistency was recognized by Pecoits et al. (2008) who highlighted that the mineralized metazoan *Cloudina* occurs between 550 and 540 Ma (Grotzinger et al., 1995; Saylor et al., 1998; Martin et al., 2000; Knoll et al., 2004; Hua et al., 2005). Hence, and following the report of *Cloudina* by Gaucher et al. (2000; 2003; 2004) in the uppermost Yermal Formation, Pecoits et al. (2008) proposed a maximum age of ca. 550 Ma for the overlying Polanco Limestones Formation.

Despite the 580 Ma age assigned by Gaucher et al. (2004) to the Polanco Limestones Formation, Gaucher et al. (2009) correlated the most negative C-isotope shift in this unit with those reported in Oman (Shuram Formation), Namibia (Nama Group), China (Doushantuo Formation), Australia (Wonoka Formation) and USA (Johnnie Formation) at ~551 Ma (Condon et al., 2005, and references therein). Although no glacial conditions have been associated with the Shuram-Wonoka-Johnnie anomaly elsewhere (Cozzi et al., 2004; Le Guerroué, 2010; Swanson-Hysell et al., 2010), a glacially-related interpretation of the  $\delta^{13}\text{C}$  drop in the Polanco Limestones Formation was suggested by Gaucher et al. (2009). Aubet et al. (2012; 2013) presented arguments negating a correlation with the Shuram-Wonoka-Johnnie and instead concluded that the negative excursion recorded in the Polanco Limestones Formation is facies-controlled and only occurs in shallow-water strata associated with storm events. It thus appears more likely to be a local rather than a basin-wide phenomenon. Furthermore, the Shuram anomaly can be clearly distinguished from other Neoproterozoic anomalies due to its amplitude ( $\delta^{13}\text{C}_{\text{carb}} < -10\text{‰}$ ) and duration as reflected by its persistence for several hundreds of meters (~700 m) in several sections worldwide (Le Guerroué et al., 2006; Halverson et al., 2010). The carbonates from the Polanco Limestones Formation, however, fall into the higher range (i.e.,  $> -5\text{‰}$ ), and unlike the rapid onset of the Wonoka anomaly, the

Polanco negative excursion at the Recalde section defines a rather gradual trend that persists for no more than 250 meters. Furthermore, a  $\delta^{13}\text{C}_{\text{carb}}$  excursion of the magnitude and duration of the Shuram-Wonoka anomaly, thought to span between 20 and 50 Ma (Le Guerroué, 2010), should be noticed in different portions of the shelf above the pycnocline. The new stable isotope data and radiometric ages presented by Aubet et al. (2012) do not support the age suggested by Pecoits et al. (2008) for the Polanco Limestones Formation either, which, as mentioned above, was mainly based on the report of the index fossil *Cloudina* by Gaucher et al. (2000; 2003; 2004). Aubet et al. (2012) inferred a depositional age of ca. 590 Ma for the lower Polanco Limestones Formation. However, this age is also problematic because it took into consideration a maximum age of  $633\pm 8$  Ma (Puntas del Santa Lucía pluton) for the Arroyo del Soldado Group, which is highly controversial as discussed above.

#### **2.3.1.4. Geological Setting**

The Arroyo del Soldado Group is thought to have been deposited on either a stable, Atlantic-type continental shelf (Gaucher, 2000; Gaucher et al., 2004) or in a foreland basin (Basei et al., 2000; Pecoits et al., 2004; Pecoits et al., 2008; Sánchez Bettucci et al., 2010; Aubet et al., 2012). This contradiction is mainly rooted in the upper Ediacaran-lowermost Cambrian age assigned to the succession (Gaucher et al., 2000; 2004). The stable Atlantic-type continental shelf setting is incompatible with the extensive evidence indicating an extensive tectono-magmatic activity during the Ediacaran in Uruguay and southern Brazil (see Pecoits et al., 2008 p. 711). Widespread magmatism, including volcanic and intrusive units, high-strain transcurrent faults, and very similar volcano-sedimentary successions deposited in strike-slip basins on both sides of the Sierra Ballena Shear Zone indicate an unstable tectonic setting (Figures 2.1, 2.3 and 2.5). Hence, many authors have proposed that during continental collision (along the Sierra Ballena Shear Zone), the original basin evolved into a foreland basin (Arroyo del Soldado and Arroyo de la Pedrera groups) (e.g., Pecoits and Oyhantçabal, 2004). At first glance, this scenario could satisfactorily explain some of the geochronological data and geological features observed in the region. However, supporting sedimentary evidence indicating a foreland setting for the Arroyo del Soldado Group has remained elusive.

In summary, there is extensive evidence arguing against a stable passive margin setting during the upper Ediacaran-lowermost Cambrian, but there is also no compelling sedimentological evidence supporting a foreland basin setting for this succession. Therefore, two scenarios are conceived here: (i) the age of the Arroyo del Soldado Group is substantially older than assumed, and (ii) convincing evidence for a foreland setting remains to be found. As discussed above, we propose that the first scenario might better explain all the available evidence, but new radiometric ages are needed to confirm this hypothesis.

### ***2.3.2. Maldonado Group***

#### **2.3.2.1. Lithostratigraphy**

The Maldonado Group includes the Playa Hermosa and Las Ventanas formations and consists of mafic and felsic volcanic rocks, pyroclastic rocks, diamictite, sandstone, conglomerate and pelite (Pecoits, 2003; Pecoits et al., 2004). Masquelin and Sánchez Bettucci (1993) suggested that both units were deposited in the same basin and that the Las Ventanas Formation was deposited later with the development of alluvial fans sourced from the Sierra de las Ánimas Complex, located to the west (Figure 2.3). Accordingly, it would be younger than the Playa Hermosa Formation (see also Midot, 1984). Nonetheless this relationship between the Playa Hermosa Formation and Las Ventanas Formation is often difficult to observe in the field due to poor outcrop between the type areas of both units. Furthermore, they show similar facies, which seem to be interlayered. Similarly, the relationship between these two units and the San Carlos Formation, which was informally included in the group, is not fully understood. Sedimentary facies of the San Carlos Formation are similar to those of the middle Las Ventanas Formation (Pecoits et al., 2008). In this regard, two possible explanations can be drawn. First, the San Carlos Formation is a lateral equivalent to the middle and upper parts of the Las Ventanas Formation, or both units, although broadly contemporaneous, were deposited in different basins.

#### 2.3.2.2. Age

Pecoits et al. (2004) suggested a depositional age of ca. 600 to 565 Ma for the group (see also Pecoits, 2002; 2003). This interpretation was supported by field relationships and the following geochronological data: (i) hypabyssal rocks of the Sierra de Las Ánimas Complex ( $520\pm 5$  Ma; Bossi et al., 1993) and the Pan de Azúcar Granite ( $559\pm 28$  Ma; Preciozzi et al., 1993) intrude the Las Ventanas Formation; (ii) the Puntas del Pan de Azúcar Lineament, which affects the Las Ventanas Formation, has a K-Ar age of  $572\pm 7$  Ma (Bossi and Campal, 1992); and (iii) Sánchez Bettucci and Linares (1996) reported radiometric ages of mafic rocks occurring at the base of the Las Ventanas Formation between  $615\pm 30$  and  $565\pm 30$  Ma (K-Ar). Despite the low quality and wide range of these data, the age suggested for the group is in agreement with new U-Pb SHRIMP ages from interbedded felsic volcanic rocks (see geochronology section below). The age of the San Carlos Formation is less well constrained. However, it is deformed by the Sierra Ballena Shear Zone whose last displacement is believed to have occurred at around 525 Ma (Bossi et al., 1993; Oyhantçabal, 2005).

Pazos et al. (2003) suggested that the Playa Hermosa Formation is a glacially-influenced succession that records the Varanger glaciation on the Río de la Plata Craton. The assignment of this unit to the Ediacaran is based on Masquelin and Sánchez Bettucci (1993), who recognized chilled margins at the contact between the sedimentary strata and trachytic dykes (see also Sánchez Bettucci et al., 2009). These hypabyssal rocks, which are part of the Sierra de las Ánimas Complex, have produced Rb-Sr and K-Ar ages between 615 and 500 Ma (Bossi et al., 1993; Sánchez Bettucci and Linares, 1996). Similarly, Pecoits (2003) and Gaucher et al. (2008) recognized probable glacial influence on the Las Ventanas Formation and also proposed a Varanger age (Pecoits et al., 2004). Based on the radiometric age constraints discussed above, a glacial event occurring sometime between ca. 590 and 570 Ma (Gaskiers) seems to be most reasonable (Pecoits et al., 2008; 2011).

### **2.3.2.2.a Geochronology**

#### *Basement and upper contact*

The group lies with an angular unconformity on metamorphic rocks of the Neoproterozoic Fuente del Puma Formation and Cerro Olivo Complex (ca. 770 Ma), the Mesoproterozoic Zanja del Tigre Formation (ca. 1.4 Ga) and granitoids of undetermined age (Figure 2.3). Although the Maldonado Group was thought to underlie the Arroyo del Soldado Group (Gaucher et al., 2008), the relationship and nature of the contact between the Maldonado Group and the Arroyo del Soldado Group is not firmly established. Reconnaissance work to the north of the Minas area, where both units are closely exposed but not in contact, suggests the presence of an angular unconformity between them. Here, the Maldonado Group is clearly less deformed than the Arroyo del Soldado Group, which suggests that the former is younger, further supporting other geochronological evidence.

#### 1) Metamorphic basement

Las Ventanas strata lay unconformably on the Neoproterozoic Fuente del Puma Formation and Mesoproterozoic Zanja del Tigre Formation (cf. Oyhantçabal et al., 2001). The San Carlos Formation overlies the metamorphic Cerro Olivo Complex (770-800 Ma) of Masquelin (2004) whose metamorphism, which was not recorded in the San Carlos Formation, occurred ca. 670-630 Ma (Oyhantçabal et al., 2009; Lenz et al., 2011; Masquelin et al., 2012; Figure 2.3).

#### 2) Granitoids

The Playa Hermosa and Las Ventanas formations unconformably overlie pink leucocratic granites of unknown age (Pecoits et al., 2008). In the case of Las Ventanas Formation, the granitic body (La Nativa Granite of Pecoits (2002; 2003)) is cross-cut by Cambrian syenitic and trachytic dykes of the Sierra de las Ánimas Complex (Figure 2.3). Similar to the granite underlying the Playa Hermosa Formation, this granite does not show strong ductile deformation, and thus both granites are most likely of Neoproterozoic age.

### *Intrusives*

Field relationships show that syenites and trachytes of the Sierra de las Ánimas Complex intrude the Las Ventanas Formation, thereby providing definite evidence of the older age of the Las Ventanas strata. Trachytes, syenites and granophyres dated by K-Ar and Rb-Sr methods yield ages between 487 and 552 Ma (Umpierre, 1966; Bossi et al., 1993). Mafic dykes cross-cutting the Las Ventanas Formation, immediately to the south of Minas City, yield a K-Ar age of  $485 \pm 13$  Ma (Poiré et al., 2005).

### *Volcanic rocks and faults*

At present, no detrital zircon or clay geochronology has been performed on the Maldonado Group or the San Carlos Formation. Mafic volcanics (El Ombú Basalt) interbedded with sedimentary rocks of the Las Ventanas Formation display ages between  $615 \pm 30$  and  $565 \pm 30$  Ma (K-Ar method; Sánchez Bettucci and Linares, 1996). Basal volcaniclastic rocks of the Las Ventanas Formation dated at  $573 \pm 11$  Ma (U-Pb SHRIMP on zircon; Oyhantçabal et al., 2009) constitute the best age constraint for the group.

The last reactivation of the Puntas del Pan de Azúcar Lineament affected the Las Ventanas Formation and took place at  $572 \pm 7$  Ma (K-Ar in syn-kinematic muscovites) (Bossi and Campal, 1992). The San Carlos Formation is intensely deformed by the Sierra Ballena Shear Zone, in which the third and final deformation phase occurred at ca. 550-500 Ma (Oyhantçabal, 2005).

#### ***2.3.2.2.b The Problem of the Volcanic Rocks and Metamorphism***

Volcanic and intrusive rocks of the Sierra de las Ánimas Complex have produced Rb-Sr and K-Ar ages between ca. 615 and 500 Ma (Umpierre, 1966; Bossi et al., 1993; Sánchez Bettucci and Linares, 1996; Oyhantçabal et al., 2007). This geochronologic data suggests the presence of at least two main magmatic pulses at approximately (i) 590-560 Ma and (ii) 550-500 Ma (cf. Sánchez Bettucci and Linares, 1996; Sánchez Bettucci et al., 2009). During the older pulse, volcanic rocks were generated and assigned to the lower Las Ventanas Formation (Pecoits, 2003; Pecoits et al., 2004) and upper Playa Hermosa Formation (Sánchez Bettucci et al., 2009). However, the rhyolitic tuffs that were assigned to the top of the Las Ventanas Formation by Blanco and Gaucher (2005) and Gaucher et

al. (2008) do not belong to the unit and are dykes cross-cutting the conglomerates. These rhyolites were dated by U-Pb (TIMS) method and yielded an age of  $65 \pm 1$  Ma (see Appendix 1; outcrop coordinates:  $34^{\circ}41'56''$  S,  $55^{\circ}13'22''$  W). Furthermore, the volcanic rocks originally described for the Las Ventanas Formation (Pecoits, 2003; Pecoits et al., 2004) are located in the base of the unit, not in top.

One crucial aspect that demands further research is the distinction between volcanic rocks assigned to the older pulse of the Sierra de las Ánimas Complex, which are intercalated with sedimentary strata of the Maldonado Group, and those traditionally assigned to the Neoproterozoic Fuente del Puma Formation (previously called the Lavalleja Group) in the type area of the Las Ventanas Formation. Although the structural and metamorphic characteristics of both units might provide some clues, it is difficult to observe such differences in the field, particularly in felsic volcanic units. To date, the stratigraphic relationship between the Fuente del Puma Formation and the Maldonado Group remains unclear.

Pecoits (2003) proposed that the Las Ventanas Formation was deformed and metamorphosed under low greenschist facies conditions (chlorite zone). This suggestion was based on the mineral paragenesis described for the basal mafic lavas: epidote + calcite + quartz + albite + muscovite + chlorite. In the same area, the mafic lavas belonging to the Fuente del Puma Formation show the following mineral paragenesis: chlorite + epidote  $\pm$  actinolite  $\pm$  calcite  $\pm$  plagioclase  $\pm$  quartz  $\pm$  sericite, which also corresponds to the greenschist facies conditions. Sánchez Bettucci et al. (2009) described similar mineral paragenesis for lavas occurring in the upper part of the Playa Hermosa Formation. However, the presence of palagonite in some basalts assigned to this unit argues against pervasive metamorphism because this mineral transforms into chlorite during the late stage of diagenesis or very low-grade metamorphism. When describing the petrography of the Las Flores basalt (Sierra de las Ánimas Complex), Oyhançabal et al. (2007) suggested that the abundance of chlorite and epidote, and the occurrence of pumpellyite and prehnite, indicate very low to low-grade metamorphism. No metamorphic minerals have yet been reported in the San Carlos Formation or in other occurrences of the Maldonado Group in the Minas area. Hence, it is still premature to conclude that a very low regional metamorphism affected the Maldonado Group because

if these rocks underwent localized deuteric or hydrothermal alteration, secondary chlorite, epidote, albite and prehnite could also be generated. In any case, the local metamorphic conditions reached by the Maldonado Group at some locations (e.g., Las Ventanas Formation at its type area) makes difficult its distinction from the Fuente del Puma Formation. Ongoing studies on detrital zircon geochronology on both units will help in determining, if any, the stratigraphic relationship between these two units.

#### **2.3.2.2.c Biostratigraphy**

The first organic-walled microfossils (*Bavlinella faveolata*) in the Las Ventanas Formation and San Carlos Formation were reported by Pecoits (2003) and Pecoits et al. (2004), respectively. Later, Blanco and Gaucher (2005) reported the presence of *Leiosphaeridia tenuissima*, *Leiosphaeridia minutissima*, *Lophosphaeridium sp.*, *Soldadophycus bossii*, *Soldadophycus major*, *Soldadophycus sp.*, *Vendotaenia sp.* No fossils have been yet reported for the Playa Hermosa Formation. The above listed microfossils, unfortunately, have little biostratigraphic value for the reasons discussed above.

#### **2.3.2.3. Geological Setting**

As discussed above (see geological setting for the Arroyo del Soldado Group), the Ediacaran of Uruguay is characterized by widespread magmatism and tectonic activity. In this regard, Masquelin and Sánchez Bettucci (1993) first suggested that Las Ventanas and Playa Hermosa formations were deposited in a pull-apart basin. Pecoits et al. (2008) also suggested an extensional basin (strike-slip and late-orogenic extensional collapse basins) for the Maldonado Group and the San Carlos Formation. Pazos et al. (2003) described the lower section of the Playa Hermosa Formation and recognized two distinct facies: (i) primarily medium to coarse-grained, and (ii) dominantly fine-grained units. The coarse-grained units consist of interbedded breccias, conglomerates, sandstones and minor mudstones that occur at the base and top of the succession; they were taken to represent depositional conditions with slope instability and high rates of sedimentation and were interpreted as being proximal to source. The fine-grained units are mainly composed of diamictites, rhythmites, sandstones and mudstones, which are interpreted to have been

deposited in a distal, glacially-influenced environment. Both facies accumulated in a sub-aqueous marine environment and represent a proximal to distal depositional trend. The Las Ventanas Formation was interpreted as a product of sheetflood-dominated fan deltas intercalated with minor marine deposits that were generated in a tectonically-active and glacially-influenced basin (Pecoits, 2002; 2003; Pecoits et al., 2004; 2008; 2011). Conglomerate-dominated lithofacies (proximal facies association) dominate the basal part of the Las Ventanas Formation, including clast-supported conglomerate and breccia, diamictite, massive sandstone and conglomerate-sandstone couplets. Upsection, pelites become more abundant with occasional conglomerate beds (pelite-dominated lithofacies or distal facies association). This lithofacies includes laminated siltstone and sandstone-pelite rhythmites, and massive sandstone and conglomerate. Therefore, Pecoits et al. (2008; 2011) concluded that the Las Ventanas and San Carlos formations were deposited in a strike-slip basin as indicated by the diverse depositional facies and their abrupt lateral changes. Furthermore, the Maldonado Group is extensively deformed, although variably, throughout the region. Strike-slip faults, westward-verging detachment faults, and folds with axis sub-parallel to the strike-slip planes are common features (Pecoits et al., 2011). This style of sedimentation, tectonics and associated magmatism is not exclusive of this unit and has been recorded all over the region (e.g., Sierra de Aguirre Formation), which confirms the active strike-slip tectonics and magmatism during that time as discussed above.

#### **2.4. Final Remarks**

Earlier stratigraphic models suggested an evolution from a rift basin (Maldonado Group) to a passive margin setting (Arroyo del Soldado Group) (e.g., Blanco and Gaucher, 2005; Gaucher et al., 2008). However, if we discard the controversial biostratigraphic data from the Arroyo del Soldado Group, and instead base our conclusions solely on radiometric age constraints, then the age of this group remains unknown but it was likely deposited between 700 and 1,000 Ma (Figure 2.5). Even if we take the age inferred in the models discussed above, the Arroyo del Soldado Group would be contemporaneous with the Maldonado Group and thereby subjected to intense syndepositional tectonism and magmatism; this is incompatible with passive-margin tectonics (see below). It also seems

difficult to explain the opening and development of a rift basin followed by the generation of an Atlantic-type passive margin and closure of the basin in just 50 Ma. For example, the Red Sea, whose rifting started in the late Oligocene (30 Ma), is still a semi-enclosed and embryonic ocean basin (oceanic spreading centers first appeared at ca. 5 Ma). At its widest point, the basin is 355 km, and shows metal-enriched sedimentation and other characteristics typical of rift-drift phases (Favre and Stampfli, 1992; Bosworth et al., 2005) that are not present in the Arroyo del Soldado Group. In this regard, no evidence exists to support substantially different basin-forming mechanisms, opening rates and sedimentary filling patterns in the Neoproterozoic. Accordingly, if we accept the principle of uniformitarianism, then the existence of a stable, Atlantic-type margin in the Ediacaran is, at the very least, highly questionable. Although there are alternative models for the development of the Arroyo del Soldado and Maldonado groups (e.g., Basei et al., 2000; Pecoits et al., 2008), no consensus currently exists in terms of their lithostratigraphy and geological setting.

The best age constraint obtained for the Las Ventanas Formation ( $573 \pm 11$  Ma; Oyhançabal et al., 2009) from volcanoclastic rocks supports the idea that an important extensional and synkinematic magmatism took place during the Ediacaran in Uruguay (see Pecoits et al., 2008 for discussion). This event, which ranges in age from ca. 560 to 600 Ma, is also represented by other regionally distributed volcanic and volcano-sedimentary successions (e.g., Sierra de Ríos and Sierra de Aguirre formations) and intrusive bodies (Nico Pérez mafic dyke swarm, synkinematic granites). Associated with this magmatism, tectonic activity constituted a primary controlling element on basin development and basin-fill architecture. The two largest, high-strain transcurrent structures present in Uruguay were reactivated during that time. Both, the Sierra Ballena and Sarandí del Yí shear zones (Figures 3.1 and 3.3) were reactivated between ca. 600 and 570 Ma. Collectively, these features suggest important tectono-magmatic activity during basin generation and deposition on both the Nico Pérez and Cuchilla Dionisio terranes. This evidence also does not support the existence of a stable, Atlantic-type continental margin during the Ediacaran-lowermost Cambrian, as proposed for the Arroyo del Soldado Group (Gaucher, 2000; Gaucher et al., 2004). Significantly, the purported glacial evidence from the Playa Hermosa and Las Ventanas formations

(Maldonado Group) and in the Tacuarí Formation suggest regional glacial conditions ca. 570-590 Ma. Hence, the Arroyo del Soldado Group is most likely older (pre-Ediacaran) than previously thought (Figure 3.5).

Finally, and although not exclusively applicable to the ‘Ediacaran’ units, a recurrent issue in the Precambrian stratigraphic nomenclature in Uruguay is the use and abuse of stratigraphic names. Naming, revising, ignoring and abandoning formal stratigraphic names with no apparent scientific reason (i.e., without following stratigraphic guides or simply without supporting evidence) has resulted in serious nomenclatural confusion. One such example is the use of different names for the same units by different authors. These recurring problems reveal the lack of a complete understanding of the stratigraphy, distribution, geological setting and age of the different units involved. In this regard, future research should be directed at outlining clear stratigraphic schemes supported by radiometric ages that fully satisfy the observation gathered in the field.

## **2.5. References**

- Amthor, J.E., Grotzinger, J.P., Schröder, S., Bowring, S.A., Ramezani, J., Martin, M.W. Matter, A., 2003. Extinction of Cloudina and Namacalathus at the Precambrian-Cambrian boundary in Oman. *Geol. Soc. Am. Bull.* 31, 431-434.
- Aubet, N., Pecoits, E., Bekker, A., Gingras, M.K., Zwingmann, H., Veroslavsky, G., de Santa Ana, H., Konhauser, K.O., 2012. Chemostratigraphic constraints on early Ediacaran carbonate ramp dynamics, Río de la Plata craton, Uruguay. *Gondw. Res.* 22, 1073-1090.
- Aubet, N., Pecoits, E., Bekker, A., Gingras, M.K., Zwingmann, H., Veroslavsky, G., de Santa Ana, H., Konhauser, K.O., 2013. Reply to Comment by C. Gaucher et al. on “Chemostratigraphic constraints on early Ediacaran carbonate ramp dynamics, Río de la Plata craton, Uruguay”. *Gondw. Res.* 23, 1186-1188.
- Basei, M., Siga, Jr.O., Masquelin, H., Harara, O., Reis Neto, J. and Preciozzi, F., 2000. The Dom Feliciano Belt of Brazil and Uruguay and its foreland domain, the Río de la

Plata Craton. In: Cordani, U., Milani, E., Thomaz F.A., Campos, D. (Eds.), Tectonic evolution of South America, pp. 311-334.

Basei, M.A.S., Frimmel, H.E., Nutman, A.P., Preciozzi, F., Jacob, J., 2005. The connection between the Neoproterozoic Dom Feliciano (Brazil/Uruguay) and Gariep (Namibia/South Africa) orogenic belts. *Prec. Res.* 139, 139-221.

Blanco, G., Gaucher, C., 2005. Estratigrafía, paleontología y edad de la Formación Las Ventanas (Neoproterozoico, Uruguay). *Lat. Am. J. Sedimentol. Basin Anal.* 12, 109-124

Blanco, G., Rajesh, H.M., Gaucher, C., Germs, G.J.B., Chemale Jr., F., 2009. Provenance of the Arroyo del Soldado Group (Ediacaran to Cambrian, Uruguay): Implications for the paleogeographic evolution of southwestern Gondwana. *Prec. Res.* 171, 57-73.

Borba, A.W., Mizusaki, A.M.P., 2003. Santa Bárbara Formation (Caçapava do Sul, southern Brazil): depositional sequences and evolution of an Early Paleozoic post-collisional basin. *J. South Am. Earth Sci.* 16, 365-380.

Bossi, J., 1966. Geología del Uruguay. Departamento de Publicaciones de la Universidad de la República, Montevideo.

Bossi, J., Campal, N., 1992. Magmatismo y tectónica transcurrente durante el Paleozoico Inferior en Uruguay. In: Gutiérrez-Marco, J.G., Saavedra, J., Rabano, I. (Eds.), Paleozoico Inferior de Iberoamérica. Universidad de Extremadura, Mérida, pp. 343-356.

Bossi, J., Cingolani, C., Llambías, E., Varela, R., Campal, N., 1993. Características del magmatismo post-orogénico finibrasiliano en el Uruguay: formaciones Sierra de Ríos y Sierra de Ánimas. *Rev. Brasil. Geocien.* 23, 282-288.

Bossi, J., Ferrando, L., Montaña, J., Campal, N., Morales, H., Gancio, F., Schipilov, A., Piñeyro, D., Sprechmann, P., 1998. Carta Geológica del Uruguay. Escala 1:500.000. Versión digital. Geoeditores, Montevideo.

Bosworth, W., Huchon, P., McClay, K., 2005. The Red Sea and Gulf of Aden Basins. *J. Afr. Earth Sci.* 43, 334-378.

Bowring, S., Myrow, P., Landing, E., Ramezani, J., Grotzinger, J., 2003. Geochronological constraints on terminal Neoproterozoic events and the rise of metazoans. *Geophys. Res. Abstracts* 5, 219.

Campal, N., Schipilov, A., 2005. La Formación Cerros de Aguirre: evidencias de magmatismo Vendiano en el Uruguay. *Lat. Amer. J. Sedimentol. Basin Anal.* 12, 161-174.

Campal, N., Schipilov, A., (1998) Evolución paleogeográfica del nudo tectónico de puntas del Arroyo Mansavillagra durante el proceso de formación del Supercontinente Gondwana (1500 a 500 Ma). Volumen 2, Ciclo Grenvilliano. Fac. de Agronomía-CONICYT, Montevideo.

Condon, D., Zhu, M., Bowring, S., Wang, W., 2005. U-Pb ages from the Neoproterozoic Doushantuo Formation, China. *Science* 308, 95-98.

Cozzi, A., Allen, P.A., Grotzinger, J.P., 2004. Understanding carbonate ramp dynamics using  $\delta^{13}C$  profiles: examples from the Neoproterozoic Buah Formation of Oman. *Terra Nova* 16, 62-67.

Elizalde, G., 1979. Carta Geológica de la Costa. Conservación y Mejora de Playas. Ministerio de Transporte y Obras Públicas, Programa de las Naciones Unidas para el Desarrollo – UNESCO, Montevideo. pp. 101-235.

Fambrini, G.L., Fragoso-Cesar, A.R.S., Almeida, R.P., Riccomini, C., 2005. A Formação Barriga Negra (Ediacarano do Uruguai): caracterização estratigráfica e correlação com unidades do Estado do Rio Grande do Sul, Brasil. *Rev. Brasil. Geoc.* 35, 515-524.

Fantin, M., 2003. Geología de la Sierra de Aguirre, Departamento de Rocha, Uruguay. Trabajo Final de la Licenciatura, Universidad de Buenos Aires, 92 pp.

Favre, P., Stampfli, G.M., 1992. From rifting to passive margin: the examples of the Red Sea, Central Atlantic and Alpine Tethys. *Tectonophysics* 215, 69-97.

Fragoso-Cesar, A.R.S., Machado, R.Y., Gómez Rifas, C., 1987. Observações sobre o Cinturão Dom Feliciano no Escudo Uruguaio e correlações com o Escudo do Rio Grande do Sul. In: III Symposium Sul-Brasileiro de Geologia, Curitiba, Brasil, Vol. 2, pp. 791-809.

Frei, R., Gaucher, C., Døssing, L.N., Sial, A.N., 2011. Chromium isotopes in carbonates - a tracer for climate change and for reconstructing the redox state of ancient seawater.

EPSL 312, 114-125.

Frei, R., Gaucher, C., Stolper, D., Canfield, D.E., 2013. Fluctuations in late Neoproterozoic atmospheric oxidation - Cr isotope chemostratigraphy and iron speciation of the late Ediacaran lower Arroyo del Soldado Group (Uruguay). *Gondw. Res.* 23, 797-811.

Gaucher, C., Sprechmann, P., Schipilov, A., 1996. Upper and Middle Proterozoic fossiliferous sedimentary sequences of the Nico Pérez Terrane of Uruguay: Lithostratigraphic units, paleontology, depositional environments and correlations. *N. Jb. Geol. Paläontol. Abh.* 199, 339-367.

Gaucher, C., Sprechmann, P., Montaña, J., 1998. New advances in the geology and paleontology of the Vendian to Cambrian Arroyo del soldado Group of the Nico Perez Tarrane of Uruguay. *N. Jb. Geol. Paläont. Mh.* 2, 106-118.

Gaucher, C., 2000. Sedimentology, paleontology and stratigraphy of the Arroyo del Soldado Group (Vendian to Cambrian, Uruguay). *Beringeria* 26, 1-120.

Gaucher, C., Boggiani, P., Sprechmann, P., Sial, A.N., Fairchild, T., 2003. Integrated correlation of the Vendian to Cambrian Arroyo del Soldado and Corumbá Groups (Uruguay and Brazil): paleogeographic, paleoclimatic and paleobiologic implications. *Prec. Res.* 120, 241-278.

Gaucher, C., Sial, A.N., Blanco, G., Sprechmann, P., 2004. Chemostratigraphy of the lower Arroyo del Soldado Group (Vendian, Uruguay) and paleoclimatic implications. *Gondw. Res.* 7, 715-730.

Gaucher, C., Blanco, G., Chigolino, L., Poiré, D., Germs, G.J.B., 2008. Acritarchs of the Las Ventanas Formation (Ediacaran, Uruguay): Implications for the timing of coeval rifting and glacial events in western Gondwana. *Gondw. Res.* 13, 488-501.

Gaucher, C., Sial, A.N., Poiré, D., Gómez-Peral, L., Ferreira, V.P., Pimentel, M.M., 2009. Chemostratigraphy. In: Gaucher, C., Sial, A.N., Halverson, G.P. and Frimmel, H.E.

(Eds.), Neoproterozoic-Cambrian tectonics, global change and evolution: a focus on southwestern Gondwana. *Develop. Prec. Geol.* 16, 115-122.

Gaucher, C., Poiré, D., 2009. Biostratigraphy. Neoproterozoic-Cambrian evolution of the Río de la Plata Palaeocontinent. In: Gaucher, C., Sial, A.N., Halverson, G.P., Frimmel, H.E. (Eds.), Neoproterozoic-Cambrian tectonics, global change and evolution: a focus on southwestern Gondwana. *Develop. Prec. Geol.* 16, 103-114.

Gaucher, C., Poiré, D.G., Bossi, J., Bettucci S.L., Beri, A. 2013. Comment on "Bilaterian Burrows and Grazing Behavior at >585 Million Years Ago". *Science* 339, 906.

Geyer, G. 2005. The Fish River Subgroup in Namibia: stratigraphy, depositional environments and the Proterozoic-Cambrian boundary problem revisited. *Geol. Mag.*, 142, 465-498.

Goñi, J.C., Hoffstetter, R., 1964. Uruguay. In: Hoffstetter, R. (Ed.) *Lexique stratigraphique international*. Centre National de la Recherche Scientifique, Paris, France, Fascicule 9a, pp. 1-202.

Grey, K., Calver, C.R., 2007. Correlating the Ediacaran of Australia. *Geol. Soc. London, Spec. Pub.* 286, 115-135.

Grotzinger, J.P., Bowring, S.A., Saylor, B.Z., Kaufman, A.J., 1995. Biostratigraphic and geochronologic constraints on early animal evolution. *Science* 270, 598-604.

Halverson, G.P., Hurtgen, M.T., Porter, S.M., Collins, A.C., 2010. Neoproterozoic-Cambrian biogeochemical evolution. In: Gaucher, C., Sial, A.N., Halverson, G.P. and Frimmel, H.E. (Eds.), Neoproterozoic-Cambrian tectonics, global change and evolution: a focus on southwestern Gondwana. *Develop. Prec. Geol.* 16, 351-356.

Hartmann, L.A., Santos, J.O., Bossi, J., Campal, N., Schipilov, A., Mac Naughton, N. J., 2002. Zircon and titanite U-Pb SHRIMP geochronology of Neoproterozoic felsic magmatism on the eastern border of the Río de la Plata Craton, Uruguay. *J. South Am. Earth Sci.* 15, 229-236.

Hartmann, L.A., Campal, N., Santos, J.O.S., McNaughton, N.J., Bossi, J., Schipilov, A., Lafon, J.-M., 2001. Archean crust in the Rio de la Plata Craton, Uruguay-SHRIMP U-Pb zircon reconnaissance geochronology. *J. South Am. Earth Sci.* 14, 557-570.

Hasui Y., Cameiro C. dal R., Coimbra A.M., 1975. The Ribera Folded Belt. *Rev. Bras. Geoc.* 5, 257-266.

Hua, H., Chen, Z., Yuan, X., Zhang, L., Xiao, S., 2005. Skeletogenesis and asexual reproduction in the earliest biomineralizing animal Cloudina. *Geol. Soc. Am. Bull.* 33, 277-280.

Janikian, L., Almeida, R.P., Fragoso-Cesar, A.R.S., Souza Martins, V.T., Dantas, E.L., Tohver, E., McReath, I., D'Agrella-Filho, M.S., 2012. Ages (U–Pb SHRIMP and LA ICPMS) and stratigraphic evolution of the Neoproterozoic volcano-sedimentary successions from the extensional Camaquã Basin, Southern Brazil. *Gondw. Res.* 21, 466-482.

Javaux, E.J., Knoll, A.H., Walter, M.R., 2001. Morphological and ecological complexity in early eukaryotic ecosystems. *Nature* 412, 66-69.

Javaux, E.J., Knoll, A.H., Walter, M.R., 2004. TEM evidence for eukaryotic diversity in mid-Proterozoic oceans. *Geobiology* 2, 121-132.

Jiang, G., Shi, X., Zhang, S., Wang, Y., Xiao, S. 2011. Stratigraphy and paleogeography of the Ediacaran Doushantuo Formation (ca. 635-551 Ma) in South China. *Gondw. Res.* 19, 831-849.

Johnston, D.T., Poulton, S.W., Goldberg, T., Sergeev, V.N., Podkovyrov, V., Vorob'eva, N.G., Bekker, A., Knoll, A.H., 2012. Late Ediacaran redox stability and metazoan evolution. *EPSL* 335-336, 25-35.

Kawashita, K., Gaucher, C., Sprechmann, P., Teixeira, W., Victória, R., 1999. Preliminary chemostratigraphic insights on carbonate rocks from Nico Pérez Terrane (Uruguay), In: *Actas II South American Symposium on Isotope Geology*, Córdoba, Argentina, pp. 399-402.

Knoll, A.H. Walter, M.R., Narbonne, G.M., Christie-Blick, N., 2004. A new Period for the geologic time scale. *Science* 3005, 621-622.

Knoll, A.H., Walter, M.R., Narbonne, M.G., Christie-Blick, N., 2006. The Ediacaran Period: a new addition to the geologic time scale. *Lethaia* 39, 13-30.

- Le Guerroué, E., 2010. Duration and synchronicity of the largest negative carbon isotope excursion on Earth: The Shuram/Wonoka anomaly. *Comptes Rendus Geosc.* 342, 204-214.
- Lenz, C., Fernandes, L.A.D., McNaughton, N.J., Porcher, C.C., and Masquelin, H., 2011. Magmatic and metamorphic U-Pb SHRIMP ages in zircons for the Cerro Bori Orthogneisses, Dom Feliciano Belt in Uruguay: *Prec. Res.* 185, 149-163.
- Martin, M.W., Grazhdankin, D.V., Bowring, S.A., Evans, D.A.D., Fedonkin, M.A., Kirschvink, J.L., 2000. Age of Neoproterozoic bilaterian body and trace fossils, White Sea, Russia: Implications for metazoan evolution. *Science* 288, 841-845.
- Masquelin and Tabó (1988). Carta Geologica del Uruguay, Escala 1/100.000, Hoja Carape, E-26. DINAMIGE-UdelaR, Montevideo, pp. 11.
- Masquelin, H., Pías, J., 1989. Carta geológica de las Hojas San Carlos - Punta del Este, escala 1:100.000. DINAMIGE, Montevideo.
- Masquelin, H., 1990. Análisis estructural de las zonas de cizalla en las migmatitas de Punta del Este-Uruguay. *Acta Geol. Leopold.* 30, 139-158.
- Masquelin, H., Sánchez, L., 1993. Propuesta de evolución tectono-sedimentaria para la fosa tardi-brasiliana en la región de Piriápolis, Uruguay. *Rev. Brasil. Geocienc.* 23, 313-322.
- Masquelin, H., 2004. El Complejo Cerro Olivo, Sureste de Uruguay: una revisión estratigráfica y tectónica. In: IV Congreso Uruguayo de Geología Actas CD-ROM version. Montevideo, Uruguay.
- Masquelin, H., Fernandes, L.A.D., Lenz, C., Porcher, C.C., and McNaughton, N.J., 2011. The Cerro Olivo Complex: a pre-collisional Neoproterozoic magmatic arc in Eastern Uruguay. *Int. Geol. Rev.* 54, 1161-1183.
- McCall, G.J.H., 2006. The Vendian (Ediacaran) in the geological record: Enigmas in geology's prelude to the Cambrian explosion. *Earth Sci. Rev.* 77, 1-229.

- Melezhik, V.A., Gorokhov, I.M., Kuznetsov, A.B., Fallick, A.E., 2001. Chemostratigraphy of Neoproterozoic carbonates: implications for 'blind dating'. *Terra Nova* 13, 1-11.
- Midot, D., 1984. Etude geologique et diagnostic metallogénique pour l'exploration du secteur de Minas (Uruguay). Diplome de Docteur de 3e Cycle. Université Pierre et Marie Curie, Paris.
- Montaña, J., Sprechmann, P., 1993. Calizas estromatolíticas y oolíticas y definición de la Formación Arroyo de la Pedrera (?Vendiano, Uruguay). *Rev. Brasil. Geocienc.* 23, 306-312.
- Narbonne, G.M., 2005. The Ediacara biota: Neoproterozoic origin of animals and their ecosystems. *Annu. Rev. Earth Planet. Sci.* 33, 421-42.
- Narbonne, G.M., S. Xiao, J.G. Gehling, Shields-Zhou, G.A., 2012. The Ediacaran Period. In: F. M. Gradstein, J. G. Ogg, M. Schmitz, and G. Ogg (Eds.), *Geological Time Scale 2012*. Cambridge University Press, Cambridge, pp. 413-435.
- O'Brien, S.J., King, A.F., 2005. Late Neoproterozoic (Ediacaran) stratigraphy of Avalon Zone sedimentary rocks, Bonavista Peninsula, Newfoundland. Newfoundland and Labrador Department of Natural Resources, Geological Survey, Report 05-1, pp. 101-113.
- Oyhantçabal, P., 2005. The Sierra Ballena Shear zone: kinematics, timing and its significance for the geotectonic evolution of southeast Uruguay. *Georg-August Universität zu Göttingen, Göttingen*, pp. 139.
- Oyhantçabal, P. Heimann, A., Miranda, S., 2001. An evaluation of strain in the syntectonic Solís de Mataojo Granitic Complex, Uruguay. *J. Struct. Geol.* 23, 807-817.
- Oyhantçabal, P., Siegesmund, S., Wemmer, K., Frei, R., Layer, P., 2007. Post-collisional transition from calc-alkaline to alkaline magmatism during transcurrent deformation in the southernmost Dom Feliciano Belt (Braziliano-Pan-African, Uruguay). *Lithos* 98, 141-159.

Oyhantçabal, P., Siegesmund, S., Wemmer, K., Presnyakov, S., Layer, P., 2009. Geochronological constraints on the evolution of the southern Dom Feliciano Belt (Uruguay). *J. Geol. Soc.* 166, 1075-1084.

Oyhantçabal, P., Wagner-Eimer, M., Wemmer, K., Schulz, B., Frei, R., Siegesmund, S., 2012. Paleo- and Neoproterozoic magmatic and tectonometamorphic evolution of the Isla Cristalina de Rivera (Nico Pérez Terrane, Uruguay). *Int. J. Earth Sci. (Geol. Rundsch.)*, DOI 10.1007/s00531-012-0757-4.

Pazos, P., Tófaló, R., Sánchez Bettucci, L., 2003. The record of the Varanger Glaciation at the Río de la Plata Craton, Vendian-Cambrian of Uruguay. *Gondw. Res.* 6, 65-77.

Pazos, P., Sánchez Bettucci, L., Loureiro, J. 2008. The Neoproterozoic glacial record in the Río de la Plata Craton: a critical reappraisal. *Geol. Soc. London, Spec. Pub.*, 294, 343-364.

Pecoits, E., 2002. Análisis faciológico y aspectos geológicos de la Formación Las Ventanas; un nuevo enfoque. In: Pecoits, E. and Masquelin, H. (Eds.), *II Taller Sobre la Estratigrafía del Precámbrico del Uruguay*. pp. 34-36. Facultad de Ciencias, Montevideo, Uruguay.

Pecoits, E., 2003a. Sedimentología y consideraciones estratigráficas de la Formación Las Ventanas en su área tipo, departamento de Maldonado, Uruguay. In: Pecoits, E. (Ed.), *Estratigrafía del Precámbrico del Uruguay*. *Rev. Soc. Uruguay. Geol. Spec. Publ.* 1, 124-140.

Pecoits, E., 2003b. Age and preliminary correlation of the Las Ventanas Formation and Bom Jardim-Cerro do Bugio allogroups (Vendian, Uruguay and Brazil). In: Frimmel, H.E (Ed.), *III International Colloquium Vendian-Cambrian of W-Gondwana, Programme and Extended Abstracts*, pp. 32-34. Cape Town, South Africa.

Pecoits, E., 2010. Ediacaran iron formations and carbonates of Uruguay: palaeoceanographic, palaeoclimatic and palaeobiologic implications. Ph.D. thesis, University of Alberta.

- Pecoits, E., Aubet, N., Oyhantçabal, P., Sánchez Bettucci, L., 2004. Estratigrafía de sucesiones sedimentarias y volcanosedimentarias Neoproterozoicas del Uruguay. *Rev. Soc. Uruguay. Geol.* 11, 18-27.
- Pecoits, E., Oyhantçabal, P., 2004. Geotectonic evolution of Uruguay during the Neoproterozoic-Cambrian. In: I Symposium on Neoproterozoic-Early Paleozoic events in SW-Gondwana. Extended Abstracts, IGCP Project 478, pp. 43-45, Brazil.
- Pecoits, E., Gingras, M., Aubet, N., Konhauser, K., 2008. Ediacaran in Uruguay: palaeoclimatic and palaeobiological implications. *Sedimentology* 55, 689-719.
- Pecoits, E., Gingras, M.K., Konhauser, K.O., 2011. Las Ventanas and San Carlos formations, Maldonado Group, Uruguay. *Geological Society, London, Memoirs* 36, 555-564.
- Pecoits, E., Konhauser, K.O., Aubet, N.R., Heaman, L.M., Veroslavsky, G., Stern, R.A., Gingras, M.K., 2012. Bilaterian Burrows and Grazing Behavior at >585 Million Years Ago. *Science* 336, 1693-1696.
- Pecoits, E., Konhauser, K.O., Aubet, N.R., Heaman, L.M., Veroslavsky, G., Stern, R.A., Gingras, M.K., 2012. Response to Comment on "Bilaterian Burrows and Grazing Behavior at >585 Million Years Ago". *Science* 339, 906.
- Poiré, D.G., González, P.D., Canalicchio, J. M., Repetto, F.G., Canessa, N.D., 2005. Estratigrafía del Grupo Mina Verdún, Proterozoico de Minas, Uruguay. *Latin Am. J. Sediment. Basin Anal.* 12, 125-143.
- Preciozzi, F., 1988. Carta geológica del Uruguay, Hoja F-23 Pirarajá, Escala 1:100.000. Memoria explicativa. DINAMIGE-UdelaR, Montevideo, pp. 15.
- Preciozzi, F., Spoturno, J., Heinzen, W., Rossi, P., 1988. Carta Geológica del Uruguay a escala 1:500.000. Memoria explicativa. DINAMIGE, Montevideo, pp. 90.
- Preciozzi, F., Pena, S., Masquelin, E., Pías, J., Tabó, F., 1989. Memoria explicativa del fotoplano Piriápolis. DINAMIGE-UdelaR, Montevideo, pp. 11.

Preciozzi, F., Masquelin, H., Sánchez Bettucci, L., 1993. Geología de la Porción Sur del Cinturón Cuchilla de Dionisio. In: I Simp. Int. Neoproterozoico - Cámbrico de la Cuenca del Plata), Guía de Excursiones, La Paloma, pp. 1-39.

Sánchez, L., Linares, E., 1996. Primeras edades en basaltos del Complejo Sierra de las Ánimas, Uruguay. In: XIII Congreso Geológico Argentino y III Congreso de Exploración de Hidrocarburos, Actas I pp. 399-404. La Plata.

Sánchez, L., Koukharsky, M., Pazos, P.J., Stareczek, S., 2009. Neoproterozoic subaqueous extrusive-intrusive rocks in the Playa Hermosa Formation in Uruguay: Regional and stratigraphic significance. *Gondw. Res.* 16, 134-144.

Sánchez, L., Masquelin, E., Peel, E., Oyhantçabal, P., Muzio, R., Ledesma, J.J., Preciozzi, F., 2010. Comment on “Provenance of the Arroyo del Soldado Group (Ediacaran to Cambrian, Uruguay): implications for the palaeogeographic evolution of southwestern Gondwana”. *Prec. Res.* 180, 328-333.

Saalmann, K., Gerdes, A., Lahaye, Y., Hartmann, L.A., Remus, M.V.D., Läufer, A., 2011. Multiple accretion at the eastern margin of the Río de la Plata craton: the prolonged Brasiliano orogeny in southernmost Brazil. *Int. J. Earth Sci. (Geol. Rundsch)* 100, 355-378.

Saylor, B.Z., Kaufman, A.J., Grotzinger, J.P., Urban, F., 1998. A composite reference section for terminal Proterozoic strata of southern Namibia. *J. Sed. Res.* 68, 1223-1235.

Sprechmann, P., Gaucher, C., Blanco, G., Montaña, J., 2004. Stromatolitic and trace fossils community of the Cerro Victoria Formation, Arroyo del Soldado Group (Lowermost Cambrian, Uruguay). *Gondw. Res.* 7, 753-766.

Swanson-Hysell, N.L., Rose, C.V., Calmet, C.C., Halverson, G.P., Hurtgen, M.T., Maloof, A.C., 2010. Cryogenian glaciation and the onset of carbon-isotope decoupling. *Science* 328, 608-611.

Umpierre, M., 1966. Edades de las lavas Mezoicas del Uruguay. In: Bossi, J., Geología del Uruguay. Departamento de Publicaciones de la Universidad de la República. Montevideo. Uruguay.

Umpierre, M., Halpern, M., 1971. Edades Sr-Rb del Sur de la República Oriental del Uruguay. *Rev. Asoc. Geol. Arg.* 26, 133-155.

Verdel, Ch., Wernicke, B.P., Bowring, S.A., 2011. The Shuram and subsequent Ediacaran carbon isotope excursions from southwest Laurentia, and implications for environmental stability during the metazoan radiation *GSA Bulletin* 123, 1539-1559.

Veroslavsky, G., de Santa Ana, H., Daners, G., 2006. Tacuarí Formation (Nov. Nom.): Lithostratigraphy, facies, environment, age and geological significance (Cerro Largo-Uruguay). *Rev. Soc. Uru. Geol.* 13, 23-35.

Zimmermann, U., 2011. Comment on “Provenance of the Arroyo del Soldado Group (Ediacaran to Cambrian, Uruguay): Implications for the palaeogeographic evolution of southwestern Gondwana”. *Prec. Res.* 186, 233-236.

## CHAPTER 3: U-PB DETRITAL ZIRCON AGES FROM SOME NEOPROTEROZOIC SUCCESSIONS OF URUGUAY: PROVENANCE, STRATIGRAPHY AND TECTONIC EVOLUTION

### 3.1. Introduction

The analysis of the U-Pb age spectra on detrital zircons is a useful tool for determining the provenance, maximum depositional age and stratigraphic correlations of clastic sedimentary successions. This is particularly the case in the Precambrian rock record where biostratigraphical markers are lacking and whose original stratigraphic relationships have been obliterated by deformation and metamorphism. Despite the alleged importance of the Neoproterozoic successions of Uruguay, which have been suggested to record global climatic, biogeochemical and biotic events, a recent review by Aubet et al. (2014) concluded that the stratigraphy and age of these units remain ambiguous. Consequently, existing basin models and their tectonic evolution remain poorly resolved.

With the exception of the easternmost Cuchilla Dionisio Terrane (Figure 3.1.), the early Neoproterozoic (1,000-700 Ma) rock record of Uruguay is characterized by the absence of evidence indicating significant tectono-magmatic activity (Aubet et al., 2014). In contrast, part of the late Neoproterozoic (560-650 Ma) record is punctuated by extensive magmatism accompanied by major changes in the regional tectonic regime (Oyhantçabal et al., 2007), i.e., accretion and transport of allochthonous terranes, the so-called Brasiliano/Pan-African Orogeny. This differential tectono-magmatic activity was expressed by the deposition of volcano-sedimentary successions showing a distinct stratigraphic architecture. The early Neoproterozoic record, represented by the Arroyo del Soldado Group, comprises epicontinental sea deposits that covered the passive margin of the Nico Pérez Terrane, while late Neoproterozoic successions, which includes the Playa Hermosa, Las Ventanas, San Carlos, Barriga Negra, Fuente del Puma, Sierra de Aguirre, Tacuarí and Rocha formations, points to an active tectono-magmatic settings for their deposition in both, the Nico Pérez and the Cuchilla Dionisio terranes (Figure 3.1). However, for most of these units the depositional age is still controversial due to the lack

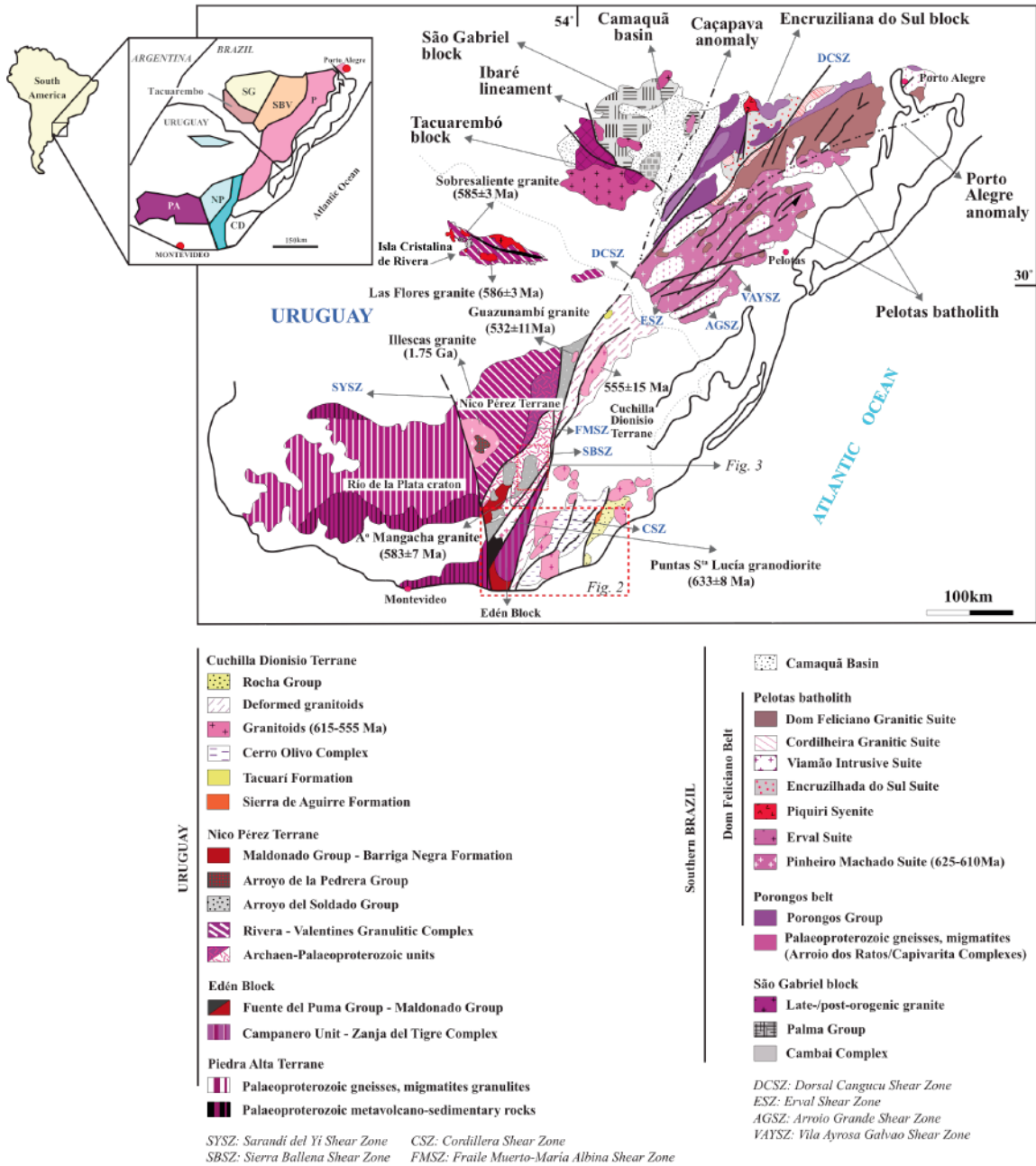


**Figure 3.1.** Simplified geologic map of Uruguay and southern Brazil (modified from Saalman et al., 2011 and references therein). Inset: PA-Piedra Alta, NP-Nico Pérez, and CD-Cuchilla Dionisio terranes of Uruguay; SG-São Gabriel, SBV-Santana da Boa Vista, P-Pelotas and Tacuarembó blocks of southern Brazil.

of radiometric ages. Additionally, the lack of a solid chronostratigraphic framework has prevented the development of a coherent tectonic model during terrane accretion.

The primary objective of this study is to constrain the maximum depositional age and provenance of Neoproterozoic volcano-sedimentary successions of Uruguay. In this regard, detrital zircon geochronology from these units is a crucial step for testing previous stratigraphic models and for determining depositional basin histories. Furthermore, by comparing the detrital zircon age provenance patterns in samples investigated in this study with published geochronological studies on basement units, we aim to establish the relationship between these Neoproterozoic successions and the surrounding tectono-stratigraphic terranes.

### **3.2. Geological Setting**

The crystalline basement of Uruguay comprises three major terranes separated by large-scale shear zones: (1) the Paleoproterozoic Piedra Alta Terrane, located to the west of the Sarandí del Yí Shear Zone, (2) the Archean to Paleoproterozoic Nico Pérez Terrane, between the Sarandí del Yí and the Sierra Ballena Shear Zones, and (3) the Neoproterozoic Cuchilla Dionisio Terrane, to the east of the Sierra Ballena Shear Zone (Figure 3.1). The Piedra Alta and Nico Pérez terranes have been traditionally considered as forming part of the Río de la Plata Craton. However, Oyhantçabal et al. (2011) recently proposed that the Nico Pérez Terrane should be considered an allochthonous block, and thus the Río de la Plata Craton in Uruguay is restricted to the Piedra Alta Terrane. In contrast to the Piedra Alta Terrane, the Nico Pérez and the Cuchilla Dionisio terranes have been strongly reworked during the Brasiliano Cycle forming the Neoproterozoic Dom Feliciano Belt (Oyhantçabal et al., 2009), thought to have occurred between 650 and 550 Ma (Cordani et al., 2000). According to Basei et al. (2000), this orogenic belt is composed of three distinct domains: the eastern granitoid belt, the central supracrustal schist belt and the western foreland basin domain, wherein the latter is less affected by deformation and metamorphism than the adjacent schist belt. Following this model, it has recently been proposed that the eastern boundary of the Nico Pérez Terrane should be placed at the Fraile Muerto-María Albina Shear Zone and not at the Sierra Ballena Shear Zone (Figure 3.1) (Basei et al., 2000; Oyhantçabal et al., 2011). Therefore, the basement block (Campanero Unit and Zanja del Tigre Complex) located to the west

of the Sierra Ballena Shear Zone is considered as a basement inlier of the Dom Feliciano Belt and not part of the Nico Pérez Terrane (Figure 3.1).

The units focused on in this study have previously been included in both, the schist belt and the foreland belt (including syn- to post-collisional strike slip settings) and thought to have been deposited between ~1,000 and 450 Ma (see Aubet et al., 2014 for a recent review). For instance, the Las Ventanas Formation (Figure 3.2) was long considered to be an alluvial-fan system operating during the Ordovician (Midot, 1984; Pazos et al., 2003). Alternatively, Pecoits et al. (2003) suggested an Ediacaran age (570-590 Ma) and redefined the unit as a volcano-sedimentary succession deposited in a fan-delta sedimentary system formed in a strike-slip basin. Similarly, the Playa Hermosa Formation (Figure 3.2) was deposited in a tectonically active basin with locally fast subsidence rates and correlated to the Varanger (Ediacaran) glacial event by Pazos et al. (2003). Although the less studied San Carlos Formation (Figure 3.2) was thought to represent a meandering fluvial depositional system of Ordovician age (Sánchez-Bettucci, 1998), a more recent study suggested that the unit possesses similar sedimentological characteristics to those shown by the Las Ventanas Formation, and is likely similar in age (Pecoits et al., 2008). The Playa Hermosa and Las Ventanas formations were grouped into the Maldonado Group (Pecoits et al., 2004), however, their relationship with the San Carlos Formation (located to the east of the Sierra Ballena Shear Zone) remains unknown. The age and depositional environment of the Arroyo del Soldado Group are also controversial. The group has been assigned to the upper Ediacaran (<583 Ma) and to the Cryogenian-Tonian (~700-1,000 Ma) deposited in conflicting tectonic settings, either in a passive margin or in a foreland basin (Aubet et al., 2014 and references therein). Furthermore, some units that were originally included in this group were later shown to be independent successions. For example, the Barriga Negra Formation (Figure 3.3) has been considered as a late- to post-orogenic (Midot, 1984; Fambrini et al., 2005), or alternatively as a pre-orogenic unit when included within the Arroyo del Soldado Group (Gaucher et al., 2008).

The depositional ages of other units are better constrained, including the Rocha, Sierra de Aguirre and Tacuarí formations (Figures 3.1 and 3.2). According to Basei et al. (2005), sedimentation of the Rocha Formation took place between ~600-550 Ma,

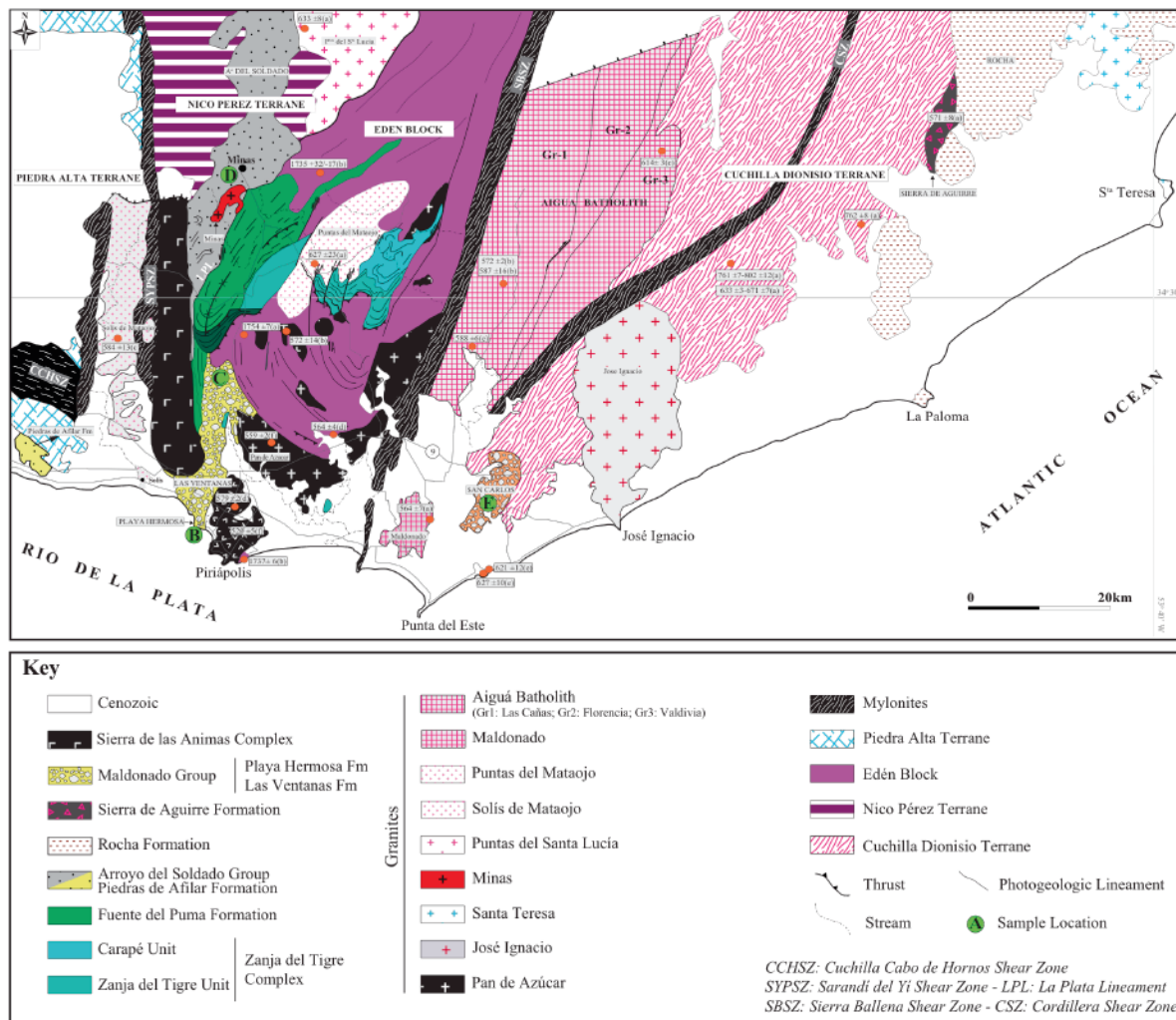


**Figure 3.2.** Geologic map of southeastern Uruguay showing published U-Pb geochronological data and sample locations. Modified from Oyhançabal (2005), Oyhançabal et al. (2009) and Pecoits et al. (2011). Radiometric ages: (a) U-Pb SHRIMP zircon, (b) U-Pb TIMS zircon, (c) Pb-Pb sphene, (d) Ar-Ar hornblende, (e) K-Ar muscovite, (f) Rb-Sr whole rock.

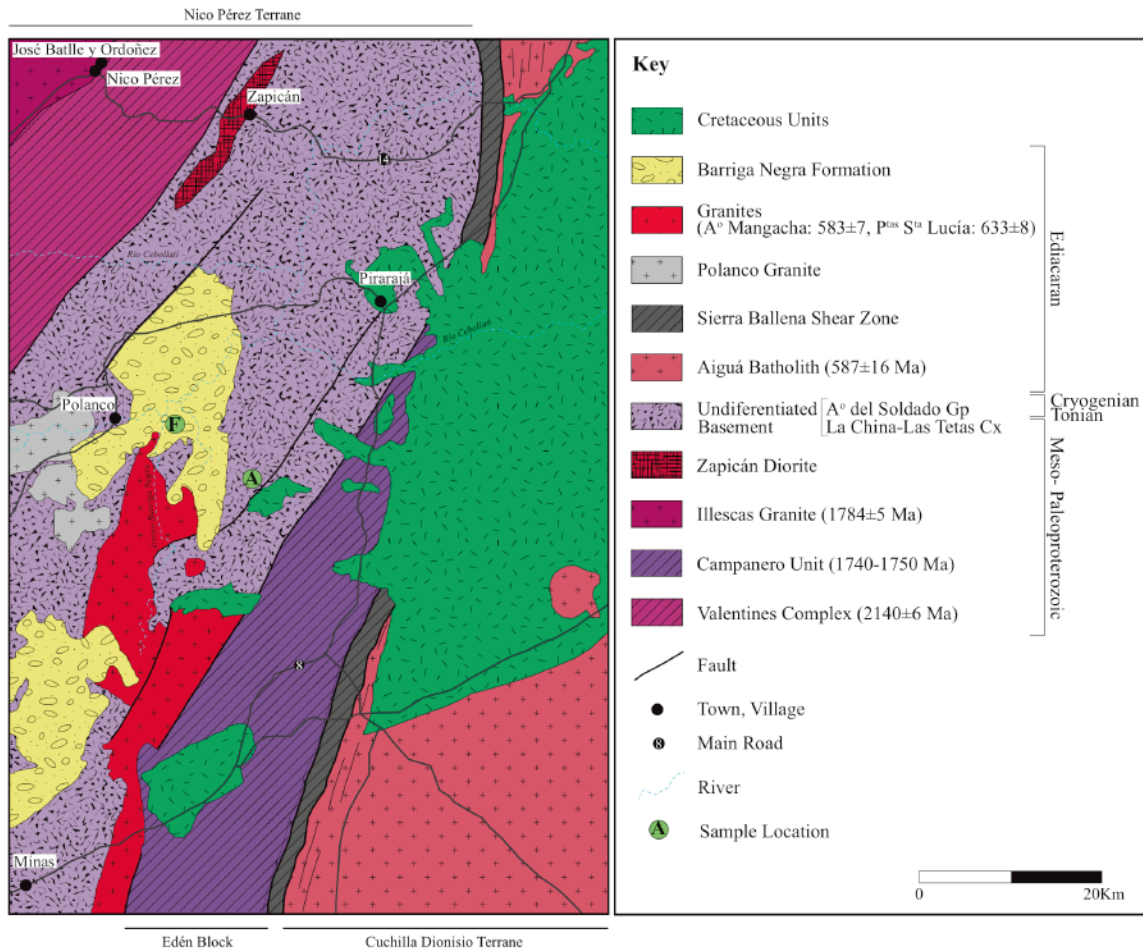


**Figure 3.3.** Simplified geologic map of the type area of the Barriga Negra Formation. Modified from Fambrini et al. (2005) and references therein.

constrained by the youngest detrital zircon grains and the onset of post-tectonic alkaline magmatism, respectively. Based on their similar lithologies, comparable structural setting and the detrital zircon age patterns, Basei et al. (2005) further suggested that the Oranjemund Group (Namibia) and the Rocha Formation are stratigraphic equivalents, and probably represent sediment fills of the same basin. The volcanoclastic Sierra de Aguirre Formation was deposited in a shallow marine and deltaic settings and is thought to have accumulated in a pull-apart basin (Campal and Schipilov, 2005). A dacite from this unit yielded a SHRIMP U-Pb concordia age of 571±8 Ma (Hartman et al., 2002). The glacially influenced Tacuarí Formation is the best-constrained unit. U-Pb zircon ages (LA-MC-ICPMS and SHRIMP) obtained from a cross-cutting granitic dyke places a

585±3 Ma minimum depositional age for this unit. A maximum depositional age for the Tacuarí Formation is 600±9 Ma, based on the youngest detrital zircon age cluster recorded (Pecoits et al., 2012, 2013).

### 3.3. Methodology

Zircon was recovered from six sandstone samples in this study using standard mineral separation techniques. Approximately 2-3 kg of rock material from each sample was pulverized to a fine powder using a jaw crusher and a rotary disc mill. Zircon concentrates were obtained by a combination of hydro-gravimetric (Wilfley table), magnetic (Frantz isodynamic separator) and density (methylene iodide) separation techniques followed by handpicking individual crystals under a binocular microscope. Zircon grains were secured in epoxy mounts, polished to expose the interior of the crystals, and imaged using a custom modified Zeiss Axioskop 40 cathodoluminescence microscope. The U-Pb analyses were performed with a Nu Plasma I multi-collector ICP-MS equipped with 12 Faraday detectors and 3 ion counter detectors. The zircons were ablated with a 213nm New Wave laser (4 Hz; 1.13 J/cm<sup>3</sup>) and typical analysis spots were 40 microns in diameter. Lead isotope fractionation was monitored by simultaneously aspirating a thallium-doped solution. Three zircon standards were analyzed with each sample, a Proterozoic zircon (LH94-15) was used to monitor U/Pb fractionation and a Neoproterozoic (GJ-32-1; 605 Ma) and Mesoarchean (OG-1; 3465 Ma) zircons were analysed as blind standards to evaluate the accuracy of the method, a summary of the blind standard results for each session is presented in the supplementary material. In general the results for the blind standards are in agreement with or slightly younger than their recommended ages. The exception is GJ-32-1 analysed during session 4 where the <sup>206</sup>Pb/<sup>238</sup>U date is 10% lower than the recommended age. Common lead corrections were not applied to the data. Long-term monitoring of zircon standards with a range of ages using this protocol indicates that uncorrected <sup>206</sup>Pb/<sup>238</sup>U dates are more accurate for grains younger than 800 Ma, for all other analyses <sup>207</sup>Pb/<sup>206</sup>Pb dates are used to compile probability density plots. Details of the U-Pb LA-MC-ICPMS technique used at the University of Alberta are outlined in Simonetti et al. (2005; 2006). Data reduction was conducted with an in-house program and data presentation (concordia diagrams,

probability density plots) was constructed using Isoplot/Ex (Ludwig, 2008). In some samples the identification of age populations was evaluated using a mixture modelling treatment (Sambridge and Compston, 1984). Ages were calculated using the uranium decay constants and  $^{238}\text{U}/^{235}\text{U}$  value recommended by Jaffey et al. (1971). The analytical data referred to in this paper are available as supplementary data (Appendix 2, Tables 3.1-3.7).

### **3.4. Results**

#### ***3.4.1. U-Pb Detrital Zircon Geochronology***

A total of 662 zircons were analyzed in six samples from five different lithostratigraphic units, namely: Yermal (Arroyo del Soldado Group), Playa Hermosa, Las Ventanas (two samples), San Carlos and Barriga Negra formations. Results are displayed in  $^{206}\text{Pb}/^{238}\text{U}$  and  $^{207}\text{Pb}/^{206}\text{Pb}$  age histograms and probability density plots calculated using the Isoplot 3.7 software by Ludwig (2008). Sample locations (coordinates) and their stratigraphic positions are provided in supplementary material (Appendix 2, Table 3.8) and shown in Figures 3.2-3.4.

##### ***3.4.1.1 Yermal Formation***

A total of 105 zircon ages were obtained from a coarse sandstone interbedded with dark siltstones and shales of the uppermost Yermal Formation (sample 101115/1). At this location (Arroyo Tapes Grande area), the unit is overlain by a thick package of limestones and dolostones of the Polanco Limestones Formation and dark shales of the Cerro Espuelitas Formation (Figure 3.4A). The probability density plot for this sample displays two distinct age clusters, a Paleoproterozoic population at  $2,212 \pm 4$  Ma ( $n=24$ ) and a larger Mesoarchean population ( $n=57$ ) with two nodes computed from the unmixing treatment at  $2915.8 \pm 2.0$  Ma (34%) and  $3038.1 \pm 1.3$  Ma (66%). The youngest detrital zircon (grain 80) has a  $^{207}\text{Pb}/^{206}\text{Pb}$  date of 1794 Ma and provides a maximum age for deposition of the Yermal Formation (Figure 3.5A).

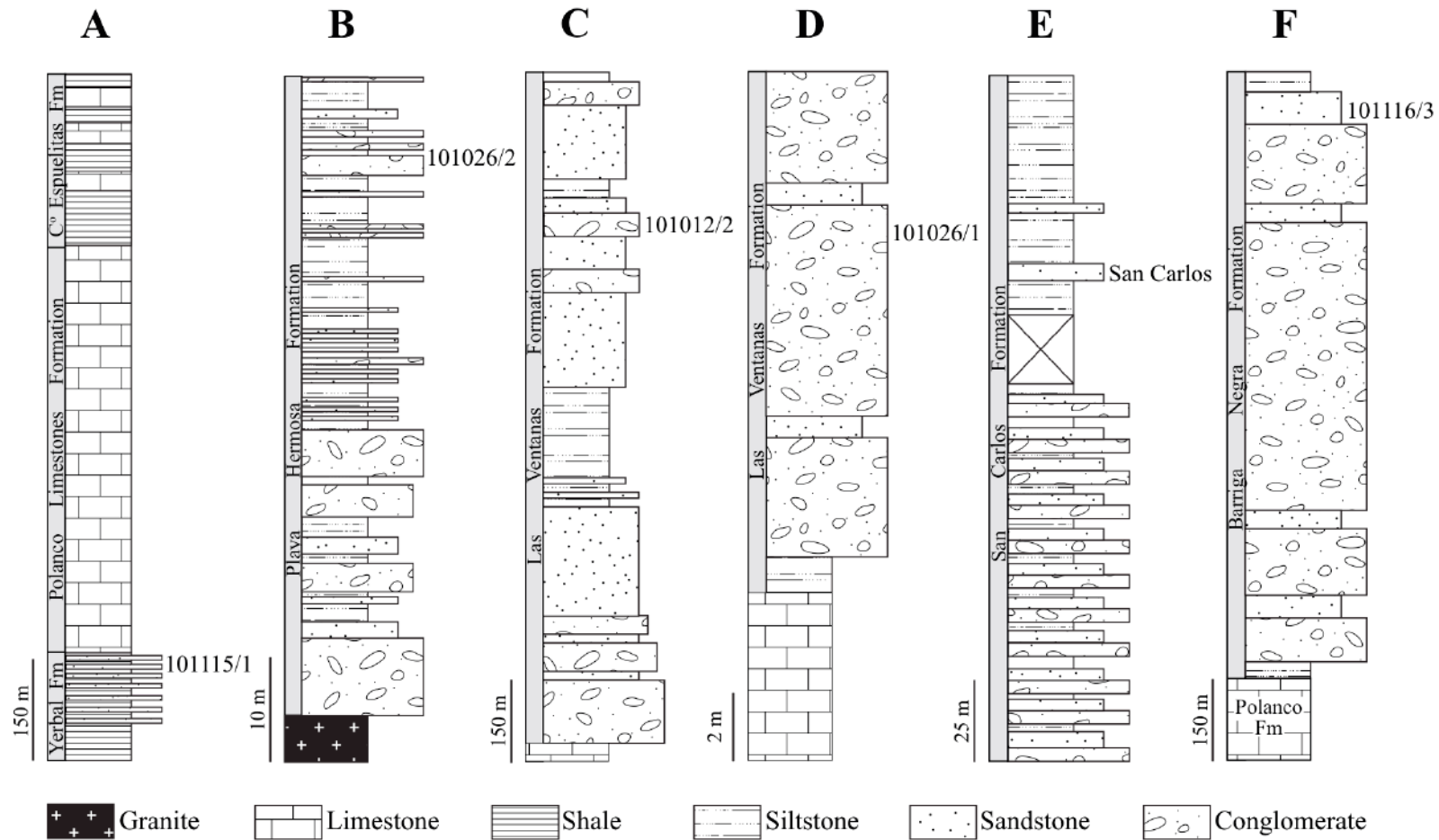


**Figure 3.4.** Stratigraphic profiles at sample locations. **(A)** Yermal Formation (sample 101115/1). **(B)** Playa Hermosa Formation (sample 101026/2). **(C)** Las Ventanas Formation (sample 101012/2). **(D)** Las Ventanas Formation (sample 101012/1). **(E)** San Carlos Formation (sample San Carlos). **(F)** Barriga Negra Formation (sample 101116/3). See Figures 3.2 and 3.3 for sample locations.



**Figure 3.5.** Combined relative probability density and histogram plots. **(A)** Yerbal Formation (sample 101115/1, n=105). **(B)** Playa Hermosa Formation (sample 101026/2, n=107). **(C)** Las Ventanas Formation (sample 101012/2, n=111). **(D)** Las Ventanas Formation (sample 101026/1, n=115). **(E-F)** San Carlos Formation (sample San Carlos, n=111). In (F) results are displayed in  $^{206}\text{Pb}/^{238}\text{U}$  ages. **(G)** Barriga Negra Formation (sample 101116/3, n=115). Representative detrital zircon grains from each sample are shown in Supplementary Material, Appendix 2 (Figure 3.1).

#### ***3.4.1.2 Playa Hermosa Formation***

A total of 107 zircon grains were analysed from a pebbly sandstone of the Playa Hermosa Formation (sample 101026/2). The sample was collected from the upper part of the stratotype of the unit, in the Hermosa Beach near Piriápolis city, where it is interbedded with siltstones and conglomerates (Figure 3.4B). This sandstone contains two distinct zircon populations, a Cambrian cluster at  $563\pm 13$  Ma ( $n=6$ ), providing a maximum age for deposition of this unit, and a dominant Paleoproterozoic cluster with 90 analyses recording dates between 2000 and 2320 Ma. A mixture modelling treatment of the Paleoproterozoic cluster identifies two similar abundance populations at  $2073.2\pm 3.1$  and  $2128.7\pm 2.7$  Ma. Figure 3.5B displays the zircon distribution of the Playa Hermosa Formation where there is a clear dominance of Paleoproterozoic zircons. Only one zircon (#12) has a near-concordant date that plots between these two peaks at  $\sim 1,730$  Ma.

#### ***3.4.1.3 Las Ventanas Formation***

Two pebbly sandstone units were analyzed from the Las Ventanas Formation. At its type area (sample 101012/2; Figure 3.4C), detrital zircon spot analyses ( $n=111$ ) display a prominent peak at  $590\pm 5$  Ma ( $n=42$ ) and two less pronounced peaks at  $2,127.9\pm 2.1$  and  $2,649.4\pm 2.8$  Ma based on an unmixing treatment of the ages between 2.0 and 2.7 Ga (Figure 3.5C). The second sample ( $n=115$ ), taken from west of Minas city (sample 101026/1; Figure 3.4D), exhibits two main populations at  $548\pm 19$  and  $2,083\pm 11$  Ma, and contains a broad range of zircon ages between  $\sim 1,050$  and  $1,950$ , and between  $\sim 2,250$  and  $2,650$  Ma (Figure 3.5D).

#### ***3.4.1.4 San Carlos Formation***

For the San Carlos Formation (sample San Carlos), 111 zircon dates were obtained from a pebbly sandstone at its type area, wherein sandstone layers are interbedded with grey plane parallel stratified siltstones in the upper part of the unit (Figure 3.4E). Three age clusters are observed at  $552\pm 3$ ,  $647\pm 10$  and  $764\pm 12$  Ma, along with Meso- and Paleoproterozoic zircon grains with dates between  $\sim 1,100$  and  $2,000$  Ma (Figures 3.5E, 3.5F).

#### ***3.4.1.5 Barriga Negra Formation***

The Barriga Negra sample (101116/3) was collected from a sandstone layer overlying coarse conglomerates of the type area of the unit (Francisco Vidal Farm; Figures 3.3 and 3.4F). Detrital zircons (n=115) from the Barriga Negra Formation display two dominant peaks at  $581\pm 6$  and  $2,028\pm 15$  Ma. Archean zircons are also abundant and range from  $\sim 2,600$  to  $3,400$  Ma with a noticeable cluster at  $2,669\pm 15$  Ma. A few scattered zircons occur between  $\sim 1,000$  and  $1,800$  Ma (Figure 3.5).

### **3.5. Discussion**

#### ***3.5.1. Possible Source Areas***

The sample from the Yermal Formation is dominated by Paleoproterozoic and Archean detrital zircon grains (Figure 3.5A). Possible sources for the  $2,212\pm 4$  Ma zircons include Paleoproterozoic units of the Piedra Alta and Nico Pérez terranes (Figures 3.1 and 3.2). For example, similar U-Pb ages were obtained from orthogneisses of the San José ( $\sim 2,200$  Ma) and Montevideo belts ( $\sim 2,160$  Ma) (Table 3.1). Similarly, this zircon population mirrors inherited ( $\sim 2,220$  Ma) and magmatic ( $\sim 2,160$ - $2,114$  Ma) ages of the Valentines and Rivera Granulitic complexes of the Nico Pérez Terrane. Archean ages ( $\sim 2,700$ - $3,400$  Ma) are restricted to the La China and Las Tetas complexes of the Nico Pérez Terrane (Figure 3.1). Although statistically insignificant, the only zircon at  $\sim 1,794$  Ma was most likely derived from Nico Pérez Terrane (Illescas Granite) (Table 3.1). Other potential sources, such as metatuffs of the Paso Severino Belt in the Piedra Alta Terrane or the Campanero Unit, are unlikely given the younger ages shown ( $1,730$ - $1,760$  Ma). Furthermore, the latter unit is also associated with younger Mesoproterozoic volcano-sedimentary successions of the Zanja del Tigre Complex ( $1,435$ - $1,490$  Ma) and the absence of zircons with this age in the Yermal Formation suggests that these Paleo- and Mesoproterozoic units (herein included within the Edén Terrane; see below) were not part of the source area.

Two samples were previously analyzed from the Yermal Formation. One sample (92 zircon grains) yielded an essentially unimodal concentration centered at  $2,450$  Ma, two grains showed an age of  $2,045$  Ma and five grains were dated between  $2,660$  and  $2,895$  Ma (Gaucher et al., 2008, their sample 'MIN 14'). The second sample (29 zircon

Terrane	Unit	Rock Type	Age	Method	Reference	
Piedra Alta	San José	Amphibolite gneiss	2202±8	TIMS	Peel and Preciozzi (2006)	
	Montevideo Granite (Pajat Blancas)	Porphyritic granite	2158±24-23	TIMS	Peel and Preciozzi (2006)	
	Montevideo Gneiss	Orthogneiss	2165±38	SHRIMP	Cordani in Santos et al. (2003)	
	Paso Severino	Metadacite	2146±8	SHRIMP	Santos et al. (2003)	
	Isla Mala Pluton	Granodiorite	2122±4	SHRIMP	Santos et al. (2003)	
	Isla Mala Pluton	Monzogranite	2111±9	SHRIMP	Santos et al. (2003)	
	Isla Mala Pluton	Granodiorite	2088±12 (MSWD=36)	TIMS	Preciozzi et al. (1999a)	
	Isla Mala Pluton	Granodiorite	2086±11 (MSWD=100)	TIMS	Peel and Preciozzi (2006)	
	Rospide Gabbro	Gabbro	2086±7	SHRIMP	Hartmann et al. (2000)	
	Soca Granite	Monzogranite (charnockite)	2078±8	TIMS	Peel and Preciozzi (2006)	
	Rospide Gabbro	Gabbro	2076±6	SHRIMP	Hartmann et al. (2008)	
	Isla Mala Pluton	Granodiorite	2074±6	SHRIMP	Hartmann et al. (2000)	
	Isla Mala Pluton	Monzogranite	2065±9	SHRIMP	Hartmann et al. (2000)	
	Soca Granite	Monzogranite (charnockite)	2056±6	SHRIMP	Santos et al. (2003)	
	Soca Granite	Monzogranite (charnockite)	2054±11	SHRIMP	Bossi et al. (2001)	
	Cufre Granite	Granite	2053±14	TIMS	Peel and Preciozzi (2006)	
	Granodiorite Florida	Porphyritic Granodiorite	2011±15/-5	TIMS	Peel and Preciozzi (2006)	
	Boca del Rosario Migmatite	Melanosome	2007±14	TIMS	Peel and Preciozzi (2006)	
	Florida Matic Dyke Swarm	Dolerite	1790±5	TIMS (Buddleyite)	Halls et al. (2001)	
	Paso Severino	Felsic metatuffs	1753±6/-4	TIMS	Peel and Preciozzi (2006)	
	Solís de Matajojo Granite	Tonalite	584±13	Pb-Pb (Sphene)	Oyhantçabal et al. (2007)	
	Sarandi del Yi Shear Zone	La China Complex	Metatonalite orthogneiss	3404±8	SHRIMP	Hartmann et al. (2001)
		La China Complex	Metatonalite orthogneiss	3340±19	SHRIMP	Hartmann et al. (2001)
		La China Complex	Metatonalite orthogneiss	3281±17	SHRIMP	Hartmann et al. (2001)
La China Complex		Metatonalite orthogneiss	3101±4	SHRIMP	Hartmann et al. (2001)	
La China Complex		Metatonalite orthogneiss	3096±45	TIMS (upper intercept)	Gaucher et al. (2011)	
La China Complex		Metatonalite orthogneiss	2721±7	SHRIMP	Hartmann et al. (2001)	
Las Tetra Complex		Muscovite quartzite	<3145±4	SHRIMP	Hartmann et al. (2001)	
Las Tetra Complex		Metaconglomerate	<2762±8	SHRIMP	Hartmann et al. (2001)	
Valentines Complex		Tonalitic granulite	2619±8	SHRIMP	Santos et al. (2003)	
Valentines Complex		Tonalitic granulite	2600	SHRIMP	Hartmann et al. (2001)	
Valentines Complex		Tonalitic granulite	2535±12	SHRIMP	Santos et al. (2003)	
Valentines Complex		Tonalitic granulite	2224±4	SHRIMP	Hartmann et al. (2001)	
Valentines Complex		Granitic granulite	2224±4	SHRIMP	Santos et al. (2003)	
Rivera Granulitic Complex		Granulite gneiss	2172±8	SHRIMP	Oyhantçabal et al. (2012)	
Rivera Granulitic Complex		Trochiliform gneiss	2163±8	SHRIMP	Santos et al. (2003)	
Valentines Complex		Tonalitic granulite	2163±22	SHRIMP	Santos et al. (2003)	
Las Flores Granite		Granite	2161±14	SHRIMP	Oyhantçabal et al. (2012)	
Rivera Granulitic Complex		Granulite gneiss	2147±9	SHRIMP	Oyhantçabal et al. (2012)	
Rivera Granulitic Complex		Trochiliform gneiss	2140±6	SHRIMP	Santos et al. (2003)	
Rivera Granulitic Complex		Granulite gneiss	2114±3	SHRIMP	Oyhantçabal et al. (2012)	
Rivera Granulitic Complex		Granulite gneiss	2093±36	SHRIMP	Oyhantçabal et al. (2012)	
Las Flores Granite		Granite	2083±14	SHRIMP	Oyhantçabal et al. (2012)	
Rivera Granulitic Complex		Trochiliform gneiss	2077±6	SHRIMP	Santos et al. (2003)	
Valentines Complex		Tonalitic granulite	2058±3	SHRIMP	Santos et al. (2003)	
Rivera Granulitic Complex		Granulite gneiss	1975±5	SHRIMP	Oyhantçabal et al. (2012)	
Illescas Granite		Rapakivi granite	1784±5	TIMS	Heaman in Campal and Schipilov (1995)	
Puntas del Santa Lucia Pluton		Granite	633±8	SHRIMP	Hartmann et al. (2002)	
Sobresaliente Granite		Granite	585±3	SHRIMP	Oyhantçabal et al. (2012)	
Las Flores Granite		Granite	586±3	SHRIMP	Oyhantçabal et al. (2012)	
Arroyo Mangacha Granite		Granite	583±7	SIMS	Gaucher et al. (2008)	
Edén Block		Zanja del Tigre Complex	Metasandstone	1800-3400	SHRIMP	Oyhantçabal et al. (2005)
		Zanja del Tigre Complex	Sandstone	1950-3550	SHRIMP	Mallmann et al. (2007)
		Campanero Unit	Orthogneiss	1754±7	SHRIMP	Mallmann et al. (2007)
		Campanero Unit	Orthogneiss	1737±6/-8	TIMS	Oyhantçabal et al. (2005)
		Campanero Unit	Orthogneiss	1735±32/-17	TIMS	Sánchez-Bettucci et al. (2003)
		Zanja del Tigre Complex	Metagabbro	1492±4	SHRIMP	Oyhantçabal et al. (2005)
		Zanja del Tigre Complex	Volcaniclastics	1433±6	TIMS	Gaucher et al. (2011)
	Zanja del Tigre Complex	Volcaniclastics	1429±21	TIMS	Oyhantçabal et al. (2005)	
	Fuente del Puma Formation (Lavalleja)	Matabasalt	667±4	TIMS	Sánchez-Bettucci et al. (2003)	
	Puntas del Matajojo Granite	Granite	627±23	SHRIMP	Oyhantçabal et al. (2009)	
	Fuente del Puma Formation (ex-Lavalleja)	Metasandstone	700-3400	SHRIMP	Oyhantçabal et al. (2005)	
	Las Ventanas Formation	Gabbro	590±2	SHRIMP	Mallmann et al. (2007)	
	Las Ventanas Formation	Volcaniclastic	573±11	SHRIMP	Oyhantçabal et al. (2009)	
	Carapé Complex	Granite	572±14 (MSWD=93)	TIMS	Sánchez-Bettucci et al. (2003)	
	Unnamed Alkaline Granite	Granite	530±14	TIMS	Oyhantçabal et al. (2005)	
	Cuchilla Dionisio	Cerro Olivo Complex	Orthogneiss	2058±10	SHRIMP	Hartmann et al. (2002)
		Cerro Olivo Complex	Orthogneiss	1073±28	SHRIMP	Basei et al. (2011)
		Cerro Olivo Complex	Orthogneiss	1081±58	TIMS	Basei et al. (2011)
		Cerro Olivo Complex	Orthogneiss	1008±60	TIMS	Preciozzi et al. (1999b)
		Cerro Olivo Complex	Orthogneiss	1006±37	TIMS	Preciozzi et al. (1999b)
		Cerro Olivo Complex	Orthogneiss	1005±20	TIMS	Basei et al. (2011)
Cerro Olivo Complex		Orthogneiss	1001±17	TIMS	Basei et al. (2011)	
Cerro Olivo Complex		Orthogneiss	ca. 990-1,000	SHRIMP (xenocryst)	Masquelin et al. (2012)	
Cerro Olivo Complex		Orthogneiss	984±64	TIMS	Preciozzi et al. (1999b)	
Cerro Olivo Complex		Orthogneiss	961±5	TIMS	Basei et al. (2011)	
Cerro Olivo Complex		Orthogneiss	802±12	SHRIMP	Lenz et al. (2011)	
Cerro Olivo Complex		Orthogneiss	796±8	SHRIMP	Lenz et al. (2011)	
Cerro Olivo Complex		Orthogneiss	797±8	SHRIMP	Lenz et al. (2011)	
Cerro Olivo Complex		Orthogneiss	795±8	SHRIMP	Lenz et al. (2011)	
Cerro Olivo Complex		Orthogneiss	794±8	SHRIMP	Lenz et al. (2011)	
Cerro Olivo Complex		Orthogneiss	793±4	SHRIMP	Lenz et al. (2011)	
Cerro Olivo Complex		Orthogneiss	788±6	SHRIMP	Lenz et al. (2011)	
Cerro Olivo Complex		Orthogneiss	786±9	SHRIMP	Lenz et al. (2011)	
Cerro Olivo Complex		Orthogneiss	780±5	SHRIMP	Lenz et al. (2011)	
Cerro Olivo Complex		Orthogneiss	778±7	SHRIMP	Masquelin et al. (2012)	
Cerro Olivo Complex		Orthogneiss	776±12	SHRIMP	Oyhantçabal et al. (2009)	
Cerro Olivo Complex		Orthogneiss	771±6	SHRIMP	Lenz et al. (2011)	
Cerro Olivo Complex		Orthogneiss	767±9	SHRIMP	Lenz et al. (2011)	
Cerro Olivo Complex		Orthogneiss	762±8	SHRIMP	Hartmann et al. (2002)	
Cerro Olivo Complex		Orthogneiss	761±7	SHRIMP	Basei et al. (2011)	
Cerro Olivo Complex		Orthogneiss	753±14	SHRIMP	Basei et al. (2011)	
Cerro Olivo Complex		Orthogneiss	743±7	SHRIMP	Hartmann et al. (2002)	
Cerro Olivo Complex		Migmatite	704±17	TIMS	Preciozzi et al. (2001)	
Cerro Olivo Complex		Orthogneiss	671±7	SHRIMP	Masquelin et al. (2012)	
Cerro Olivo Complex		Migmatite	655±6	TIMS	Basei et al. (2011)	
Cerro Olivo Complex		Paragneiss	645±4	TIMS (Monazite)	Basei et al. (2011)	
Cerro Olivo Complex		Orthogneiss	641±17	SHRIMP	Oyhantçabal et al. (2009)	
Cerro Olivo Complex		Orthogneiss and Pegmatitic Veins	637±11	SHRIMP	Masquelin et al. (2012)	
Cerro Olivo Complex		Augen Gneiss	636±19	TIMS	Basei et al. (2011)	
Cerro Olivo Complex		Paragneiss	633±5	TIMS	Basei et al. (2011)	
Rocha Group		Sandstone	629±17-2611±7	SHRIMP	Basei et al. (2005)	
Cerro Olivo Complex		Migmatite	626±25	TIMS (Zircon+Monazite)	Preciozzi et al. (2001)	
Cerro Olivo Complex		Paragneiss	616±19	TIMS	Basei et al. (2011)	
Valdivia Granite		Granite	614±5	TIMS (Titanite)	Oyhantçabal et al. (2007)	
Aguila Granite		Granite	587±16	TIMS	Basei et al. (2000)	
Tacuri Granite		Granite	585±5	LA-ICP-MS/TIMS/SHRIMP	Pessis et al. (2012)	
Florencia Granite	Granite	572±2	TIMS	Basei et al. (2000)		
Sierra de Aguirre Formation	Dacite	571±8	SHRIMP	Hartmann et al. (2002)		
Maldonado Granite	Granite	564±7	SHRIMP	Oyhantçabal et al. (2009)		
Cerro Olivo Complex	Migmatite (leucosome)	546±69	TIMS	Preciozzi et al. (2001)		
Cerro Olivo Complex	Migmatite (leucosome)	520-540	TIMS	Preciozzi et al. (1999b)		
El Pintor Granite	Monzogranite	525±9	TIMS	Basei et al. (2011)		
Cerro Olivo Complex	Migmatite (leucosome)	510±130	TIMS (lower intercept)	Preciozzi et al. (1999b)		

**Table 3.1.** Compilation of published U-Pb zircon (unless otherwise indicated) geochronology data (see also Figures 3.1 and 3.2).

grains) showed a predominance of Paleoproterozoic zircons (76%), with ages ranging from 1,900 to 2,220 Ma and a smaller late Mesoproterozoic cluster between 1,010 and 1,065 Ma (17%). The oldest zircon displays a Mesoarchean age (3,030 Ma), while the youngest and the only Neoproterozoic aged zircon was dated at  $664\pm 14$  Ma (Blanco et al., 2009, their sample ‘Yerbal Fm.’). As discussed by Aubet et al. (2014), the interpretation of the Neoproterozoic zircon in this sample is problematic because this single grain is statistically insignificant and it has not been recorded in any other sample from the Yerbal Formation, and thus it should be taken with caution. Here, we further support this suggestion based on the following arguments: (1) the new dated sample from the Yerbal Formation does not show any Neoproterozoic zircon; in fact, none of the three samples dated from that unit have zircon grains younger than 1,036 Ma; (2) none of the Neoproterozoic volcano-sedimentary units focused on in this study (located to the west of the Sierra Ballena Shear Zone) show detrital zircons of that age (all of them show a clear gap between ~650 and 1,000 Ma); and (3) as pointed out by Aubet et al. (2014), the same gap exists in basement rocks, which would explain the lack of detrital zircons of that age in the Neoproterozoic cover. Hence, the  $664\pm 14$  Ma-age zircon reported by Blanco et al. (2009) is not considered valid herein.

When the three Yerbal samples are analyzed in detail, some differences arise. The two northernmost samples (‘Yerbal Fm.’ and 101115/1) display a marked peak at ~2,200 Ma (76% and 37%, respectively), while the southernmost sample (‘MIN 14’) shows no zircons at that age but it displays a significant cluster at 2,450 Ma (92%). Similarly, the former two samples show relatively abundant Archean zircons whereas the latter only shows four Archean grains. Another striking difference is the presence of Mesoproterozoic (~1,036 Ma) zircons in the northernmost sample (‘Yerbal Fm.’), which are completely absent in the other two samples. Taken together, these results suggest that the Yerbal Formation was mainly sourced from the Nico Pérez Terrane. Even though the Piedra Alta Terrane could source 2,200 Ma zircons, their presence in the Yerbal samples is accompanied by Archean zircon grains, which only occur in the Nico Pérez Terrane and are not accompanied by younger (~1,750-2,100 Ma) grains also common in the Piedra Alta Terrane (Table 3.1). Furthermore, the southernmost Yerbal sample (‘MIN 14’), which is closest to the Piedra Alta Terrane at its present position, shows no zircons

from this terrane. Strikingly, this sample displays a Paleoproterozoic cluster at 2,450 Ma. There is no record of rocks with this age in the Nico Pérez Terrane and the only relatively nearby rocks of similar age (2,480-2,440 Ma) are found in the São Gabriel Block, in southern Brazil (Figure 3.1) (Hartmann et al., 2004). However, this sample is a very coarse-grained subarkose characterized by abundant relatively fresh feldspars, which would indicate a proximal source area (Gaucher et al., 2008), and discount recycled-secondary sources. Hence, we predict that future studies will identify basement rocks of this age in the Nico Pérez Terrane that are hitherto unknown in Uruguay.

Similarly, the ~1,036 Ma peak recorded in the Yermal Formation does not correspond to any known basement unit of the Nico Pérez Terrane. These zircons could derive either from (1) the Cuchilla Dioniso Terrane, (2) Mesoproterozoic rocks from elsewhere, (3) basement rocks not yet identified in the Nico Pérez Terrane or, alternatively, (4) the source rocks were simply eroded away. The Cuchilla Dioniso and Nico Pérez terranes were suggested to have amalgamated in the mid-Ediacaran (Pecoits et al., 2004; 2008; Oyhançabal et al., 2009), and their proximity during the deposition of the Tonian-Cryogenian Yermal Formation (see section 3.5.2 below) is unknown. Although similar ages (~1,000 Ma) were obtained in the Cuchilla Dioniso Terrane (Preciozzi et al., 1999b), they correspond to inherited zircon grains (Oyhançabal et al., 2009) and new geochronological studies on this terrane indicated magmatism at ~800-760 Ma, followed by high-grade metamorphism at ~670-630 Ma (Hartmann et al., 2002; Oyhançabal et al., 2009; Lenz et al., 2011; Masquelin et al., 2012; Basei et al., 2011). Therefore, it is very unlikely that those Mesoproterozoic zircons were sourced from this terrane without showing any evidence of the more typical Neoproterozoic ages (Table 3.1 and Figure 3.2). The same holds true if an African source is considered. This is further supported by paleocurrent directions measured in the Yermal Formation indicating source areas located to the northwest. Hence, possible source areas were located to the west of the Sierra Ballena Shear Zone and not to the east. In this regard, alternative sources for these Mesoproterozoic zircons are represented by the ‘Grenvillian-type age’ Sunsas orogenic belt at the southwestern corner of the Amazonian Craton (Cordani et al., 2010), and the proto-Andean belt in the western Río de la Plata Craton (Rapela et al., 2010; Ramos, 2010). In either case, the Mesoproterozoic zircons found in the Yermal Formation

(Blanco et al., 2009 their Fig. 7) are less rounded than other Paleoproterozoic-Archean zircons sourced from local areas (Zimmermann, 2011). This last point is difficult to reconcile with the more than 1,000 km that separates these areas from the Arroyo del Soldado outcrops at their present position. Therefore, excluding the above mentioned hypotheses to explain the presence of the  $\sim 1,036$  Ma zircons in the Yermal Formation we are left with three alternatives: (1) the Nico Pérez Terrane was closer to the above mentioned (Sunsas and proto-Andean belts) or other Grenville-age source areas during the deposition of the Yermal Formation (Arroyo del Soldado Group); (2)  $\sim 1,036$  Ma rocks have not yet been identified in the Nico Pérez Terrane; or (3) they have been eroded away.

The dominance of Paleoproterozoic dates with two age nodes at  $2073.2 \pm 3.1$  and  $2128.7 \pm 2.7$  Ma in the detrital zircon age spectra of the Playa Hermosa Formation is readily explained when considering Paleoproterozoic units of the Piedra Alta and Nico Pérez terranes as possible source areas. For example, the oldest ages overlap with U-Pb ages obtained from granites and gneisses of the Montevideo Belt and metavolcanics of the Paso Severino Belt, whereas the youngest peak is similar within error to the age of late tectonic granites, such as the Isla Mala Granitic Suite of the Piedra Alta Terrane (Table 3.1). Similarly, these two zircon populations mirror the magmatic ( $\sim 2,160$ - $2,114$  Ma) and metamorphic ( $\sim 2,060$ - $2,090$  Ma) ages of the Valentines and Rivera Granulitic complexes of the Nico Pérez Terrane (Figure 3.1). The only zircon at  $\sim 1,730$  Ma could also derive from any of these two terranes and even from the Edén Terrane (Campanero Unit:  $1,730$ - $1,760$  Ma). Considering the lack of the typical Archean ages found in the Nico Pérez Terrane and present in all the Neoproterozoic successions located to the west of the Sierra Ballena Shear Zone, we suggest that the Piedra Alta was the most important source area, if not the only one, for the Playa Hermosa Formation. This is further supported by paleocurrent and paleoslope directions measured in this unit indicating source areas located to the southwest (Pazos et al., 2003; Pecoits et al., 2008). A maximum depositional age for the Playa Hermosa Formation is constrained by the youngest zircon population at  $563 \pm 13$  Ma. This age coincides with that obtained from basal volcanoclastic deposits in the Las Ventanas Formation at  $573 \pm 11$  Ma (Table 3.1). Intense magmatism represented by volcanic, sub-volcanic and intrusive units has been

reported in the area, but no U-Pb ages are available. The most reliable age is that obtained from the Pan de Azúcar Pluton at  $579 \pm 2$  Ma ( $^{40}\text{Ar}/^{39}\text{Ar}$  in hornblende; Oyhantçabal et al., 2007), which are similar to both the volcanoclastic deposits and the youngest zircon population found in the Playa Hermosa Formation.

At its type area, the zircon age spectra of the Las Ventanas Formation show three main age clusters: (1)  $2,649 \pm 3$ ; (2)  $2,128 \pm 2$ ; and (3)  $590 \pm 5$  Ma. The oldest zircon population ( $2,649 \pm 3$  Ma) suggests that basement of the Nico Pérez Terrane contributed to this unit because no igneous Archean rocks have been found elsewhere in the basement of Uruguay. For example, similar ages have been obtained in La China, Las Tetas and Valentines complexes of the Nico Pérez Terrane (Table 3.1). The second cluster ( $2,128 \pm 2$  Ma) could be sourced from the Piedra Alta or Nico Pérez terranes. Both terranes have units with ages well within this range (Table 3.1). The few zircon grains dated at  $\sim 3,100$ ,  $2,400$ , and between  $1,750$  and  $1,100$  Ma, can also be explained by inputs from the basement of the Nico Pérez and Edén terranes. Based on the available U-Pb data, source units for these zircons include, La China ( $2,720$ - $3,400$  Ma) and Las Tetas ( $2,762$ - $3,262$  Ma) complexes in the Nico Pérez Terrane, and the Campanero Unit ( $1,737$ - $1,754$  Ma) and Zanja del Tigre Complex ( $1,429$ - $1,492$  Ma) of the Edén Terrane (Table 3.1). The Piedra Alta Terrane could only source  $1,750$  Ma zircons because similar ages were obtained in felsic metatuffs of the Paso Severio Belt (Table 3.1). Hence, the unit seems to have been mainly sourced from the Nico Pérez Terrane and Edén terranes. The large Ediacaran cluster at  $590 \pm 5$  Ma defines the maximum depositional age for the Las Ventanas Formation. Similar to the Playa Hermosa Formation, this peak is most likely related to the Ediacaran magmatism described in the area, and it fits with the age reported for basal volcanoclastic rocks of the Las Ventanas Formation at  $573 \pm 11$  Ma (Table 3.1).

The sample taken from the conglomerates near Minas city shows two prominent peaks at  $548 \pm 19$  Ma, and between  $2,083 \pm 11$  and  $2,150$  Ma. The latter range is virtually the same to that shown by the Playa Hermosa Formation, and as such, it can largely be explained by contributions from the Piedra Alta Terrane. However, this sample also shows a wide range of zircon grains with ages between  $\sim 1,050$  and  $2,650$  Ma. Considering that the Piedra Alta Terrane does not record magmatic activity, with the exception of the La Paz Neoproterozoic granite and some Paleoproterozoic metatuffs

(~1753 Ma) after the intrusion of the Florida dyke swarm at  $1,790 \pm 5$  Ma (Halls et al., 2001), it can be argued that both the Piedra Alta and the Nico Pérez terranes were source areas. The same is true for the Archean zircons. As stated above, there is no record of ~1,050 Ma zircons in basement rocks of the Nico Pérez Terrane. However, the detrital zircon spectra of the Arroyo del Soldado Group also shows zircons of this age, which indicate that the ~1,050 Ma zircons recorded in the Las Ventanas Formation were likely sourced by the Arroyo del Soldado Group. If so, these zircons would represent second-cycle grains. On the other hand, with the exception of the Illescas Rapakivi granite ( $1784 \pm 5$  Ma; Figure 3.1), zircons between ~1,200 and 1,800 Ma are not recorded in the basement of the Nico Pérez Terrane or in the Arroyo del Soldado Group implying that rocks from the Edén Terrane (1,400-1,800 Ma) also sourced the Las Ventanas Formation at this location. The youngest zircon cluster at  $548 \pm 19$  Ma constrains the maximum age of deposition for this conglomerate, which overlaps with that of the Playa Hermosa Formation and is slightly younger than that of the Las Ventanas Formation at its type area.

In summary, the results for the Playa Hermosa and Las Ventanas formations (Maldonado Group) show that, although spatially variable, the Piedra Alta, Nico Pérez and Edén terranes were important source areas. Both samples from the Las Ventanas Formation show a wide range of zircons that could only be sourced from the Nico Pérez and Edén terranes. Although the Playa Hermosa Formation also shows Paleoproterozoic zircons that could be sourced from the same areas, the lack of Archean, Meso- and upper Paleoproterozoic ages (except for one single grain at ~1,730 Ma), also typical in the Nico Pérez Terrane, seems to indicate that the Piedra Alta Terrane was the ultimate origin of the above mentioned Paleoproterozoic cluster in the Playa Hermosa Formation. Therefore, we suggest that the main source area of the Playa Hermosa Formation was the Piedra Alta Terrane, although minor inputs from the Nico Pérez cannot be excluded. The sedimentological features and internal architecture of the Maldonado Group, together with the variations observed in the zircon age distribution in all the three samples, most likely reflects tectonic adjustments during basin(s) infill, and thus, changes in the contribution of the source areas. At first glance, when combining the youngest detrital zircon populations of the Las Ventanas and Playa Hermosa formations at their respective

type areas, we can conclude that the maximum age of the deposition is ~595 Ma. However, if we also consider the data from conglomerates (Las Ventanas Formation) near Minas city, the maximum age can be further constrained to ~570 Ma. This last age is within error of that obtained in basal volcanoclastic rocks of the Las Ventanas Formation at its type area dated by U-Pb SHRIMP to  $573 \pm 11$  Ma (Oyhantçabal et al., 2007). Hence, we suggest that the deposition of both units started between 570 and 562 Ma, as indicated by the maximum age for the Minas conglomerates and the youngest age possible for the volcanoclastics, respectively.

The age pattern for the San Carlos Formation shows a strong contribution from a Neoproterozoic basement that can be correlated with the gneissic-migmatitic and intrusive rocks of the Cuchilla Dioniso Terrane (Table 3.1). Although the Cuchilla Dioniso Terrane and the Nico Pérez-Piedra Alta terranes were amalgamated in the mid-Ediacaran and before the deposition of the San Carlos Formation (Pecoits et al., 2004; 2008; Oyhantçabal et al., 2009), the absence of typical ages recorded in the Piedra Alta and Nico Pérez terranes strongly suggests that these blocks were not source areas for the sediments of the San Carlos Formation. However, the occurrence of Meso- and Paleoproterozoic ages account for some contribution from the Edén Terrane, which typically shows the same ages (Table 3.1). A maximum depositional age for the unit is constrained by the youngest zircon cluster at  $552 \pm 3$  Ma. Showing similar features to the Playa Hermosa and Las Ventanas formations, the San Carlos Formation was informally included in the Maldonado Group until new data became available (Pecoits et al., 2004). In this regard, two scenarios were proposed by the same authors: (1) the San Carlos Formation, along with the Las Ventanas and Playa Hermosa formations, were deposited in the same basin, which subsequently was dismantled by the Sierra Ballena Shear Zone (Figure 3.2), or (2) the Maldonado Group *s.s.* and the San Carlos Formation, although most likely contemporaneous, were deposited in different basins. Based on the new data presented here, we suggest that the San Carlos Formation was deposited in a different basin whose main source was its own basement. Taking into account the youngest zircon cluster observed in the San Carlos Formation ( $552 \pm 3$  Ma), it seems that the initiation of deposition could have occurred slightly later (~10 Ma) than that in the Playa Hermosa and Las Ventanas formations, although they probably overlapped during basin infill.

The Barriga Negra Formation shows a zircon age spectra typical of that found in the basement of the Nico Pérez Terrane, ranging from ~1,750 to 3,400 Ma (Table 431). Similar to samples from the Las Ventanas Formation, there are some few grains (three) between ~1,000 and 1,500 Ma. The two zircons with ages at ~1,300-1,500 Ma could be sourced from the Edén Terrane, while that at ~1,000 Ma probably corresponds to reworking of the underlying Arroyo del Soldado Group outcropping in the area. A Cuchilla Dionisio source for this zircon is discounted based on the lack of the more widespread Neoproterozoic ages found in this terrane (Table 3.1 and Figure 3.2). The youngest zircon population constrains the maximum depositional age of the Barriga Negra Formation to  $\sim 581 \pm 6$  Ma, which fits well within the chronostratigraphic framework established for the Las Ventanas and Playa Hermosa formations. As for the Maldonado Group, the San Carlos Formation and other Ediacaran units (e.g., Sierra de Aguirre Formation), the ubiquitous occurrence of Ediacaran zircons clearly suggests the presence of active magmatic activity at that time and the contemporaneous development of extensional basins, some of them accompanied with important volcanic activity in both the Nico Pérez and Cuchilla Dionisio terranes (see section 3.5.2 below).

Recent work by Aubet et al. (2014) showed compelling evidence demonstrating the existence of an angular unconformity between the slightly deformed Barriga Negra Formation (above) and the strongly deformed Arroyo del Soldado Group (below), and thus both units are demonstratively unrelated (see also Fragoso-Cesar et al., 1987; Fambrini et al., 2005). Therefore, the age presented here constraining the maximum depositional age for the Barriga Negra Formation ( $581 \pm 6$  Ma), also helps to constrain the minimum age for the Arroyo del Soldado Group. A similar maximum age constraint of  $\sim 589$  Ma for the Barriga Negra Formation was presented by Blanco et al. (2009). Although the data presented by the authors have been strongly questioned (see for example Sánchez-Bettucci et al., 2010; Zimmermann, 2011; Aubet et al., 2014) some general comparison can be made. Besides the youngest cluster ( $\sim 589$  Ma), Blanco et al. (2009) reported a couple of important peaks at 1,795-1,723, 631-566, and 2,890-3,155 Ma with only two grains around 2,157-2,284 Ma. As described above, our zircon age spectra is also characterized by Paleoproterozoic and Archean ages but it is noteworthy the absence of the 1,795-1,723 Ma cluster reported by Blanco et al. (2009). The sample

dated by these authors comes from the middle-lower part of the Barriga Negra Formation, while our sample was taken from the upper most part of the unit. This difference, together with the sedimentological features of the succession, indicates active tectonism and changing source areas during deposition. In this scenario, the lower section of the Barriga Negra Formation would be dominated by Paleoproterozoic zircons sourced from the Edén Terrane (~1,740-1,750 Ma, Campanero Unit), located to the southeast (Figure 3.3). Paleocurrent measurements obtained in the succession further support this source area (Fambrini et al., 2005). In contrast, the upper half of the unit is dominated by Ediacaran zircons (~581 Ma) and early Paleoproterozoic and Archean zircons from local granites and basement rocks of the Nico Pérez Terrane, respectively (Figure 3.3).

### ***3.5.2. Chronostratigraphy and geological setting***

The evolution of the Neoproterozoic Dom Feliciano Belt in Uruguay has been subject of many geotectonic interpretations. Proposals have included subduction models towards the east and the west accompanied by the development of one or more volcanic arcs. For example, Frago-Cesar (1980) proposed subduction to the west, which would have produced a magmatic arc represented by the granite domain (Aiguá Batholith) of the Cuchilla Dionisio Terrane (Figure 3.1). Based on this model, it was later suggested a back arc basin represented by the Neoproterozoic supracrustal succession (schist domain) was located to the west of the magmatic arc (Fernandes et al., 1992; Sánchez-Bettucci and Ramos, 1999). In contrast, other models suggested the existence of a passive margin represented by the Arroyo del Soldado Group, which evolved from rift deposits of the Maldonado Group (e.g., Gaucher et al., 2008; Blanco et al., 2009). In an attempt to reconcile this inconsistency, Basei et al. (2000) suggested that the strata assigned to a passive margin setting (Arroyo del Soldado Group) were deposited instead in a foreland basin along with the volcano-sedimentary Maldonado Group, and that the rest of the supracrustal rocks belonging to the schist domain (e.g., Fuente del Puma Formation) were produced in a different context to that of the magmatic arc (see also Pecoits et al. 2008). Hence, Basei et al. (2000; 2005; 2008) proposed eastward subduction toward the Kalahari Craton building up the granite domain, and that this granite belt (i.e., magmatic arc) and the schist domain were juxtaposed later during a late Brasiliano Event. Oyhantçabal et al.

(2007) proposed a west-directed subduction and suggested that slab beak-off was the most likely mechanism associated with the generation of the granitic magmas shortly after the collision, and thus the granites (Aiguá Batholith) were not part of the magmatic arc.

In a recent study, Aubet et al. (2014) concluded that the stratigraphic model suggesting the evolution from a rift basin (Maldonado Group) to a passive margin setting (Arroyo del Soldado Group) is not supported by stratigraphic relations. Indeed, when detrital zircon age spectra of the Playa Hermosa and Las Ventanas formations (Maldonado Group) are compared to those of the Yermal Formation (Arroyo del Soldado Group), it is clear that differences in their tectonic settings exist. The Maldonado Group record important Ediacaran zircon clusters, whilst the Yermal Formation does not record ages younger than ~1,036 Ma (Gaucher et al., 2008; Blanco et al., 2009; this study). This is not a trivial aspect given the voluminous record of Ediacaran magmatism in the region, particularly in the Nico Pérez Terrane, which is the basement of the Arroyo del Soldado Group. Furthermore, this magmatism is accompanied by marked strike-slip tectonics, which also contradicts the idea of an Atlantic-type continental shelf during the Ediacaran-lowermost Cambrian, as proposed for the Arroyo del Soldado Group (Gaucher et al., 2008; Blanco et al., 2009). Therefore, our data indicates that the Maldonado Group is younger than the Arroyo del Soldado Group. The same conclusion was reached by Aubet et al. (2014), where the authors presented an extensive review of the stratigraphy, radiometric ages and existing models for the origin of those basins.

As shown in the present study, this tectono-magmatic activity is clearly recorded in the Maldonado Group, and in the San Carlos and Barriga Negra formations as evidenced by the presence of Ediacaran zircon ages in all these units - these are totally absent in the Arroyo del Soldado Group. With the exception of the San Carlos Formation, which is developed on the Cuchilla Dionisio Terrane, detrital zircons between ~1,000 and 650 Ma are lacking in all the units studied here. This would suggest that magmatism was absent during that time in the Nico Pérez Terrane. Significantly, zircons younger than 1,036 Ma are also absent in the Yermal Formation of the Arroyo del Soldado Group. This is further supported by the lack of magmatic ages at that time in Piedra Alta and Nico Pérez terranes (Aubet et al., 2014), which explains their absence in the Barriga Negra

Formation, Maldonado and Arroyo del Soldado groups. When U-Pb ages of the basement are considered (Table 3.1), it appears as though the last magmatic events (prior to deposition of the Arroyo del Soldado Group) in the Nico Pérez and Edén terranes occurred at ~1,785 and ~1,430 Ma, respectively (Figure 3.6). This is further supported by considering all the available U-Pb, Rb-Sr and K-Ar ages of the basement, which shows that the same gap exists Aubet et al. (2014; their Figure 5). Similarly, the first magmatic event after deposition of the Arroyo del Soldado Group is represented by the Puntas del Santa Lucía Batholith at ~633 Ma (Table 3.1). Hence, we suggest that the mixed carbonate-siliciclastic Arroyo del Soldado Group was deposited in a shallow epicontinental sea that transgressed the Nico Pérez Terrane between ~1,000 and 650 Ma (Figure 3.6).

A radically different tectonic setting has been proposed for the Playa Hermosa, Las Ventanas, San Carlos and Barriga Negra formations. Masquelin and Sánchez-Bettucci (1993) suggested that Las Ventanas and Playa Hermosa formations were deposited in a pull-apart basin. Later, Pecoits et al. (2008) proposed a strike-slip system for the Maldonado Group and the San Carlos Formation. A similar tectonic regime was also indicated for the Sierra de Aguirre (Campal and Schipilov, 2005) and Barriga Negra formations (Fambrini et al., 2005). A comparable scenario has been proposed for the Ediacaran-Early Cambrian (605-530 Ma) basins (e.g., Camaquã, Castro and Itajaí basins) in southern Brazil (Almeida et al., 2010). However, those authors suggested an extensional origin for this basin system and concluded that the strike-slip deformation occurred after basin formation, in the Early Cambrian. In Uruguay, the Ediacaran basins are spatially related to major strike-slip faults and seem to be directly related to the tangential collisional event. Furthermore, typical structures found in strike-slip basins, such as post-diagenetic inverse faulting in the Playa Hermosa Formation Masquelin and Sánchez-Bettucci (1993), apparent migration of the depocentre in the Las Ventanas Formation (Pecoits et al., 2011), and the rhombohedral shape of the Sierra de Aguirre Basin (Campal and Schipilov, 2005) have all been suggested. Most importantly, and as shown by radiometric ages, the synchronicity between deposition and regional shearing, at least for the best-constrained basins, seems clear. Therefore, we suggest that the deposition of the Maldonado Group (<562-570 Ma), Sierra de Aguirre Formation (571±8

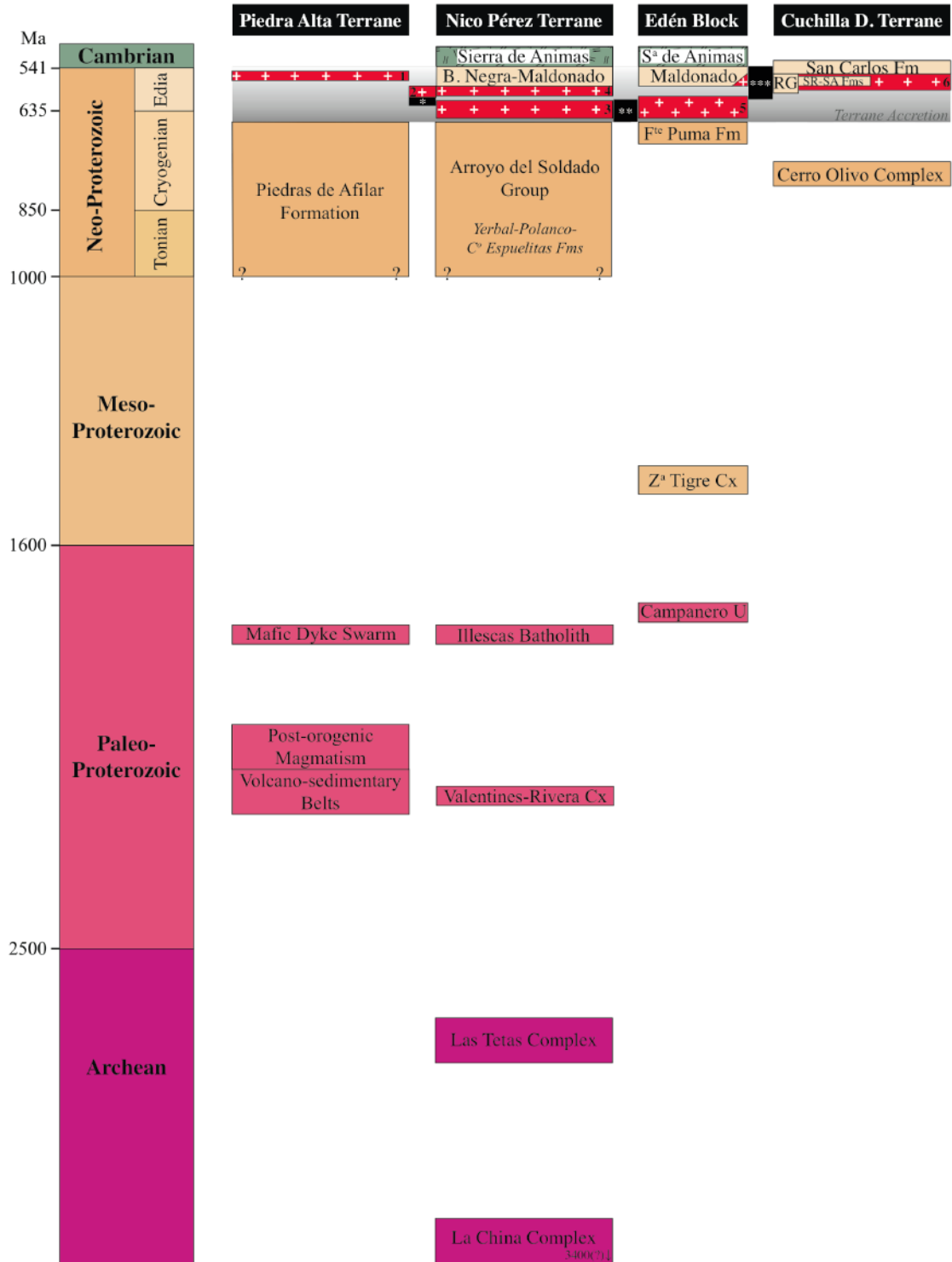


**Figure 3.6.** Stratigraphic columns for tectono-stratigraphic terranes of Uruguay. Time scale from Gradstein et al. (2012). Granites: (1) La Paz (Rb/Sr age); (2) Solís de Mataojo; (3) Puntas del Santa Lucía; (4) Sobresaliente, Mangacha, Las Flores; (5) Mataojo; (6) Tacuarí, Aiguá, Florencia, Maldonado. FP: Fuente del Puma Formation; RG: Rocha Group; SR-SA: Sierra de Ríos and Sierra de Aguirre formations. Accretionary events: (\*) Piedra Alta; (\*\*) Edén; (\*\*\*) Cuchilla Dionisio.

Ma), and Barriga Negra Formation ( $<581\pm6$  Ma) overlaps with the synkinematic granites, ranging from  $584\pm13$  (Solís de Mataojo Granite) to  $564\pm7$  Ma (Maldonado Granite), which support that these faults were active during basin infill.

One crucial aspect recognized by Aubet et al. (2014) is the difficulty in distinguishing between volcanic rocks previously assigned to the older volcanic pulse of the Sierra de Animas Complex, which were thought to be interdigitated with the Maldonado Group, and those traditionally assigned to Neoproterozoic Fuente del Puma Formation (ex Lavalleja Group) in the type area of the Las Ventanas Formation (Figure 3.2). Unfortunately, the geochronological data from the Fuente del Puma Formation is scarce. Basei et al. (2008) reported U-Pb SHRIMP detrital zircon ages from one quartz-sericite schist of this unit showing seven Archean zircons (2,600-3,400 Ma), six between (1,780-2,400 Ma), and five Neoproterozoic ages between 600 and 1,060 Ma, with three values close to the youngest age (data not presented). However, Oyhantçabal et al. (2005) pointed out that zircon ages younger than 650 Ma are highly discordant, and thus only one single zircon dated at  $715\pm26$  Ma would constrain the maximum depositional age of the unit. Sánchez-Bettucci et al. (2003) also reported some preliminary conventional U-Pb ages on zircon (four analyses) and one rutile from a metabasalt of this unit. According to the same authors (data not presented), it yielded a possible crystallization age of  $667\pm4$  Ma and a metamorphic age of  $624\pm14$  Ma. Hence, by combining the magmatic, metamorphic and detrital zircon ages reported for the Fuente del Puma Formation, magmatism and deposition seems to have occurred roughly between 660 and 690 Ma.

At its type area, the Las Ventanas Formation overlies the Mesoproterozoic Zanja del Tigre Complex with a marked angular unconformity, whereas its relation with the underlying volcanic and sedimentary rocks traditionally assigned to the Fuente del Puma Formation is less clear (Figure 3.2). In the first instance, this basement-cover relationship is clearly reflected in the detrital zircon spectra of the Las Ventanas Formation, which contains Mesoproterozoic zircon grains of the Zanja del Tigre Complex (see above). However, this is not the case for the Fuente del Puma Formation; i.e., being the Fuente del Puma Formation the basement of the Las Ventanas Formation, this is not reflected in the detrital age spectra of the latter. In this sense, there is a clear absence of magmatism between 1,000 and  $590\pm5$  Ma in the Las Ventanas Formation at its type area where the

relationships with its basement (Fuente del Puma Formation and Zanja del Tigre Complex) is observed. Interestingly, Oyhantçabal et al. (2007) obtained an U-Pb SHRIMP age of  $573\pm 11$  Ma for volcanoclastic rocks of the Fuente del Puma Formation immediately underlying the Las Ventanas Formation. This age is similar to that reported by Mallmann et al. (2007) at  $590\pm 2$  Ma in gabbros also correlated by the same authors to the Fuente del Puma Formation. These ages are recorded in the detrital zircon spectra of the Las Ventanas Formation and indicate that the magmatism assigned to the Fuente del Puma Formation took place in two stages, approximately at 667, and from 590 to 560 Ma. Therefore, it can be concluded that while the first stage corresponds to the Fuente del Puma Formation in the strict sense, which did not constitute a source area for the Las Ventanas Formation, the younger magmatism is coeval with the deposition of the Las Ventanas Formation and would rather be part of this unit.

Although further geochronologic studies are necessary to better constrain the Fuente del Puma Formation (*sensu stricto*), these ranges agree with the magmatic and detrital zircon data presented by Sánchez-Bettucci et al. (2003), Mallmann et al. (2007), Oyhantçabal et al. (2007) and Basei et al. (2008), and with the detrital zircon spectra reported in this study for the Las Ventanas Formation. We suggest that the volcanic rocks of the Las Ventanas Formation, previously assigned to the Fuente del Puma Formation, might represent the base of the rift basin wherein the Las Ventanas Formation was later deposited, accompanied and capped by volcanism of the Sierra de Animas Complex. A similar scenario was described for contemporaneous Ediacaran basins in southern Brazil where age constraints demonstrated that the Brazilian basins were formed between 605 and 530 Ma, and they record two major periods of basin formation and volcanic activity from 605 to 570 Ma and from 550-535 Ma (Almeida et al., 2010). The first period is characterized by thick volcano-sedimentary successions related to basic and intermediate volcanic rocks, with minor acid volcanics, and the second period is characterized by thick siliciclastic successions and discrete events of acid volcanism (Almeida et al., 2010). If the correlation suggested here between volcanic rocks once considered part of the Fuente del Puma Formation and basal volcanics of the Las Ventanas Formation is confirmed, an extensional origin for this basin, as suggested for the Ediacaran-Early Cambrian in southern Brazil (Almeida et al., 2010), is the most likely scenario.

### *3.5.3. Accretion of the Piedra Alta and Nico Pérez Terranes*

One important question regarding the configuration of the Río de la Plata Craton is, when did the Piedra Alta and Nico Pérez terranes accrete? This craton has been long considered as a single unit that was in place at least ~1,200 Ma (Bossi and Ferrando, 2001). However, in a recent review, Oyhantçabal et al. (2011) did not include the Nico Pérez Terrane in the Río de la Plata Craton and pointed out that the accretion age is poorly constrained between approximately 1,750 and 600 Ma. The last important movement of the Sarandí del Yí Shear Zone, which separates the Piedra Alta and Nico Pérez terranes, is geochronologically constrained (using U-Pb on sphene) by the age obtained for the emplacement of the syntectonic Solís de Mataojo Granitic Complex at  $584 \pm 13$  Ma (Oyhantçabal et al., 2007). The Paleo- or Mesoproterozoic age for accretion is based on the idea that the Piedra Alta mafic dyke swarm, dated at  $1,790 \pm 5$  Ma (U-Pb on baddeleyite; Halls et al., 2001), is affected by the Sarandí del Yí Shear Zone where the apparent curvature of the eastern end of the dyke swarm ('drag fold') is consistent with a dextral shear sense (Bossi and Campal, 1992) and not with the sinistral sense recorded during the intrusion of the Ediacaran Solís de Mataojo Granitic Complex (Oyhantçabal et al., 2007). Low-grade hydrothermal overprint in two felsic veins and one associated dyke dated between 1,370 and 1,170 Ma (Ar-Ar and Rb-Sr; Teixeira et al., 1999) and one K-Ar age of  $1,253 \pm 32$  Ma (data not presented by the authors) for a synkinematic muscovite located on a thrust plane in the Nico Pérez Terrane have been interpreted to support the accretion of both terranes during the Mesoproterozoic (Bossi and Cingolani, 2009).

Extensive fieldwork has not confirmed the curvature of the Piedra Alta mafic dykes. The problem is probably rooted in the fact that most of these mafic dykes were identified in aerial photographs and only a small fraction could actually be recognized in the field. Hence, numerous dykes and the mentioned curvature simply correspond to photo-lineaments whose origins are not clear. The only unit that seems to have been dextrally deflected is the Cuchilla Cabo de Hornos Shear Zone (Spoturno et al., 2004). This shear zone is composed of mylonites deriving from granitic and para-metamorphic protoliths of the Piedra Alta Terrane, and although no ages are available, a Paleoproterozoic age for the mylonites was inferred (Spoturno et al., 2004); the age of deflection and its relationship with the Sarandí del Yí Shear Zone remains unknown.

Furthermore, the use of few K-Ar and Rb-Sr ages on both sides of the Sarandí del Yí Shear Zone to place constraints on the age of accretion is very speculative. Teixeira et al. (2002) hypothesized that reactivation of the fault systems, which controlled the emplacement of the dyke swarm, could have been the probable mechanism through which low temperature hydrothermal fluids disturbed the K-Ar and Rb-Sr isotopic systems. Unfortunately, the nature and extension of this event remains unclear. Similarly, the K-Ar age reported from a pegmatite in a thrust plane in the Nico Pérez Terrane is located more than 10 km away from the Sarandí del Yí Shear Zone and not in the transcurrent shear itself; the relationship between these two structures also remains unknown (Oyhantçabal et al., 2011).

The analysis of detrital zircon spectra from Neoproterozoic sedimentary successions deposited on both sides of the Sarandí del Yí Shear Zone can shed some light on this issue. The Piedras de Afilar Formation is the only known sedimentary succession deposited on the Piedra Alta Terrane. As explained below, the lack of Neoproterozoic (<1,000 Ma) detrital zircons, the absence of detrital zircons typically found in basement rocks of the neighboring Nico Pérez Terrane (located to the east), and the lack of evidence indicating a source from the western margin of the Río de la Plata Craton (proto-Andes) suggests that the Piedras de Afilar Formation was most likely deposited between 1,000 and 650 Ma, and that the Piedra Alta and the Nico Pérez terranes were not attached at that time. Previous proposals considered the Piedras de Afilar Formation as Ediacaran in age, while its Mesoproterozoic zircons (1,000-1,500 Ma) were likely sourced from the proto-Andean Mesoproterozoic Belt (Gaucher et al., 2008). However, the available evidence does not support this interpretation. If an Ediacaran age is considered, the absence of Neoproterozoic (pre-Ediacaran) zircons in the Piedras de Afilar Formation, which are extensively represented in the Nico Pérez Terrane, cannot be explained. Moreover, the extensive magmatic and tectonic activity recorded in the Ediacaran is not compatible with the stable tectonic setting for the Piedras de Afilar Formation (Pecoits et al., 2008). While the maximum depositional age for the Piedras de Afilar Formation is constrained by the youngest detrital zircon cluster recorded at ~1,000 Ma, its minimum depositional age is placed at  $584 \pm 13$  Ma, which corresponds to the synkinematic magmatism recorded in the Sarandí del Yí Shear Zone. Additionally, the

absence of Neoproterozoic ( $\leq 650$  Ma) detrital zircons mirroring source areas from the once approaching Nico Pérez Terrane (i.e., the proximity of this terrane should have caused input of  $\leq 650$  Ma zircons), suggests a minimum depositional age of  $\sim 650$  Ma.

The Piedras de Afilar Formation shows 99% of the zircons with ages between 1,000-2,070 Ma (Gaucher et al., 2008). Although one can argue that some of these zircons could be sourced from the Nico Pérez Terrane, the lack of typical Archean and Paleoproterozoic zircons in the Piedras de Afilar Formation, which are common in the Nico Pérez Terrane, argues against a source from this terrane. Of particular importance for our analysis are the zircon clusters between 1,000 and 1,900 Ma in the Piedras de Afilar Formation. Older populations ( $\sim 2,000$  Ma) most likely derived from the local basement of the unit (Table 3.1). For most of these Mesoproterozoic zircons a proto-Andean source was proposed (Gaucher et al., 2008). In this regard, the basement of the Andes is formed by different blocks showing Grenville affinities, such as Chilenia, Cuyania, Antofalla, Arequipa, among others (Ramos, 2010). Particularly important for our discussion are those blocks that were left in Gondwana after the break up of Rodinia and could be part of the source areas of the Piedras de Afilar Formation. Such is the case of Pampia, which remained attached to Amazonia after the Rodinia amalgamation and never detached from it (Ramos et al., 2010). The Pampia terrane was part of the Rodinia supercontinent during the Mesoproterozoic with a Neoproterozoic ocean in its eastern side, which separated the Pampean terrane from the Río de la Plata Craton (Pampean, Brasiliano or Clymene Ocean) (Rapela et al. 2007; Cordani et al., 2009). Escayola et al. (2007) pointed out that the western part of this terrane has a strong Grenville-age source while the eastern margin shows a Brasiliano source with ages between 700 and 600 Ma. They suggested a west-dipping subduction starting at  $\sim 700$ -650 Ma between the Pampia and Río de la Plata blocks, with the development of an island arc and associated back arc basin. This Neoproterozoic magmatic arc system was the source area of the Neoproterozoic zircons found in the pampean metasediments. Further to the north, correlative rocks of the Puncoviscana Formation (late Neoproterozoic-Early Cambrian) and the overlying Mesón Group (Late Cambrian) also show a predominance of Late Neoproterozoic zircons characteristic of the widespread Brasiliano Orogeny of south central and southeast Brazil (Adams et al., 2011). The presence of an ocean basin

separating the Pampia and the Río de la Plata cratons and the absence of Neoproterozoic zircons (<1,000 Ma) in the Piedras de Afilar Formation, therefore, argue against proto-Andes being its source area. Furthermore, nearly all the Neoproterozoic-Cambrian samples reported by Escayola et al. (2007) and Adams et al. (2011) show Mesoproterozoic detrital zircon spectra different from those displayed by the Piedras de Afilar Formation.

On the other hand, Paleoproterozoic zircons are almost absent from the provenance patterns of the above-mentioned Argentinian Neoproterozoic successions, suggesting that there was little contribution from the Río de la Plata Craton (Escayola et al., 2007; Adams et al., 2011). In turn, the Late Cambrian Mesón Group shows abundant Paleoproterozoic zircons (Adams et al., 2011). This clearly suggests that the Río de la Plata and Pampia were not attached in the Neoproterozoic (e.g., Rapela et al., 2007; Ramos et al., 2010), and thus a proto-Andean source for the Piedras de Afilar Formation during the Ediacaran finds no support. In this regard, it has been suggested that Amazonia, Pampia and Arequipa-Antofalla cratonic blocks were part of the Rodinia supercontinent (Brito Neves et al., 1999; Kröner and Cordani, 2003) whereas São Francisco, Paranapanema and Río de La Plata cratons were separated from those by the Transbrasiliano lineament Cordani et al. (2009). In this model, the Neoproterozoic-Early Cambrian Araguaia-Paraguai-Pampean belts were formed (along this lineament) and represent the main suture for closing the Clymene (Brasiliano) Ocean (Rapela et al. 1998; Escayola et al., 2007; Ramos et al. 2010). Hence, the eastern margin of Pampia represents the southern extension of the Transbrasiliano lineament, which juxtaposed the Río de La Plata Craton and Pampia (Ramos et al. 2010). Differences exist in terms of the tectonic juxtaposition model. According to Rapela et al. (2007), the Río de la Plata craton was juxtaposed obliquely to the Pampean orogen, whereas Escayola et al. (2007) and Ramos et al. (2010) favored an orthogonal collision. In any case, the Río de la Plata Craton likely accreted by the Early Cambrian when it became the source for Paleoproterozoic detrital zircons in Mid- to Late Cambrian and Ordovician successions (Adams et al., 2011; Verdecchia et al., 2011). Later during the Late Cambrian-Early Ordovician, a significant displacement of the Pampia terrane with respect to the Río de la Plata (and other Gondwana cratons) through a dextral strike-slip shear positioned both cratons into their

final position (Spagnuolo et al., 2012). Therefore, the detrital zircon ages gathered from the Piedras de Afilar Formation further support the allochthony of the Piedra Alta Terrane (Río de la Plata Craton after Oyhantçabal et al. (2011)) with respect to Pampia and the Nico Pérez terranes.

Further evidence indicating the exotic nature of the Piedra Alta Terrane with respect to the Nico Pérez Terrane comes from the detrital age spectra of the Arroyo del Soldado Group, located to the east of the Sarandí del Yí Shear Zone. Considering the available U-Pb ages from the Nico Pérez basement, nearly all the detrital zircons from the Arroyo del Soldado Group can be readily explained as being sourced from it (see section 3.5.1). The only exception is the relatively small late Mesoproterozoic cluster (~1,050 Ma). Rocks of this age are unknown in the Nico Pérez Terrane, and thus three possible explanations are put forward here to explain the presence of these zircons in the Arroyo del Soldado Group: (1) Mesoproterozoic (~1,050 Ma) rocks have not yet been found in the Nico Pérez Terrane, (2) they were eroded away, or (3) these zircons were sourced from a now distant Mesoproterozoic belt. For the same reasons mentioned above for the Piedras de Afilar Formation, a Proto-Andean Mesoproterozoic source on the western side of the Río de la Plata Craton cannot explain the zircons found in the Arroyo del Soldado Group. A Piedras de Afilar source (reworking) can be also discounted for these Mesoproterozoic zircons because the Arroyo del Soldado Group does not record the same age spectrum shown by the Piedras de Afilar Formation. This implies that different areas sourced these units. It also supports the suggestion that the Nico Pérez and the Piedra Alta terranes were not accreted at the time of the Piedras de Afilar Formation and Arroyo del Soldado Group deposition.

Additional support for a Neoproterozoic accretion comes from Nd isotope data. In this regard, all the samples of the Piedras de Afilar Formation only plot within the range defined by basement rocks of the Piedra Alta Terrane (Figure 3.7A). Conversely, the Yermal and Polanco formations (Arroyo del Soldado Group), and the Cerros San Francisco Formation (Arroyo de la Pedrera Group) plot within the field of the Nico Pérez Terrane (Figure 3.7B). While all the samples from the Arroyo de la Pedrera Group only plot within the field defined by this terrane some of the samples of the Yermal and Polanco formations also overlap with that of the Piedra Alta Terrane. Nevertheless, the

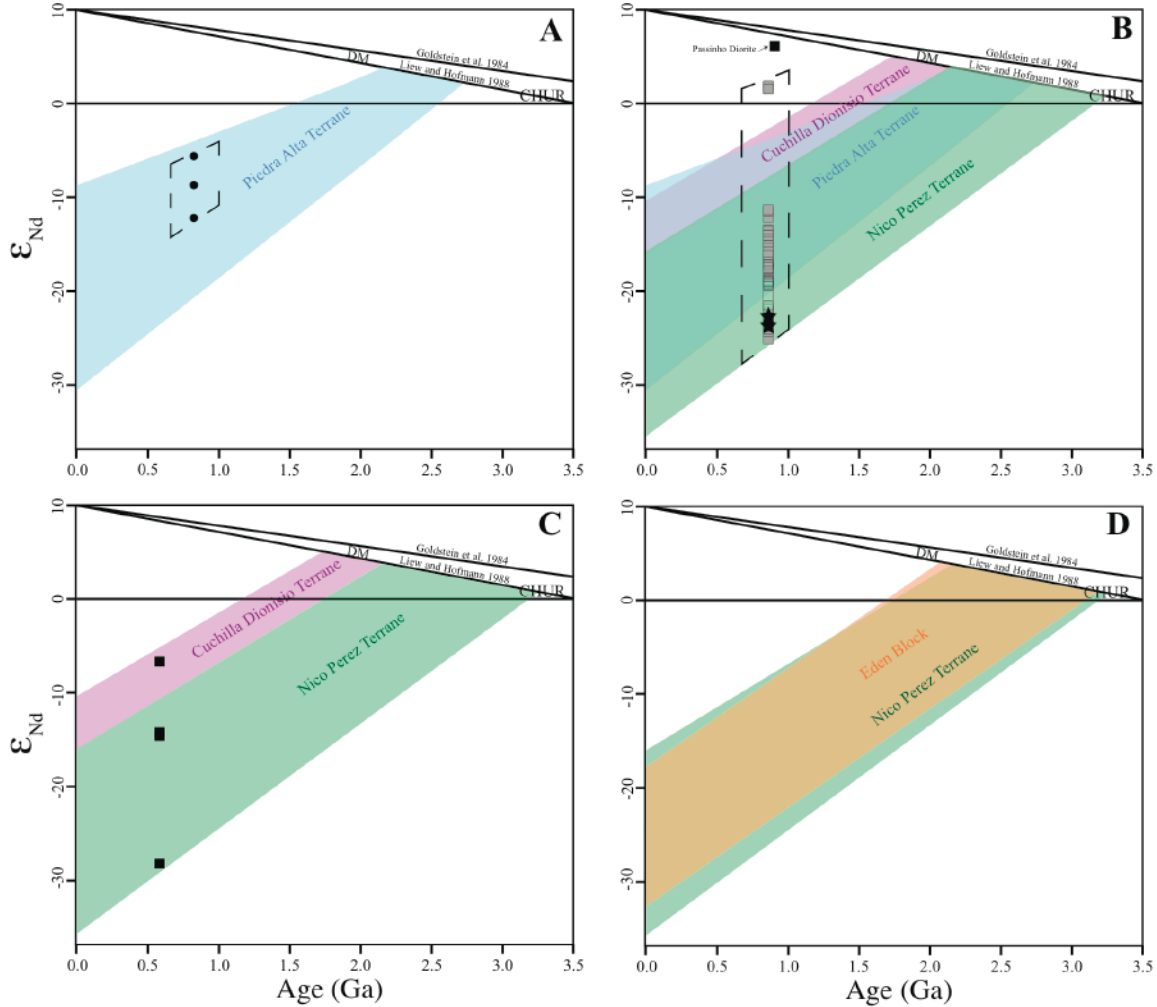


**Figure 3.7.** Diagrams of  $\epsilon_{Nd}(t)$  vs. time (Ma). Compilation of Sm-Nd isotope compositions for **(A)** Piedras de Afilar Formation (n=3); **(B)** Yerbal Formation (grey squares, n=76) and Polanco Limestones (empty squares; n=22) formations (Arroyo del Soldado Group), and Cerros San Francisco Formation (black stars, n=2; Arroyo de la Pedrera Group); **(C)** Barriga Negra Formation (n=4). Composition fields of metasedimentary and metaigneous rocks from Piedra Alta, Nico Pérez and Cuchilla Dionisio terranes are shown for reference. **(D)** Composition fields from Edén and Nico Pérez terranes. Data in A and B were plotted arbitrarily at 850 Ma but would plot somewhere within the dash-outlined areas between ~650 and 1,000 Ma. Source of data: Bossi et al., 1993; Mazzuchelli et al., 1995; Rivalenti et al., 1995; Cingolani et al., 2002; Pankhurst et al., 2003; Gastal et al., 2005; Preciozzi and Peel, 2005; Peel and Preciozzi, 2006; Mallmann et al., 2007; Blanco et al., 2009; Oyhantçabal et al., 2011; Frei et al., 2011; 2013. DM: depleted mantle evolution lines after Goldstein et al. (1984) and Liew and Hofmann (1988). CHUR: chondrite uniform reservoir after DePaolo and Wasserburg (1976).

fact that not all of them do likely indicates that the source area for both of these units was the Nico Pérez Terrane. It is also noteworthy that the two northernmost samples of the Yermal Formation show positive  $\epsilon\text{Nd}(t)$  values and do not overlap with any field defined by basement rocks of Uruguay (Figure 3.7B). One possibility is that these rocks, attributed to the Yermal Formation in the Isla Cristalina de Rivera (Figure 3.1), do not belong to this unit. Another scenario is that the Yermal Formation, at least its northernmost part, was sourced by rocks belonging to the São Gabriel Block in southern Brazil (Figure 3.1). In contrast to the crustal reworking shown by other adjacent crustal blocks, including those located in Uruguay, Sm-Nd analyses of the São Gabriel block indicate a juvenile origin for this unit (Gastal et al., 2005; Saalman et al., 2011). Particularly important for our analysis is the Passinho Diorite of the Cambaí Complex, with an age of  $\sim 880$  Ma (U-Pb SHRIMP, Leite et al., 1998), located in the southern part of the São Gabriel Block and which shows positive  $\epsilon\text{Nd}(t)$  values from +5.8 to +6.3 (Leite, 1997) (Figure 3.7B). In contrast to the Arroyo del Soldado Group (650-1,000 Ma), the Ediacaran Barriga Negra Formation ( $<581 \pm 6$  Ma) shows evidence of Nico Pérez and Cuchilla Dionisio sources (Figure 3.7C), which further supports the idea that both terranes were accreted in the Ediacaran, but before the deposition of this unit.

As stated above, the only dextrally deflected unit in the Piedra Alta Terrane is the Cuchilla Cabo de Hornos Shear Zone (Spoturno et al., 2004). Interestingly, Oyhantçabal (2005) suggested that the curvature shown by the Campanero Unit (Sierra de Cabral fold), located to the east of the Sarandí del Yí Shear Zone, represents the counterpart of the abovementioned structure and that both high temperature mylonitic foliations were rotated as a consequence of the activity of the dextral Sarandí del Yí Shear Zone. Unfortunately, no radiometric ages have been available to place constraints on the timing of this deflection, which would represent the accretion of the Piedra Alta and Edén terranes. Based on the ages obtained in this study, we suggest that this event took place between  $\sim 650$ - $585$  Ma, the minimum depositional age for the Arroyo del Soldado Group and the Piedras de Afilar Formation, and the sinistral shear reactivation of the Sarandí del Yí Shear Zone, respectively. As discussed in more detail in the following section, the accretion of the Edén Terrane, where the Sierra de Cabral fold occurs, took place  $\sim 650$ - $620$  Ma ago. Therefore, if the observation made by Oyhantçabal (2005) holds true, this

would indicate that the accretion of the Piedra Alta and Nico Pérez terranes occurred afterwards, approximately between 620-600 Ma (see section 3.5.4 below).

#### ***3.5.4. Paleogeographic and Paleotectonic Implications***

Paleogeographic reconstructions of the Río de la Plata Craton for the Meso- and Neoproterozoic differ widely. For example, Li et al. (2008) placed the Río de la Plata Craton at the heart of Rodinia adjacent to the southern Grenville margin of Laurentia between the Congo-São Francisco Craton and Laurentia, close to the Amazonia and Kalahari Cratons. In turn, Johansson (2014) positioned the Río de la Plata Craton at some distance away from Laurentia and Amazonia, and separated from the latter by a wide Brasiliano (Clymene) ocean embayment; i.e., not forming part of Rodinia. Although Johansson (2014) located the Río de la Plata Craton adjacent to the present-day west side of the Kalahari Craton, the author pointed out that a position in between this craton and the Laurentian margin cannot be ruled out (Figure 3.8A). The location of the Río de la Plata Craton between Laurentia and Congo cratons by Li et al. (2008) follows the idea of Fuck et al. (2008), who mentioned the occurrence of Mesoproterozoic units to the west (Pampia) and east (Cuchilla Dionisio Terrane) of the Río de la Plata Craton at its present position (Ramos and Vujovich, 1993; Preciozzi et al., 1999b; Basei et al., 2000). In the latter case, it is noteworthy that the basement rocks of the Cuchilla Dionisio Terrane were formerly correlated with the Namaqua Belt of South Africa (Preciozzi et al., 1999b; Basei et al., 2005; Basei et al., 2011). However, new studies have suggested a correlation with the Coastal Terrane of the Kaoko Belt located at the southwestern margin of the Congo Craton (Gross et al., 2009; Oyhantçabal et al., 2009; Konopásek et al., 2014). Thus, the idea proposed by Fuck et al. (2008), and followed by Li et al. (2008), at least for the eastern margin of the Río de la Plata Craton (the relation between its western margin and Laurentia is strongly debated), finds support in more recent regional studies. Nonetheless, as previously suggested (Pecoits et al., 2004; 2008; Oyhantçabal et al., 2009), and further supported in this study, the Cuchilla Dionisio Terrane attached to the Nico Pérez Terrane in the mid-Ediacaran, and the latter was attached to the Piedra Alta slightly later. Thus, the correlation between the Cuchilla Dionisio and Coastal terranes should not be used to place precise paleogeographic constraints on the Río de la Plata Craton before the

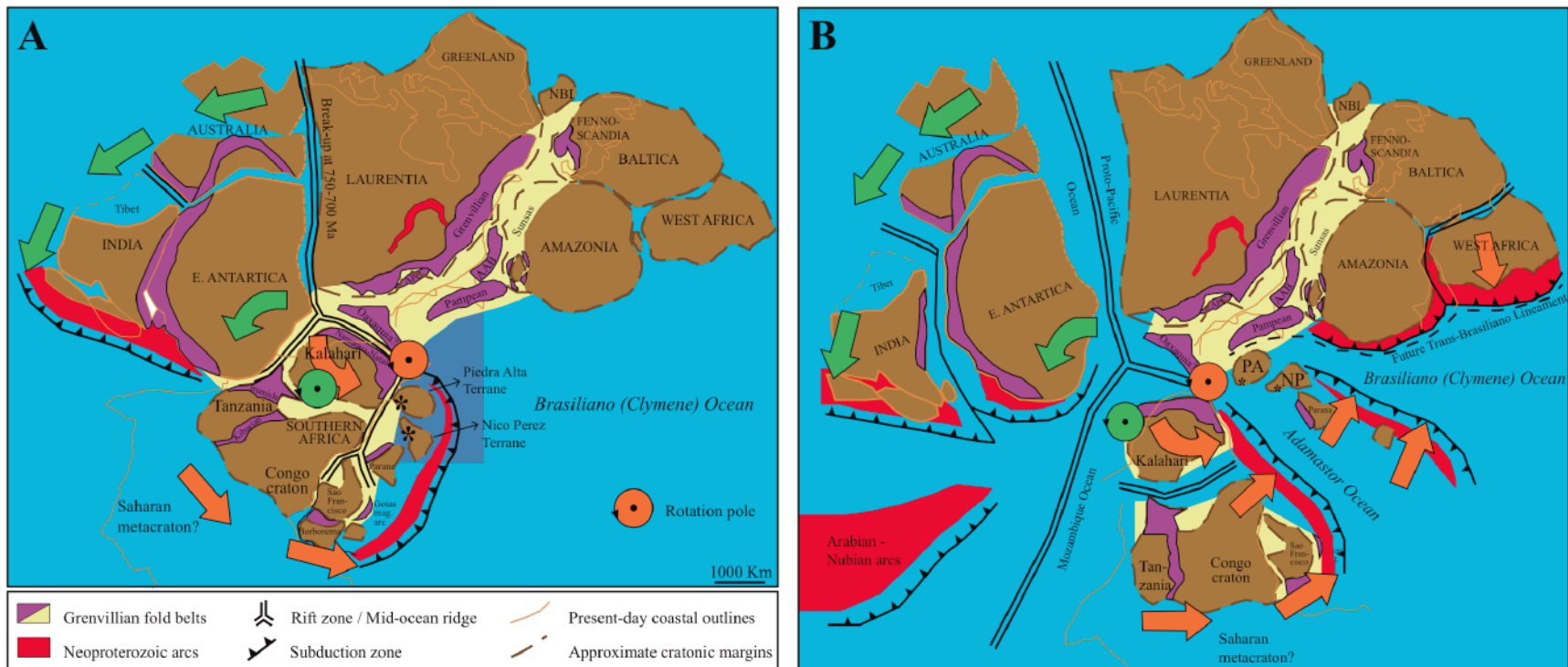


**Figure 3.8.** (A) Reconstruction of Rodinia showing the initial break-up of its western part at ca. 850-750 Ma. Piedras de Afilas (Piedra Alta Terrane=Río de la Plata Craton) and Arroyo del Soldado (Nico Pérez Terrane) basins indicated by asterisks. The dark blue shaded area indicates possible location of Piedra Alta and Nico Pérez terranes in the Clymene Ocean (see text for explanation). (B) Shift from Rodinia to Gondwana ca. 750-650. Modified from Johansson (2014). PA; Piedra Alta Terrane. NA; Nico Pérez Terrane.

Ediacaran when these terranes were independent blocks (Figure 3.8A). In turn, Johansson (2014) placed the Río de la Plata Craton attached to the Kalahari Craton through the Namaqua-Natal Belt based on the presence of Mesoproterozoic rocks of the Edén Terrane (Zanja del Tigre Complex). As for the Cuchilla Dioniso Terrane, the Edén Terrane is allochthonous with respect to the Río de la Plata Craton (i.e., the Piedra Alta and Nico Pérez terranes), and thus cannot be used either for paleogeographic reconstructions of the craton. Although both Li et al. (2008) and Johansson (2014) positioned the Río de la Plata Craton close to the Kalahari and Congo-São Francisco cratons, Johansson (2014) considered that all these blocks were not part of Rodinia (cf. Li et al., 2008).

Although it is still premature to draw a definite Paleogeographic model, the ages obtained in this and previous studies (Oyhantçabal et al., 2011; 2012 and references therein) accompanied with updated geological mapping (e.g., Spoturno et al., 2004; 2012) and a better understanding of the stratigraphy of the Neoproterozoic successions and their basement (Aubert et al., 2014) allow us to set a baseline for future research. As stated above, the Piedra Alta and the Nico Pérez terranes were independent blocks until ~620-600 Ma. The presence of clearly different Mesoproterozoic zircon age spectra in the Piedras de Afilar Formation and Arroyo del Soldado Group indicates that these units had different source areas and were deposited in different basins. We suggest that the position of the Piedra Alta and Nico Pérez terranes in Rodinia was somewhere in the Clymene (Brasiliano) ocean between the Laurentian and west Africa (Kalahari and Congo-São Francisco Cratons) as hypothesized by Johansson (2014) (Figure 3.8A). In this context, both sedimentary successions (Piedras de Afilar Formation and Arroyo del Soldado Group) were deposited in stable tectonic settings and sourced from the west-northwest (at present coordinates), and so any link with Mesoproterozoic orogenic systems should be located in that direction with respect to the Piedra Alta and Nico Pérez terranes. Likewise, any model should consider a stronger influence of Mesoproterozoic sources in the case of the Piedras de Afilar Formation (Piedra Alta Terrane) when compared with the Arroyo del Soldado Group (Nico Pérez Terrane).

The source of the Mesoproterozoic zircons in the Arroyo del Soldado Group (1,050 Ma) and the Meso- and upper Paleoproterozoic zircons (1,000-1,900 Ma) in the Piedras de Afilar Formation remains unknown. Regardless, these units clearly had

different source areas, which further supports that the Piedra Alta and Nico Pérez terranes were allochthonous with respect to each other at that time. Although both units show typical Grenville ages (900-1,300 Ma; Rivers, 1997), the Piedras de Afilar Formation also display detrital zircon populations between 1,350 and 1,900 Ma that are characteristic of Grenville basement areas, such as the Laurentian craton interior in North America (e.g., Thomas et al., 2004) or its counterpart at the southwestern corner of the Amazonian Craton in South America. The latter is represented by the Ventuari-Tapajós (2000–1800 Ma), Rio Negro-Juruena (1780–1550 Ma) and Rondonian-San Ignacio (1550–1300 Ma) tectonic provinces, whose orogenic evolution has been compared to that of the North American Grenvillian Province (Cordani et al., 2010). However, Laurentia along with some cratonic blocks from South America, including Amazonia, Pampia and Arequipa-Antofalla, were part of the Rodinia supercontinent, whereas São Francisco, Paranapanema and Río de La Plata cratons (along with Kalahari and Congo cratons from Africa) were separated from those by the Transbrasiliano lineament (Figure 3.8B) (Brito Neves et al., 1999; Kröner and Cordani, 2003; Cordani et al., 2009). If this holds true, the Piedras de Afilar (Piedra Alta Terrane) and the Arroyo del Soldado (Nico Pérez Terrane) were not sourced from Rodinia-Grenvillian Provinces. Based on available paleomagnetic data from Africa and South America, Tohver et al. (2006) placed the São Francisco-Congo, Kalahari and Río de la Plata cratons very close to each other and likely forming a single continental mass that agglutinated more or less contemporaneously to Rodinia. Therefore, some of the Mesoproterozoic mobile belts of central Brazil (e.g., Espinhaço) and central-southern Africa, collectively known as Kibaran (e.g., Kibaran, Irumide, Namaqua, Natal), formed between 1,400 and 1,000 Ma (Cordani et al., 2010 and references therein), are favoured here as the sources of the Uruguayan successions (Figure 3.8A).

The global reconfiguration from Rodinia to Gondwana (~850 to 650 Ma) has been described as a counterclockwise rotation of western and southern Rodinia, relative to a fixed Laurentia, Amazonia, Baltica and West Africa cratons with the concomitant opening of the Proto-Pacific ocean (west of Laurentia) and closure of the Brasiliano (Clymene) ocean (Johannsson, 2014) (Figure 3.8). It was during this reconfiguration that the Arroyo del Soldado Group was likely deposited and subsequently the basin was

closed. On a more regional scale, Saalman et al. (2011) suggested that following the subduction of oceanic crust beneath the Río de la Plata Craton margin in its northeastern side the collision of a microcontinent (Encantadas) with the Río de la Plata Craton and the São Gabriel Block (Figure 3.1) took place at ~730-690 Ma (São Gabriel Event). The presence of this microcontinent and the São Gabriel Event in Uruguay as responsible for the closure of the Arroyo del Soldado Basin, however, has not been previously discussed.

The Encantadas Block (in southern Brazil) comprises Paleoproterozoic (~2,200 Ma) basement rocks of the Encantadas Complex, the Porongos schist belt and to east, separated by the transcurrent Dorsal de Canguçu Shear Zone, the Pelotas batholith (Figure 3.1). In Uruguay, both units have been correlated with the Fuente del Puma Formation (ex-Lavalleja Group) and the Aiguá batholith, respectively. The Sierra Ballena Shear Zone is considered the southern extension of the Dorsal de Canguçu Shear Zone. In the first case, the available ages for the Fuente del Puma Formation (see above) and the Porongos belt (~790 Ma; Porcher et al., 1999; Saalman et al., 2011) differ greatly (~130-100 Ma). Nonetheless, more radiometric determinations are necessary to draw definite conclusions in this case. The Pelotas batholith comprises several suites of 635-590 Ma granites (Figure 3.1) and shows TDM model ages between 2,000 and 1,300 Ma (Saalman et al., 2011 and references therein). Similarly, the Aiguá Batholith, situated to the east of the Sierra Ballena Shear Zone, shows an age between 560 and 615 Ma (Table 3.1) and a TDM model age between 1,700 and 2,200 Ma (Figure 3.7B-C).

In contrast to the basement of these units in Brazil (Encantadas Complex), when the basement located on both sides of the Sierra Ballena Shear Zone in southern Uruguay is considered, some clear differences arise. The Edén Terrane, located to the west, comprises a Paleoproterozoic (~1,750 Ma) gneissic basement (Campanero Unit) and Mesoproterozoic supracrustal rocks of the Zanja del Tigre Complex (~1,430 Ma). In contrast, the Cerro Olivo Complex, situated to the east, comprises ortho- and para-derived metamorphic rocks with ages between 750 and 800 Ma for the magmatism and 650-600 Ma for the high-grade metamorphic event. Additionally, when TDM model ages from both sides of the Sierra Ballena Shear Zone are compared they also show differences. The Edén Terrane displays a TDM model age roughly between 2,100 and 3,300 Ma, which overlap with those of the Nico Pérez Terrane; see Figure 3.7D), while the Cuchilla

Dioniso Terrane shows younger ages between 1,700 and 2,200 Ma (Figure 3.7C). Other differences include: (1) the absence of inherited ~1,000 Ma zircons in ortho-derived rocks to the west of the Sierra Ballena Shear Zone, which are common in the Cerro Olivo Complex located to the east (Table 3.1); (2) only granites occurring in the Cuchilla Dionisio Terrane (e.g., Valdivia granite) show a source of Pb with ages of ~1,000 Ma (Oyhantçabal et al., 2007); and (3) only granites found in the Edén Terrane (e.g., Puntas del Mataojo Granite) have inherited zircon cores displaying concordant Paleoproterozoic/Archean ages (see for example Oyhantçabal et al., 2009). Therefore, while favouring a possible affinity between the Edén Terrane and the Nico Pérez Terrane (see below), these features argue in favour of a different tectonic evolution for the Edén and Cuchilla Dioniso terranes. Hence, the boundary between these two domains (Sierra Ballena Shear Zone) would represent a suture zone.

The apparent similarities found in the basement on both sides of the Dorsal de Canguçu Shear Zone in southern Brazil led Saalman et al. (2011) to propose a common tectonic evolution, thereby arguing against this shear zone being a suture zone. In this regard, the significance of the Dorsal de Canguçu and Sierra Ballena Shear Zones has been a matter of debate. While some thought it to represent a suture between two lithospheric plates (e.g., Basei et al., 2000), others suggested that it represents an intra-continental fault (e.g., Fernandes and Koester, 1999). In Uruguay, the Sierra Ballena Shear Zone was argued to represent an intra-continental shear zone based on the occurrence of calc-alkaline granitic intrusions on both sides with ages in the range of 650-600 Ma (Oyhantçabal et al., 2009). Under close scrutiny, however, the age and spatial distribution of these granites show differences. For example, the oldest U-Pb SHRIMP ages (~630 Ma; Table 3.1) are only found in the Nico Pérez Terrane and in the Edén Terrane. Available geochemical data for one of these granites (Puntas del Mataojo Granite) indicates a high-K<sub>2</sub>O calc-alkaline signature compatible with a magmatic arc or a post-collisional tectonic setting (Sánchez-Bettucci et al. 2003; Oyhantçabal et al., 2009). Here, we suggest that these granites were most likely emplaced after the closure of the Arroyo del Soldado Basin and as a result of the collision between the Edén and the Nico Pérez terranes (Figure 3.9). This event, herein named the "Edén Accretionary Event" might also be reflected in U-Pb ages (~630 Ma) of metamorphic rutile in the

Fuente del Puma Formation (see above). Following this collision, the Cuchilla Dionisio Terrane accreted, via the Sierra Ballena Shear Zone, to the Nico Pérez and the Edén terranes producing a second magmatic event between 615 and 560 Ma (Figure 3.9), which is manifested in all those blocks (Cuchilla Dionisio Accretionary Event; Table 3.1). Therefore, the Sierra Ballena Shear Zone would represent a suture whose main activity in Uruguay spans from 580 to 560 Ma, as indicated by the occurrence of the associated transpressional magmatism (see also Oyhantçabal et al., 2009). Older granites located to the west of this shear zone are related to an earlier accretionary event (Edén Event), located further to the west, and should not be considered in dating the evolution of the Sierra Ballena Shear Zone, which is rather associated to the accretion of the Cuchilla Dionisio Terrane.

The provenance of the Edén Terrane is uncertain, although its basement and that of the Nico Pérez Terrane might have the same affinity. This observation is supported by the overlapping TDM model ages of Neoproterozoic granites, gneissic basement and supracrustal rocks from both domains (Figure 3.7D). As stated above, the fact that the coeval Illescas Rapakivi Granite in the Nico Pérez Terrane corresponds to an anorogenic setting, which did not experience high-grade metamorphism, as did the arc-related protoliths of the Campanero Unit of the Edén Terrane, suggests that both units drifted away before 1,780-1,750 Ma. This is further supported by the lack of Mesoproterozoic (~1,430 Ma) rocks in the Nico Pérez Terrane which can be used to argue that the Paleoproterozoic and Archean detrital zircons recorded in the Mesoproterozoic (~1,430 Ma) Zanja del Tigre Complex were derived from a domain other than the Nico Pérez Terrane. As shown in this study, the Edén Terrane was not part of the basement of the Arroyo del Soldado Group, and therefore, we suggest that these two blocks were attached in the Neoproterozoic likely during the lower Ediacaran-upper Cryogenian (~650-620 Ma). Although fundamental questions still exist with regards to the nature and age of the Fuente del Puma Formation (*s.s.*), this unit occurs within the Edén Terrane (e.g., Oyhantçabal et al., 2005). Thus, the boundary between this allochthonous block and the Nico Pérez Terrane is placed at the La Plata Lineament (Oyhantçabal, 2005; Figures 3.2 and 3.3). As demonstrated by the occurrence of basement windows belonging to the Zanja del Tigre Complex (e.g., Burgueño and COMSA quarries) and orthogneisses of the

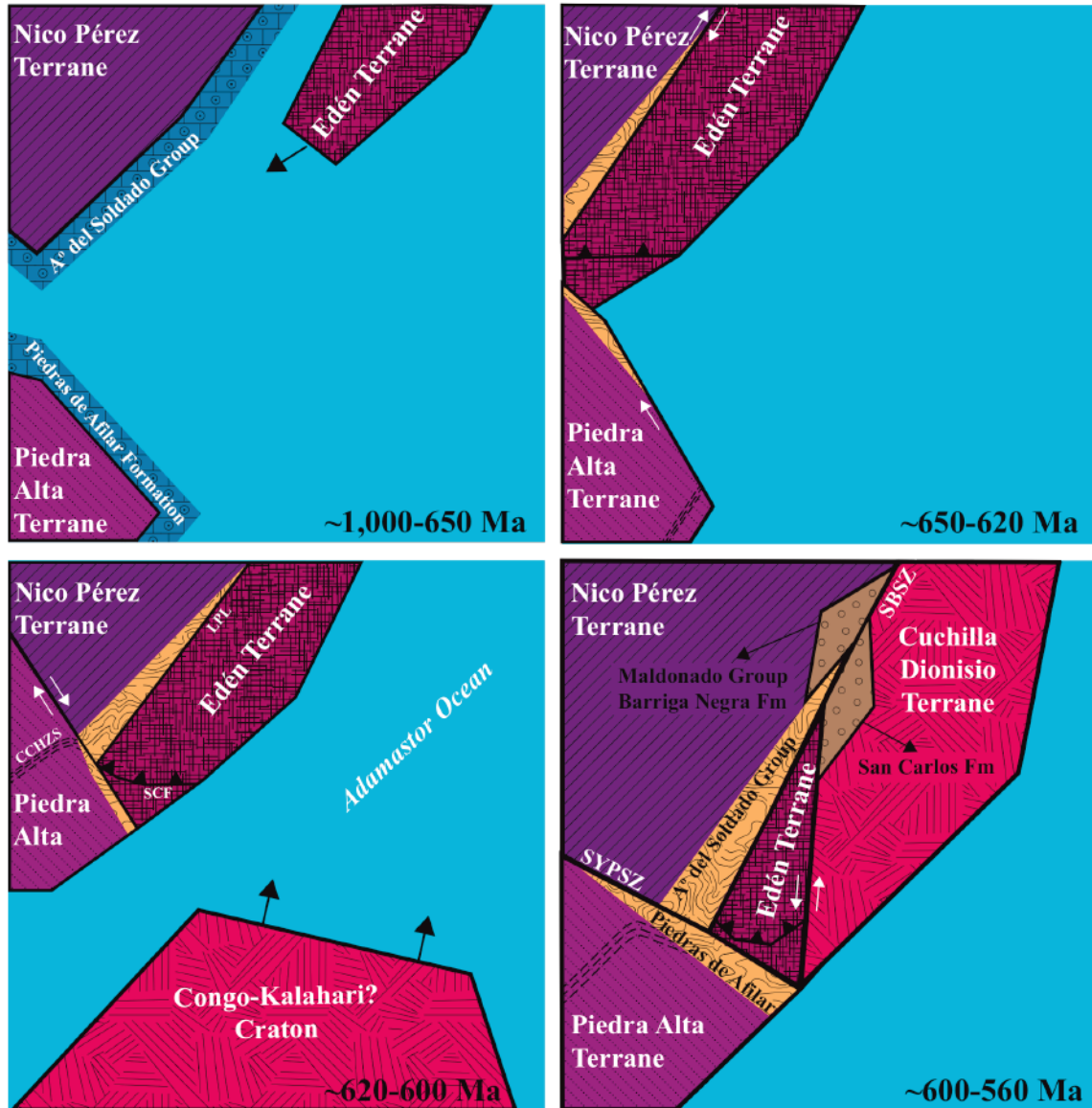


**Figure 3.9.** Schematic reconstruction showing a possible scenario of episodic oblique terrane collisions during the Neoproterozoic (see text for details). CCHZS: Cuchilla Cabo de Hornos Shear Zone; SCF: Sierra de Cabral Fold; SYPSZ: LPL: La Plata Lineament; Sarandí del Yí-Piriápolis Shear Zone; SBSZ: Sierra Ballena Shear Zone.

Campanero Unit in Punta Rasa (Figure 3.2), this block extends to the south under the Maldonado Group and Sierra de Animas Complex (Piriápolis area) up to the Atlantic coast. The boundaries of this block coincides with the once informally defined but later abandoned Serrana Block (Gaucher et al., 2004).

Sometime around 600-550 Ma, the closure of the Adamastor Ocean and collision with the Congo (Kalahari?) craton took place (Figure 3.9). Eastward (Basei et al., 2008)

and westward (Oyhantçabal et al., 2007) subduction models have been proposed. In either case, the collisional history in southeastern Uruguay was characterized by NE-SW plate convergence, evident as sinistral transcurrent shearing mainly through the Sierra Ballena Shear Zone. The absence of relicts preserving high-pressure paragenesis further supports an oblique collision. Additionally, syntectonic granite emplacement along the sinistral Sierra Ballena Shear Zone (and its equivalents in southern Brazil) became locally more important. In Uruguay, synkinematic granitoids include, (1) the Maldonado granite ( $564\pm 7$  Ma) emplaced between the Sierra Ballena and Cordillera Shear Zones; (2) the Aiguá granite ( $587\pm 16$  Ma), an elongated pluton in contact with mylonites of the Sierra Ballena Shear Zone to the west and the Florencia Granite to the east; (3) the Florencia granite ( $572\pm 2$  Ma), an elongated pluton located between the Aiguá and Valdivia Granites; (4) the Arroyo de los Píriz Granite ( $588\pm 6$  Ma), an elongate body emplaced directly in the eastern Sierra Ballena Shear Zone; and (5) the Solís de Mataojo granitic complex ( $584\pm 13$  Ma), an elongated intrusion related to the southern extreme of the Sarandí del Yí Shear Zone (Oyhantçabal et al., 2005; 2007; 2009) (Figure 3.2). Contrary to previous proposals, which considered this granitic magmatism to be the root of a continental arc (Basei et al., 2008), Oyhantçabal et al. (2007) suggested that slab beak-off was the most likely mechanism associated with the generation of the granitic magmas shortly after the collision, and thus these granites were not part of the magmatic arc. Furthermore, Oyhantçabal et al. (2007) suggested that this magmatism shows an evolution beginning with highly-fractionated calc-alkaline granites (Solís the Mataojo Granitic Complex  $\sim 584$  Ma), followed by mildly alkaline granites and shoshonitic volcanics (Maldonado Granite  $\sim 575$  Ma, and Las Flores Basalt), and concluding with peralkaline intrusions and volcanics (Sierra de Animas Complex  $\sim 540$ - $520$  Ma). The signature of this magmatism indicates a post-collision setting during the activity of the Sierra Ballena Shear Zone, which played a major role in the emplacement of these magmatic associations.

Brittle deformation was associated with the Sierra Ballena Shear Zone. Its conjugate shears or faults are related to anisotropy of the local basement, and led to formation of fault bounded pull-apart basins in transtensional segments (Figure 3.9). Prevailing fault orientations show NNE-SSW trends coinciding with the direction of main

compressional deformation generating the NW-SE extension in these basins. Similar paleostress fields have been recognized in Ediacaran basins of Brazil (Almeida et al., 2010) suggested that the age constraints, lithological similarities, and structural aspects point to the correlation of all Ediacaran to Cambrian basins of southeastern South America in a common basin system, with recurrent events of subsidence, magmatic activity, and brittle deformation from 605 to 530 Ma. Once established, these pull-apart basins subsided very quickly and accumulate large thicknesses of alluvial, marine and volcanic deposits. Such is the case of the Maldonado Group (alluvial conglomerates, sandstones, sand-mud rhythmites, basic and acid volcanic and volcanoclastic rocks), San Carlos Formation (fluvial sandstones and conglomerates; siltstones), Cerros de Aguirre Formation (acidic volcanic and volcanoclastic rocks), Barriga Negra Formation (alluvial conglomerates, sandstones and mudstones), Sierra de Ríos Formation (acidic volcanic rocks), and the Tacuarí Formation (conglomerates, sandstones and sand-mud rhythmites).

The Rocha Group, located in the extreme southeastern Uruguay, was also deposited in the Ediacaran (Basei et al., 2008) and similar to its own basement (Cerro Olivo Complex) shows an African affinity. In the latter case, magmatic ages at 800-750 Ma on zircon and high-temperature metamorphism dated at 650-600 Ma would support the correlation between the Cuchilla Dionisio Terrane and the Coastal Terrane of the Kaoko Belt (Oyhantçabal et al., 2009; Gross et al., 2009; Konopásek et al., 2014). The Rocha Group has been correlated with successions in the Gariep belt in Southern Africa, based on detrital zircon record, suggesting that it was deposited in the back-arc to the Gariep magmatic arc (Basei et al., 2000; 2005; cf. Oyhantçabal et al., 2007).

#### **4.6. Conclusions**

The purpose of the present study was to constrain the maximum depositional age and provenance of Neoproterozoic volcano-sedimentary successions of Uruguay with the ultimate goal of better understanding the regional paleogeography, and the timing and dynamics of terrane accretion. The following conclusions can now be drawn:

1. The mixed siliciclastic-carbonate Arroyo del Soldado Group was deposited during the Tonian-Cryogenian, between ~1,000 and 650 Ma, in a passive continental margin

developed along the southeastern margin of the Nico Pérez Terrane. In contrast, the deposition of the siliciclastic and volcanoclastic Playa Hermosa, Las Ventanas, San Carlos and Barriga Negra formations occurred during the upper Ediacaran (<585 Ma) in small fault-bounded basins developed over the Nico Pérez, Edén and Cuchilla Dionisio terranes.

2. Evidence of tectonic and magmatic activity during the Tonian-Cryogenian is absent in the Nico Pérez Terrane, which further supports the existence of a stable continental margin at that time. The Ediacaran, however, is characterized by extensive tectonic activity and voluminous magmatism in all the domains. This tectonic and magmatic activity is largely associated with the accretion of continental blocks.

3. Far from being a definite model, our results suggest that the present-day terrane configuration took place in a relatively short (~100 Ma long) period of time between ~650 and 560 Ma. In this regard, the Edén and Nico Pérez terranes likely accreted at ~650-620 Ma (Edén Accretionary Event), followed by their accretion to the Piedra Alta Terrane at ~620-600 Ma (Piedra Alta Accretionary Event), and culminating with the accretion of the Cuchilla Dionisio Terrane at ~600-560 Ma (Cuchilla Dionisio Accretionary Event).

4. Based on the distinct stratigraphy, geology, U-Pb zircon ages and Nd isotopes, a new terrane, named Edén Terrane, is now defined. As for the above-mentioned terranes, the boundaries between this block and the adjacent terranes are highly tectonized, with large-scale ductile shear zones implying that the geodynamic history of the Ediacaran is dominated by oblique movements with episodes of emplacement of granite complexes during transpressional and posterior extensional events.

#### **4.7. References**

Adams, C.J., Miller, H., Aceñolaza, F.G., Toselli, A.J., Griffin, W.L. 2011. The Pacific Gondwana margin in the late Neoproterozoic-early Paleozoic: Detrital zircon U–Pb ages

from metasediments in northwest Argentina reveal their maximum age, provenance and tectonic setting. *Gondw. Res.* 19, 71-83.

Almeida, R.P., Janikian, L., Fragoso-Cesar, A.R., Fambrini, G.L., 2010. The Ediacaran to Cambrian rift system of southeastern South America: tectonic implications. *Jour. Geol.* 118, 145-161.

Aubet, N.R., Pecoits, E., Heaman, L.M., Veroslavsky, G., Gingras, M.K., Konhauser, K.O., 2014. Ediacaran in Uruguay: Facts and Controversies, *Journal of South American Earth Sciences*, doi: 10.1016/j.jsames.2014.06.007.

Basei, M., Siga, Jr.O., Masquelin, H., Harara, O., Reis Neto, J. and Preciozzi, F., 2000. The Dom Feliciano Belt of Brazil and Uruguay and its foreland domain, the Río de la Plata Craton. In: Cordani, U., Milani, E., Thomaz F.A., Campos, D. (Eds.), *Tectonic evolution of South America*, pp. 311-334.

Basei, M.A.S., Frimmel, H.E., Nutman, A.P., Preciozzi, F., Jacob, J., 2005. The connection between the Neoproterozoic Dom Feliciano (Brazil/Uruguay) and Gariep (Namibia/South Africa) orogenic belts. *Prec. Res.* 139, 139-221.

Basei, M.A.S., Frimmel, H.E., Nutman, A.P., Preciozzi, F., 2008. West Gondwana amalgamation based on detrital zircon ages from Neoproterozoic Ribeira and Dom Feliciano belts of South America and comparison with coeval sequences from SW Africa. In: Pankhurst RJ, Trouw RAJ, de Brito Neves BB, De Wit MJ (Eds.) *West Gondwana: Pre-Cenozoic Correlations Across the South Atlantic Region* vol 294. Geological Society, London, special publications, pp 239-256.

Basei, M.A.S., Peel, E., Sanchez-Bettucci, L., Preciozzi, F., Nutman, A.P., 2011. The basement of the Punta del Este Terrane (Uruguay): an African Mesoproterozoic fragment at the eastern border of the South American Rio de la Plata craton. *Int. J. Earth Sci. (Geol Rundsch)* 100, 289-304.

Blanco, G., Rajesh, H.M., Gaucher, C., Germs, G.J.B., Chemale Jr., F., 2009. Provenance of the Arroyo del Soldado Group (Ediacaran to Cambrian, Uruguay): Implications for the paleogeographic evolution of southwestern Gondwana. *Prec. Res.* 171, 57-73.

- Bossi, J., Campal, N., 1992. Magmatismo y tectónica transcurrente durante el Paleozoico Inferior en Uruguay. In: Gutiérrez-Marco, J.G., Saavedra, J., Rabano, I. (Eds.), *Paleozoico Inferior de Iberoamérica*. Universidad de Extremadura, Mérida, pp. 343-356.
- Bossi, J., Campal, N., Civetta, L., Demarchi, G., Girardi, V.A.V., Mazzucchelli, M., Negrini, L., Rivalenti, G., Fragoso Cesar, A.R.S., Sinigoi, S., Teixeira, W., Piccirillo, E.M., Molesini, M. 1993. Early Proterozoic dike swarms from Western Uruguay: geochemistry, Sr-Nd isotopes and petrogenesis. *Chem. Geol.* 106, 263-277.
- Bossi, J., Cingolani, C., 2009. Extension and general evolution of the Rio de la Plata Craton. In: Gaucher C, Sial AN, Halverson GP, Frimmel HE (Eds.) *Neoproterozoic-Cambrian tectonics, global change and evolution: a focus on southwestern Gondwana*. *Developments in Precambrian Geology*, vol 16, Elsevier, pp 73-85.
- Bossi, J., Ferrando, L., 2001. Carta Geológica del Uruguay, Escala 1:500.000. Versión 2.0 Digital, Facultad de Agronomía, Montevideo.
- Bossi, J., Campal, N., Hartmann, L.A., Schipilov, A. 2001. Predevoniano en el Uruguay; terrenos y SHRIMP II. *Actas XI Cong. Latinoam. Geol. Montevideo*. CD-ROM version.
- Brito Neves, B.B., Campos Neto, M.C., Fuck, R.A., 1999. From Rodinia to Western Gondwana: an approach to the Brasiliano-Pan African cycle and orogenic collage. *Episodes* 22, 155-166.
- Campal, N., Schipilov, A., 2005. La Formación Cerros de Aguirre: evidencias de magmatismo Vendiano en el Uruguay. *Lat. Amer. J. Sedimentol. Basin Anal.* 12, 161-174.
- Campal, N., Schipilov, A., 1995. The Illescas bluish quartz rapakivi granite (Uruguay-South America): some geological features. In: *Symp. Rapakivi Granites and Related Rocks*, Belem, Brazil, p. 18.
- Cingolani, C.A., Hartmann, L.A., Santos, J.O.S., McNaughton, N.J., 2012. U-Pb SHRIMP dating of zircons from the Buenos Aires Complex of the Tandilia Belt, Rio de la Plata Craton, Argentina. *Actas del XV Congreso Geológico Argentino*. El Calafate.
- Cordani, U.G., Sato, K., Teixeira, W., Tassinari, C.C.G., and Basei, M.A.S., 2000. Crustal evolution of the South American platform. In: Cordani, U.G., Milani, E.J.,

Thomaz-Filho, A., and Campos, D.A. (Eds.), Tectonic evolution of South America, pp. 19-40.

Cordani, U.G., Teixeira, W., Tassinari, C.C.G., Coutinho, J.M.V., Ruiz, A.S., 2010. The Rio Apa Craton in Mato Grosso do Sul (Brazil) and northern Paraguay: Geochronological evolution, correlations and tectonic implications for Rodinia and Gondwana. *A. Jour. Sci.* 310, 981-1023.

Cordani, U.G., Teixeira, W., D'Agrella-Filho, M.S., Trindade, R.I. 2009. The position of the Amazonian craton in supercontinents. *Gondw. Res.* 15, 396-407.

DePaolo, D.J., Wasserburg, G.J., 1976. Nd isotopic variations and petrogenetic models. *Geophys. Res. Lett.* 3, 249-252.

Escayola, M.P., Pimentel, M.M., Armstrong, R., 2007. Neoproterozoic backarc basin: sensitive high-resolution ion microprobe U-Pb and Sm-Nd isotopic evidence from the Eastern Pampean Ranges, Argentina. *Geology* 35, 495-498.

Fambrini, G.L., Frago-Cesar, A.R.S., Almeida, R.P., Riccomini, C., 2005. A Formação Barriga Negra (Ediacarano do Uruguai): caracterização estratigráfica e correlação com unidades do Estado do Rio Grande do Sul, Brasil. *Rev. Brasil. Geoc.* 35, 515-524.

Fernandes, L.A.D. Tommasi, A., Porcher, C.C., 1992. Deformation patterns in the southern Brazilian branch of the Dom Feliciano Belt: A reappraisal. *Jour. South Amer. Earth Sci.* 5, 77-96.

Fernandes, L.A.D., Koester, E., 1999. The Neoproterozoic Dorsal de Canguçu strike-slip shear zone: its nature and role in the tectonic evolution of southern Brazil. *J. Afr. Earth Sci.* 29, 3-24.

Fragoso-Cesar, A.R.S., 1980. O Cratón do Rio de la Plata e o Cinturão Dom Feliciano no Escudo Uruguaio-Sul-Rio-Grandense. *Soc. Bras. Geol.* 5, 2879-2892.

Fragoso-Cesar, A.R.S., Machado, R.Y., Gómez Rifas, C., 1987. Observações sobre o Cinturão Dom Feliciano no Escudo Uruguaio e correlações com o Escudo do Rio Grande do Sul. In: III Symposium Sul-Brasileiro de Geologia, Curitiba, Brasil, Vol. 2, pp. 791-809.

- Frei, R., Gaucher, C., Stolper, D., Canfield, D.E., 2013. Fluctuations in late Neoproterozoic atmospheric oxidation – Cr isotope chemostratigraphy and iron speciation of the late Ediacaran lower Arroyo del Soldado Group (Uruguay). *Gond. Res.* 23, 797-811.
- Frei, R., Gaucher, C., Dossing, L.N., Sial, A.N., 2011. Chromium isotopes in carbonates – A tracer for climate change and for reconstructing the redox state of ancient seawater. *EPSL* 312, 114-125.
- Fuck, R.A., Brito Neves, B.B., Schobbenhaus, C., 2008. Rodinia descendants in South America. *Prec. Res.* 160, 108-126.
- Gastal, M.C.P., Lafon, J.M., Hartmann, L.A., Koester, E., 2005. Sm-Nd isotope compositions as a proxy for magmatic processes during the Neoproterozoic of southern Brazilian shield. *J. South Am. Earth Sci.* 18, 255-276.
- Gaucher, C., Chiglino, L., Pecoits, E., 2004. Southernmost exposures of the Arroyo del Soldado Group (Venidan to Cambrian, Uruguay): palaeogeographic implications for the amalgamation of W-Gondwana. *Gondw. Res.* 3, 701-714.
- Gaucher, C., Blanco, G., Chiglino, L., Poiré, D., Germs, G.J.B., 2008. Acritarchs of the Las Ventanas Formation (Ediacaran, Uruguay): Implications for the timing of coeval rifting and glacial events in western Gondwana. *Gondw. Res.* 13, 488-501.
- Gaucher, C., Frei, R., Chemale, Jr.F., Frei, D., Bossi, J., Martínez, G., Chiglino, L., Cernuschi, F., 2011. Mesoproterozoic evolution of the Rio de la Plata Craton in Uruguay: at the heart of Rodinia? *Int. J. Earth Sci. (Geol Rundsch)* 100, 273-288.
- Goldstein, S.L., O’Nions, R.K., Hamilton, P.J., 1984. A Sm-Nd isotopic study of atmospheric dusts and particulates from major river systems. *Earth Planet. Sci. Lett.* 70, 221-236.
- Gradstein, F.M., Ogg, J.G., Schmitz, M., Ogg, G., 2012. *Geological Time Scale*. Cambridge University Press, Cambridge, pp. 413-435.
- Gross, A.O.M.S., Droop, G.T.R., Porcher, C.C., Fernandes, L.A.D., 2009. Petrology and thermobarometry of mafic granulites and migmatites from the Chafalote Metamorphic

Suite: new insights into the Neoproterozoic P-T evolution of the Uruguayan-Sul-Rio-Grandense Shield. *Prec. Res.* 170, 157-174.

Halls, H.C., Campal, N., Davis, D.W., Bossi, J., 2001. Magnetic studies and U–Pb geochronology of the Uruguayan dyke swarm, Río de la Plata craton, Uruguay: paleomagnetic and economic implications. *J. South A. Earth Sci.* 14, 349-361.

Hartmann, L.A., Santos, J.O., Bossi, J., Campal, N., Schipilov, A., Mac Naughton, N. J., 2002. Zircon and titanite U-Pb SHRIMP geochronology of Neoproterozoic felsic magmatism on the eastern border of the Río de la Plata Craton, Uruguay. *J. South Am. Earth Sci.* 15, 229-236.

Hartmann, L.A., Philipp, R.P., Liu, D., Wan, Y., Wang, Y., Santos, J.O., Vasconcellos, M.A.Z., 2004. Paleoproterozoic magmatic provenance of detrital zircons, Porongos Complex Quartzites, Southern Brazilian Shield. *International Geology Review*, 46, 127-157.

Hartmann, L.A., Campal, N., Santos, J.O.S., McNaughton, N.J., Bossi, J., Schipilov, A., Lafon, J.-M., 2001. Archean crust in the Rio de la Plata Craton, Uruguay-SHRIMP U-Pb zircon reconnaissance geochronology. *J. South Am. Earth Sci.* 14, 557-570.

Hartmann, L.A., Piñeyro, D., Bossi, J., Leite, J.A.D., Mcnaughton, N.J., 2000. Zircon U-Pb SHRIMP dating of Paleoproterozoic Isla Mala granitic magmatism in the Rio de la Plata Craton, Uruguay. *J. South A. Earth Sci.* 13, 105-113.

Jaffey, A.H., Flynn, K.F., Glendenin, L.E., Bentley, W.C., Essling, A. M., 1971. Precision measurement of half-lives and specific of <sup>235</sup>U and <sup>238</sup>U. *Phys. Rev. C4*, 1889-1906.

Johansson, A., 2014. From Rodinia to Gondwana with ‘SAMBA’ model – A distant view from Baltica towards Amazonia and beyond. *Prec. Res.* 244, 226-235.

Konopásek, J., Košler, J., Sláma, J., Janoušek, V. 2014. Timing and sources of pre-collisional Neoproterozoic sedimentation along the SW margin of the Congo Craton (Kaoko Belt, NW Namibia). *Gondw. Res.* 26, 386-401.

- Kröner, A., Cordani, U., 2003. African, southern Indian and South American cratons were not part of the Rodinia supercontinent: evidence from field relationships and geochronology. *Tectonophysics* 375, 325-352.
- Leite, J.A.D., Hartmann, L.A., McNaughton, N.J., Chemale F.Jr., 1998. SHRIMP U-Pb Zircon geochronology of Neoproterozoic juvenile and crustal-reworked terranes in southernmost Brazil. *Int. Geol. Rev.* 40, 688-705.
- Lenz, C., Fernandes, L.A.D., McNaughton, N.J., Porcher, C.C., and Masquelin, H., 2011. Magmatic and metamorphic U-Pb SHRIMP ages in zircons for the Cerro Bori Orthogneisses, Dom Feliciano Belt in Uruguay. *Prec. Research* 185, 149-163.
- Li, Z.X., Bogdanova, S.V., Collins, A.S., Davidson, A., De Waele, B., Ernst, R.E., Fitzsimons, I.C.W., Fuck, R.A., Gladkochub, D.P., Jacobs, J., Karlstrom, K.E., Lu, S., Natapov, L.M., Pease, V., Pisarevsky, S.A., Thrane, K., Vernikovsky, V., 2008. Assembly, configuration, and break-up history of Rodinia: a synthesis. *Prec. Res.* 160, 179-210.
- Liew, T.C., Hofmann, A.W., 1988. Precambrian crustal components, plutonic associations, plate environment of the Hercynian Fold Belt of Central Europe: indications from a Nd and Sr isotopic study. *Contr. Miner. Petr.* 98, 129-138.
- Ludwig K.R., 2008. Isoplot version 3.7, User's Manual, Berkeley Geochronology Center Special Publication 4.
- Mallmann, G., Chemale Jr.F., Avila, J.N., Kawashita, K., Armstrong, R., 2007. Isotope geochemistry and geochronology of the Nico Perez Terrane, Río de La Plata Craton, Uruguay. *Gondw. Res.* 12, 489-508.
- Masquelin, H., Fernandes, L.A.D., Lenz, C., Porcher, C.C., McNaughton, N.J., 2012. The Cerro Olivo Complex: a pre-collisional Neoproterozoic magmatic arc in Eastern Uruguay. *Int. Geol. Review* 54, 1161-1183.
- Masquelin, H., Sánchez-Bettucci, L., 1993. Propuesta de evolución tectono-sedimentaria para la fosa tardi-brasiliana en la región de Piriápolis, Uruguay. *Rev. Brasil. Geocienc.* 23, 313-322.

- Mazzuchelli, M., Rivalenti, G., Piccirillo, E.M., Girardi, V.A.V., Civetta, L., Petrini, R., 1995. Petrology of the Proterozoic mafic dyke swarms of Uruguay and constraints on their mantle source composition. *Prec. Res.* 74, 177-194.
- Midot, D., 1984. Etude géologique et diagnostic métallogénique pour l'exploration du secteur de Minas (Uruguay). Diplôme de Docteur de 3e Cycle. Université Pierre et Marie Curie, Paris.
- Oyhantçabal, P., 2005. The Sierra Ballena Shear zone: kinematics, timing and its significance for the geotectonic evolution of southeast Uruguay. *Georg-August Universität zu Göttingen, Göttingen*, pp. 139.
- Oyhantçabal, P., Siegesmund, S., Wemmer, K., Frei, R., Layer, P., 2007. Post-collisional transition from calc-alkaline to alkaline magmatism during transcurrent deformation in the southernmost Dom Feliciano Belt (Braziliano-Pan-African, Uruguay). *Lithos* 98, 141-159.
- Oyhantçabal, P., Siegesmund, S., Wemmer, K., 2011. The Río de la Plata Craton: a review of units, boundaries, ages and isotopic signature. *Int. J. Earth Sci.* 100, 201-220.
- Oyhantçabal, P., Siegesmund, S., Wemmer, K., Presnyakov, S., Layer, P., 2009. Geochronological constraints on the evolution of the southern Dom Feliciano Belt (Uruguay). *J. Geol. Soc.* 166, 1075-1084.
- Oyhantçabal, P., Wagner-Eimer, M., Wemmer, K., Schulz, B., Frei, R., Siegesmund, S., 2012. Paleo- and Neoproterozoic magmatic and tectonometamorphic evolution of the Isla Cristalina de Rivera (Nico Perez Terrane, Uruguay). *Int. J. Earth Sci. (Geol Rundsch)* doi:10.1007/s00531-012-0757-4.
- Pankhurst, R.J., Ramos, A., Linares, E., 2003. Antiquity of the Rio de la Plata Craton in Tandilia, southern Buenos Aires province, Argentina. *J. South Am. Earth Sci.* 16, 5-13.
- Pazos P., Tófaló, R., Sánchez-Bettucci, L., 2003. The record of the Varanger Glaciation at the Rio de la Plata Craton, Vendian-Cambrian of Uruguay. *Gondw. Res.* 6, 65-77.

Peel, E., Preciozzi, F., 2006. Geochronologic synthesis of the Piedra Alta Terrane, Uruguay. V South American Symposium on Isotope Geology. Punta del Este, Uruguay, pp. 234-237.

Pecoits, E., 2003. Sedimentología y consideraciones estratigráficas de la Formación Las Ventanas en su área tipo, departamento de Maldonado, Uruguay. Rev. Soc. Urug. Geol. Spec. Publ. 1, 124-140.

Pecoits, E., Aubet, N., Oyhantçabal, P., Sánchez-Bettucci, L., 2004. Estratigrafía de sucesiones sedimentarias y volcanosedimentarias Neoproterozoicas del Uruguay. Rev. Soc. Uruguay. Geol. 11, 18-27.

Pecoits, E., Gingras, M., Aubet, N., Konhauser, K., 2008. Ediacaran in Uruguay: palaeoclimatic and palaeobiological implications. Sedimentology 55, 689-719.

Pecoits, E., Gingras, M.K., Konhauser, K.O., 2011. Las Ventanas and San Carlos formations, Maldonado Group, Uruguay. Geological Society, London, Memoirs 36, 555-564.

Pecoits, E., Konhauser, K.O., Aubet, N.R., Heaman, L.M., Veroslavsky, G., Stern, R.A., Gingras, M.K., 2012. Bilaterian Burrows and Grazing Behavior at >585 Million Years Ago. Science 336, 1693-1696.

Porcher, C.C., McNaughton, N.J., Leite, J.A.D., Hartmann, L.A., Fernandes, L.A.D., 1999. Idade Shrimp em zircão: vulcanismo ácido do Complexo Metamórfico Porongos. In: Simpósio sobre Vulcanismo e Ambientes Associados. Abstracts, Gramado, 110.

Preciozzi, F., Basei, M.A.S., Masquelin, H., 1999a. New geochronological data from the Piedra Alta Terrane (Rio de La Plata Craton). In: II South American Symposium on Isotope Geology, Córdoba, pp. 341-343.

Preciozzi, F., Masquelin, H., Basei, M.A.S., 1999b. The Namaqua/Grenville terrane of eastern Uruguay. In: Proceedings of the II South American Symposium on Isotope Geology, Actas, Córdoba (Argentina), pp. 338-340.

Preciozzi, F., Peel, E., Muzio, R., Ledesma, J.J. and Guerequiz, R., 2001. Dom Feliciano Belt and Punta del Este Terrane: Geochronological features. III South Amer. Symp. Isotope Geol. Pucón, Chile.

Preciozzi, F., Peel, E., 2005. El cinturón Dom Feliciano y sus relaciones con el craton del Río de la Plata y el Terreno Punta del Este - geología y geocronología. Informe Final, Proyecto Conicyt-FCE #6009.

Ramos, V.A., 2010. The Grenville-age basement of the Andes. *J. South A. Earth Sci.* 29, 77-91.

Ramos, V.A., Vujovich, G., Martino, R., Otamendi, J. 2010. Pampia: a large cratonic block missing in the Rodinia supercontinent. *Jour. Geod.* 50, 243-255.

Ramos, V.A., Vujovich, G.I., 1993. The Pampia Craton within Western Gondwanaland. In: Ortega-Gutierrez, F., Coney, P., Centeno-García, E., Gomez-Caballero, A. (Eds.), *Proceedings of The First Circum-Pacific and Circum-Atlantic Terrane Conference*. Mexico, pp. 113-116.

Rapela, C.W., Pankhurst, R.J., Casquet, C., Baldo, E., Saavedra, J., Galindo, C., Fanning, C.M., 1998. The Pampean Orogeny of the southern proto-Andes: evidence for Cambrian continental collision in the Sierras de Cordoba. In: Pankhurst, R.J., Rapela, C.W. (Eds.), *The proto-Andean Margin of Gondwana*, vol. 142. Geological Society, London, Sp. Pub, pp. 181-217.

Rapela, C.W., Pankhurst, R.J., Casquet, C., Baldo, E., Saavedra, J., Galindo, C., Fanning, C.M., 2007. The Pampean Orogeny of the southern proto-Andes: Cambrian continental collision in the Sierras de Cordoba. *Earth Sci. Rev.* 142, 181-217.

Rapela, C.W., Pankhurst, R.J., Casquet, C., Baldo, E., Galindo, C., Fanning, C.M., Dahlquist, J.M., 2010. The Western Sierras Pampeanas: protracted Grenville-age history (1330-1030 Ma) of intra-oceanic arcs, subduction-accretion at continental-edge and AMCG intraplate magmatism. *J. South A. Earth Sci.* 29, 105-127.

Rivers, T., 1997. Lithotectonic elements of the Grenville Province: review and tectonic implications. *Prec. Res.* 86, 117-154.

Rivalenti, G., Mazzucchelli, M., Molesini, M., Petrini, R., Girardi, V.A.V., Bossi, J., Campal, N., 1995. Petrology of Late Proterozoic mafic dikes in the Nico Perez region, central Uruguay. *Mineral. Petrol.* 55, 239-263.

Sambridge, M.S., Compston, W., 1994. Mixture modelling of multi-component data sets with application to ion-probe zircon ages: *Earth Planet. Sci. Lett.* 128, 373-390.

Sánchez-Bettucci, L., Ramos, V.A., 1999. Aspectos geológicos de las rocas metavolcanicas y metasedimentarias del Grupo Lavalleja, sudeste de Uruguay. *Rev. Bras. Geoc.* 29, 557-570.

Sánchez-Bettucci, Masquelin, E., Peel, E., Oyhantçabal, P., Muzio, R., Ledesma, J.J., Preciozzi, F., 2010. Comment on “Provenance of the Arroyo del Soldado Group (Ediacaran to Cambrian, Uruguay): implications for the palaeogeographic evolution of southwestern Gondwana”. *Prec. Res.* 180, 328-333.

Sánchez-Bettucci, L., 1998. Evolución tectónica del cinturón Dom Feliciano en la región Minas-Piriapolis, Uruguay. Ph.D. Thesis. Universidad de Buenos Aires, Argentina.

Sánchez-Bettucci, L. Preciozzi, F. Basei, M.A.S., Oyhantçabal, P. Peel, E., Loureiro, J., 2003. Campanero Unit: A Probable Paleoproterozoic Basement and its Correlation to other Units of Southeastern Uruguay. IV South Amer. Symp. Isotope Geol. Salvador, Brazil.

Santos, J.O.S., Hartmann, L.A., Bossi, J., Campal, N., Schipilov, A., Piñeyro, D., McNaughton, N.J., 2003. Duration of the Transamazonian and its correlation within South America based on U-Pb SHRIMP geochronology of the La Plata Craton, Uruguay. *Int. Geol. Rev.* 45, 27-48.

Spagnuolo, C.M., Rapalini, A.E., Astini, R.A., 2012. Assembly of Pampia to the SW Gondwana margin: a case of strike-slip docking? *Gondw. Res.* 2-3, 406-421.

Saalmann, K., Gerdes, A., Lahaye, Y., Hartmann, L.A., Remus, M.V.D., Läufer, A., 2011. Multiple accretion at the eastern margin of the Río de la Plata craton: the prolonged Brasiliano orogeny in southernmost Brazil. *Int. J. Earth Sci. (Geol. Rundsch)* 100, 355-378.

Simonetti, A., Heaman, L.M., Hartlaub, R.P., Creaser, R.A., MacHattie, T.G., Bohm, C., 2005. U-Pb zircon dating by laser ablation-MC-ICP-MS using a new multiple ion counting Faraday collector array. *J. Anal. Atom. Spectrom.* 20, 677-686.

Simonetti, A., Heaman, L.M., Chacko, T., Banerjee, N.R., 2006. In situ petrographic thin section U-Pb dating of zircon, monazite, and titanite using laser ablation-MC-ICP-MS. *Int. Jour. Mass. Spectrom.* 253, 87-97.

Spoturno, J., Oyhançabal, P., Goso, C., Aubet, N., Cazaux, S., 2004. Mapa Geologico y de Recursos Minerales del Departamento de Canelones a Escala 1/100 000. DINAMIGE-Facultad de Ciencias.

Spoturno, J., Loureiro, J., Oyhançabal, P., Pascale, A., 2012. Mapa Geologico y de Recursos Minerales del Departamento de Maldonado a Escala 1/100 000. DINAMIGE-Facultad de Ciencias.

Teixeira, W., Renne, P., Bossi, J., Campal, N., D'Agrella, F., 1999.  $^{40}\text{Ar}/^{39}\text{Ar}$  and Rb/Sr geochronology of the Uruguayan dike swarm, Río de la Plata Craton and implications for Proterozoic intraplate activity in western Gondwana. *Prec. Res.* 93, 153-180.

Thomas, W.A., Astini, R.A., Mueller, P.A., Gehrels, G.E., Wooden, J.L., 2004. Transfer of the Argentine Precordillera terrane from Laurentia: constraints from detrital-zircon geochronology. *Geology* 32, 965-968.

Tohver, E., D'Agrella-Filho, M.S., Trindade, R.I.F., 2006. Paleomagnetic record of Africa and South America for the 1200–500 Ma interval, and evaluation of Rodinia and Gondwana assemblies. *Prec. Res.* 147, 193-222.

Verdecchia, S.O., Casquet, C., Baldo, E.G., Pankhurst, R.J., Rapela, C.W., Fanning, M., Galindo, C., 2011. Mid- to Late Cambrian docking of the Rio de la Plata craton to southwestern Gondwana: age constraints from U-Pb SHRIMP detrital zircon ages from Sierras de Ambato and Velasco (Sierras Pampeanas, Argentina). *Jour. Geol. Soc.* 168, 1061-1071.

Zimmermann, U., 2011. Comment on “Provenance of the Arroyo del Soldado Group (Ediacaran to Cambrian, Uruguay): Implications for the palaeogeographic evolution of southwestern Gondwana”. *Prec. Res.* 186, 233-236.

## CHAPTER 4: CHEMOSTRATIGRAPHIC CONSTRAINTS ON EARLY EDIACARAN CARBONATE RAMP DYNAMICS, RÍO DE LA PLATA CRATON (URUGUAY)

### 4.1. Introduction

The geochemical analyses of carbonate rocks has proven extremely useful at unravelling the palaeo-oceanographic conditions during deposition and establishing chemostratigraphic age constraints, particularly when strata lack recognizable fossils or are radiometrically undatable (e.g., Derry et al., 1989; Knoll and Walter, 1992; Jacobsen and Kaufman, 1999; Halverson et al., 2005; Azmy et al., 2006; Bekker et al., 2006; Ohno et al., 2008; Sawaki et al., 2010). Based on the premise that carbonate carbon isotope signatures reflect seawater composition at the time of deposition, significant negative carbon isotope anomalies in Neoproterozoic rocks has been interpreted as a proxy of decreased bioproductivity in association with glacial events (e.g., Knoll et al., 1986; Kaufman and Knoll, 1995; Kaufman et al., 1997; Halverson et al., 2005). However, secular variations in carbon isotope composition of marine carbonates ( $\delta^{13}\text{C}_{\text{carb}}$ ) are also known to reflect the influence of several other factors, including post-depositional alteration and diverse sources of the  $^{13}\text{C}$ -depleted carbon (Hayes et al., 1999; Knauth and Kennedy, 2009).

In Uruguay, previous chemostratigraphic studies on Ediacaran carbonates, the Polanco Limestones Formation, have identified a significant  $\delta^{13}\text{C}$  depletion in shallow-water facies (down to -4.5‰) and a connection to glaciation has been suggested as the most likely explanation for this excursion (Gaucher et al., 2004; 2009). According to the same authors, the absence of glaciogenic rocks associated to this anomaly would be consistent with deposition at low latitudes under tropical conditions and this negative anomaly would reflect seawater composition in the aftermath of a non-global post-Gaskiers glaciation occurred elsewhere. Crucially, the apparent synchronicity between this excursion, correlated with the Shuram-Wonoka-Johnnie carbon isotope anomaly (Gaucher et al., 2009), and glacial conditions carries important implications for the palaeo-oceanographic and palaeo-climatic evolution in the Ediacaran and ultimately, for the rise of animal life (Canfield et al., 2008; Ishikawa et al., 2008; Maruyama and

Santosh, 2008; Meert and Lieberman, 2008; Sawaki et al., 2010; Jiang et al., 2011). In order to assess the extent of this negative excursion across the Polanco basin and therefore, to evaluate the relative contributions of local versus global carbon cycles this study aims to: (a) present detailed carbon isotopic profiles from deep-water and shallow-water facies, (b) constrain the age of the Polanco Limestones Formation by means of new radiometric data, and (c) discuss the possible mechanisms that could have initiated this prominent negative excursion.

#### **4.2. Geologic setting and stratigraphy**

Ediacaran sedimentary and subordinate volcanic rock successions are well exposed on the southeastern and eastern margins of the Río de la Plata craton in Uruguay. These rocks were deposited and deformed during the Neoproterozoic Brasiliano/Pan-African orogeny. This orogeny constitutes the final stages of West Gondwana's assembly (Rapela et al., 2011), which occurred when the eastern margin of the Río de la Plata craton collided along the Sierra Ballena Shear Zone with island-arc terranes that approached from the southeast (Oyhantçabal et al., 2007). The Polanco Limestones Formation forms part of a marine, mixed carbonate-siliciclastic succession, the Arroyo del Soldado Group, which is traceable over 300 km along the eastern border of the Río de la Plata craton and covers an area of approximately 2,400 km<sup>2</sup> (Figure 4.1). The group reaches almost 3,000 m in thickness, and has been subdivided into four formations: the Yermal, Polanco Limestones, Cerro Espuelitas and Barriga Negra formations (*sensu* Pecoits et al., 2008; 2011) that record deep- to shallow-water marine environments developed during an overall transgression-regression-transgression (Figure 4.2).

At the base, the Arroyo del Soldado Group comprises a fining- and thinning-upward succession with a maximum-recorded thickness of 900 m. It contains interbedded mudstones and sandstones with minor amounts of carbonates, cherts and iron formations (Yermal Formation). The overlying Polanco Limestones Formation is a coarsening-upward succession, composed of minor higher-frequency coarsening-upward cycles. Typical lithologies include dark-grey limestones and dolostones rhythmically interbedded on mm- to meter -scales with rare chert layers. Bracketed between siliciclastic units, the

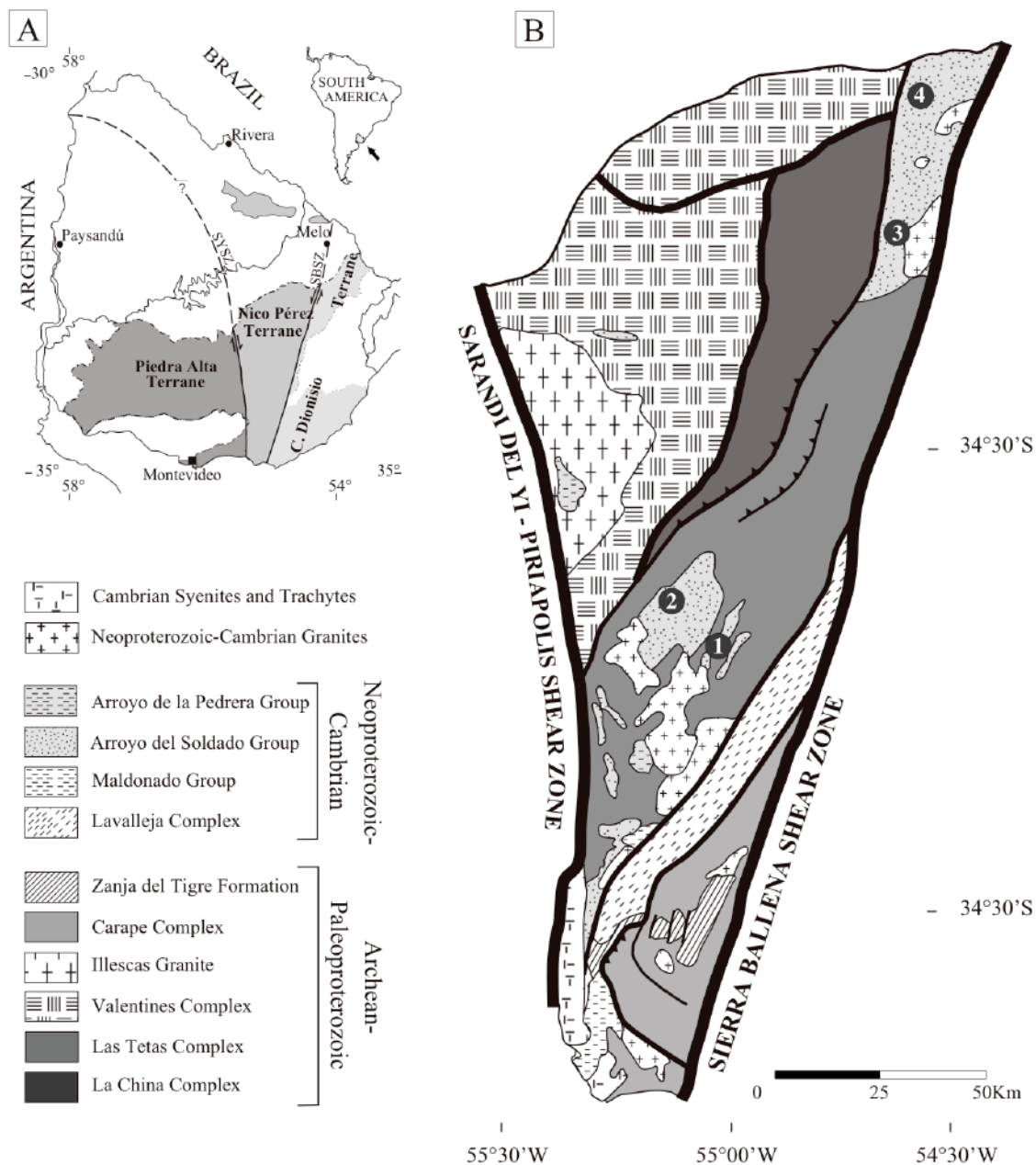


**Figure 4.1.** (A) Location map of Uruguay and tectonostratigraphic subdivision of the crystalline basement. (B) Schematic geological map of part of the Río de la Plata craton (Nico Pérez terrane) showing the distribution of the Arroyo del Soldado Group and location of the sections (1: Los Tapes; 2: Barriga Negra; 3: South Isla Patrulla; 4: Recalde).

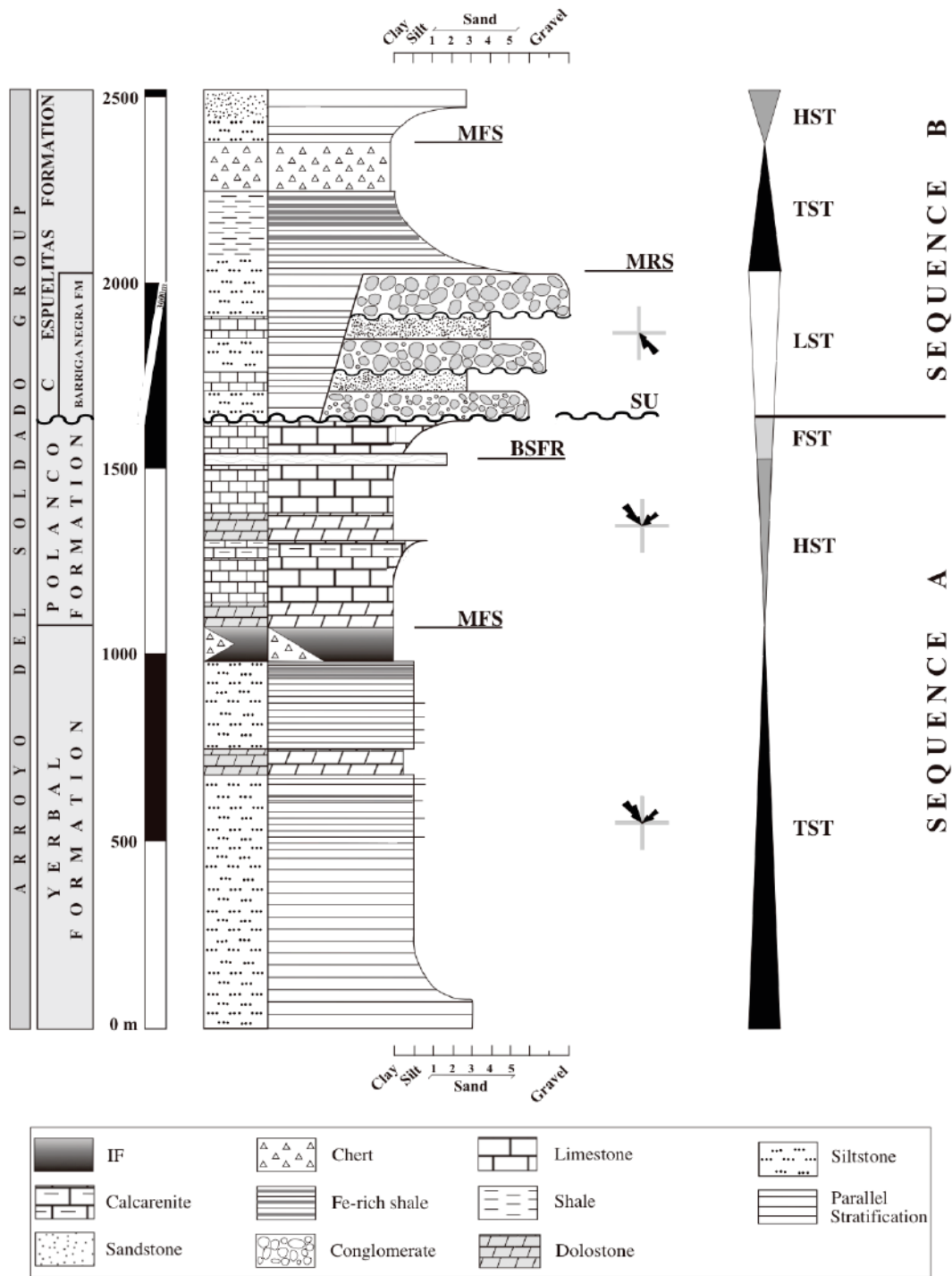


**Figure 4.2.** Simplified stratigraphical column of the Arroyo del Soldado Group (after Pecoits et al., 2008), and sequence stratigraphic interpretation. Abbreviations: SU = subaerial unconformity; BSFR = basal surface of forced regression; MRS = maximum regressive surface; MFS = maximum flooding surface; LST = lowstand systems tract (*sensu* Hunt and Tucker, 1992); TST = transgressive systems tract; HST = highstand system tract; FSST = falling-stage systems tract. Palaeocurrents indicated by rose diagrams.

carbonate succession thickens from less than 75 m to more than 900 m (Figure 4.2). The Barriga Negra Formation is restricted to the western landward margin where it unconformably overlies the Polanco Limestones Formation and consists of basin-margin alluvial fans. The unit comprises thickly bedded conglomerates, carbonate breccias, sandstones and mudstones, which gradationally pass into the Cerro Espuelitas Formation. The latter consists of an alternation of siltstones, black- and iron-rich shales and cherts, with minor occurrences of sandstones and carbonates and locally reaches a thickness of more than 550 m (Figure 4.2).

### 4.3. Analytical methods

Rock samples were collected at intervals between 5 to 10 m. Petrographic analyses were performed on sixty-four thin sections, which were stained with Alizarin Red S and potassium ferricyanide to identify calcite, dolomite, and iron content in both mineral phases. Trace element geochemistry was determined using a PerkinElmer Elan6000 Quad-ICP-MS (quadrupole inductively coupled plasma mass-spectrometer) following  $\text{Na}_2\text{O}_2$  sintering digestion (Longerich et al., 1990). Precision was 4-6% for abundances  $> 0.01$  ppm and  $\leq 10\%$  for the most depleted elements.

Carbonate powders were obtained by using a dental drill, and were analyzed for carbon and oxygen isotopes in the Stable Isotope Laboratory at the University of Alberta. Carbonates phases (calcite and dolomite) were extracted separately, and a total of twenty-nine dolostones and fifty-seven limestones were analyzed.  $\text{CO}_2$  gas was extracted from these powdered carbonate samples on a high vacuum line by reacting 20-40 mg of sample with 100% phosphoric acid at  $25^\circ\text{C}$  for approximately 24 hours of reaction for limestones or 3 days for dolostones (McCrea, 1950). The released  $\text{CO}_2$  gas was analyzed for O and C isotopes on a Finnigan MAT 252 mass spectrometer. All carbon-isotope data are expressed in the  $\delta$ -notation in parts per thousand (‰) using the Vienna Pee Dee Belemnite (V-PDB) international standard. Reproducibility was checked providing an analytical precision of better than  $\pm 0.1\text{‰}$  for  $\delta^{13}\text{C}$  ( $1\sigma$ ) and  $\delta^{18}\text{O}$  ( $1\sigma$ ). From analysis of reference standards, analytical accuracy was estimated to be  $\pm 0.1\text{‰}$ .

Strontium isotope ratios of seventeen limestones were determined using 20 mg aliquots of sample powder following the procedures detailed in Holmden et al. (1996).

Strontium isotopes were measured using a NuPlasma MC-ICP-MS instrument at the University of Alberta. Subsequent to ion chromatographic treatment, the Sr-bearing aliquots were diluted in a 2% HNO<sub>3</sub> solution and aspirated into the ICP. Strontium isotope data were acquired in static, multicollection mode using five Faraday collectors for a total of 400 seconds. Prior to the aspiration of a sample, a 30-second measurement of the gas (+ acid) blank was conducted for the correction of the <sup>86</sup>Kr and <sup>84</sup>Kr isobaric (plasma-based) interferences. The isobaric interference of <sup>87</sup>Rb was monitored and corrected for using the <sup>85</sup>Rb ion signal; however, the latter was negligible for all of the results reported here. Accuracy and reproducibility of the analytical protocol were verified by the repeated analysis of a 100 ppb solution of the NIST SRM 987 Sr isotope standard during the course of this study yielding an average value of 0.710255 ± 0.000020 (1SD; n = 7 analyses) and is indistinguishable compared to the accepted value of 0.710245. The typical internal precision ('error') associated with individual Sr isotope analysis ranges from 0.00001 to 0.00003 (2σ level).

The K-Ar dating was performed on illite samples from the uppermost Yerbal Formation, at CSIRO ESRE facilities, Perth, Western Australia. The sample was gently disaggregated using a repetitive freezing and heating technique to avoid artificial reduction of rock components with K-bearing minerals such as micas or K-feldspars (Liewig et al., 1987). Grain size fractions <2 and 2-6 μm were separated in distilled water according to Stoke's law and a <0.4 μm was separated using a high-speed centrifuge. Clay mineralogy and polytypes were characterized by X-ray Diffraction (XRD). The K-Ar dating technique follows methods described in detail elsewhere (Dalrymple and Lanphere, 1969). Conventional K-Ar isotopic determinations were performed using a VG3600 with an on-line <sup>38</sup>Ar spike following Bonhomme et al. (1975). Argon was extracted from the separated mineral fractions by fusing samples within a vacuum line serviced by an on-line <sup>38</sup>Ar spike pipette. The isotopic composition of the spiked Ar was measured with an on-line VG3600 mass spectrometer using a Faraday cup. The <sup>38</sup>Ar spike was calibrated against biotite GA1550 (McDougall and Roksandic, 1974). During the course of the study 2 standards and 2 airshot values were measured. The K-Ar dating standard and airshot results are summarised in Supplementary Table 1. The error for Argon analyses is below 1% and the <sup>40</sup>Ar/<sup>36</sup>Ar value for airshots averaged 294.28 ± 0.29.

The K-Ar ages were calculated using  $^{40}\text{K}$  abundance and decay constants recommended by Steiger and Jäger (1977). The age uncertainties take into account the errors during sample weighing,  $^{38}\text{Ar}/^{36}\text{Ar}$  and  $^{40}\text{Ar}/^{38}\text{Ar}$  measurements and K analysis. K-Ar age errors are within  $2\sigma$  uncertainty. See Supplementary material (Appendix 3) for full details on XRD and radiometric techniques.

## **4.4. Results**

### ***4.4.1. Facies Associations***

Three main facies associations were recognized and interpreted to represent: inner, mid and outer ramp settings (see description below). The scarcity of gravity-induced deposits related to platform margin, the absence of barred restricted marine conditions (e.g., absence of platform-margin buildups), and the gradual transitions between facies suggest deposition on a homoclinal ramp (Read, 1985; Burchette and Wright, 1992).

#### *4.4.1.1. Medium- to coarse-grained calcarenites with occasional sandstone beds*

##### *Description*

These deposits, up to 200 m thick, are documented in the middle and upper Polanco Limestones Formation at the Recalde and Barriga Negra (parastratotype) sections (see locations in Figure 4.1B). Three main facies are recognized in this facies association: (F1) amalgamated hummocky cross-stratified calcarenites (Figure 4.3A), (F2) trough cross-stratified calcarenites (Figure 4.3B) with sporadic swaley cross-stratification, and (F3) alternations of low-angle cross-stratified and asymmetrically-rippled laminated calcarenites (Figures 4.3C and 4.3D) showing current direction towards the northwest, although a subordinate, reverse current has also been noted. This facies association typically form coarsening- and thickening-upward regressive units. Facies 1 forms the basal parts of this facies association and overlies mid-ramp deposits (see below) with an erosional contact that locally exhibits rip-up clasts. The dominantly trough cross-stratified calcarenites of F2 commonly appear bracketed between F1 and F3 where the latter, positioned erosionally above F2, occurs at the top of the upper coarsening-and thickening-upward cycles.

### *Interpretation*

These deposits are interpreted to represent a storm-dominated inner ramp setting. Facies 1 is taken to represent sedimentation in the upper shoreface environment where well-sorted, low-angle planar cross-bedded calcarenites are interpreted as being produced on a wave-dominated beach face (Dott and Bourgeois, 1982; Dott, 1983). The underlying trough cross-stratified and swaley cross-stratified calcarenites (F2) are characteristic of a storm-dominated middle shoreface environment (Plint, 2011). Trough cross-bedding is generally directed parallel to the shoreline in response to longshore currents; at deeper depths they are sometimes oriented offshore and most likely reflect offshore movement during storms (Hart and Plint, 1989). Thus, the transition from trough cross-stratified and swaley cross-strata into planar cross-stratification and rippled beds with occasional siliciclastic arenite layers suggests a transition to a shallower, higher energy upper shoreface setting where storm and longshore currents were able to form 3-D subaqueous dunes. Hummocky-dominated calcarenites of facies 3 (F3) are interpreted as deposited in the transition between mid-ramp and lower shoreface setting. Their sedimentary structures record frequent storm events indicating water depth above storm-weather wave base (Dott and Bourgeois, 1982).

#### *4.4.1.2. Parallel laminated or thinly interbedded limestone and dolostone calcisiltites*

##### *Description*

This facies association, which is a few meters to more than 200 m thick, is the predominant component within the lower part of the Recalde section and towards the top interfingers with inner ramp facies 3. It is characterized by alternations of grey, parallel laminated or thinly interbedded limestone and dolostone calcisiltites (Figure 4.3E). Occasional hummocky cross-stratified calcarenites and thin massive-appearing to parallel stratified calcarenite beds are also present. The finer-grained sediments dominate. Thinner calcisiltite layers are accompanied by correspondingly thinner hummocky cross-stratified beds and calcarenite intercalations. Dark-grey organic-rich, medium to coarse calcisiltites are finely-interbedded with fine dolosiltites layers. Individual layers are a few millimetres to a few decimetres thick, have sharp contacts, tabular geometries and are laterally continuous. The thicker (0.2-2m) calcarenite beds have erosional bases,

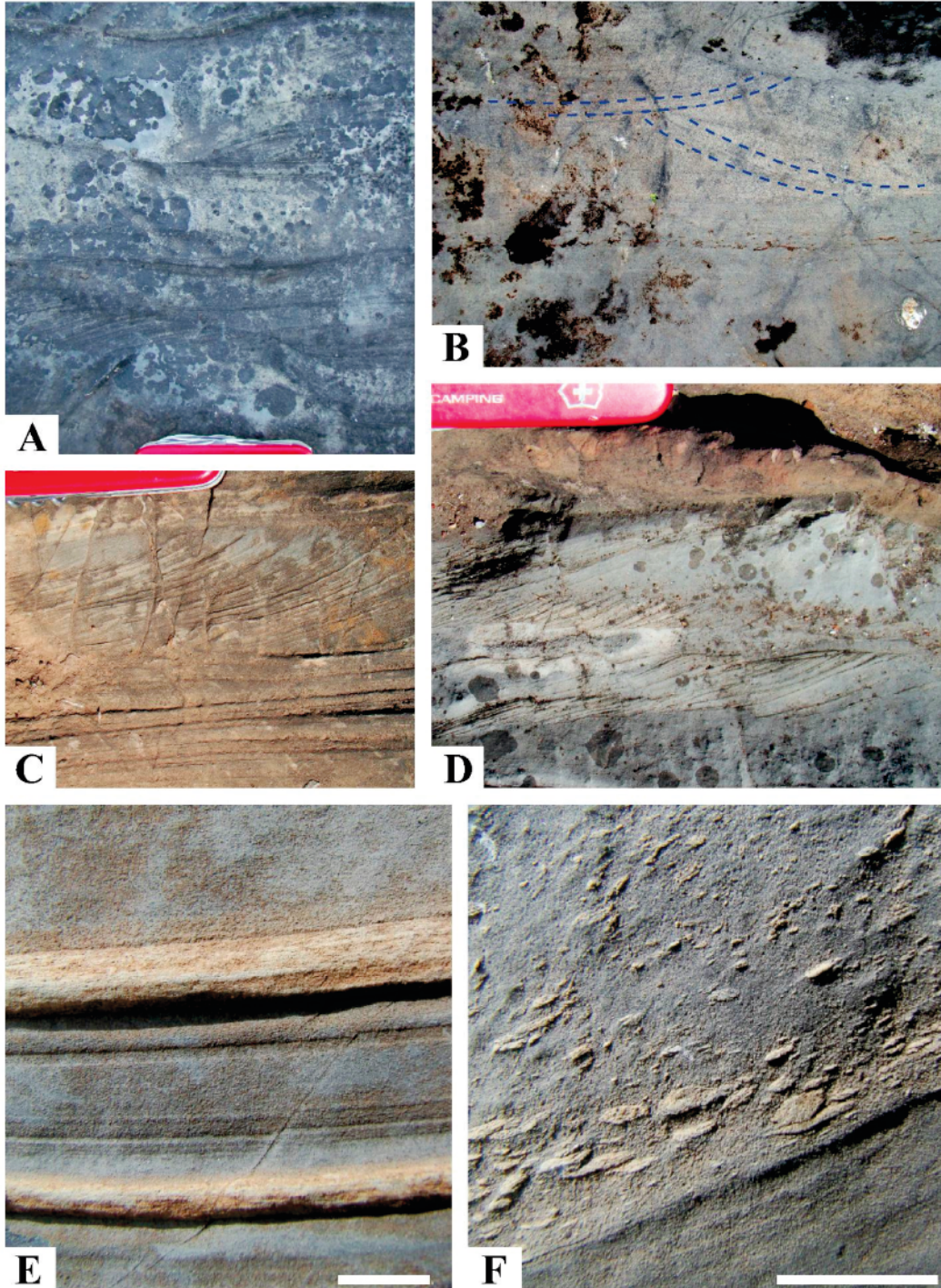


**Figure 4.3.** Inner and middle ramp facies at the Recalde and South Isla Patrulla sections. **(A)** Hummocky cross-bedded sets in medium grained calcarenites. **(B)** Trough cross-stratification showing truncation of foreset laminae. **(C)** and **(D)** Ripple cross-laminated calcarenites. **(E)** Grey laminated limestones interbedded with dolostone calcisiltites. **(F)** Rip-up clasts in normally-graded calcarenite bed. Length of knife = 10cm; Length of scale bar = 3cm.

particularly when present in association with hummocky cross-stratification, may possess intraformational rip-up clasts at the base and normally graded upper portions (Figure 4.3F).

#### *Interpretation*

The position of this lithofacies in stratigraphic sections and the sedimentary features observed suggest that these finely interbedded carbonates formed in a mid- to proximal outer ramp setting characterized by moderate energy, and episodic storm events as indicated by the hummocky cross-stratification. Likewise, repetitive alternation of fine-grained rhythmites and coarser calcarenite beds reflects alternating storm- and fair-weather deposition in more distal outer ramp areas wherein episodic storms were able to transport coarser sediment into deeper waters (e.g., Seguret et al., 2001). Thus, hummocky cross-stratified and graded sandstones were formed as storm sheets on the mid-ramp above the storm wave-base, whereas finer sediments were deposited from suspension during periods of quiescence after cessation of storms. Palaeocurrent trends from interbedded coarser lithologies (calcarenites), lateral changes in facies and thickness, as well as the rare slumps measured indicate that the ramp deepened gradually to the southeast and the coastline was roughly oriented northeast-southwest (see palaeocurrent diagrams in Figure 4.2).

#### *4.4.1.3. Laminated to bedded limestones and dolostones*

##### *Description*

These deposits are best represented in the Los Tapes and the south Isla Patrulla sections (see locations in Figure 4.1B). Two main facies can be distinguished: (F1) thinly bedded limestone-dolostone (Figure 4.4A-D), and (F2) laminated to bedded dolostones. This facies association thickens in the palaeoseaward direction and is characterized by parallel lamination, demarcated by subtle changes in grain size, and occasional chert layers and nodules with no obvious evidence of storm reworking. The limestone and dolostone beds are typically 0.01-1 m thick and grey in colour (Figure 4.4E). The dolostone layers show well-developed grading and display finer-grain size than the limestone and tend to be thinner and more even-bedded and laminated. Light grey, fine-grained, thin- to medium-

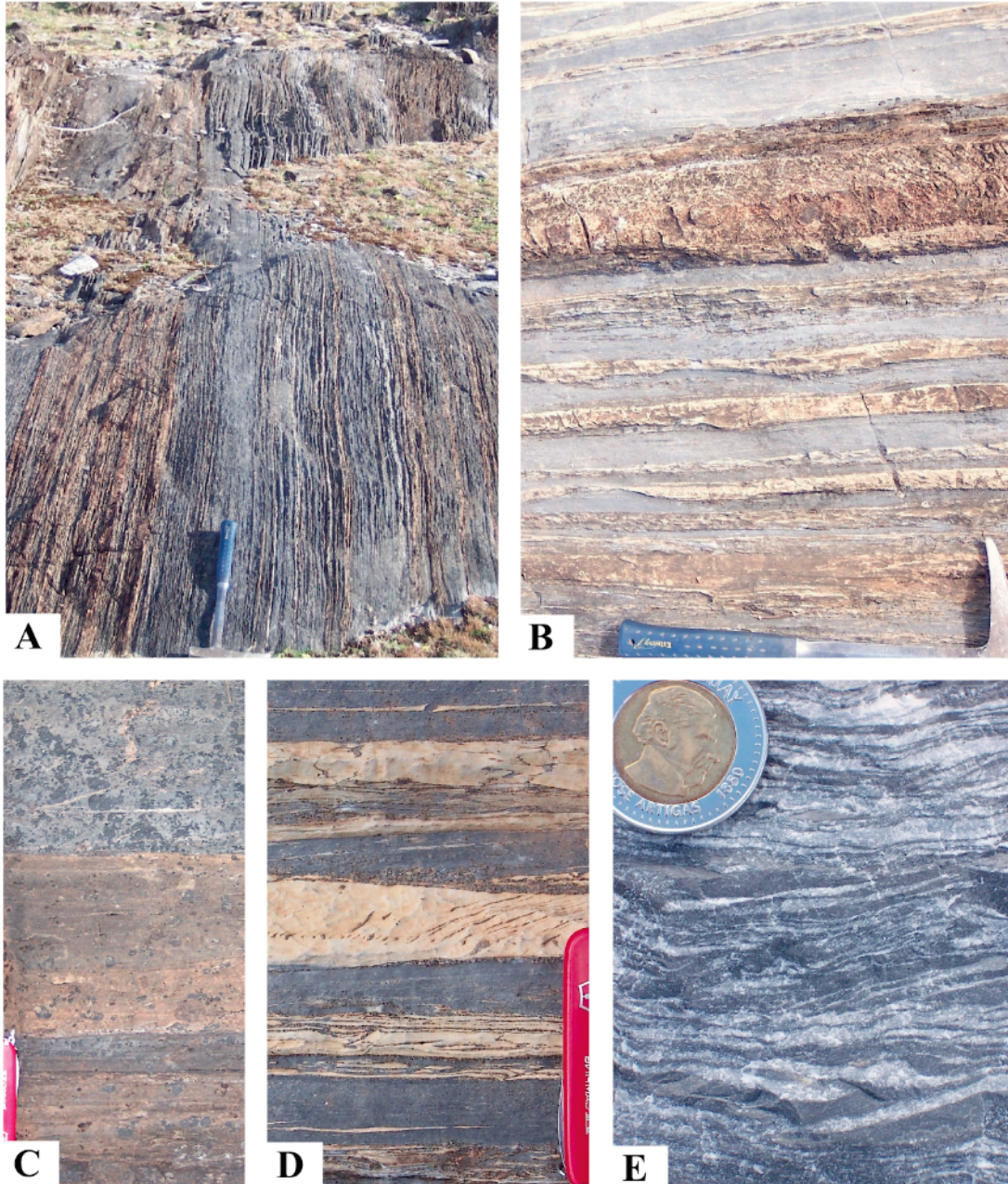


**Figure 4.4.** Outer ramp facies at the Los Tapes section. The carbonate rhythmites represent the most common lithotype of the Polanco Limestone Formation. Rhythmites consist of millimetre- to decimetre-thick alternations of limestone and dolostone layers (A, B). Dolostone predominates over limestone at the base of the section (A). Massive dolostones are usually light beige in colour and form beds up to 25cm thick (C). The contact between dolostone and limestone layers is always sharp, showing no transition (C, D). Colour of the limestones is typically gray, with darker colours at the base passing into lighter shades towards the top (E). Weathered dolostone beds commonly have light beige color due to the iron content of the dolomite, while limestone beds weather gray (A, B, C, D). Length of hammer = 40cm; length of knife = 10cm.

bedded dolostones with chert nodules occur at the top of the Polanco Limestones Formation in the distal parts of the basin (e.g., Cerro Espuelitas area).

#### *Interpretation*

Grain size and sedimentary structures indicate a relatively deep-marine depositional environment characterised by low to moderate energy in an outer ramp setting. The depositional setting was below storm wave base, as suggested by the paucity of graded beds, the presence of fine, parallel lamination and the lack of any evidence of storm or fair-weather wave activity. This facies association was deposited at sufficient depths to be unaffected by wave and storm activity and thus, the cycles recognized in the two other zones are missing in this outer shelf setting. The dark colour of the laminated rhythmites and dolostones, which is due to the organic matter content, suggests anoxic conditions. The poorly-oxygenated, deep-water masses were, however, most likely non-sulfidic as indicated by the abundant organic matter and low S concentrations (<0.012 wt%) in the dolostones and limestones.

#### **4.4.2. Petrography**

The analysis of the different carbonate phases and microfabric is important to interpret isotopic geochemistry of carbonates. Microscopic observations were conducted in order to identify carbonate components and to evaluate crystal size, percentages of clastic and authigenic minerals, extent of dissolution-recrystallization, and other alteration features. The composition of all studied samples was rather uniform, mostly fine-crystalline dolomite (grain size 5-20 $\mu\text{m}$ ) and calcite (< 50 $\mu\text{m}$ ), with few samples showing partial recrystallization (Figure 4.5A-D).

The Polanco carbonates at the Los Tapes and South Isla Patrulla sections are characterized by the alternation of dolostones and limestones (Figure 4.4). Two main types of dolostones, massive and laminated, are developed. Massive dolostones are composed of a xenotopic mosaic of subhedral to anhedral fine-grained dolomite crystals (<20 $\mu\text{m}$ ) with occasional disseminated euhedral pyrite crystals. Laminated dolostones are composed mainly of an idiotopic mosaic of subeuhedral (planar-s) dolomite crystals with sizes ranging between 5 and 20  $\mu\text{m}$  (Figure 4.5A-C). Lamination in dolostones is defined

by the presence of variable amounts of silt-sized quartz and authigenic chert (Figure 4.5A-B), while the lamination in limestones is composed of fine- to medium-grained equigranular calcite ( $<50\mu\text{m}$ ) (Figure 4.5C-D). Pressure-dissolution is indicated by micrometer-sized stylolites, which are generally defined by a residue of kerogen or pyrobitumen. Stylolites are common in areas where dolomite and calcite co-occur (Figure 4.5A). When present, intercrystalline porosity is occluded by sparry calcite and dolomite cements (Figure 4.5D), and, occasionally, chert. Those carbonate cements occur in less than 5% of the rock volume indicating that recrystallization was not extensive. Fractures are usually narrow (up to 25mm wide) and mineral filled. Two types of fracture-filling cement have been recognized: (1) sub-euhedral blocky spar ( $> 200\mu\text{m}$  to  $< 1\text{cm}$ ), and (2) euhedral to sub-euhedral saddle dolomite ( $> 300\mu\text{m}$  to  $< 500\mu\text{m}$ ) (Figure 4.5E-F).

The near micritic crystal size and retention of the primary fabric might indicate that diagenesis and deformation did not greatly alter the original sediment. On the other hand, the presence of blocky spar and fracture-healing cements suggest intermediate to deep burial depth for their origin. Therefore, the relative chronology of the diagenetic phases observed in the Polanco Limestones Formation can be summarized as: (1) depositional and immediately post-depositional phases (micritic to microspar dolostones and limestones); and (2) burial phases (blocky cementation of microfenestral cavities, and healing fractures).

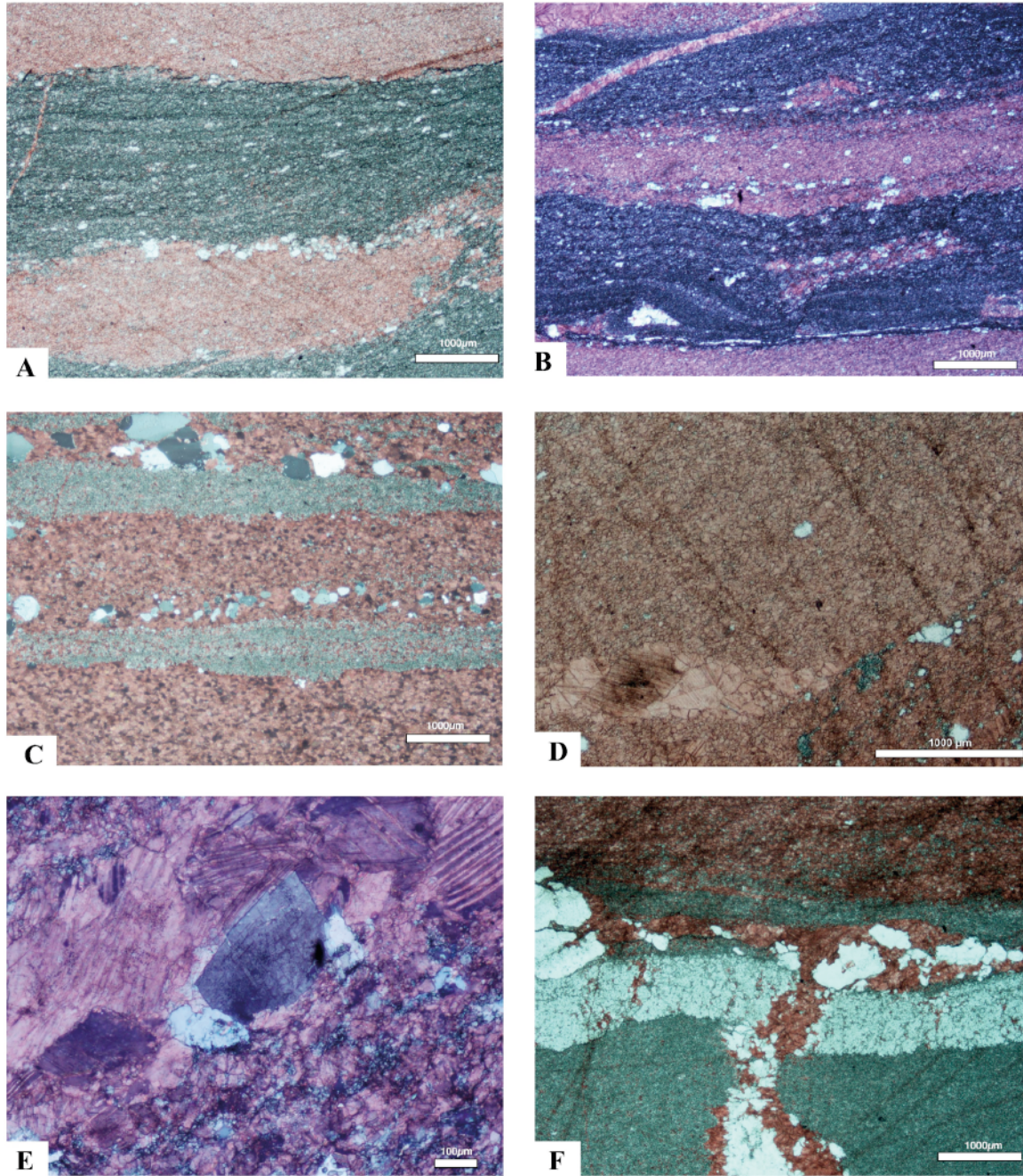


**Figure 4.5.** Thin section microphotographs of carbonate rocks of the Polanco Limestones Formation. Thinly laminated rhythmites show the alternation of microspar laminae with finely laminated dolomicrospar (**A**, **B**) and massive impure dolostone laminae (**C**). Detrital quartz grains are common but never constitute more than the 5% of the rock (**A**, **B**, **C**). Details of fenestral fabric in microspar; blocky calcite oclusing porosity (**D**). Saddle dolomite occurs as a late diagenetic phase filling fractures and in intimate association with subeuhedral blocky spar (**E**). Silicification pulses were probably contemporaneous with fracturing and carbonate filling (**F**).

### 4.4.3. Carbonate geochemistry

#### 4.4.3.1. Oxygen and carbon isotopes

Results of isotopic analyses on microdrilled carbonates are presented in Table 4.1 and are plotted relative to their stratigraphic position on Figures 4.6 and 4.7. The range of  $\delta^{13}\text{C}$  values of dolomite and calcite at the Los Tapes section is narrow (standard deviation for dolomite is 0.8‰ and for calcite is 0.6‰). Carbon isotopic values of dolostones range between -2.7‰ and +0.2‰ (mean = -1.4‰), whereas limestone compositions are between -3.1‰ and -0.4‰ (mean = -1.9‰). The carbon isotope values of both limestones and dolostones show a relatively unimodal distribution, clustered around -1.5‰. At the South Isla Patrulla section (Figure 4.7),  $\delta^{13}\text{C}$  values range between -1.9‰ and +2.0‰ (mean = +0.2‰; standard deviation = 1.3‰). Most of the  $\delta^{18}\text{O}$  values of the Los Tapes limestones (-7.2 to -13.7‰, mean =  $-11.0 \pm 1.8$ ‰) overlap with the range of the dolostones (-6.2 to -12.3‰; mean =  $-8.6 \pm 2.2$ ‰). The oxygen isotope ratios of limestones in the shallow water facies at Recalde reported by Gaucher et al. (2004) (-6.1 to -10.7‰; mean =  $-7.9 \pm 1.5$ ‰) overlap the field of the deep-water facies limestones of Tapes and those from the South Isla Patrulla section, whereas carbon isotope ratios are more variable in their study (-3.3 to +5.3‰).

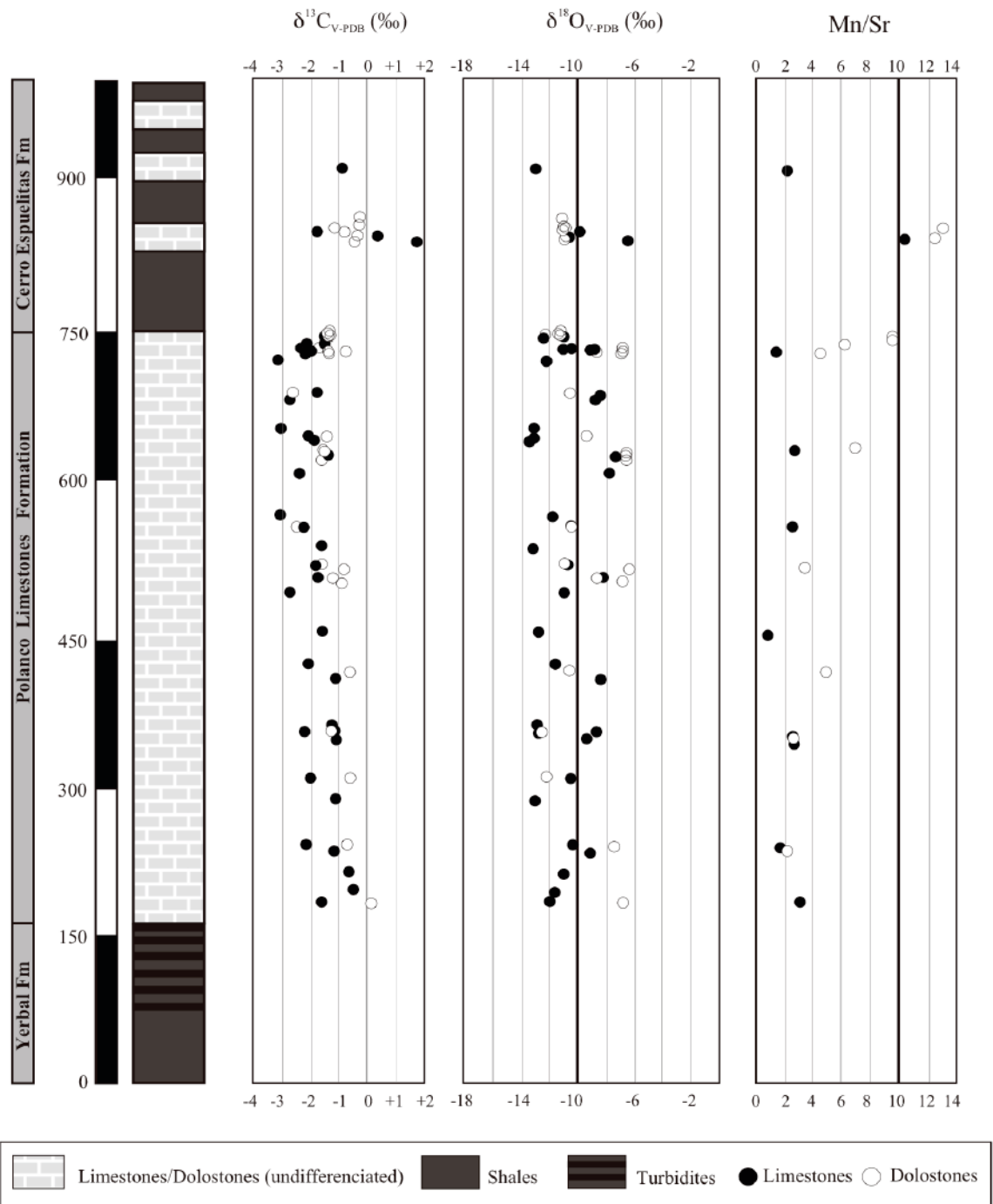
#### 4.4.3.2. Trace elements

Table 4.1 summarizes the concentrations and ratios of Mn and Sr in the Polanco Limestones Formation at the Los Tapes, South Isla Patrulla and Recalde sections. The dolostones and limestones from Los Tapes have relatively low and constant Mn concentrations ( $\text{Mn}_{\text{dolostones}}$  range between 120 and  $\pm 249$ ppm;  $\text{Mn}_{\text{limestones}}$  ranges between 103 and 256ppm) and Sr contents ( $\text{Sr}_{\text{dolostones}}$  range between 21 and 81 ppm;  $\text{Sr}_{\text{limestones}}$  between 36 and 87ppm). Sr concentrations are more variable in the Recalde limestones (from 627 to 2241ppm), corresponding to a narrow range of Mn content (between 37 and 138ppm). The South Isla Patrulla section shows similar Mn (74-92 ppm) and Sr (538-619 ppm) concentrations as those found in the Recalde section.

Unit	Lithology	Sample	$\delta^{18}\text{O}_{\text{PDB}}$	$\delta^{13}\text{C}_{\text{PDB}}$	$\delta^{18}\text{O}_{\text{SMOW}}$	$^{87}\text{Sr}/^{86}\text{Sr}$	2 $\sigma$	Mn/Sr	Mn	Sr	Al	K	Rb
Polanco Limestone Fm. (Los Tapes)	Limestone	060524/1	-11.969	-0.488	18.572								
Polanco Limestone Fm. (Los Tapes)	Limestone	060524/1	-12.005	-1.65	18.534	0.72436	0.000030	3.4	216	63.1	5836	8545	14.6
Polanco Limestone Fm. (Los Tapes)	Limestone	060524/2	-10.93	-0.717	19.642								
Polanco Limestone Fm. (Los Tapes)	Limestone	060524/3	-9.25	-1.289	21.374								
Polanco Limestone Fm. (Los Tapes)	Limestone	060524/3	-10.133	-2.246	20.463	0.73083	0.000030	1.9	148	79.7	4530	5546	9.08
Polanco Limestone Fm. (Los Tapes)	Limestone	060524/4	-13.512	-1.005	16.98								
Polanco Limestone Fm. (Los Tapes)	Limestone	060524/4	-10.288	-2.058	20.304								
Polanco Limestone Fm. (Los Tapes)	Limestone	060524/5	-12.869	-2.273	17.643								
Polanco Limestone Fm. (Los Tapes)	Limestone	060524/5	-9.795	-1.199	20.182								
Polanco Limestone Fm. (Los Tapes)	Limestone	060524/5	-8.86	-1.27	21.776	0.73701	0.000033	2.4	139	59	6933	5240	14.9
Polanco Limestone Fm. (Los Tapes)	Limestone	060524/5	-12.902	-1.287	17.609			2.4	143	58.5	6909	5243	15
Polanco Limestone Fm. (Los Tapes)	Limestone	060524/6	-8.393	-1.283	22.258								
Polanco Limestone Fm. (Los Tapes)	Limestone	060524/6	-11.881	-2.146	18.661								
Polanco Limestone Fm. (Los Tapes)	Limestone	060524/7	-13.161	-1.567	17.342	0.73673	0.000016	1.2	103	84.3	2239	1893	3.35
Polanco Limestone Fm. (Los Tapes)	Limestone	060524/7	-13.161	-1.567	17.342								
Polanco Limestone Fm. (Los Tapes)	Limestone	060524/8	-8.357	-1.815	22.294								
Polanco Limestone Fm. (Los Tapes)	Limestone	060524/8	-11.351	-2.813	19.208								
Polanco Limestone Fm. (Los Tapes)	Limestone	060524/9	-10.872	-1.908	19.702								
Polanco Limestone Fm. (Los Tapes)	Limestone	060524/10	-13.481	-1.697	17.013								
Polanco Limestone Fm. (Los Tapes)	Limestone	060524/11	-10.328	-2.408	20.263	0.73769	0.000022	2.5	138	55.5	1494	1741	2.42
Polanco Limestone Fm. (Los Tapes)	Limestone	060524/11	-11.977	-3.079	18.563								
Polanco Limestone Fm. (Los Tapes)	Limestone	060524/12	-7.23	-1.622	23.457								
Polanco Limestone Fm. (Los Tapes)	Limestone	060524/12	-7.999	-2.47	22.664	0.74823	0.000026						
Polanco Limestone Fm. (Los Tapes)	Limestone	060524/13	-13.079	-3.112	17.427								
Polanco Limestone Fm. (Los Tapes)	Limestone	060524/13	-13.676	-2.002	16.811								
Polanco Limestone Fm. (Los Tapes)	Limestone	060524/13	-13.745	-1.973	16.741								
Polanco Limestone Fm. (Los Tapes)	Limestone	060524/14	-8.299	-1.849	22.354								
Polanco Limestone Fm. (Los Tapes)	Limestone	060524/14	-8.622	-2.942	22.022								
Polanco Limestone Fm. (Los Tapes)	Limestone	060524/15	-12.003	-3.179	18.536								
Polanco Limestone Fm. (Los Tapes)	Limestone	060524/15	-9.58	-2.109	21.034								
Polanco Limestone Fm. (Los Tapes)	Limestone	060524/15	-9.58	-2.109	21.034								
Polanco Limestone Fm. (Los Tapes)	Limestone	060524/15	-9.319	-2.165	21.303								
Polanco Limestone Fm. (Los Tapes)	Limestone	060524/15	-11.099	-2.22	19.468								
Polanco Limestone Fm. (Los Tapes)	Limestone	060524/15	-10.105	-2.073	20.493	0.73645	0.000021	1.6	140	87	3238	2682	4.62
Polanco Limestone Fm. (Los Tapes)	Limestone	060524/16				0.74361	0.000030		256	36.1	15065.8	11735	24.9
Polanco Limestone Fm. (Los Tapes)	Limestone	060524/17	-11.315	-1.53	19.245								
Polanco Limestone Fm. (Los Tapes)	Limestone	060524/17	-12.391	-1.661	18.136								
Cerro Espueltas Formation (Los Tapes)	Limestone	060525/2	-6.405	1.856	24.307	0.74532	0.000021	10.6	704	66.3	8206	4554	18.6
Cerro Espueltas Formation (Los Tapes)	Limestone	060525/2	-10.227	0.369	20.367								
Cerro Espueltas Formation (Los Tapes)	Limestone	060525/2	-9.999	-1.978	20.602								
Cerro Espueltas Formation (Los Tapes)	Limestone	060525/3	-13.194	-0.944	17.308	0.73100	0.000014	2.2	249	112	2666	1597	9.6
Polanco Limestone Fm. (Los Tapes)	Dolostone	060524/1	-6.993	0.21	23.701								
Polanco Limestone Fm. (Los Tapes)	Dolostone	060524/3	-7.892	-0.773	22.774			2	161	80.9	4300	5407	8.9
Polanco Limestone Fm. (Los Tapes)	Dolostone	060524/4	-12.312	-0.695	18.217								
Polanco Limestone Fm. (Los Tapes)	Dolostone	060524/5	-12.349	-1.064	18.18			2.3	141	62.5	7476	6141	15.9
Polanco Limestone Fm. (Los Tapes)	Dolostone	060524/6	-10.245	-0.662	20.349			4.9	213	43.6	8204	6871	14.6
Polanco Limestone Fm. (Los Tapes)	Dolostone	060524/8	-7.19	-0.942	23.497								
Polanco Limestone Fm. (Los Tapes)	Dolostone	060524/8	-6.247	-0.915	24.469								
Polanco Limestone Fm. (Los Tapes)	Dolostone	060524/8	-8.59	-1.185	22.055								
Polanco Limestone Fm. (Los Tapes)	Dolostone	060524/9	-11.04	-1.869	19.529			3.2	120	38.1	32448	24590	50.2

Unit	Lithology	Sample	$\delta^{18}\text{O}_{\text{PDB}}$	$\delta^{13}\text{C}_{\text{PDB}}$	$\delta^{18}\text{O}_{\text{SMOW}}$	$^{87}\text{Sr}/^{86}\text{Sr}$	2 $\sigma$	Mn/Sr	Mn	Sr	Al	K	Rb
Polanco Limestone Fm. (Los Tapes)	Limestone	060524/1	-11.969	-0.488	18.572								
Polanco Limestone Fm. (Los Tapes)	Limestone	060524/1	-12.005	-1.65	18.534	0.72436	0.000030	3.4	216	63.1	5836	8545	14.6
Polanco Limestone Fm. (Los Tapes)	Limestone	060524/2	-10.93	-0.717	19.642								
Polanco Limestone Fm. (Los Tapes)	Limestone	060524/3	-9.25	-1.289	21.374								
Polanco Limestone Fm. (Los Tapes)	Limestone	060524/3	-10.133	-2.246	20.463	0.73083	0.000030	1.9	148	79.7	4530	5546	9.08
Polanco Limestone Fm. (Los Tapes)	Limestone	060524/4	-13.512	-1.005	16.98								
Polanco Limestone Fm. (Los Tapes)	Limestone	060524/4	-10.288	-2.058	20.304								
Polanco Limestone Fm. (Los Tapes)	Limestone	060524/5	-12.869	-2.273	17.643								
Polanco Limestone Fm. (Los Tapes)	Limestone	060524/5	-9.795	-1.199	20.182								
Polanco Limestone Fm. (Los Tapes)	Limestone	060524/5	-8.86	-1.27	21.776	0.73701	0.000033	2.4	139	59	6933	5240	14.9
Polanco Limestone Fm. (Los Tapes)	Limestone	060524/5	-12.902	-1.287	17.609			2.4	143	58.5	6909	5243	15
Polanco Limestone Fm. (Los Tapes)	Limestone	060524/6	-8.393	-1.283	22.258								
Polanco Limestone Fm. (Los Tapes)	Limestone	060524/6	-11.881	-2.146	18.661								
Polanco Limestone Fm. (Los Tapes)	Limestone	060524/7	-13.161	-1.567	17.342	0.73673	0.000016	1.2	103	84.3	2239	1893	3.35
Polanco Limestone Fm. (Los Tapes)	Limestone	060524/7	-13.161	-1.567	17.342								
Polanco Limestone Fm. (Los Tapes)	Limestone	060524/8	-8.357	-1.815	22.294								
Polanco Limestone Fm. (Los Tapes)	Limestone	060524/8	-11.351	-2.813	19.208								
Polanco Limestone Fm. (Los Tapes)	Limestone	060524/9	-10.872	-1.908	19.702								
Polanco Limestone Fm. (Los Tapes)	Limestone	060524/10	-13.481	-1.697	17.013								
Polanco Limestone Fm. (Los Tapes)	Limestone	060524/11	-10.328	-2.408	20.263	0.73769	0.000022	2.5	138	55.5	1494	1741	2.42
Polanco Limestone Fm. (Los Tapes)	Limestone	060524/11	-11.977	-3.079	18.563								
Polanco Limestone Fm. (Los Tapes)	Limestone	060524/12	-7.23	-1.622	23.457								
Polanco Limestone Fm. (Los Tapes)	Limestone	060524/12	-7.999	-2.47	22.664	0.74823	0.000026						
Polanco Limestone Fm. (Los Tapes)	Limestone	060524/13	-13.079	-3.112	17.427								
Polanco Limestone Fm. (Los Tapes)	Limestone	060524/13	-13.676	-2.002	16.811								
Polanco Limestone Fm. (Los Tapes)	Limestone	060524/13	-13.745	-1.973	16.741								
Polanco Limestone Fm. (Los Tapes)	Limestone	060524/14	-8.299	-1.849	22.354								
Polanco Limestone Fm. (Los Tapes)	Limestone	060524/14	-8.622	-2.942	22.022								
Polanco Limestone Fm. (Los Tapes)	Limestone	060524/15	-12.003	-3.179	18.536								
Polanco Limestone Fm. (Los Tapes)	Limestone	060524/15	-9.58	-2.109	21.034								
Polanco Limestone Fm. (Los Tapes)	Limestone	060524/15	-9.58	-2.109	21.034								
Polanco Limestone Fm. (Los Tapes)	Limestone	060524/15	-9.319	-2.165	21.303								
Polanco Limestone Fm. (Los Tapes)	Limestone	060524/15	-11.099	-2.22	19.468								
Polanco Limestone Fm. (Los Tapes)	Limestone	060524/15	-10.105	-2.073	20.493	0.73645	0.000021	1.6	140	87	3238	2682	4.62
Polanco Limestone Fm. (Los Tapes)	Limestone	060524/16				0.74361	0.000030		256	36.1	15065.8	11735	24.9
Polanco Limestone Fm. (Los Tapes)	Limestone	060524/17	-11.315	-1.53	19.245								
Polanco Limestone Fm. (Los Tapes)	Limestone	060524/17	-12.391	-1.661	18.136								
Cerro Espueltas Formation (Los Tapes)	Limestone	060525/2	-6.405	1.856	24.307	0.74532	0.000021	10.6	704	66.3	8206	4554	18.6
Cerro Espueltas Formation (Los Tapes)	Limestone	060525/2	-10.227	0.369	20.367								
Cerro Espueltas Formation (Los Tapes)	Limestone	060525/2	-9.999	-1.978	20.602								
Cerro Espueltas Formation (Los Tapes)	Limestone	060525/3	-13.194	-0.944	17.308	0.73100	0.000014	2.2	249	112	2666	1597	9.6
Polanco Limestone Fm. (Los Tapes)	Dolostone	060524/1	-6.993	0.21	23.701								
Polanco Limestone Fm. (Los Tapes)	Dolostone	060524/3	-7.892	-0.773	22.774			2	161	80.9	4300	5407	8.9
Polanco Limestone Fm. (Los Tapes)	Dolostone	060524/4	-12.312	-0.695	18.217								
Polanco Limestone Fm. (Los Tapes)	Dolostone	060524/5	-12.349	-1.064	18.18			2.3	141	62.5	7476	6141	15.9
Polanco Limestone Fm. (Los Tapes)	Dolostone	060524/6	-10.245	-0.662	20.349			4.9	213	43.6	8204	6871	14.6
Polanco Limestone Fm. (Los Tapes)	Dolostone	060524/8	-7.19	-0.942	23.497								
Polanco Limestone Fm. (Los Tapes)	Dolostone	060524/8	-6.247	-0.915	24.469								
Polanco Limestone Fm. (Los Tapes)	Dolostone	060524/8	-8.59	-1.185	22.055								
Polanco Limestone Fm. (Los Tapes)	Dolostone	060524/9	-11.04	-1.869	19.529			3.2	120	38.1	32448	24590	50.2

**Table 4.1.** Oxygen, C, and Sr isotope values as well as trace element concentrations of carbonates from the Polanco Limestones and Cerro Espueltas formations.



**Figure 4.6.** Schematic stratigraphic profile of the Polanco Limestones Formation at the Los Tapes section and corresponding vertical variations in  $\delta^{13}\text{C}$ ,  $\delta^{18}\text{O}$ , and Mn/Sr values.

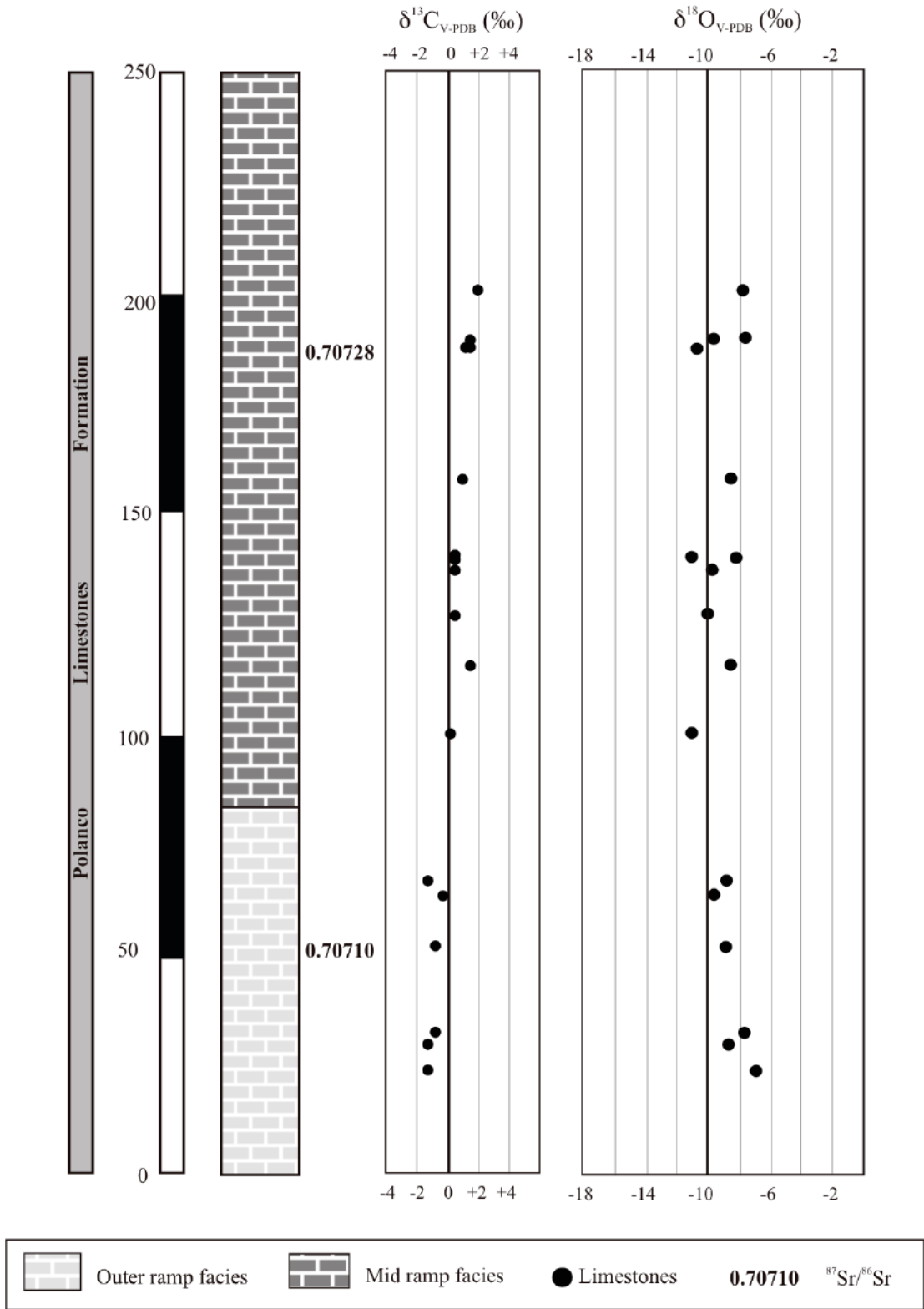


**Figure 4.7.** Schematic stratigraphic profile of the Polanco Limestones Formation at the South Isla Patrulla section and corresponding vertical variations in  $\delta^{13}\text{C}$  and  $\delta^{18}\text{O}$  values.

#### **4.4.3.3. Strontium isotopes**

The range of Sr isotope values (Table 4.1) is similar in both South Isla Patrulla ( $^{87}\text{Sr}/^{86}\text{Sr} = 0.70710$  to  $0.70728$ ) and Recalde ( $^{87}\text{Sr}/^{86}\text{Sr} = 0.70677$  to  $0.70791$ ) carbonates. In contrast, Sr isotopic ratios from the Los Tapes section are significantly higher ( $^{87}\text{Sr}/^{86}\text{Sr} = 0.72436$  to  $0.74823$ ).

#### **4.4.4. Clay mineralogy**

The dominant clay minerals present are  $2M_1$  illite and kaolinite. The sample fractions contain variable amounts of quartz and  $2M_1$  illite is enriched in the finest  $<0.4 \mu\text{m}$  fraction (see Supplementary Table 2.2). No low temperature  $1M/1M_d$  polytype could be identified by XRD.

#### **4.4.5. K-Ar dating**

Three clay fractions  $<0.4$ ,  $<2$  and  $2-6 \mu\text{m}$  from sample 101025/1 (uppermost Yerbal Formation) were analyzed. The K-Ar ages are referred to the Gradstein et al. (2004) timescale and vary significantly (Supplementary Appendix 3 Table 2.3.3). The  $<0.4 \mu\text{m}$  illite fraction yields the youngest age of  $513.8 \pm 10.4$  Ma (Cambrian-Series 2-Stage 4). The  $<2 \mu\text{m}$  illite fraction yields an intermittent age of  $574.7 \pm 11.6$  Ma (Neoproterozoic-Ediacaran), whereas the coarse grained  $2-6 \mu\text{m}$  illite fraction yields the oldest age of  $636.5 \pm 12.8$  Ma (Neoproterozoic-Cryogenian). Radiogenic  $^{40}\text{Ar}$  ranges from 96.4 to 98.9% indicating negligible atmospheric Ar contamination and reliable analytical conditions for all analyses. The K contents range homogeneously from 4.2 to 4.3%.

### **4.5. Discussion**

#### ***4.5.1. Effect of diagenetic alteration on carbonate carbon, oxygen and strontium isotope compositions***

A crucial question in any study of carbon isotope composition of ancient carbonates is whether primary marine signature is preserved. One widely-used screening method for evaluating the effects of diagenesis on primary carbon and oxygen isotope compositions is their comparison with absolute and relative trace element abundances (e.g., Brand and Veizer, 1980). For Precambrian carbonates, different abundance ratios and combinations

of trace elements and isotopic data are used; one of the most commonly used proxies for post-depositional alteration is the Mn/Sr ratio which is used for assessing post-depositional alterations of  $\delta^{13}\text{C}$  values (e.g., Kaufman et al., 1991; Jacobsen and Kaufman, 1999; Bekker et al., 2003). During diagenesis, enrichment in Mn is accompanied by the depletion in Sr, increasing the overall Mn/Sr ratios (Brand and Veizer, 1980; Banner and Hanson, 1990). Carbonates with Mn/Sr ratios less than 3.0 are considered to be best-preserved (Derry et al. 1992; Kaufman et al. 1993).

Strontium concentrations in the Los Tapes section are lower and more homogeneous than those found in the South Isla Patrulla and Recalde areas (see Table 4.1). The low Sr concentrations in the Los Tapes section, however, do not correlate with an increase in the Mn concentrations, which suggests that both Mn and Sr concentrations are not controlled by the degree of diagenetic alteration. The Mn/Sr ratios of limestones, although lower, are within the range of those displayed by dolostones. This difference might be explained by a better fit of Sr into the crystal lattice of calcite (Veizer, 1983). Although limestones with Mn/Sr ratios above 3.0 might reflect some post-depositional alteration, the consistency of  $\delta^{13}\text{C}$  values among closely-spaced samples with different Mn/Sr ratios supports a near-to-primary carbon isotope composition. In contrast, Mn/Sr values in the Recalde and South Isla Patrulla areas are  $<0.25$  (Table 4.1). This difference in Mn/Sr ratios at studied sections may be explained by distinct degrees of alteration in shallow and deep sections. Additionally, the common presence of dolomite in the Los Tapes section (Figure 4.5) might be responsible for the overall increase in Mn/Sr ratios of the rhythmites, because Mn easily substitute for Mg during precipitation of either primary or secondary dolomite (Brand and Veizer, 1980; Fairchild et al., 1990; Vasconcelos and McKenzie, 1997). Importantly, the lack of correlation between the Mn/Sr ratios and  $\delta^{13}\text{C}$  (or  $\delta^{18}\text{O}$ ) values and  $\delta^{13}\text{C}$  values and Mn (or Sr) contents suggests that carbon isotope values from both the Los Tapes and Recalde sections were not strongly influenced by post-depositional alteration (Figure 4.8). Therefore, the measured  $\delta^{13}\text{C}$  values most likely reflect contemporaneous seawater composition.

The  $\delta^{18}\text{O}$  values can be also used to evaluate diagenetic alteration and the degree of interaction between carbonates and post-depositional fluids (Jacobsen and Kaufman, 1999). As expected,  $\delta^{18}\text{O}$  values of the dolostones at the Los Tapes section are slightly

enriched with respect to coexisting limestones (Figure 4.6) (O’Neil and Epstein, 1966). Additionally, the smaller grain size (Figure 4.5A and B), earlier stabilization in the post-depositional history and the resulting lower permeability of dolostones might have contributed to better preservation of their original geochemical signature (Pelechaty, 1998). Many of the limestone and dolostone samples display oxygen isotope values above -10‰, similar to least-altered Neoproterozoic carbonates (Figure 4.9) (Kaufman and Knoll, 1995).

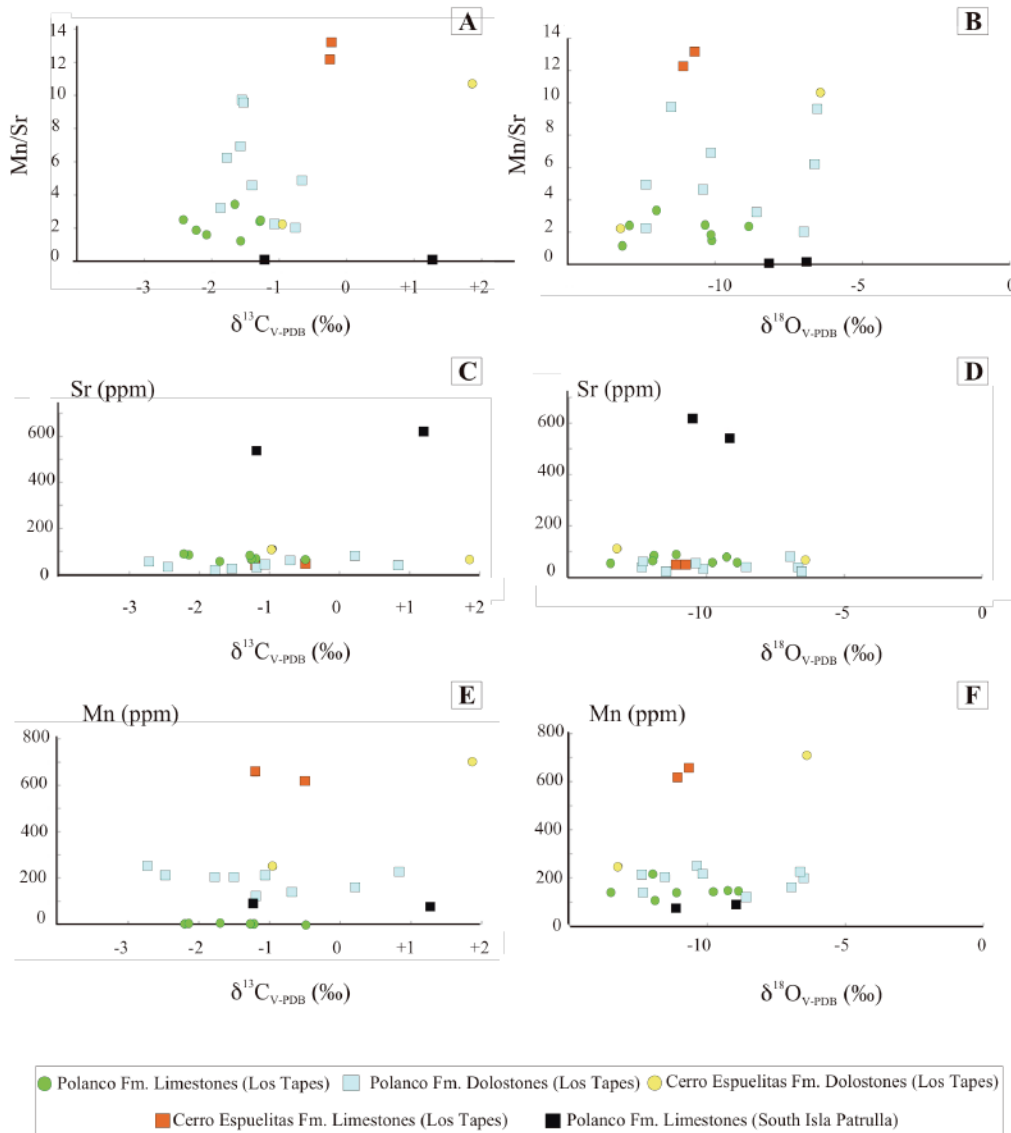


**Figure 4.8.** Scatter diagrams for the Polanco Limestones Formation and the overlying Cerro Espuelitas Formation at the Los Tapes and South Isla Patrulla sections (A) Mn/Sr vs.  $\delta^{13}\text{C}$ , (B) Mn/Sr vs.  $\delta^{18}\text{O}$ , (C) Sr vs.  $\delta^{13}\text{C}$ , (D) Sr vs.  $\delta^{18}\text{O}$ , (E) Mn vs.  $\delta^{13}\text{C}$ , and (F) Mn/Sr vs.  $\delta^{18}\text{O}$ .

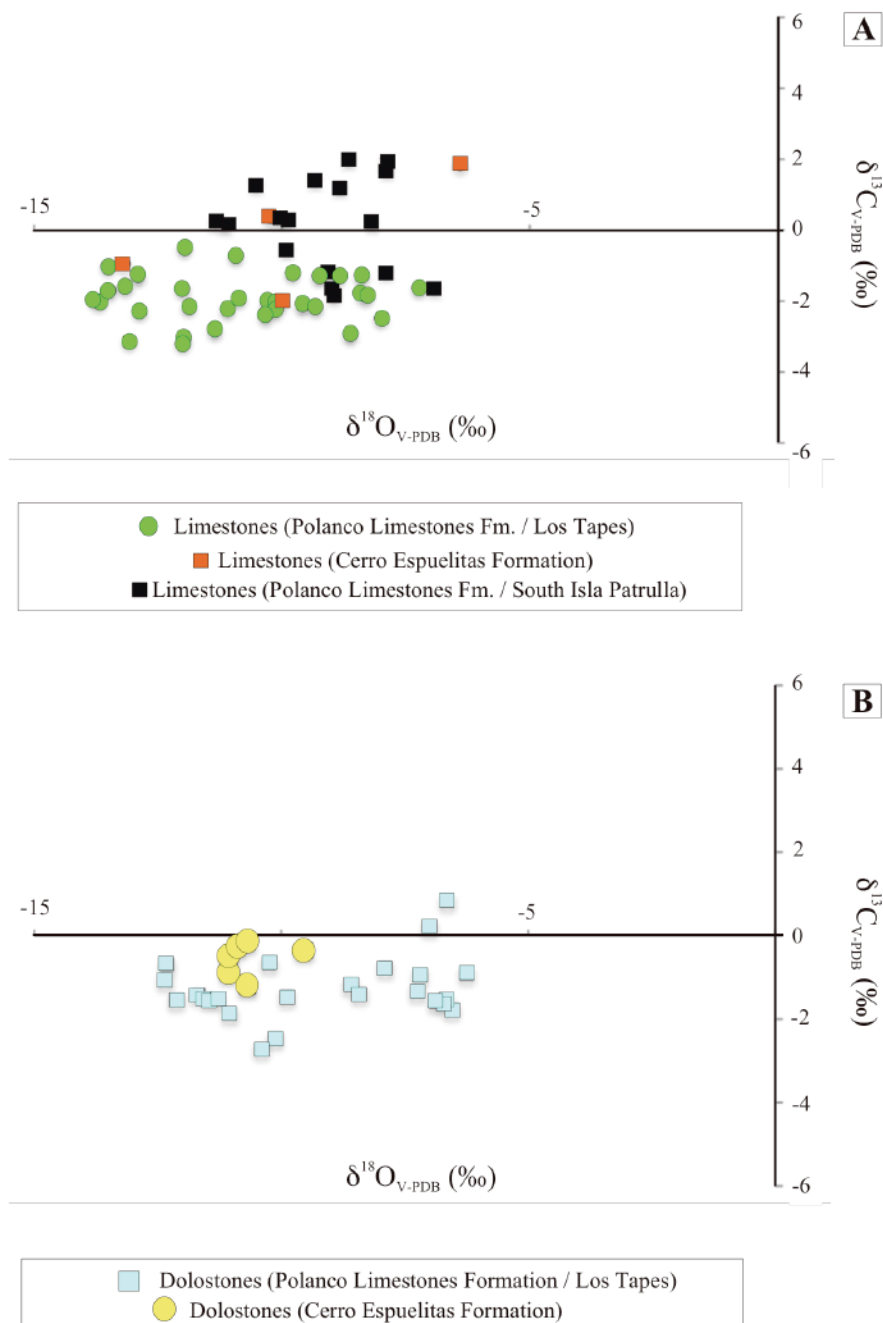


**Figure 4.9.**  $\delta^{18}\text{O}$  vs.  $\delta^{13}\text{C}_{\text{carb}}$  cross plot for carbonates from the Polanco Limestones Formation and the overlying Cerro Espuelitas Formation at the Los Tapes and South Isla Patrulla sections. The  $R^2$  coefficient of co-variation for the  $\delta^{18}\text{O}$  and  $\delta^{13}\text{C}_{\text{carb}}$  values for the limestones (**A**) and dolostones (**B**) is less than 0.01 indicating no clear correlation between the isotopic data.

Overprinting of primary  $^{87}\text{Sr}/^{86}\text{Sr}$  compositions may result from the mixing of Sr derived from seawater with that derived from external sources (Montañez et al., 1996; Sawaki et al., 2008). Regardless the cause of these elevated values, the  $^{87}\text{Sr}/^{86}\text{Sr}$  ratios from Los Tapes are unlikely to record seawater composition. In turn, the majority of samples from the Recalde area do not show correlation of  $^{87}\text{Sr}/^{86}\text{Sr}$  ratios with  $\delta^{13}\text{C}$ , Mn/Sr or Sr values, which supports preservation of depositional Sr isotope values (Figure 4.10).

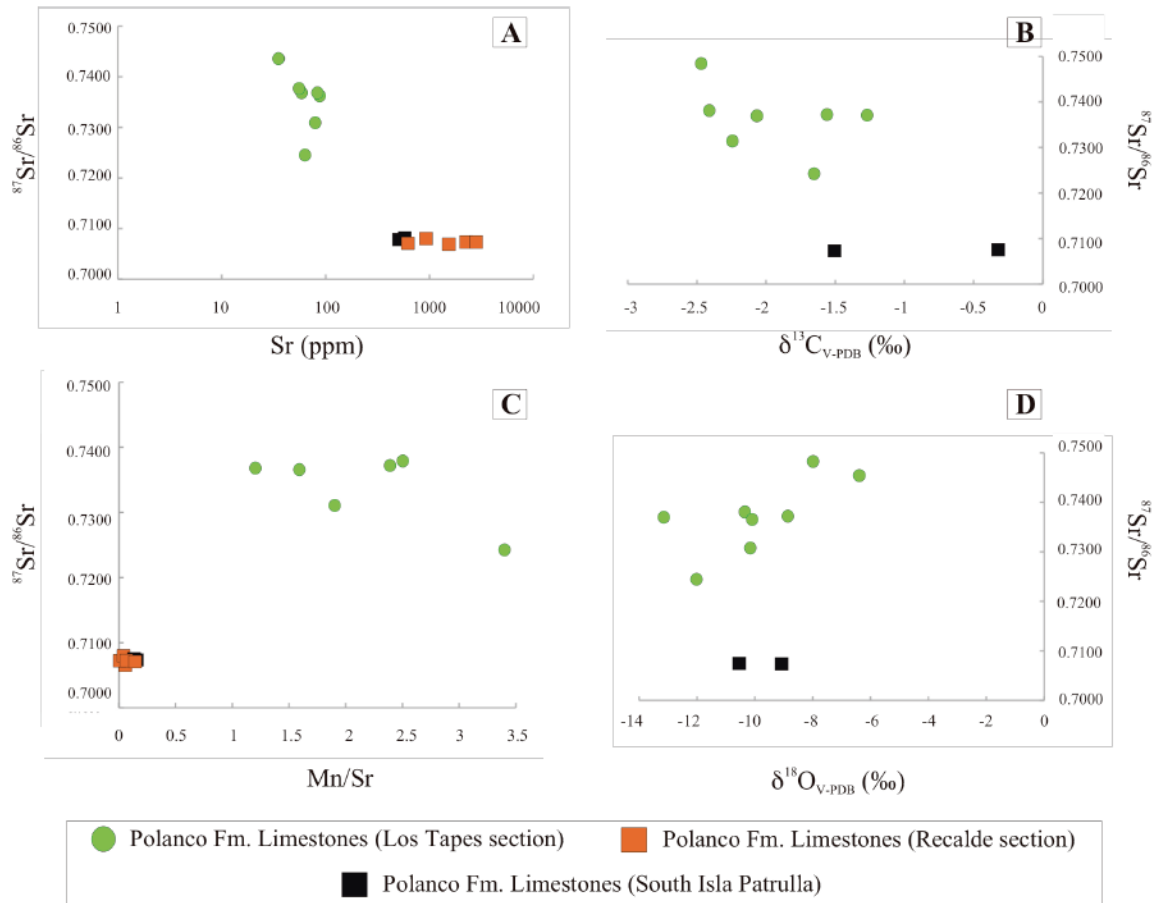


**Figure 4.10.** Scatter diagrams for limestones from the Los Tapes, South Isla Patrulla and Recalde sections. **(A)**  $^{87}\text{Sr}/^{86}\text{Sr}$  vs. Sr (ppm).  $R^2_{\text{Tapes}} = 0.15$ , **(B)**  $^{87}\text{Sr}/^{86}\text{Sr}$  vs.  $\delta^{13}\text{C}$ .  $R^2_{\text{Tapes}} = 0.16$ , **(C)**  $^{87}\text{Sr}/^{86}\text{Sr}$  vs. Mn/Sr.  $R^2_{\text{Tapes}} = 0.31$ , and **(D)**  $^{87}\text{Sr}/^{86}\text{Sr}$  vs.  $\delta^{18}\text{O}$ .  $R^2_{\text{Tapes}} = 0.49$ .

#### 4.5.2. C- and Sr-isotope chemostratigraphy

Well-preserved C- and Sr-isotope data obtained for marine carbonates have provided a detailed record of isotopic variations in seawater through time (Melezhik et al., 2001;

Shields and Veizer, 2002). Variations in the isotopic composition of carbon in carbonates is a particularly useful indicator of biogeochemical changes over the geological time, reflecting the isotopic composition of carbon inputs to the ocean-atmosphere system, the average fractionation between dissolved inorganic carbon and organic matter, and the proportion of organic matter to carbonate buried in sediments (Kump and Arthur, 1999). In contrast, the  $^{87}\text{Sr}/^{86}\text{Sr}$  of seawater tracks the balance between riverine inputs to the ocean, which result from continental weathering, and inputs from submarine hydrothermal systems (Goldstein and Jacobsen, 1987; Palmer and Edmond, 1989). Hence,  $^{87}\text{Sr}/^{86}\text{Sr}$  ratios are considered a useful proxy to trace global-scale changes in tectonics and climate on a geologic timescale.

The dominant features of the carbon and strontium isotope variations in the Neoproterozoic-Cambrian seawater are generally known, and reference curves of secular variations have been presented by several authors (Melezhik et al., 2001; Halverson et al., 2010; Sawaki et al., 2010). Characteristic features include: (i) high average  $\delta^{13}\text{C}$  values ( $\approx 5\text{‰}$ ) during the Tonian (1,000-850 Ma) and Cryogenian (850-635 Ma), punctuated by three negative  $\delta^{13}\text{C}$  anomalies during the Bitter Spring Stage and in association with the Sturtian and Marinoan glaciations, (ii) highly variable, and on average low  $\delta^{13}\text{C}$  values, during the Ediacaran Period, including a distinctive negative anomaly to values as low as  $-12\text{‰}$  (Shuram-Wonoka-Johnnie anomaly), and (iii) variable but near average  $\approx 0\text{‰}$  values during the Cambrian, following an apparently short-lived negative excursion at the Precambrian-Cambrian boundary (Halverson et al., 2007; Ishikawa et al., 2008). In contrast, the general pattern of the  $^{87}\text{Sr}/^{86}\text{Sr}$  record shows a progressive rise through most of the Neoproterozoic (Halverson et al., 2010; Sawaki et al., 2010). However, some differences arise when different compilations are compared. Whereas some authors suggest a virtually monotonic rise with only minor shifts associated with glaciations (e.g., Halverson et al., 2007; 2010), others have interpreted shifts as discrete, incremental steps (e.g., Melezhik et al., 2001). Overall, low  $^{87}\text{Sr}/^{86}\text{Sr}$  values between 0.7054 and 0.7070 characterize the time span between 900 and 690 Ma, whereas  $^{87}\text{Sr}/^{86}\text{Sr}$  ratios increase from 0.7071 to 0.7086 between 670 and 542 Ma, reaching values as high as 0.7095 in the Cambrian.

As a whole, the carbon isotope composition of the limestones and dolostones of the Polanco Limestones Formation is fairly uniform throughout the Los Tapes section. Other than one exception, all of our values are systematically below 0‰ and the trend shows a gradual shift from +0.2‰, at the base, to -3‰ in the upper part of the section. The South Isla Patrulla section shows a similar trend but with a range of  $\delta^{13}\text{C}$  values from -1.9‰ to +2‰, and the Recalde section displays more positive  $\delta^{13}\text{C}$  values ranging from +2.5‰ to +5.3‰ in the lower part of the stratigraphic profile (Figure 4.11). These values gradually decrease to -3.3‰, defining a negative excursion, and return to positive values between +0.7‰ and +2.8‰.

The high  $^{87}\text{Sr}/^{86}\text{Sr}$  ratios ( $> 0.72436$ ) of the limestones in the Los Tapes section indicate varying degree of alteration during diagenesis. Limestones with the highest  $^{87}\text{Sr}/^{86}\text{Sr}$  ratios also have much lower Sr contents and thus, were likely more strongly affected by diagenetic fluids. Accordingly, they cannot be used for Sr chemostratigraphy. In addition to the previously reported  $^{87}\text{Sr}/^{86}\text{Sr}$  values (Gaucher et al., 2004; 2009), new  $^{87}\text{Sr}/^{86}\text{Sr}$  data for five limestones from the Recalde (Figure 4.11) and two limestones from South Isla Patrulla (Figure 4.7) sections were used to chemostratigraphic considerations. The lowest measured  $^{87}\text{Sr}/^{86}\text{Sr}$  ratio (0.70677) is found below the main wave-influenced interval and is from a limestone containing 1541 ppm Sr, which is among the highest concentrations in this study and indicating aragonite precursor, and the lowest content of lithophile elements (Table 2.1). Furthermore, petrographic observations suggest excellent preservation for this sample, implying that its  $\delta^{13}\text{C}$  value of +4‰ is probably closest to primary seawater composition.

Following recent compilations of Neoproterozoic seawater Sr isotope curves (Halverson et al., 2010; Sawaki et al., 2010), most of the samples reported herein (0.70708-0.70791) fall within the range defined for the early Ediacaran (ca. 635-580 Ma). The least radiogenic value obtained (0.70677), however, is significantly lower and would imply either a Cryogenian age (ca. 700 Ma) or, considering a maximum depositional age of 600 Ma for the Polanco Limestones Formation (see Geochronology below), a contribution from a non-radiogenic source of Sr. The rare earth element plus yttrium pattern for this sample share the essential shale-normalised characteristics of marine precipitates (i.e., La, Gd and Y anomalies) but show no Eu anomaly, typical of high-T

hydrothermal fluids (see Supplementary Appendix 3) (Bau and Dulski, 1996). In this regard, Pecoits et al. (2011) concluded that iron formations from the uppermost Yermal Formation were influenced by low-temperature hydrothermal fluids. These young iron deposits differ from typical Archaean and Palaeoproterozoic BIF in that high-temperature hydrothermal input did not influence their chemistry and thus, do not display the characteristic Eu anomaly shown by their older counterparts. Similarly, low-T hydrothermalism could influence the chemistry of the Polanco seawater by lowering its  $^{87}\text{Sr}/^{86}\text{Sr}$  ratio, although not producing positive Eu anomalies.

#### 4.5.3. $^{40}\text{K}$ - $^{40}\text{Ar}$ geochronology

According to Gaucher (2004), the maximum depositional age of the Arroyo del Soldado Group is radiometrically constrained by U-Pb crystallization ages of basement rocks from the Puntas del Santa Lucía pluton dated at  $633 \pm 8$  Ma (Hartmann et al., 2002). Minimum age constraints are provided by the intrusive Guazunambí and Polanco granites which yield Rb-Sr isochron ages of  $532 \pm 11$  and  $548 \pm 11$  Ma, respectively (Umpierre and Halpern, 1971; Kawashita et al., 1999). Additionally, the age of the Polanco Limestones Formation is broadly constrained by the youngest detrital zircon U-Pb ages obtained from the underlying Yermal Formation ( $\sim 664$  Ma) and the overlying Barriga Negra Formation ( $\sim 566$  Ma) (Blanco et al., 2009). This age range is consistent with recently reported K-Ar geochronology of diagenetic illites of the uppermost Yermal Formation, which indicates a minimum age between 600 and 580 Ma for the unit (Pecoits et al., 2011). Here, we report new K-Ar illite ages from the uppermost Yermal Formation to further understand the relative timing of diagenesis in the Yermal shales and infer the depositional age of the overlying Polanco limestones.

The K-Ar illite ages obtained from the Yermal shales scatter significantly (from  $636.5 \pm 12.8$  Ma to  $513.8 \pm 10.4$  Ma) but fit within the above mentioned timeframe if considered in the context of a regional very low temperature thermal overprint. Based on the maximum age constraint for the whole group (Puntas del Santa Lucía pluton) and the thermal history of the Arroyo del Soldado Basin, a potential thermal overprint on the ages

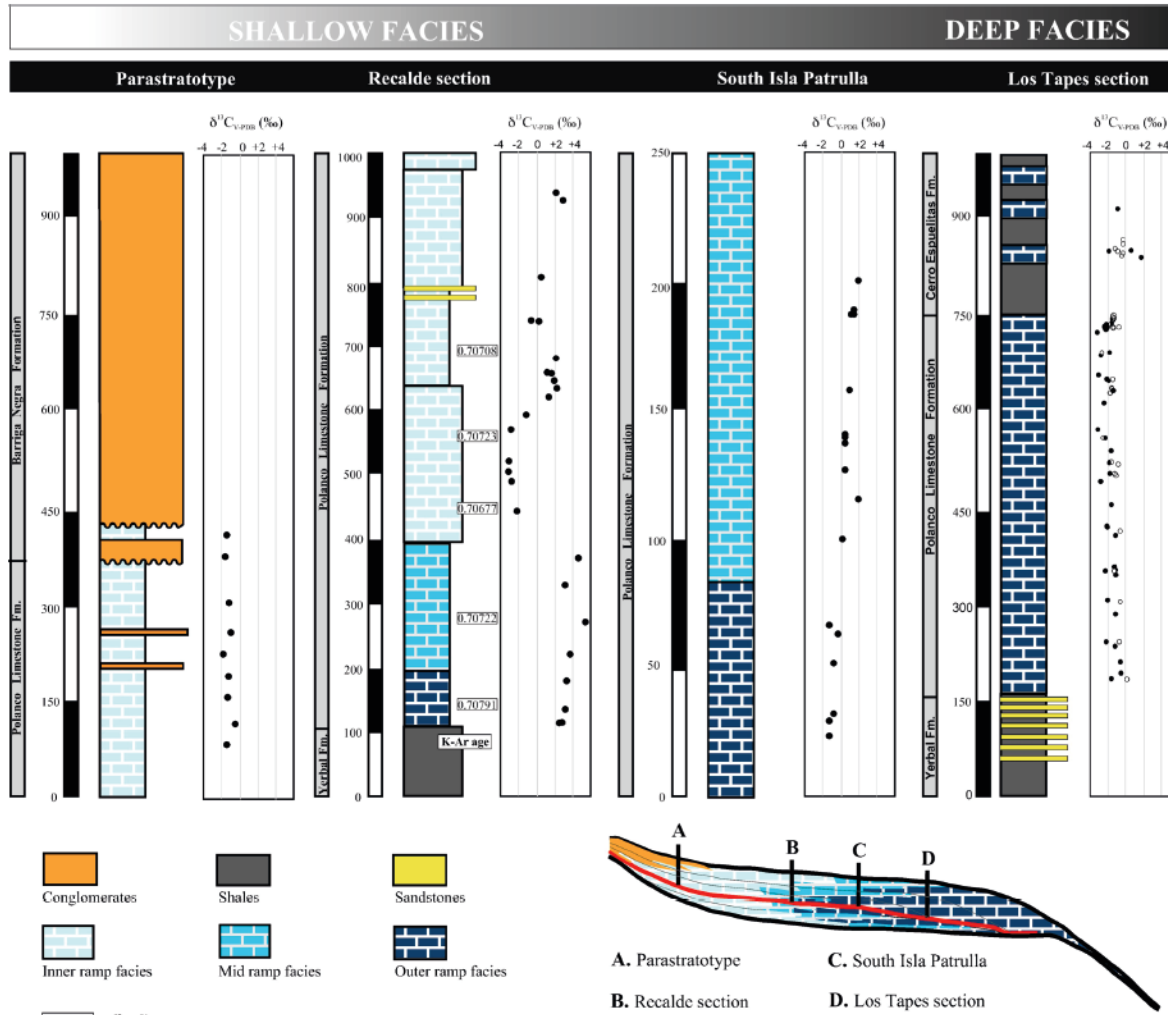


**Figure 4.11.** Comparison of carbon isotope profiles from the deep- and shallow-water sections. Data for the Barriga Negra (parastratotype) and Recalde sections are from Gaucher et al. (2004).

of the illite fractions was evaluated by basic Ar diffusion calculations as outlined by Zwingmann et al. (2010). Three maximum grain sizes comprising 6, 2 and 0.4  $\mu\text{m}$  and a temperature range of 200 and 250°C, with a thermal overprint timeframe range of 0.1, 0.5 and 1Ma, were used. As the geometry of fine grained clay minerals will strongly influence diffusion, cylindrical, plane and sphere geometric shapes were applied. For diffusion calculations of fine grained clay minerals, original parameters listed in Huon et al. (1993) were used in this study with  $D_0$  and  $E_a$  values  $6.03 \times 10^{-7} \text{ cm}^2/\text{s}$  and  $40 \times 10^3 \text{ cal/mol}$  respectively (Wijbrans and McDougall, 1986). The results of these calculations are summarized in Supplementary Table 2.4 and Figure 4.12. A potential thermal overprint on the 2 and 2-6 $\mu\text{m}$  grain size fractions is negligible if the temperature is as low as 200°C up to a modeled 1 Ma range. At a 250°C range, Argon diffusion will start to reduce the ages of a <0.4  $\mu\text{m}$  fraction whereas the coarser <2 and 2-6 $\mu\text{m}$  fractions will suffer only minor radiogenic  $^{40}\text{Ar}$  loss. Calculations indicate that a temperature of 250°C over a 1 Ma time span would affect and thermally-disturb mainly the ages of <0.4  $\mu\text{m}$  illite fraction. Figure 4.12 and Supplementary Table 2.5 compile recalculated illite ages via a radiogenic  $^{40}\text{Ar}$  loss caused by a 0.1, 0.5 and 1 Ma thermal event at 200 and 250°C on 0.4, 2 and 2-6  $\mu\text{m}$  grain sizes. The average value from cylinder, plate and sphere geometry modeling was used for this calculation. These conditions would suggest indirectly a sedimentation age of the uppermost Yerbál Formation at 600-580 Ma (see Figure 4.12).

Therefore, this new data constrain the onset of sedimentation of the Polanco Limestones Formation to a maximum age of 600 Ma. If we assume that the minimum age of deposition is already constrained by the youngest zircons present in the Barriga Negra Formation at ~566 Ma then, the carbonate sedimentation lasted less than 35 Ma. Considering a maximum thickness of ~900m recorded for the unit, this time frame indicates that the decompacted average sedimentation rate for the Polanco Limestone Formation was ~50 m/Ma. This average value is well within the range of sedimentation rates compiled from similar modern and ancient carbonate systems (Sadler 1999; Bosscher and Schagler, 1993).

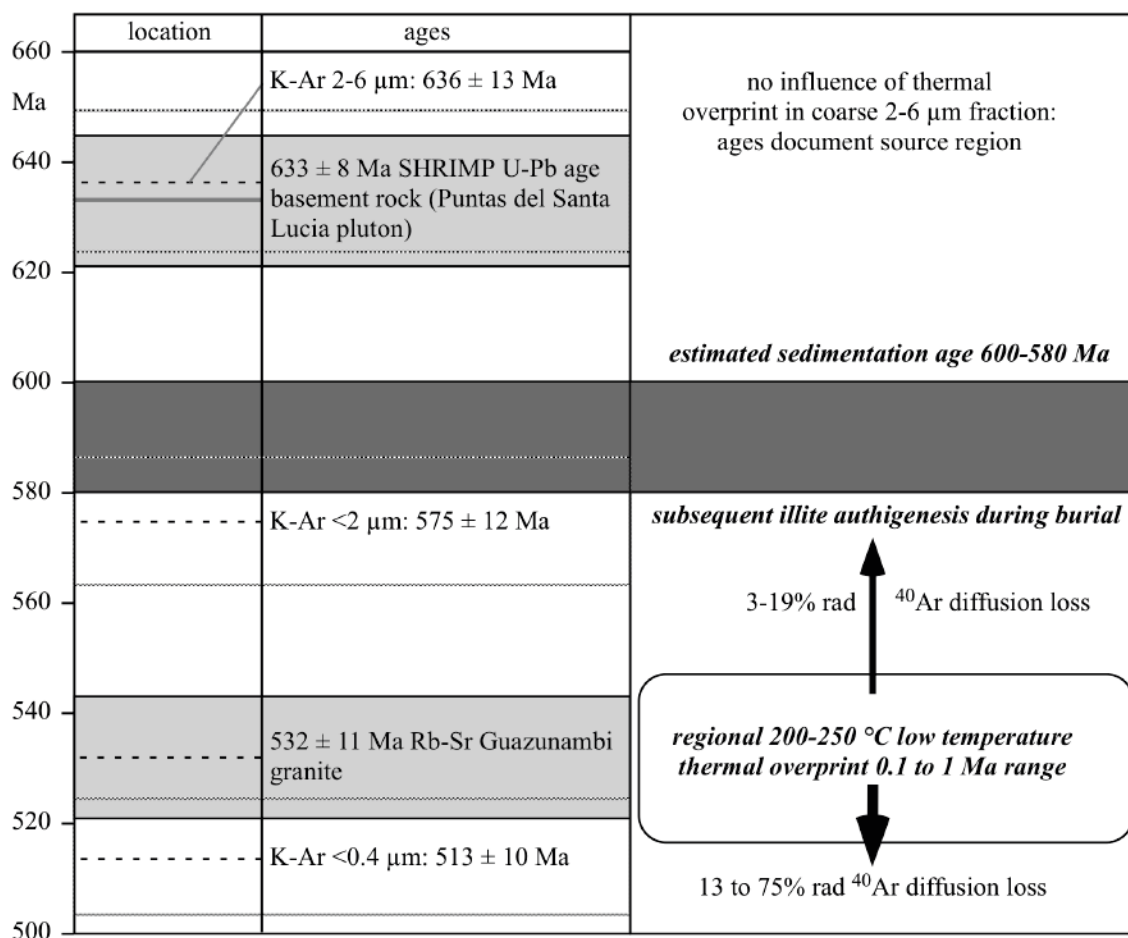


**Figure 4.12.** Summary of the illite age data from the uppermost Yerbal Formation.

#### 4.5.4. Palaeo-oceanographic significance of the C- and Sr-isotope records

The long-term secular variations in the carbon isotope composition of marine carbonates ( $\delta^{13}\text{C}_{\text{carb}}$ ) reflect the influence of several factors. Under steady-state conditions, positive excursions are likely driven by higher productivity due to higher nutrient influx to the surface ocean or an increase in the burial efficiency of organic matter (Halverson et al., 2009). Conversely, negative excursions result from either a decrease in primary productivity or lower burial efficiency of organic matter in sediments (i.e., more organic matter oxidation in the sediments), which ultimately result in decreased burial of organic matter (Halverson et al., 2009). Rapid carbon isotope excursions, especially negative, may also occur under non-steady-state conditions and are most likely a result of input and oxidation of massive amounts of  $^{13}\text{C}$ -depleted carbon from sedimentary methane

clathrates (Jiang et al., 2003; Bejrrum and Canfield, 2011), labile organic matter (Kaufman et al., 2007), or dissolved organic carbon (Rothman et al., 2003).

Comparison of carbon isotope values along a palaeo-depth gradient provides an opportunity to differentiate between local and global signals. In this context, critical to the interpretation of the  $\delta^{13}\text{C}_{\text{carb}}$  chemostratigraphy of the Ediacaran Arroyo del Soldado Group and extrabasinal correlations is the understanding of the origin of the  $\delta^{13}\text{C}$  values recorded by the Polanco Limestones Formation. In the following, we discuss the conditions that might have caused the negative carbon isotope excursion and its palaeo-environmental implications.

#### *4.5.3.1. Non-steady state conditions*

One scenario that could explain the negative carbon isotope values in shallow-water settings is the oxidation of the dissolved organic carbon pool (DOC). The marked  $^{13}\text{C}$ -enrichment of Neoproterozoic limestones has been argued to reflect the development of a stratified ocean with a lower anoxic layer depleted in  $^{13}\text{C}$  (Kaufman et al., 1991; Derry et al., 1992; Grotzinger and Knoll, 1995; Knoll et al., 1996). These authors hypothesized that intense ocean stratification, with a simultaneous build-up of alkalinity via sulphate reduction and  $^{13}\text{C}$ -depletion in anoxic deep waters, might explain the observed geochemical signatures (see also Canfield et al., 2007). This non-steady state process would transfer large volumes of deep-waters with  $^{13}\text{C}$ -depleted carbon to the much smaller volume of shallow-water settings, generating large negative  $\delta^{13}\text{C}_{\text{carb}}$  excursions during ocean overturns. Notably some of these large negative  $\delta^{13}\text{C}_{\text{carb}}$  excursions in the Neoproterozoic are not accompanied by parallel  $\delta^{13}\text{C}_{\text{org}}$  excursions, which was explained by a much larger DOC pool in the Neoproterozoic ocean than now (Rothman et al., 2003). It was further suggested that  $\delta^{13}\text{C}_{\text{carb}}$  values would be high at times when the DOC pool was growing (Rothman et al., 2003; Fike et al., 2006; McFadden et al., 2008). The stratified ocean model predicts a  $^{13}\text{C}$ -enrichment in carbonates due to high biological productivity in shallow-marine environments and a  $^{13}\text{C}$ -depletion in deep waters by remineralisation of organic matter (Knoll et al., 1996; Calver, 2000).

The relative contribution of carbon exchange, between surface and deep ocean waters, to the  $\delta^{13}\text{C}_{\text{carb}}$  signal depends on the water-column structure and depth, as well as

on the rates of seawater circulation across the ocean (Calver, 2000). Nonetheless, the Wonoka anomaly can be clearly distinguished from other Neoproterozoic anomalies due to its amplitude ( $\delta^{13}\text{C}_{\text{carb}} < -10\text{‰}$ ) and persistence for several hundred of meters (ca. 700 m) (Le Guerroué et al., 2006; Halverson et al., 2010). Significantly, the carbonates from the Polanco Limestones Formation fall into the range of what are generally considered normal marine carbonates (i.e.,  $> -5\text{‰}$ ; Summons and Hayes, 1992) and, conversely to the rapid onset of the Wonoka anomaly, the Polanco negative excursion –at the Recalde section- defines a rather gradual trend and persists for no more than 250 meters (Figure 4.11). Furthermore, a  $\delta^{13}\text{C}_{\text{carb}}$  excursion of the magnitude and duration of the Shuram/Wonoka anomaly, thought to span between 20 and 50 Ma (Le Guerroué, 2010), should be noticed in different portions of the shelf above the pycnocline. The negative excursion recorded in the Polanco Limestones Formation, however, is facies controlled and only occurs in shallow-water strata associated with storm events and thus, it appears to be likely a local rather than a basin-wide phenomenon.

#### 4.5.3.2. *Steady-state conditions*

Negative  $\delta^{13}\text{C}$  excursions may also indicate an increased rate of oxidation of organic carbon or a decrease in its burial rate (Kump and Arthur, 1999). In this context, the prominent negative excursion recorded in the middle Polanco Limestones Formation (Recalde section), might reflect recycling of organic carbon either through aerobic respiration in the upper water column (where oxygen was available) or anaerobically in deeper waters or bottom sediment (i.e., sulphate-reducing bacteria). Comparatively, the stratigraphically homogenous and less negative  $\delta^{13}\text{C}_{\text{carb}}$  values ( $> -3\text{‰}$ ) found in the more distal Los Tapes section can reflect global carbon isotope signal; i.e., carbon isotope fractionation associated with photosynthetic carbon fixation. In modern oceans, DIC of surface waters is enriched in  $\delta^{13}\text{C}$  up to 3‰ relative to deeper waters by the ‘biological pump effect’; i.e., fixation of carbon in the photic zone and delivery of dead organic matter into deeper waters where it is remineralized (Kroopnick, 1985; Berger and Vincent, 1986). In poorly mixed basins, the difference in  $\delta^{13}\text{C}_{\text{DIC}}$  between surface and bottom waters can be even greater (e.g., 7‰ in the Black Sea; Deuser, 1970). The apparent depth gradient in  $\delta^{13}\text{C}_{\text{DIC}}$  between the shallow- and deeper-water carbonates in

the Polanco depositional basin is inferred to have been ca. 2-7‰, which is still comparable to the gradient in modern oceans ( $\leq 3\text{‰}$ ) and in stratified basins ( $\leq 7\text{‰}$ ). Water column stratification during the deposition of the lower part of the Arroyo del Soldado Group has been suggested based on the development of iron formation in the upper part of the Yermal Formation (Pecoits et al., 2008; 2011) and it might explain the difference between the positive and slightly negative carbon isotope values of carbonates in the lower Recalde and Los Tapes sections, respectively. Additionally, when Ce signatures of deep and shallow water facies are compared the former show the absence of Ce anomaly whilst the shallowest samples display negative Ce anomalies (see Supplementary Appendix 3). Such stratification, however, could not have caused the stratigraphically restricted negative excursion found in the tempestitic carbonates of the middle Recalde section; i.e., through oxidation of the DOC pool (see above). In this regard, the carbonate facies of the south Isla Patrulla section, palaeogeographically located between the Los Tapes and the Recalde sections, shows a transition towards consistently positive values best exemplified in the lower Recalde section (Figure 4.11). Furthermore, the negative values reached in the shallow tempestite-bearing carbonates are systematically more negative with respect to the ones found in the deeper Los Tapes section providing further support to this hypothesis and arguing against any destratification event.

Hence, the larger carbon isotope gradient between distal (Los Tapes section) and more proximal facies as those recorded in the South Isla Patrulla and lower Recalde sections, could be explained by the effect of a stratified basin. Degradation of organic material below the redox boundary would lead to the mentioned chemical gradient with depth, wherein  $\delta^{13}\text{C}$  values are more positive in shallow waters. This stratification, however, cannot explain the negative excursion recorded in storm-related shallow-water facies. According to the view advanced here, the higher levels of reworking under storm-dominated conditions are expected to increase oxidation of organic matter and ultimately, to produce negative  $\delta^{13}\text{C}$  signatures.

#### **4.6. Conclusions**

Sedimentological, petrographic, geochemical and isotopic data were combined to

constrain the depositional environment and the age of the Polanco Limestones Formation and to understand the platform dynamics. By comparing chemostratigraphic profiles across the basin (i.e., shallow- vs. deep-water settings), we show that this type of integrated analysis can help to interpret Precambrian carbonate systems, especially those associated with major palaeo-climatic and palaeo-environmental events. The following conclusions can be drawn from this study:

1. Facies analyses indicates that the Polanco Limestones Formation was deposited on a storm-dominated homoclinal ramp, where inner-, mid- and outer-ramp facies associations were recognized and described. Inner ramp facies association is characterized by coarsening- and thickening-upward regressive cycles of calcarenites representing upper, middle and lower shoreface environments deposited above the mean fair-weather wave base in well-oxygenated waters. Mid-ramp facies association consists of thinly-bedded calcisiltite and dolosiltite with hummocky and swaley cross-stratified calcarenites and thin massive or parallel-stratified calcarenite beds. Outer ramp deposits comprise limestone and dolostone rhythmites and bedded dolostones deposited below the mean storm wave-base and under anoxic conditions.

2. Petrographic observations permits the recognition of two major diagenetic stages affecting carbonates and their relative chronology: (1) depositional and early diagenetic phases (micritic to microsparitic dolostones and limestones), and (2) late diagenetic phases (blocky and fracture-filling cements).

3. Petrographic, textural and diverse geochemical proxies used here suggest that most of the studied samples did not experience significant post-depositional alteration of the carbon isotope composition and thus, these carbonates record near-primary seawater signature. Accordingly, the carbonates can be used for chemostratigraphic comparisons. In contrast, Sr isotope compositions are more variable, reflecting the effects of diagenesis and probable exchange with clay minerals or simply changes in relative riverine input. In this regard, carbonates from the South Isla Patrulla and Recalde sections are suitable for Sr chemostratigraphy whereas those from the Los Tapes section should be excluded.

4. Carbon and most importantly, strontium isotope data from the Polanco Limestones Formation exhibit values compatible with those of the global seawater reference curves for the early Ediacaran (635-580 Ma). This interpretation is supported by previously reported radiometric data indicating a depositional age between ~600 and ~566 Ma. New radiometric ages on diagenetic illite of the uppermost Yermal Formation further support this time interval.

5. The lack of a basin-wide negative carbon isotope excursion and good correlation between  $\delta^{13}\text{C}$  data and facies associations suggests that ramp dynamics strongly influenced the carbon cycle. The results presented are consistent with a strong remineralization of organic matter within the hummocky-bearing inner-ramp sediments, which might account for the most negative  $\delta^{13}\text{C}$  values in the middle Recalde section. Because organic carbon is  $^{13}\text{C}$ -depleted relative to normal marine DIC, precipitation of carbonate derived from remineralized organic carbon will decrease the  $\delta^{13}\text{C}$  of the limestone and thus, the more efficient respiration of organic matter can produce the negative  $\delta^{13}\text{C}$  values recorded in these strata. The  $\delta^{13}\text{C}$  gradient between relatively shallow-water (non-storm dominated) and deep-water facies can be explained by the 'photic pump' effect. When compared with the modern ocean gradient, the slightly larger  $\delta^{13}\text{C}$  gradient found in the Polanco Limestones Formation may result from either higher primary productivity at that time, or most likely, a more prominent stratification of the water column.

#### **4.7. References**

Azmy, K., Kaufman, A.J. Misi, A., Oliveira, T.F., 2006. Isotope stratigraphy of the Lapa Formation, São Francisco Basin, Brazil: implications for Late Neoproterozoic glacial events in South America. *Precambrian Research* 149, 231-248.

Baadsgard, H., 1987. Rb-Sr and K-Ca isotope systematics in minerals from potassium horizons in the Prairie Evaporite Formation, Saskatchewan, Canada. *Chemical Geology* 66, 1-15.

Banner, J.L., Hanson, G.N., 1990. Calculation of simultaneous isotopic and trace element variations during water-rock interaction with application to carbonate diagenesis. *Geochimica et Cosmochimica Acta* 54, 3123-3137.

Bau, M., Dulski, P., 1996. Distribution of yttrium and rare-earth elements in the Penge and Kuruman iron-formations, Transvaal Supergroup, South Africa. *Precambrian Research* 79, 37-55.

Bekker, A., Sial, A.N., Karhu, J.A., Ferrerira, V.P., Noce, C.M., Kaufman, A.J., Romano, A.W., Pimentel, M.M., 2003. Chemostratigraphy of carbonates from the Minas Supergroup, Quadrilátero Ferrífero (Iron Quadrangle), Brazil: A stratigraphic record of early Proterozoic atmospheric, biogeochemical and climatic change. *American Journal of Science* 303, 865-904.

Bekker, A., Karhu, J.A., Kaufman, A.J., 2006. Carbon isotope record for the onset of the Lomagundi carbon isotope excursion in the Great Lakes area, North America. *Precambrian Research* 148, 145-180.

Berger, W.H., Vincent, E., 1986. Deep-sea carbonate: Reading the carbon-isotope signal, *Geologische Rundschau* 75, 249-269.

Bjerrum, C.J., Canfield, D.E., 2011. Towards a quantitative understanding of the late Neoproterozoic carbon cycle. *Proceedings of the National Academy of Sciences* 108, 5542-5547.

Blanco, G., Rajesh, H.M., Gaucher, C., Germs, G.J.B., Chemale Jr., F., 2009. Provenance of the Arroyo del Soldado Group (Ediacaran to Cambrian, Uruguay): Implications for the paleogeographic evolution of southwestern Gondwana. *Precambrian Research* 171, 57-73.

Bonhomme, M., Thuizat, G.R., Pinault, Y., Clauer, N., Wendling, R., Winkler, R., 1975. Méthode de datation potassium-argon. *Appareillage et Technique*, Strasbourg, 53.

Brand, U., Veizer, J., 1980. Chemical diagenesis of a multi component carbonate system: 1. Trace elements. *Journal of Sedimentary Petrology* 50, 1219-1236.

Bristow, T.F., Kennedy, M.J., 2008. Carbon isotope excursions and the oxidant budget of the Ediacaran atmosphere and ocean. *Geology* 36, 863-866.

- Burchette, T.P., Wright, V.P., 1992. Carbonate ramp depositional systems. *Sedimentary Geology* 79, 3-57.
- Calver, C., 2000. Isotope stratigraphy of the Ediacaran (Neoproterozoic III) of the Adelaide rift complex, Australia, and the overprint of water column stratification. *Precambrian Research* 100, 121-150.
- Canfield, D.E., Poulton, S.W., Knoll, A.H., Narbonne, G.M., Ross, G., Goldberg, T., Strauss, H., 2008. Ferruginous Conditions Dominated Later Neoproterozoic Deep-Water Chemistry. *Science* 321, 949-952.
- Canfield, D.E., Poulton, S.W., Narbonne, G.M., 2007. Late-Neoproterozoic Deep-Ocean Oxygenation and the Rise of Animal Life. *Science* 315, 92-95.
- Clauer, N., Chaudhuri, S., 1995. *Clays in crustal environments: isotope dating and tracing*, Springer, Berlin.
- Condon, D., Zhu, M., Bowring, S., Wang, W., 2005. U-Pb ages from the Neoproterozoic Doushantuo Formation, China. *Science* 308, 95-98.
- Cozzi, A., Allen, P.A., Grotzinger, J.P., 2004. Understanding carbonate ramp dynamics using  $\delta^{13}\text{C}$  profiles: examples from the Neoproterozoic Buah Formation of Oman. *Terra Nova* 16, 62-67.
- Crank, J., 1975. *The Mathematics of Diffusion*, second ed. Oxford University Press, Oxford.
- Dalrymple, G.B., Lanphere, M.A., 1969. *Potassium-argon dating: principles, techniques and applications to geochronology*, W.H. Freeman, San Francisco.
- Derry, L.A., Kaufman, A.J., Jacobsen, S.B., 1992. Sedimentary cycling and environmental change in the Late Proterozoic: evidence from stable and radiogenic isotopes. *Geochimica et Cosmochimica Acta* 56, 1317-1329.
- Derry, L.A., Keto, L.S., Jacobsen, S.B., Knoll, A.H., Swett, K., 1989. Strontium isotopic variations in Upper Proterozoic carbonates from Svalbard and East Greenland. *Geochimica et Cosmochimica Acta* 53, 2331-2339.

- Derry, L.A., 2010. A burial diagenesis origin for the Ediacaran Shuram-Wonoka carbon. *Earth and Planetary Science Letters* 294, 152-162.
- Deuser W.G., 1970. Carbon-13 in Black Sea Waters and Implications for the Origin of Hydrogen Sulfide. *Science* 168, 1575-1577.
- Dott Jr, R.H., 1983. Episodic sedimentation; how normal is average? How rare is rare? Does it matter? *Journal of Sedimentary Research* 53, 5-23.
- Dott Jr, R.H., Bourgeois, J., 1982. Hummocky stratification: significance of its variable bedding sequences. *GSA Bulletin* 93, 663-680.
- Fairchild, I.J., Marshall, J.D., Bertrand-Sarfati, J., 1990. Stratigraphic shifts in carbon isotopes from Proterozoic stromatolitic carbonates (Mauritania): influences of primary mineralogy and diagenesis. *American Journal of Sciences* 290, 46-79.
- Fike, D.A., Grotzinger, J.P., Pratt, L.M., Summons, R.E., 2006. Oxidation of the Ediacaran ocean. *Nature* 444, 744-747.
- Gaucher, C., Boggiani, P., Sprechmann, P., Sial, A.N., Fairchild, T., 2003. Integrated correlation of the Vendian to Cambrian Arroyo del Soldado and Corumba Groups (Uruguay and Brazil): paleogeographic, paleoclimatic and paleobiologic implications. *Precambrian Research* 120, 241-278.
- Gaucher, C., Sial, A.N., Blanco, G., Sprechmann, P., 2004. Chemostratigraphy of the lower Arroyo del Soldado Group (Vendian, Uruguay) and paleoclimatic implications. *Gondwana Research* 7, 715-730.
- Gaucher, C., Sial, A.N., Poiré, D., Gómez-Peral, L., Ferreira, V.P., Pimentel, M.M., 2009. Chemostratigraphy. In: Gaucher, C., Sial, A.N., Halverson, G.P. and Frimmel, H.E. (Eds.), *Neoproterozoic-Cambrian tectonics, global change and evolution: a focus on southwestern Gondwana. Developments in Precambrian Geology* 16, Elsevier, Amsterdam, 115-122.
- Germis, G.J.B., 1972. New shelly fossils from Nama Group, South West Africa. *American Journal of Science* 272, 752-761.
- Goldstein, S.J., Jacobsen, S.B., 1988. Nd and Sr isotopic systematics of river water

suspended material: implications for crustal evolution. *Earth and Planetary Science Letters* 87, 249-265.

Gradstein, F. J., Ogg, A., Smith, A., 2004. *Geologic Time Scale*, Cambridge University Press, Cambridge.

Grotzinger, J.P., Bowring, S.A., Saylor, B.Z., Kaufman, A.J., 1995. Biostratigraphic and geochronologic constraints on early animal evolution. *Science* 270, 598-604.

Halverson, G.P., Dudas, F.O., Maloof, A.C., Bowring, S.A., 2007. Evolution of the  $^{87}\text{Sr}/^{86}\text{Sr}$  composition of Neoproterozoic seawater. *Palaeogeography, Palaeoclimatology, Palaeoecology* 256, 103-129.

Halverson, G.P., Hoffman, P.F., Schrag, D.P., Maloof, A.C., Rice, A.H.N., 2005. Toward a Neoproterozoic composite carbon-isotope record. *Geological Society of America Bulletin* 117, 1181-1207.

Halverson, G.P., Hurtgen, M.T., Porter, S.M., Collins, A.C., 2010. Neoproterozoic-Cambrian biogeochemical evolution. In: Gaucher, C., Sial, A.N., Halverson, G.P. and Frimmel, H.E. (Eds.), *Neoproterozoic-Cambrian tectonics, global change and evolution: a focus on southwestern Gondwana*. *Developments in Precambrian Geology* 16, Elsevier, Amsterdam, 351-356.

Hart, B.S., Plint, A.G., 1989. Gravelly shoreface deposits: a comparison of modern and ancient sequences. *Sedimentology* 36, 551-557.

Hartmann, L.A., Santos, J.O., Bossi, J., Campal, N., Schipilov, A., Mac Naughton, N. J., 2002. Zircon and titanite U-Pb SHRIMP geochronology of Neoproterozoic felsic magmatism on the eastern border of the Rio de la Plata Craton, Uruguay. *Journal of South American Earth Sciences* 15, 229-236.

Hayes, J.M., Strauss, H., Kaufman, A.J., 1999. The abundance of  $^{13}\text{C}$  in marine organic matter and isotopic fractionation in the global biogeochemical cycle of carbon during the past 800 Ma. *Chemical Geology* 161, 103-125.

Holmden, C., Creaser, R.A., Muehlenbachs, K., Leslie, S.A., Bergstrom, S.M., 1996. Isotopic and elemental systematics of Sr and Nd in 454 Ma biogenic apatites: implications for paleoseawater studies. *Earth and Planetary Science Letters* 142, 425-437.

Horodyski, R.J., Knauth, L.P., 1994. Life on Land in the Precambrian. *Science* 263, 494-498.

Hua, H., Chen, Z., Yuan, X., Zhang, L. and Xiao, S., 2005. Skeletogenesis and asexual reproduction in the earliest biomineralizing animal Cloudina. *Geology* 33, 277-280.

Huon, S., Cornee, J.J., Pique, A., Rais, N., Clauer, N., Liewig, N., Zayane, R., 1993. Mise en évidence au Maroc d'événements thermiques d'âge triasico-liasique à l'ouverture de l'Atlantique. *Bulletin de la Société Géologique de France* 164, 165-176.

Ishikawa, T., Ueno, Y., Komiya, T., Sawaki, Y., Han, J., Shu, D., Li, Y., Maruyama, S., Yoshida, N., 2008, Carbon isotope chemostratigraphy of a Precambrian/Cambrian boundary section in the Three Gorge area, South China: Prominent global-scale isotope excursions just before the Cambrian Explosion. *Gondwana Research* 14, 193-208.

Jacobsen, S.B., Kaufman, A.J., 1999. The Sr, C and O isotopic evolution of Neoproterozoic seawater. *Chemical Geology* 161, 37-57.

Jiang, G., Kennedy, M.J., Christie-Blick, N., 2003. Stable isotopic evidence for methane seeps in Neoproterozoic postglacial cap carbonates. *Nature* 426, 822-826.

Jiang, G., Shi, X., Zhang, S., Wang, Y., Xiao, S., 2011. Stratigraphy and paleogeography of the Ediacaran Doushantuo Formation (ca. 635–551 Ma) in South China. *Gondwana Research* 19, 831-849.

Jiang, G., Kaufman, A. J., Christie-Blick, N., Zhang, S., Wu, H., 2007. Carbon isotope variability across the Ediacaran Yangtze platform in South China: Implications for a large surface-to-deep ocean gradient. *Earth and Planetary Science Letters* 261, 303-320.

Kaufman, A.J. Knoll, A.H., 1995. Neoproterozoic variations in the carbon isotopic composition of seawater: Stratigraphic and biogeochemical implications. *Precambrian Research* 73, 27-49.

Kaufman, A.J., Hayes, J.M., Knoll, A.H., Germs, G.J.B., 1991. Isotopic compositions of carbonates and organic carbon from upper Proterozoic successions in Namibia: stratigraphic variation and the effects of diagenesis and metamorphism. *Precambrian Research* 49, 301-327.

- Kaufman, A.J., Jacobsen, S.B., Knoll, A.H., 1993. The Vendian record of Sr and C isotopic variations in seawater: Implications for tectonics and paleoclimate. *Earth and Planetary Science Letters* 120, 409-430.
- Kaufman, A.J., Knoll, A.H., Narbonne, G.M., 1997. Isotopes, ice ages, and terminal Proterozoic Earth history. *Proceedings of the National Academy of Science U.S.A.* 94, 6600-6605.
- Kaufman, A.J., Corsetti, F.A., Varni, M.A., 2007. The effect of rising atmospheric oxygen on carbon and sulfur isotope anomalies in the Neoproterozoic Johnnie Formation, Death Valley, USA. *Chemical Geology* 237, 47-63.
- Kawashita, K., Gaucher, C., Sprechmann, P., Teixeira, W., Victória, R., 1999. Preliminary chemostratigraphic insights on carbonate rocks from Nico Pérez Terrane (Uruguay), In: *Actas II South American Symposium on Isotope Geology, Córdoba*, pp. 399-402.
- Knauth, L.P., Martin, J.K., 2009. The late Precambrian greening of the Earth. *Nature* 460, 728-732.
- Knoll, A.H., Hayes, J.M., Kaufman, A.J., Swett, K., Lambert, I.B., 1986. Secular variation in carbon isotope ratios from Upper Proterozoic successions of Svalbard and East Greenland. *Nature* 321, 832-838.
- Knoll, A.H., Walter, M.R., 1992. Latest Proterozoic stratigraphy and Earth history. *Nature* 356, 673-678.
- Knoll, A.H., Walter, M.R., Narbonne, G.M., Christie-Blick, N., 2004. A New Period for the geologic time scale. *Science* 3005, 621-622.
- Kroopnick, P.M., 1985. The distribution of  $^{13}\text{C}$  of  $\Sigma\text{CO}_2$  in the world oceans. *Deep-Sea Research* 32, 57-84.
- Kump, L.R., Arthur, M.A., 1999. Interpreting carbon-isotope excursions: carbonates and organic matter. *Chemical Geology* 161, 181-198.

- Le Guerroué, E., 2010. Duration and synchronicity of the largest negative carbon isotope excursion on Earth: The Shuram/Wonoka anomaly. *Comptes Rendus Geoscience* 342, 204-214.
- Le Guerroué, E., Allen, P.A., Cozzi, A., Etienne, J.L., Fanning, C., 2006. 50 Myr recovery from the largest negative carbon excursion in the Ediacaran ocean. *Terra Nova* 18, 147-153.
- Liewig, N., Clauer, N., Sommer, F., 1987. Rb-Sr and K-Ar dating of clay diagenesis in Jurassic sandstone oil reservoirs, North Sea. *AAPG Bulletin* 71, 1467-1474.
- Longerich, H.P., Jenner, G.A., Fryer, B.J., Jackson, S.E., 1990. Inductively coupled plasma-mass spectrometric analysis of geological samples; a critical evaluation based on case studies. *Chemical Geology* 83, 105-118.
- Martin, M.W., Grazhdankin, D.V., Bowring, S.A., Evans, D.A.D., Fedonkin, M.A., Kirschvink, J.L., 2000. Age of Neoproterozoic bilaterian body and trace fossils, White Sea, Russia: implications for metazoan evolution. *Science* 288, 841-845.
- Martin, M.W., Grazhdankin, D.V., Bowring, S.A., Evans, D.A.D., Fedonkin, M.A., Kirschvink, J.L., 2000. Age of Neoproterozoic bilaterian body and trace fossils, White Sea, Russia: implications for metazoan evolution. *Science* 288, 841-845.
- Maruyama, S., Santosh, M., 2008. Models on Snowball Earth and Cambrian explosion: A synopsis. *Gondwana Research* 14, 22-32.
- McCrea, J.M., 1950. On the isotopic chemistry of carbonates and a paleothermometer scale. *Journal of Chemical Physics* 5, 48-51.
- McDougall, I., Roksandic, Z., 1974. Total fusion  $^{40}\text{Ar}/^{39}\text{Ar}$  ages using HIFAR reactor. *Journal of the Geological Society of Australia* 21, 81-89.
- McDougall, I., Harrison T.M., 1999. *Geochronology and Thermochemistry by the  $^{40}\text{Ar}/^{39}\text{Ar}$  method*, second ed. Oxford University Press, Oxford.
- McFadden, K.A., Huang, J., Chu, X., Jiang, G., Kaufman, A.J., Zhou, C., Yuan, X., Xiao, S., 2008. Pulsed oxidation and biological evolution in Ediacaran Doushantuo Formation. *Proceedings of the National Academy of Science U.S.A.* 105, 3197-3202.

- Meert, J.G., Lieberman, B.S., 2008. The Neoproterozoic assembly of Gondwana and its relationship to the Ediacaran-Cambrian radiation. *Gondwana Research* 14, 5-21.
- Melezhik, V.A., Gorokhov, I.M., Kuznetsov, A.B., Fallick, A.E., 2001. Chemostratigraphy of Neoproterozoic carbonates: implications for 'blind dating'. *Terra Nova* 13, 1-11.
- Montañez, I.P., Banner, J.L., Osleger, D.A., Borg, L.E., Bosserman, P.J., 1996. Integrated Sr isotope variations and sea-level history of Middle to Upper Cambrian platform carbonates: Implications for the evolution of Cambrian seawater  $^{87}\text{Sr}/^{86}\text{Sr}$ . *Geology* 24, 917-920.
- Ohno, T., Komiya, T., Ueno, Y., Hirata, T. Maruyama, S., 2008. Determination of  $^{88}\text{Sr}/^{86}\text{Sr}$  mass-dependent isotopic fractionation and radiogenic isotope variation of  $^{88}\text{Sr}/^{86}\text{Sr}$  in the Neoproterozoic Doushantuo Formation. *Gondwana Research* 14, 126-133.
- O'Neil, J.R., Epstein, S., 1966. A method for oxygen isotope analysis of milligram quantities of water and some of its applications. *Journal of Geophysical Research* 71, 4955-4961.
- Oyhantçabal, P., Siegesmund, S., Wemmer, K., Frei, R., Layer, P., 2007. Post-collisional transition from calc-alkaline to alkaline magmatism during transcurrent deformation in the southernmost Dom Feliciano Belt (Braziliano–Pan-African, Uruguay). *Lithos* 98, 141-159.
- Palmer, M.R., Edmond, J.M., 1989. The strontium isotope budget of the modern ocean. *Earth and Planetary Science Letters* 92, 11-26.
- Pecoits, E., Aubet, N.R., Gingras, M.K., Poulton, S.W., Bekker, A., Veroslavsky, G., Konhauser, K.O., 2011. An Ediacaran iron formation: New evidence for ferruginous late Neoproterozoic seawater. *Precambrian Research*, *in press*. (doi:10.1016/j.precamres.2011.10.002).
- Pecoits, E., Gingras, M., Aubet, N., Konhauser, K., 2008. Ediacaran in Uruguay: palaeoclimatic and palaeobiological implications. *Sedimentology* 55, 689-719.

Pelechaty, S.M., 1998. Integrated chronostratigraphy of the Vendian system of Siberia: implications for a global stratigraphy. *Journal of the Geological Society of London* 155, 957-973.

Plint, A.G., 2011. Wave- and storm-dominated shoreline and shallow marine systems. In: Dalrymple, R.W. and James, N.P., (Eds.), *Facies Models*, 4th Edition, Geological Association of Canada, 167-200.

Rapela, C.W., Fanning, C.M., Casquet, C., Pankhurst, R.J., Spalletti, L., Poiré, D., Baldo, E.G., 2011. The Rio de la Plata craton and the adjoining Pan-African/brasiliano terranes: Their origins and incorporation into south-west Gondwana. *Gondwana Research in press*.

Read, J.F., 1985. Carbonate platform facies models. *American Association of Petroleum Geologists Bulletin* 69, 1-21.

Rothman, D.H., Hayes, J.M., Summons, R.E., 2003. Dynamics of the Neoproterozoic carbon cycle. *Proceedings of the National Academy of Science U.S.A.* 100, 124-129.

Ruf, M., Elmar Link, E., Pross, J., Aigner, T., 2005. A multi-proxy study of deeper-water carbonates (Upper Jurassic, southern Germany): combining sedimentology, chemostratigraphy and palynofacies. *Facies* 51, 327-349.

Sawaki, Y., Ohno, T., Fukushi, Y., Komiya, T., Ishikawa, T., Hirata, T., Maruyama, S., 2008. Sr isotope excursion across the Precambrian–Cambrian boundary in the Three Gorges area, South China. *Gondwana Research* 14, 134-147.

Sawaki, Y., Ohno, T., Tahata, M., Komiya, T., Hirata, T., Maruyama, S., Windley, B.F., Han, J., Shu, D. Li, Y., 2010. The Ediacaran radiogenic Sr isotope excursion in the Doushantuo Formation in the Three Gorges area, South China. *Precambrian Research* 176, 46-64.

Saylor, B.Z., Kaufman, A.J., Grotzinger, J.P., Urban, F., 1998. A composite reference section for terminal Proterozoic strata of southern Namibia. *Journal of Sedimentary Research* 68, 1223-1235.

Seguret, M., Moussine-Pouchkaine, A., Gabaglia, G.R., Bouchette, F., 2001. Storm deposits and storm-related coarse carbonate breccias on a pelagic outer shelf (south-east basin France). *Sedimentology* 48, 231-254.

- Shen, Y., Zhang, T., Hoffman, P. F., 2008. On the coevolution of Ediacaran oceans and animals. *Proceedings of the National Academy of Science U.S.A.* 105, 7376-7381.
- Shields, G., Veizer, J., 2002. Precambrian marine carbonate isotope database: version 1.1. *Geochemistry, Geophysics, Geosystems* 3.
- Shields, G.A., 2007. A normalized seawater strontium isotope curve: possible implications for Neoproterozoic–Cambrian weathering rates and the further oxygenation of the Earth. *Earth* 2, 35-42.
- Steiger, R. H., Jäger, E., 1977. Subcommittee on Geochronology: convention on the use of decay constants in geo- and cosmochemistry. *Earth and Planetary Science Letters* 36, 359-362.
- Summons, R.E. Hayes, J.M., 1992. Principles of molecular and isotopic biogeochemistry. In: Schopf, J.W., Klein, C. (Eds.), *The Proterozoic Biosphere: A multidisciplinary study*, Cambridge, UK, Cambridge University Press, 83-93.
- Thomas, C.W., Graham, C.M., Ellam, R.M., Fallick, A.E., 2004.  $^{87}\text{Sr}/^{86}\text{Sr}$  chemostratigraphy of Dalradian limestones of Scotland and Ireland: constraints on depositional ages and time scales. *Journal of the Geological Society of London* 161, 229-242.
- Umpierre, M., Halpern, M., 1971. Edades Sr-Rb del Sur de la República Oriental del Uruguay. *Revista de la Asociación Geológica Argentina* 26, 133-155.
- Vasconcelos, C., McKenzie, J.A., 1997. Microbial mediation of modern dolomite precipitation and diagenesis under anoxic conditions (Lagoa Vermelha, Rio de Janeiro, Brazil). *Journal of Sedimentary Research* 67, 378-390.
- Veizer, J., 1983. Chemical diagenesis of carbonates: Theory and application of trace element technique. In: Arthur, M.A., Anderson, T.F., Kaplan, I.R., Veizer, J. and Land, L.S. (Eds.), *Stable Isotopes in Sedimentary Geology*. Society of Economic Paleontologists and Mineralogists Short Course No. 10, Dallas, 3-1 to 3-100.
- Walter, M.R., Veevers, J.J., Calver, C.R., Gorjan, P., Hill, A.C., 2000. Dating the 840–544 Ma Neoproterozoic interval by isotopes of strontium, carbon, and sulfur in seawater, and some interpretative models. *Precambrian Research* 100, 371-433.

Wijbrans, J. R., McDougall I., 1986.  $^{40}\text{Ar}/^{39}\text{Ar}$  dating of white micas from an alpine high-pressure metamorphic belt on Naxos. *Contributions to Mineralogy and Petrology* 93, 187-194.

Zwingmann, H., Yamada, K., Tagami, T., 2010. Timing of brittle faulting within the Nojima fault zone, Japan. *Chemical Geology* 275, 176-185.

## CHAPTER 5: A LOW $p\text{CO}_2$ INTERGLACIAL PERIOD? INSIGHTS FROM PAIRED $\delta^{13}\text{C}_{\text{ORG}}$ AND $\delta^{13}\text{C}_{\text{CARB}}$ RECORDS OF CRYOGENIAN CARBONATES

### 5.1. Introduction

It is widely accepted that the Neoproterozoic (1,000-542 Ma) was a time of major global environmental changes that included tectonic upheaval (final breakup of Rodinia and the assembly of Gondwana), full oxygenation of the oceans and a pair of global (Snowball) glaciations (Shields-Zhou et al., 2012 and references therein). These events irreversibly changed the composition of the ocean and atmosphere, and ultimately led to the rise and explosion of animal life (Knoll et al., 2006; Budd, 2008).

One important line of evidence to understand the significance of these events derives from the stable carbon isotope records of carbonate rocks and contemporaneous sedimentary organic matter (Schidlowski, 1988; Knoll et al., 1986; Hayes et al., 1999; Kump and Arthur, 1999; Des Marais, 2001; Schrag et al., 2002; Halverson et al., 2010). Crucially, when carbon isotope records are interpreted in concert with sedimentological and geochronological data they serve as a powerful tool for elucidating the causes and consequences of secular variations in carbon isotope record.

Previous chemostratigraphic studies carried out in the Polanco Limestones Formation (Uruguay) have provided useful insights into the paleoceanographic evolution of the basin (Gaucher et al., 2004; Frei et al., 2011; Aubet et al., 2012). However, these studies were limited by the lack of paired  $\delta^{13}\text{C}_{\text{carb}}$  and  $\delta^{13}\text{C}_{\text{org}}$  as well as by the absence of radiometric age constraints.

Presented here are paired analyses of  $\delta^{13}\text{C}_{\text{carb}}$  and  $\delta^{13}\text{C}_{\text{org}}$ , Sr-isotopes, trace element data and U-Pb ages from three carbonate sections of the Polanco Limestones Formation. The documented  $\delta^{13}\text{C}$  trends are evaluated alongside previously published data from deep-water facies (Aubet et al., 2012). Our results suggest local and global carbon cycle effects on  $\delta^{13}\text{C}$ , and highlight the importance of continued study of paired  $\delta^{13}\text{C}_{\text{carb}}$  and  $\delta^{13}\text{C}_{\text{org}}$  trends in interglacial Cryogenian sections elsewhere.

## 5.2. Geological setting

The Polanco Limestones Formation was deposited in a southeast facing passive margin and comprises marine carbonates with occasional siltstone and sandstone strata. The unit overlies siltstones and iron formations of the Yerbal Formation and underlies shales and cherts of the Cerro Espuelitas Formation (Figure 5.1A). Geochronological constraints indicate deposition between ~1,000 and 650 Ma (Aubert et al., 2014). Similar to data presented by Gaucher et al. (2004) and Frei et al. (2011), the samples studied here come from the Calera de Recalde Syncline and were obtained from three different sections, which cover much of the carbonate succession (Figure 5.1B). Facies analyses indicate that the Polanco Limestones Formation was deposited on a storm-dominated homoclinal ramp, where inner-, mid- and outer-ramp facies associations are recognized (Aubert et al., 2012). Inner ramp facies association is characterized by coarsening- and thickening-upward regressive cycles of calcarenites representing upper, middle and lower shoreface environments deposited above the mean fair-weather wave base in well-oxygenated waters (Figure 5.2A-B). Mid-ramp facies association consists of thinly-bedded calcisiltite and dolosiltite with hummocky and swaley cross-stratified calcarenites and thin massive or parallel-stratified calcarenite beds (Figure 5.2C-D). Outer ramp deposits comprise limestone and dolostone rhythmites and bedded dolostones deposited below the mean storm wave-base under dominantly anoxic conditions (Figure 5.2E-F). Outer ramp facies are characterized by a progressive drop in  $\delta^{13}\text{C}_{\text{carb}}$  values between ~0 and -3.0‰ (Aubert et al., 2012). In contrast, previous work in mid- and inner-ramp facies in the Calera de Recalde Syncline shows a predominance of positive values (up to +5.3‰) interrupted by two negative shifts, one of which reaches a nadir of -3.3‰ (Gaucher et al., 2004).

## 5.3. Methods

A total of 90 carbonate samples for isotopic analyses were collected from three sections ranging from 250-500m, at 5 m intervals. Rock samples were first cut using a water-based diamond-bladed saw to produce two mirror-image billets, one for thin petrographic examination and one for microdrilling. Prior to geochemical analyses, the billets were hand polished to remove saw marks and any remnant surface contamination. Billets were then cleaned using ultrapure water (deionized, 18 M $\Omega$ ) in an ultrasonic bath to remove

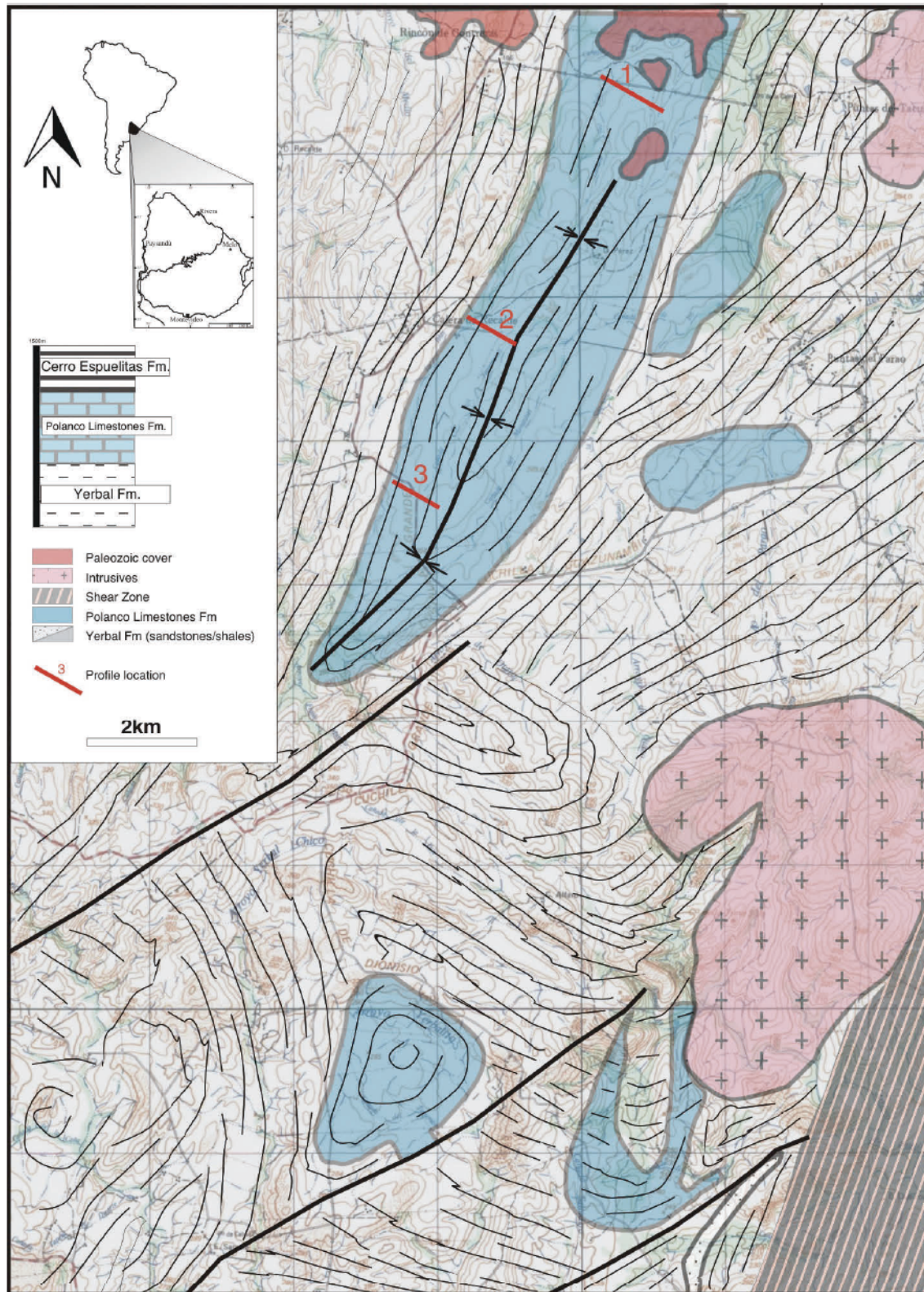


**Figure 5.1. (A)** Simplified stratigraphic column of the Arroyo del Soldado Group (after Aubet et al., 2014). **(B)** Schematic geological map of the Recalde Syncline area showing the location of the sections.

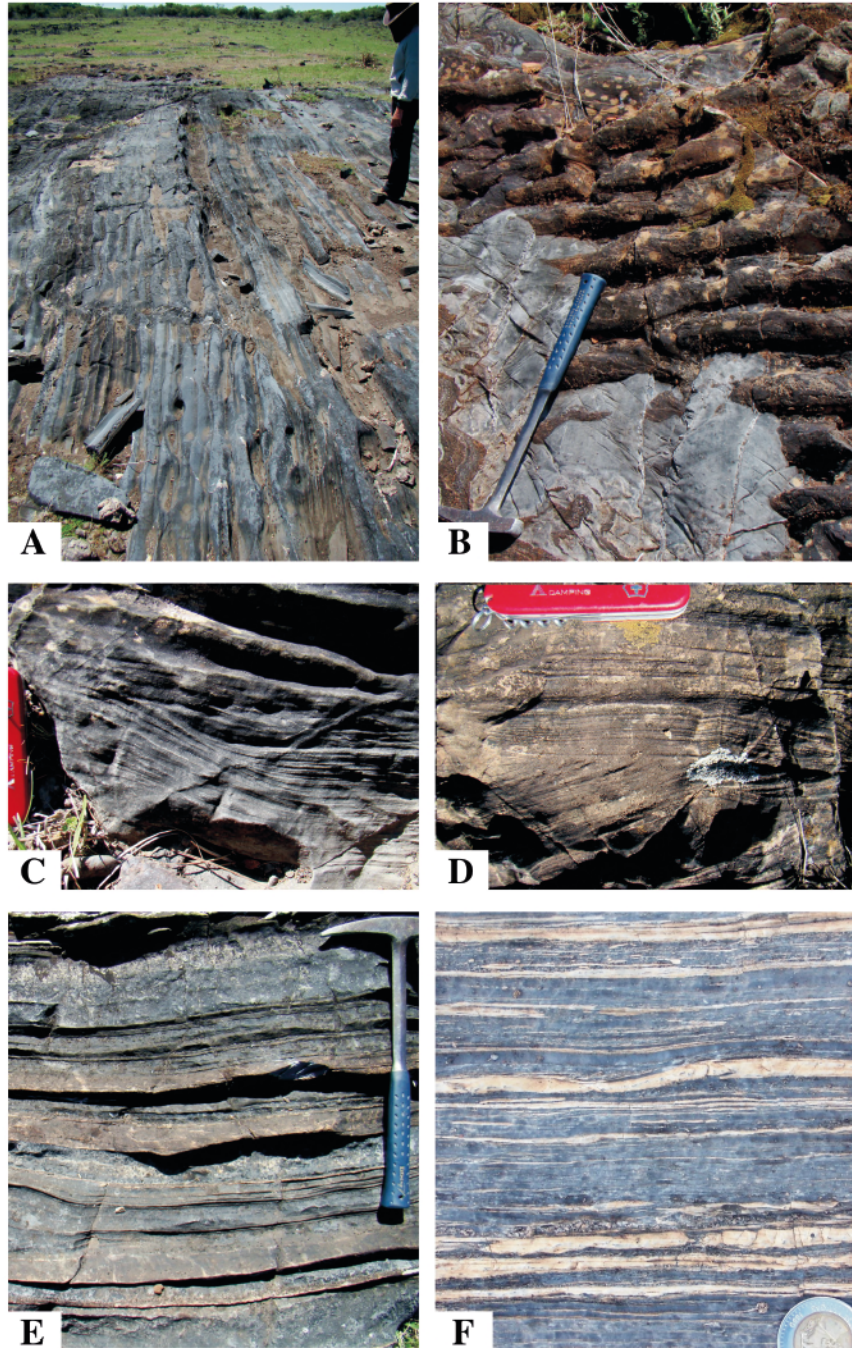


**Figure 5.2.** Photographs of the Polanco Limestones Formation showing typical features of inner, middle and outer ramp facies. (A) General view of limestone dominated carbonates characteristic of inner and middle ramp facies. (B) Ripple cross-laminated sandstones interbedded with limestones largely restricted to inner ramp facies. (C) Hummocky-bedded calcarenite (mid ramp). (D) Planar cross-bedded sandy marls from inner ramp lithofacies. (E) Rhythmites dolostone-limestone typical of outer ramp facies. (F) Laminated rhythmites dolostone-limestone. Length of hammer = 40 cm; length of knife = 10 cm.

excess sediment. Fine-grained micritic components were preferentially microdrilled with dental carbide burrs (0.5-mm diameter) for analysis and unwanted phases (e.g., veins) were avoided. In addition to C- and Sr-isotope analyses, trace element geochemistry was determined using a PerkinElmer Elan6000 Quad-ICP- MS (quadrupole inductively coupled plasma mass-spectrometer) after dissolution in 8N ultrapure HNO<sub>3</sub>. Precision was 4-6% for abundances >0.01 ppm and ≤10% for the most depleted elements.

Inorganic carbon and oxygen isotopes were analyzed in the Stable Isotope Laboratory at the University of Alberta. CO<sub>2</sub> gas was extracted on a high vacuum line by reacting 20-40 mg of sample with 100% phosphoric acid at 25 °C for approximately 24 h of reaction (McCrea, 1950). The released CO<sub>2</sub> gas was analyzed for O and C isotopes on a Finnigan MAT 252 mass spectrometer. All carbon-isotope data are expressed in the δ-notation in parts per thousand (‰) using the Vienna Pee Dee Belemnite (V-PDB) international standard. Reproducibility was checked providing an analytical precision of better than ±0.1‰ for δ<sup>13</sup>C (1σ) and δ<sup>18</sup>O (1σ). From analysis of reference standards, analytical accuracy was estimated to be ±0.1‰.

Strontium isotope ratios of thirty-five limestones were determined using 20 mg aliquots of sample powder following the procedures detailed in Holmden et al. (1996). Strontium isotopes were measured using a NuPlasma MC-ICP-MS instrument at the University of Alberta. Subsequent to ion chromatographic treatment, the Sr-bearing aliquots were diluted in a 2% HNO<sub>3</sub> solution and aspirated into the ICP. Strontium isotope data were acquired in static, multicollection mode using five Faraday collectors for a total of 400 s. Prior to the aspiration of a sample, a 30-second measurement of the gas (+acid) blank was conducted for the correction of the <sup>86</sup>Kr and <sup>84</sup>Kr isobaric (plasma-based) interferences. The isobaric interference of <sup>87</sup>Rb was monitored and corrected for using the <sup>85</sup>Rb ion signal; however, the latter was negligible for all of the results reported here. Accuracy and reproducibility of the analytical protocol were verified by the repeated analysis of a 100 ppb solution of the NIST SRM 987 Sr isotope standard during the course of this study yielding an average value of 0.710255±0.000020 (1SD; n = 7 analyses) and is indistinguishable compared to the accepted value of 0.710245. The typical internal precision ('error') associated with individual Sr isotope analysis ranges from 0.00001 to 0.00003 (2σ level).

$\delta^{13}\text{C}_{\text{org}}$  analyses were performed at the Stable Isotopes for Innovative Research (SIFIR) laboratory at the University of Manitoba. The concentration of total organic carbon was determined on an Eltra IR C/S analyzer as the difference between total carbon (determined by combustion) and total inorganic carbon (determined by acidification). The concentration of total sulphur was also determined on an Eltra IR C/S analyzer. For  $\delta^{13}\text{C}_{\text{org}}$  analyses, sample powder was weighed in a silver cup, and ultrapure 6N HCl was added to remove inorganic carbon. To improve the efficiency of sample combustion, temperature in the oxidation column was raised to 1100°C, and a ‘macro’ O<sub>2</sub> injection loop was utilized. Tin cups were used as a catalyst to increase the combustion temperature through exothermic reaction. Analyses were performed using a Costech™ 4010 Elemental Analyzer (EA) coupled to a Thermo Finnigan™ Delta V Plus isotope-ratio mass-spectrometer via an open-split interface (ConFlo III, Thermo Finnigan™). Sample normalization was performed using the two-point calibration described in Coplen et al. (2006). Two international standards (USGS40 and USGS41) were analyzed at the beginning, middle, and end of each run. A calibration line was calculated for each run by least-squares linear regression using the known and measured isotope values of the calibration standards. To monitor the quality of sample preparation and analysis performance, the international standard USGS Green River shale SGR-1b ( $\delta^{13}\text{C}_{\text{org}} = -29.3 \pm 0.1\text{‰}$  V-PDB) was treated and analyzed as an unknown. Replicate analyses of SGR-1b standard yielded the  $\delta^{13}\text{C}_{\text{org}}$  value of  $-29.5 \pm 0.1\text{‰}$  (n=24).

Uranium-lead ages were determined for six carbonate samples. The carbonate powders were weighed in an ultra-clean room using a UTM2 microbalance, and once transferred to acid-washed Teflon digestion vessels were dissolved in 6.2N HCl at 80°C for 48 hours. A measured amount of <sup>205</sup>Pb/<sup>235</sup>U tracer solution (7.55mg) was added to the acid mixture prior to digestion. Uranium and lead were purified using an HBr procedure (Heaman, 1989). The purified uranium and lead were loaded onto out-gassed Re-filaments in a mixture of silica gel and phosphoric acid. Their isotopic compositions were determined on a VG354 thermal ionization mass spectrometer (TIMS) at the University of Alberta using a Daly photomultiplier (analogue) detector mode. All errors are reported at the 2σ level.

## 5.4. Results

### 5.4.1. C, O, Sr and preliminary N isotopes

A detailed carbon isotope record for the Polanco Limestones Formation was obtained from three measured stratigraphic sections correlated through geological mapping, wherein the lower portion of the unit is reproduced in two of these profiles located ~4 km apart (Figures 5.1B and 5.3). A total of 90 samples were analyzed for  $\delta^{13}\text{C}_{\text{carb}}$  and  $\delta^{18}\text{O}$  isotopes and approximately half of them (41 samples) were selected for  $\delta^{13}\text{C}_{\text{org}}$  analyses. The best-preserved samples (35) were then selected for  $^{87}\text{Sr}/^{86}\text{Sr}$  analyses. Additionally, five preliminary analyses (only for profile 1) were performed for  $\delta^{18}\text{N}$  isotopes. Strontium, oxygen, carbon and nitrogen isotopic composition and elemental data are given in Table 5.1.

In profile 1, where the contact with the underlying Yerbal Formation is not exposed, the basal 155m define a progressive decline in  $\delta^{13}\text{C}_{\text{carb}}$  values from +2.1‰ to -2.9‰. These negative values are maintained for the next 50m, averaging -2.85‰ with a nadir of -3.4‰. This drop is followed by a recovery towards positive values (+1.7 and +1.3‰), between 240 and 270m, and back to more negative values oscillating between -0.6‰ and +0.4‰. The  $\delta^{18}\text{O}$  (PDB) profile for this section shows scattered values between -10‰ and -5‰ (92%) with only three values ranging from -10.5‰ to -11.8‰. The latter value is particularly important because is associated with the lowest  $\delta^{13}\text{C}_{\text{carb}}$  value, which should be taken with caution. Organic carbon isotope values start out at -15.8‰ and for the next 140m stay between -15.5‰ and -14.2‰. Above, between 240 and 287m, values shift towards heavier values, ranging from -10.6‰ to -13.1‰ rapidly falling to -23.4‰ at 305m. In the overlying 60m, the profile culminates with  $\delta^{13}\text{C}_{\text{org}}$  values averaging -15.9‰. Accordingly,  $\Delta^{13}\text{C}$  varies between 11.4 and 22.8‰. The measured  $^{87}\text{Sr}/^{86}\text{Sr}$  ratios on samples from profile 1 are largely variable ranging between 0.706496 and 0.708107 and defining a gradual drop up-section (Figure 5.3). All the five samples analyzed for  $\delta^{18}\text{N}$  isotopes show very low ‰N ( $\leq 0.02$ ). The two samples showing the highest N concentrations show  $\delta^{18}\text{N}$  values between 1.7‰ and 4.2‰ while the two samples with intermediate N concentrations range between -0.9‰ and 2.1‰. The sample showing the lowest N content is not considered here given the larger uncertainty on its  $\delta^{18}\text{N}$  value (-3.6).

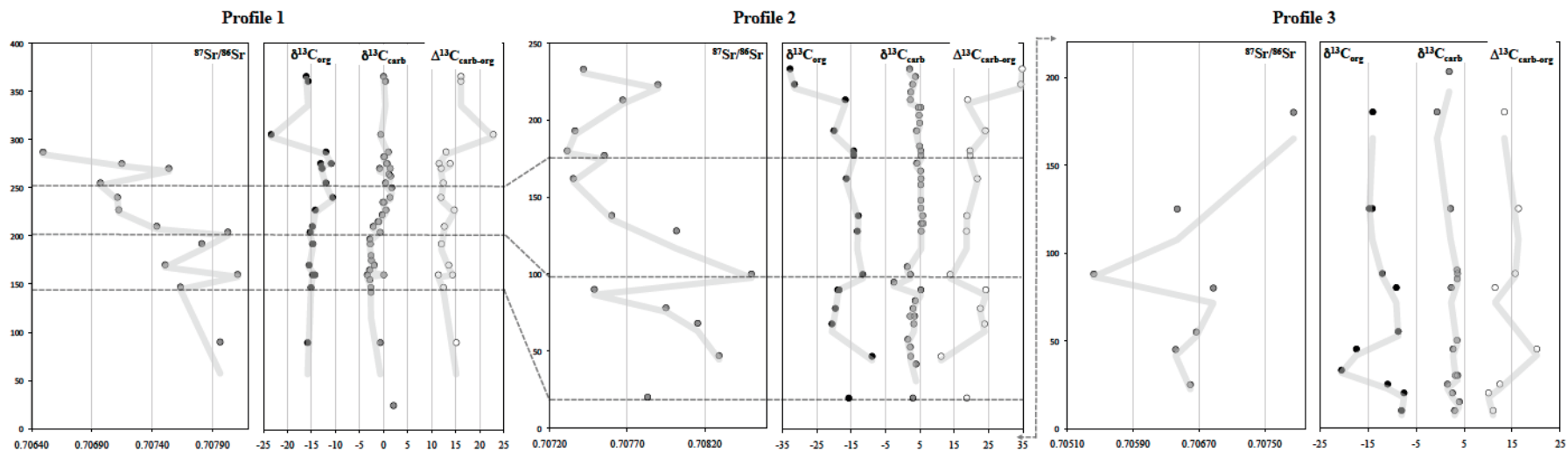


**Figure 5.3.** Profiles of the Polanco Limestones Formation at the Recalde Syncline area with corresponding vertical variations in  $\delta^{13}\text{C}_{\text{carb}}$ ,  $\delta^{13}\text{C}_{\text{org}}$ ,  $\Delta^{13}\text{C}$  and  $^{87}\text{Sr}/^{86}\text{Sr}$ . Vertical scale in meters. Correlations are suggested based upon lithostratigraphic relationships and isotope trends (dashed grey lines).

Depth (m)	$\delta^{13}\text{C}_{\text{carb}}$	$\delta^{13}\text{C}_{\text{org}}$	$\Delta^{13}\text{C}_{\text{carb-org}}$	$\delta^{18}\text{O}_{\text{PDB}}$	$\delta^{18}\text{O}_{\text{SMOW}}$	$^{87}\text{Sr}/^{86}\text{Sr}$	$2\sigma$	$\delta^{15}\text{N}$	Al	Ca	K	P	Sr	Zr	Sr/Ca	Fe/Sr	Mn/Sr	Rb/Sr
<i>Profile 1</i>																		
25	2.078			-10.536	20.048													
90	-0.676	-15.8	15.124	-8.049	22.612	0.707963	0.000015		307	247950	1258	65	1249	0.38	0.0050	1.64	0.0819	0.0038
142	-2.622			-8.356	22.295													
147	-2.658	-15.1	12.442	-8.044	22.617	0.707633	0.000017		419	278786	1429	63	1525	0.56	0.0055	1.10	0.0843	0.0038
155	-2.858			-7.26	23.425													
160	-3.401	-14.8	11.399	-11.815	18.73	0.708107	0.000029		790	258953	962	75	1069	1.68	0.0041	2.71	0.1500	0.0043
160	0.04	-14.3	14.34	-13.68	16.807													
165	-2.918			-8.488	22.16													
170	-1.947	-15.5	13.553	-7.658	23.016	0.707507	0.000018	-3.60	257	292141	603	68	1860	0.93	0.0064	1.01	0.0596	0.0017
175	-2.541			-7.807	22.862													
180	-2.615			-8.838	21.799													
192	-2.768	-14.8	12.032	-8.288	22.366	0.707810	0.000022		447	159518	1271	84	1107	0.92	0.0069	3.61	0.0941	0.0059
197	-2.864			-7.715	22.957													
204	-2.00	-15.3	13.300	-7.800	22.900	0.708026	0.000020	1.70	996	133802	996	135	765	2.56	0.0057	5.42	0.1822	0.0084
204	-0.707			-7.499	23.18													
210	-2.154	-14.8	12.646	-9.369	22.251	0.707437	0.000016		355	262674	560	67	2040	1.23	0.0078	1.19	0.0315	0.0018
215	-1.118			-8.691	21.95													
215	-0.993			-8.856	21.781													
222	-0.31			-8.322	22.331													
227	0.498	-14.2	14.698	-7.834	22.834	0.707122	0.000023		45.5	306822	68	72	3316	0.40	0.0108	0.28	0.0074	0.0001
235	0.085			-7.638	23.036													
235	-0.161			-7.839	22.828													
240	1.336	-10.6	11.936	-7.774	22.896	0.707112	0.000018		356	272090	417	82	3144	0.61	0.0116	0.55	0.0220	0.0008
250	1.705			-7.759	22.911													
255	0.42	-12.0	12.42	-5.204	25.545	0.706971	0.000019	2.10	229	290108	412	125	1914	1.07	0.0066	1.42	0.0979	0.0013
262	1.449			-7.224	23.462													
264	1.114			-7.125	23.565													
270	-0.825	-12.8	11.975	-8.887	21.749	0.707537	0.000021		906	216636	249	278	714	2.87	0.0033	7.27	0.3744	0.0019
270	1.372			-9.98	20.621													
275	0.733	-13.1	13.833	-8.903	21.732	0.707148	0.000027	-0.90	543	248680	392	257	1488	2.03	0.0060	2.97	0.1043	0.0015
275	0.632	-10.9	11.532	-9.674	20.937			4.20	945	105444	600	660	160	5.14	0.0015	66.40	4.2200	0.0130
282	0.068			-6.353	24.361													
282	0.167			-6.325	24.389													
287	0.994	-12.0	12.994	-5.941	24.785	0.706496	0.000029		55.9	296194	106	118	1269	1.01	0.0043	2.30	0.5603	0.0003
305	-0.584	-23.4	22.816	-8.355	22.297				63.0	312559	50	82	290	1.14	0.0009	9.46	3.7348	0.0003
360	0.379	-15.7	16.079	-7.53	23.148				1246	110362	171	316	153	2.74	0.0014	125.81	12.2963	0.0043
365	-0.004	-16.1	16.096	-11.045	19.523				372	255280	47	129	118	6.63	0.0005	69.98	23.8459	0.0010
<i>Profile 2</i>																		
20	2.996	-15.7	18.696	-11.881	18.662	0.707831	0.000033		295	342508	107	112	1100	2.14	0.0032	2.03	0.0475	0.0004
42	3.897			-8.655	21.988													
47	2.334	-8.9	11.234	-10.907	19.666	0.708291	0.000033		222	309631	192	117	566	2.09	0.0018	7.00	0.1323	0.0016
53	2.22			-10.152	20.444													
58	1.514			-10.922	19.65													
68	3.257	-20.6	23.857	-9.961	20.641	0.708153	0.000035		157	347672	69	64	596	1.11	0.0017	2.15	0.1146	0.0004
73	3.469			-8.821	21.816													
73	2.181			-15.551	25.539													
78	3.045	-19.6	22.645	-7.009	23.685	0.707949	0.000035		207	348238	112	94	485	1.19	0.0014	2.57	0.1429	0.0010
83	3.648			-12.244	18.288													
90	5.297	-18.9	24.197	-7.658	23.015	0.707487	0.000024		112	346231	192	110	1323	0.68	0.0038	1.58	0.1733	0.0008
95	-2.562			-20.734	9.535													
100	2.262	-11.6	13.862	-9.58	21.034	0.708500	0.000034		172	322620	74	84	500	1.06	0.0015	5.52	0.2404	0.0005
105	1.337			-7.099	23.591													
128	5.405	-13.2	18.605	-7.703	22.969	0.708017	0.000026		325	324066	293	121	1101	1.01	0.0034	2.97	0.1132	0.0015
133	5.449			-7.632	23.042													
133	5.963			-7.674	22.999													
138	5.829	-12.9	18.729	-7.007	23.687	0.707600	0.000022		1723	336069	923	108	2305	2.41	0.0069	1.20	0.0385	0.0030
143	5.331			-7.224	23.463													
148	5.3			-8.714	21.927													
158	5.271			-9.3	21.322													
162	5.356	-16.4	21.756	-8.173	22.485	0.707352	0.000026		112	411170	180	129	1519	0.79	0.0037	1.72	0.1227	0.0006
167	5.218			-10.263	20.329													
167	5.226			-8	22.663													
172	4.136			-8.148	22.51													
177	5.347	-14.3	19.647	-7.992	22.671	0.707552	0.000020		200	417898	216	79	1579	1.14	0.0038	1.12	0.0235	0.0006
180	5.305	-14.3	19.605	-7.103	23.588	0.707313	0.000026		409	413176	298	68	2656	1.51	0.0064	0.79	0.0260	0.0005
183	4.911			-10.156	20.44													
193	4.07	-20.0	24.07	-6.308	24.407	0.707363	0.000022		115	436537	158	90	1470	0.88	0.0034	0.79	0.0297	0.0004
198	4.96			-7.448	23.232													
203	4.789			-7.758	22.912													
208	4.592			-8.135	22.524													
208	4.721			-8.678	21.964													
208	5.269			-7.146	23.543													
213	2.241	-16.7	18.941	-11.933	18.608	0.707671	0.000029		389	378909	53	69	810	1.46	0.0021	2.70	0.1099	0.0001
218	2.372			-6.219	24.499													
223	2.914	-31.5	34.414	-7.745	22.925	0.707897	0.000038		98.3	428467	49	80	797	0.85	0.0019	1.32	0.0636	0.0001
228	3.733			-7.153	23.536													
233	2.023	-32.8	34.823	-7.786	22.883	0.707417	0.000022		214	454942	469	86	1304	0.33	0.0029	0.78	0.0372	0.0019
<i>Profile 3</i>																		
10	3.018	-8.0	11.018	-9.21	21.415				292	247236	262	197	416	0.68	0.0017	17.52	11.5234	0.0038
15	4.014			-5.349	25.395													
20	2.586	-7.5	10.086	-6.53	24.178				167	312663	26	87	255	0.96	0.0008	3.23	2.2438	
25	1.554	-10.9	12.454	-5.723	25.01	0.706595	0.000029		46.7	326872	33	58	210	0.45	0.0006	1.72	1.2851	0.0003
30	3.653			-6.043	24.68													
30	3.192			-5.285	25.461													
33		-20.5							74.1	192091	50	63	247	0.45	0.0013	18.14	1.5587	0.0006
45	2.713	-17.4	20.113	-5.134	25.618	0.706417	0.000019		54.9	264695	27	61	294	0.68	0.0011	5.26	0.3467	0.0001
50	3.521			-6.463	24.247													
55		-8.7				0.706667	0.000033		219	238542	67	122	307	1.60	0.0013	14.89	0.4589	0.0011
80	2.324	-9.1	11.424	-9.321	21.301	0												

Beginning approximately twenty meters above the contact with the Yermal Formation, profile 2 defines a small increase in  $\delta^{13}\text{C}_{\text{carb}}$  values from +3‰ to +3.9‰. Up section, and for the next 41m, there is a shift towards more negative values with a nadir at +1.5‰. After recovering to values of up to 5.3‰ (90m), there is another drop to +1.3‰ and then a return to +5.4‰ (128m). While a single value as low as -2.6‰ is recorded during this drop at 95m, this value is associated with an abrupt drop in  $\delta^{18}\text{O}$  (PDB), from -7.7‰ to -21‰ (see below). Between 128 and 208m  $\delta^{13}\text{C}_{\text{carb}}$  values are rather homogenous ranging from +4.07‰ to +5.96‰. Afterwards, there is a small shift to +2.2‰ increasing up to +3.7‰ and back to +2‰. Over a total of 39 samples, oxygen isotope values (PDB) in profile 2 are as follows, 74% between -10‰ and -4‰, 21% between -10‰ and -12, and 5% between -15‰ and -21‰. Of the two samples showing the lightest  $\delta^{18}\text{O}$  values (i.e., from -15‰ to -21‰), only the one with the lowest value is associated with the most negative  $\delta^{13}\text{C}$  value of -2.6‰ and thus, this value should not be considered for further analysis. Values of  $\delta^{13}\text{C}_{\text{org}}$  begin at -15.7‰ in the lowermost beds and after a shift to a heaviest value of -8.9‰, there is an abrupt drop to -20.6‰. The following 22m are characterized by a smooth rise to -18.5‰ and then an abrupt increase to -11.6‰ (100m). For the rest of the section, values trend negatively averaging -18.35‰ ca. 200m and then they rapidly fall to -32.8‰. Similar to stratigraphic section 1, samples from this profile depict an overall decreasing Sr isotope trend up-section, with minor fluctuations and values oscillating between 0.708500 and 0.707313 (Figure 5.3).

Profile 3 is largely characterized by positive  $\delta^{13}\text{C}_{\text{carb}}$  values oscillating between +1.5‰ and +4‰, with one exception at 180m showing one value of -0.6‰. Overall, the profile is expressed as a progressive decline in  $\delta^{13}\text{C}_{\text{carb}}$  starting with values around +3-4‰, diving to -0.6‰ and returning to +1.9‰. Similar to profile 1, in this section the majority of the oxygen isotope values oscillate between -10‰ and -5‰ (PDB), with two values plotting at -4.2‰ and -4.1‰ with no obvious trends.  $\delta^{13}\text{C}_{\text{org}}$  values begin near -8.0‰ and begin to decline abruptly at 25m reaching a nadir of -20.5‰. Values shift back to -8.7‰ at 55m but then decline reaching a peak value of -14.7‰ at 125m and stay near -14‰ in the upper part of the section. For this profile,  $\Delta^{13}\text{C}$  varies between 10.1‰ and 20.1‰. With the exception of one sample (0.707848), the  $^{87}\text{Sr}/^{86}\text{Sr}$  ratios in profile 3 are

among the lowest ratios reported for the entire unit ranging between 0.705423 and 0.706875 (Figure 5.3).

## 5.4.2. Geochronology

### 5.4.2.1. U-Pb (Pb-Pb) dating

The reliability of carbonate U-Pb geochronology is strongly dependant on the quality of the samples (i.e., lack of significant post-depositional alteration, U and Pb concentrations, lack of detrital contamination). Accordingly, the selection of carbonate samples for this study was based on the following criteria: (1) the use of geochemical parameters as filters to select for samples that most probably retain a near-primary composition (e.g., Mn/Sr  $\leq$  1, Rb/Sr  $\leq$  0.001); (2) variable U/Pb ratios and U and Pb concentrations at different stratigraphic intervals; (3) preservation of the original petrographic textures, excluding samples with different phases under cathodoluminescence imaging.

Isotopic data for HCl-soluble portions of twenty-six limestones from three stratigraphic sections are given in Table 5.2. With the exception of two samples, U and Pb concentrations range from 0.17 to 2.70 and 0.49 to 6.38 ppm, respectively. Corresponding  $^{238}\text{U}/^{204}\text{Pb}$  ratios (hereafter “ $\mu$ ” values) range from 8.38 to 143.30. The  $^{204}\text{Pb}/^{206}\text{Pb}$  vs.  $^{238}\text{U}/^{204}\text{Pb}$  results are plotted in Figure 5.4. When analyzed by section, each set shows a significant scatter in the U-Pb results. Samples from section 101020 define a  $^{238}\text{U}/^{204}\text{Pb}$  isochron that corresponds to an age of  $673\pm 770$  Ma and a mean square of the weighted deviates (MSWD) equal to 4710. The same scatter is recorded in section 101022 (9 points) with an age of  $556\pm 1100$  Ma (MSWD = 3218) (Table 5.2). The high degree of scatter in the U-Pb isochrons might be the result of initial Pb isotope heterogeneity and/or later disturbance of the U-Pb system.

Isochron plots from stratigraphic sections 101020 and 101022 do not show any meaningful age related to the deposition of the Polanco Limestones. However, after excluding three samples from calculation, an age of  $807\pm 58$  Ma with a MSWD = 3.1 and a probability of 0.04 from 4 points was obtained for section 101021 (Figure 5.4C). A new isochron plot built with 2 more samples from section 101020 provides an age of  $752\pm 95$  Ma (Figure 5.4D). Although with a more elevated MSWD (28), the new age is within the range of the one obtained in stratigraphic section 101021 (Figure 5.4C).

On the other hand, whole-rock Pb-isotopic data from Polanco Limestones Formation (Table 5.2) show a scatter in  $^{207}\text{Pb}/^{204}\text{Pb}$  and  $^{206}\text{Pb}/^{204}\text{Pb}$  in all the profiles. The  $^{206}\text{Pb}/^{204}\text{Pb}$  ratios grow from 21.92 to 31.70 in section 101020, from 21.31 to 53.06 in section 101021, and 20.18 to 29.61 in section 101022. Accordingly, carbonate material is heterogeneous even in the least altered limestone samples selected based on the geochemical criteria.

Regression of the all the data yields a line equivalent to an age of 1306 Ma (101020), 1604 Ma (101021), and 1306 Ma (101022) with large errors of 570 Ma, 420 Ma, and 340 Ma respectively. Because the associated errors are so large the results are not considered a reliable age estimate and consequently some data was discarded to reduce the MSWD values. Thus, five analyses in section 101020 define a linear trend in the  $^{207}\text{Pb}/^{204}\text{Pb}$  versus  $^{206}\text{Pb}/^{204}\text{Pb}$  diagram that corresponds to an age of  $1454\pm 81$  Ma (MSDW = 2.2), five data points  $1570\pm 70$  Ma (MSDW = 1.3) for section 101021, and four analysis define an age of  $1450\pm 66$  Ma (MSDW = 2.1) (Figure 5.5).

Sample (a)	Compositional Parameters							Radiogenic Isotope Ratios							Isotopic Ages					Sample (Radiogenic + Initial Pb) Isotope Ratios												
	Wt. mg (b)	U ppm (c)	Th U (d)	Pb ppm (c)	mol % <sup>208</sup> Pb* (e)	Pb* Pb <sub>i</sub> (pg) (e)	Pb <sub>c</sub> (pg) (e)	<sup>208</sup> Pb/ <sup>206</sup> Pb (f)	<sup>208</sup> Pb/ <sup>206</sup> Pb (g)	<sup>207</sup> Pb/ <sup>206</sup> Pb (g)	% err (h)	<sup>235</sup> Pb/ <sup>238</sup> U (g)	% err (h)	<sup>235</sup> Pb/ <sup>238</sup> U (g)	% err (h)	corr. coef. (i)	<sup>207</sup> Pb/ <sup>206</sup> Pb (i)	± (h)	<sup>235</sup> Pb/ <sup>238</sup> U (i)	± (h)	<sup>207</sup> Pb/ <sup>206</sup> Pb (i)	± (h)	<sup>235</sup> U/ <sup>206</sup> Pb (j)	% err (h)	<sup>208</sup> Pb/ <sup>206</sup> Pb (j)	% err (h)	corr. coef. 8/4-6/4 (j)	<sup>235</sup> U/ <sup>206</sup> Pb (j)	% err (h)	<sup>208</sup> Pb/ <sup>206</sup> Pb (j)	% err (h)	corr. coef. 5/4-7/4 (k)
<b>101020</b>																																
101020-6A	8.79	1.6	1.13	6.4	26.3%	0.12	50103	21.92	0.327	0.07507	11.15	3.5914	11.67	0.34696	1.03	0.550	1070	224	1548	93	1920.1	17.2	16.62	0.32	21.916	0.22	0.635	0.1206	0.32	15.823	0.23	0.634
101020-13A	4.15	2.7	0.75	2.5	43.0%	0.23	8521	28.32	0.228	0.06094	3.42	1.9623	3.52	0.15651	0.41	0.292	1445	65	1103	24	937.3	3.6	77.82	0.16	28.328	0.11	0.543	0.5644	0.16	16.498	0.15	0.476
101020-19	2.87	0.5	1.30	2.6	26.8%	0.13	6732	22.07	0.368	0.08989	6.91	5.4688	7.04	0.44126	0.79	0.230	1423	132	1896	60	2356.3	15.5	13.43	0.23	22.076	0.10	0.294	0.0974	0.23	15.923	0.13	0.257
101020-21	7.21	0.7	0.84	1.3	30.6%	0.14	8217	23.27	0.253	0.08778	5.98	2.3059	6.11	0.19052	0.65	0.257	1378	115	1214	43	1124.2	6.7	37.39	0.14	23.273	0.15	0.700	0.2712	0.14	16.015	0.15	0.453
101020-24	4.02	0.6	1.64	5.2	31.7%	0.17	18093	23.65	0.418	0.09419	5.95	11.6226	6.20	0.89493	0.69	0.414	1512	112	2574	58	4120.4	21.0	8.38	0.19	23.650	0.17	0.788	0.0608	0.19	16.096	0.19	0.745
101020-25B	4.78	0.9	1.55	6.0	27.8%	0.14	25100	22.37	0.417	0.08056	12.49	7.0511	13.33	0.63479	1.24	0.706	1211	246	2118	119	3168.5	31.1	9.81	0.53	22.374	0.37	0.685	0.0711	0.53	15.891	0.38	0.673
101020-25C	2.64	23.4	0.75	8.0	49.0%	0.30	16225	31.70	0.234	0.07437	4.26	0.7079	4.48	0.06994	0.44	0.527	1051	86	543	19	430.3	1.8	225.3	0.33	31.703	0.25	0.725	1.6342	0.33	16.547	0.27	0.698
101020-27	1.27	1.8	0.92	4.4	42.2%	0.23	11742	27.98	0.219	0.09006	3.71	4.8723	3.83	0.29216	0.44	0.340	1427	71	1797	32	2133.8	8.0	30.16	0.19	27.983	0.13	0.580	0.2187	0.19	16.456	0.16	0.525
101020-31	3.54	34.7	0.60	13.6	32.3%	0.14	42066	23.86	0.225	0.06262	7.65	0.3860	7.77	0.04471	0.61	0.234	695	163	331	22	281.9	1.7	172.4	0.18	23.857	0.10	0.328	1.2506	0.18	15.873	0.13	0.311
<b>101021</b>																																
101021-1	4.10	1.3	0.33	0.8	66.5%	0.55	2120	48.25	0.100	0.08149	1.70	2.5232	1.79	0.22458	0.23	0.441	1233	33	1279	13	1306.0	2.8	143.4	0.28	48.353	0.22	0.821	1.0401	0.28	18.014	0.20	0.632
101021-6	19.40	0.3	1.36	1.0	24.2%	0.11	17983	21.31	0.400	0.09748	6.38	3.7921	6.38	0.28214	0.83	0.067	1576	119	1591	51	1602.1	11.8	18.29	0.15	21.310	0.05	0.334	0.1327	0.15	15.893	0.04	0.371
101021-8	3.37	1.7	1.36	5.9	24.2%	0.11	17983	21.31	0.400	0.09748	6.38	3.7921	6.38	0.28214	0.83	0.067	1576	119	1591	51	1602.1	11.8	18.29	0.15	21.310	0.05	0.334	0.1327	0.15	15.893	0.04	0.371
101021-10	5.25	0.4	0.71	0.4	40.8%	0.21	1937	27.29	0.215	0.09697	3.20	2.3613	3.25	0.17661	0.46	0.175	1567	60	1231	23	1048.4	4.5	63.28	0.26	27.325	0.15	0.700	0.4590	0.26	16.474	0.15	0.684
101021-11	4.11	0.4	0.89	0.8	35.3%	0.18	2916	24.97	0.263	0.10248	14.10	3.6987	15.67	0.26176	1.95	0.832	1670	261	1571	125	1498.8	26.1	33.77	1.04	24.988	0.75	0.722	0.2449	1.04	16.296	0.66	0.812
101021-14	3.45	0.5	0.16	0.5	69.5%	0.62	1046	53.06	0.047	0.10757	20.45	5.2386	21.05	0.35320	2.71	0.915	1759	374	1859	197	1949.8	45.6	105.2	6.02	53.309	5.97	0.992	0.7631	6.02	19.387	5.96	0.992
101021-18A	4.32	0.9	0.85	2.1	28.6%	0.13	8214	22.63	0.254	0.09965	5.64	3.0794	5.80	0.22411	0.74	0.268	1618	105	1428	44	1303.6	8.7	28.96	0.18	22.639	0.12	0.669	0.2100	0.18	16.037	0.11	0.716
<b>101022</b>																																
101022-6	5.90	0.2	2.76	0.5	21.0%	0.12	2679	20.45	0.833	0.08115	10.61	2.2114	10.80	0.19764	1.06	0.230	1225	208	1185	76	1162.6	11.3	21.77	0.20	20.451	0.09	0.335	0.1579	0.20	15.739	0.12	0.230
101022-8	6.35	0.6	3.13	0.6	19.9%	0.12	3475	20.18	0.985	0.09238	23.77	0.7856	25.97	0.06168	2.98	0.763	1475	451	589	116	385.8	11.2	65.33	1.43	20.181	0.46	0.315	0.4738	1.43	15.762	0.40	0.372
101022-10	5.33	0.3	1.69	1.2	27.8%	0.14	5616	22.37	0.481	0.10224	5.82	5.8003	5.96	0.41571	0.74	0.244	1665	108	1955	52	2241.0	14.0	14.97	0.16	22.373	0.15	0.700	0.1086	0.16	16.026	0.15	0.392
101022-16B	5.23	0.9	0.76	1.7	45.5%	0.26	7025	29.61	0.220	0.08824	3.49	4.0907	3.63	0.33623	0.43	0.383	1388	67	1652	30	1868.5	6.9	40.08	0.22	29.625	0.14	0.567	0.2907	0.22	16.579	0.16	0.538
101022-21	3.71	0.6	1.46	1.5	32.0%	0.17	4793	23.77	0.427	0.08880	6.51	3.7009	6.81	0.30226	0.73	0.453	1400	125	1572	54	1702.5	10.9	25.23	0.24	23.774	0.18	0.675	0.1830	0.24	16.067	0.19	0.643
101022-28	7.20	0.8	0.67	1.4	44.6%	0.24	8078	29.15	0.196	0.08409	3.42	3.7109	3.50	0.32006	0.38	0.267	1295	66	1574	28	1790.0	6.0	40.66	0.14	29.162	0.09	0.374	0.2949	0.14	16.484	0.12	0.238

- (a) whole rock powders  
(b) Fraction weights determined with a Mettler microbalance, uncertainties are <0.1 mg  
(c) Concentrations determined by isotope dilution using a mixed <sup>208</sup>Pb/<sup>235</sup>U tracer solution  
(d) Model Th/U ratio calculated from radiogenic <sup>208</sup>Pb/<sup>206</sup>Pb ratio and <sup>237</sup>Pb/<sup>235</sup>U age.  
(e) Pb\* and Pbc represent radiogenic and common Pb, respectively; mol % <sup>208</sup>Pb\* with respect to radiogenic, blank and initial common Pb.  
(f) Measured ratio corrected for spike and fractionation only. Daily analyses corrected for detector bias based on analysis of NBS-981 and US50  
(g) Corrected for fractionation, spike, and common Pb; 8 pg of common Pb was assumed to be procedural blank; <sup>235</sup>Pb/<sup>238</sup>U = 18.24 ± 1.0%; <sup>207</sup>Pb/<sup>206</sup>Pb = 15.64 ± 0.25%;  
<sup>208</sup>Pb/<sup>206</sup>Pb = 37.50 ± 1.0% (all uncertainties 1-sigma). Excess over blank was assigned to initial common Pb with an isotopic composition calculated using the Stacey and Kramers (1975) model at 1.5 Ga.  
(h) Errors reported in this table are quoted at 2-sigma, propagated using the algorithms of Schmitz and Schoene (2007) and Crowley et al. (2007).  
(i) Calculations are based on the decay constants of Jaffey et al. (1971).  
(j) Corrected for fractionation, spike, and blank Pb only.

**Table 5.2.** U-Th-Pb isotopic data for the Polanco Limestones Formation Whole Rock.

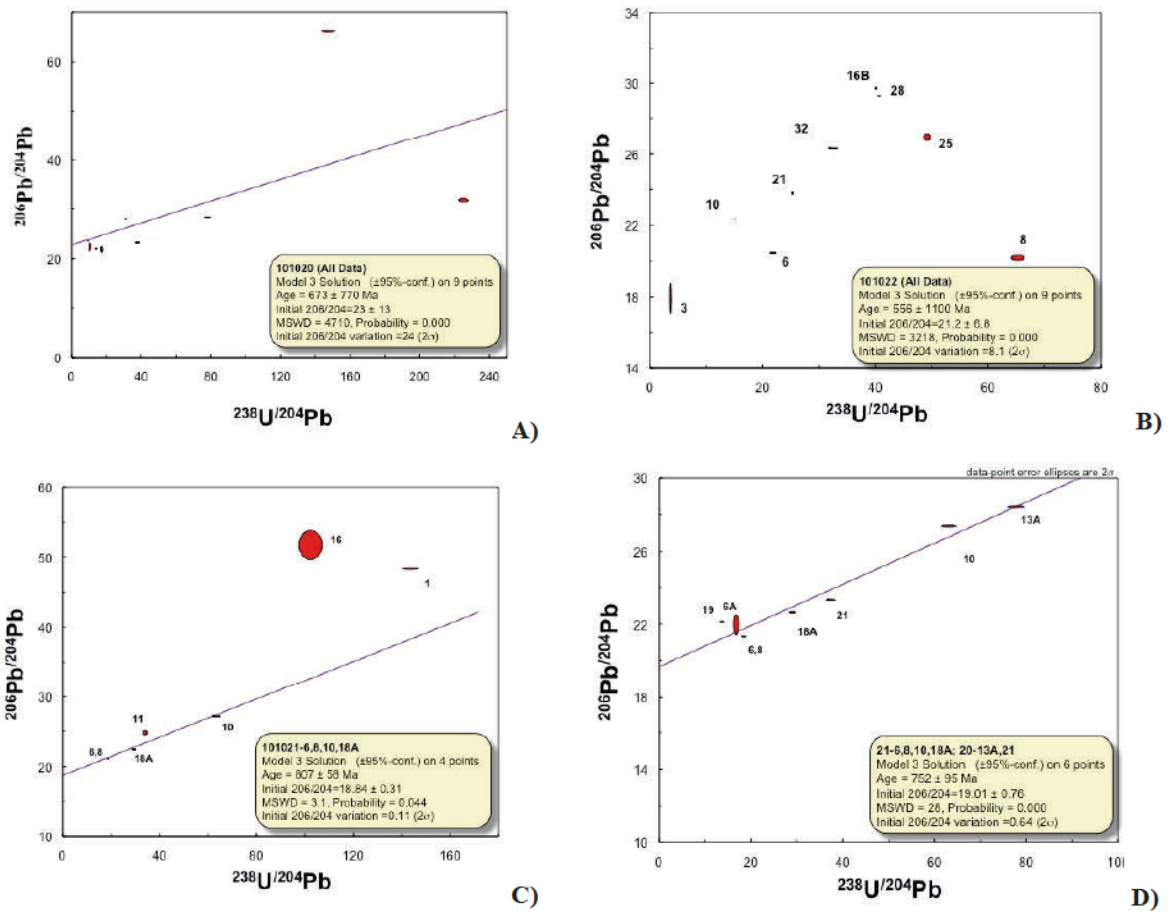


**Figure 5.4.** U-Pb isochron diagram for carbonates of the Polanco Limestones Formation. (A) and (B) all data points for sections 101020 and 101022 respectively; (C) Age calculated on selected points from section 101021, and (D) from sections 101021 and 101020.

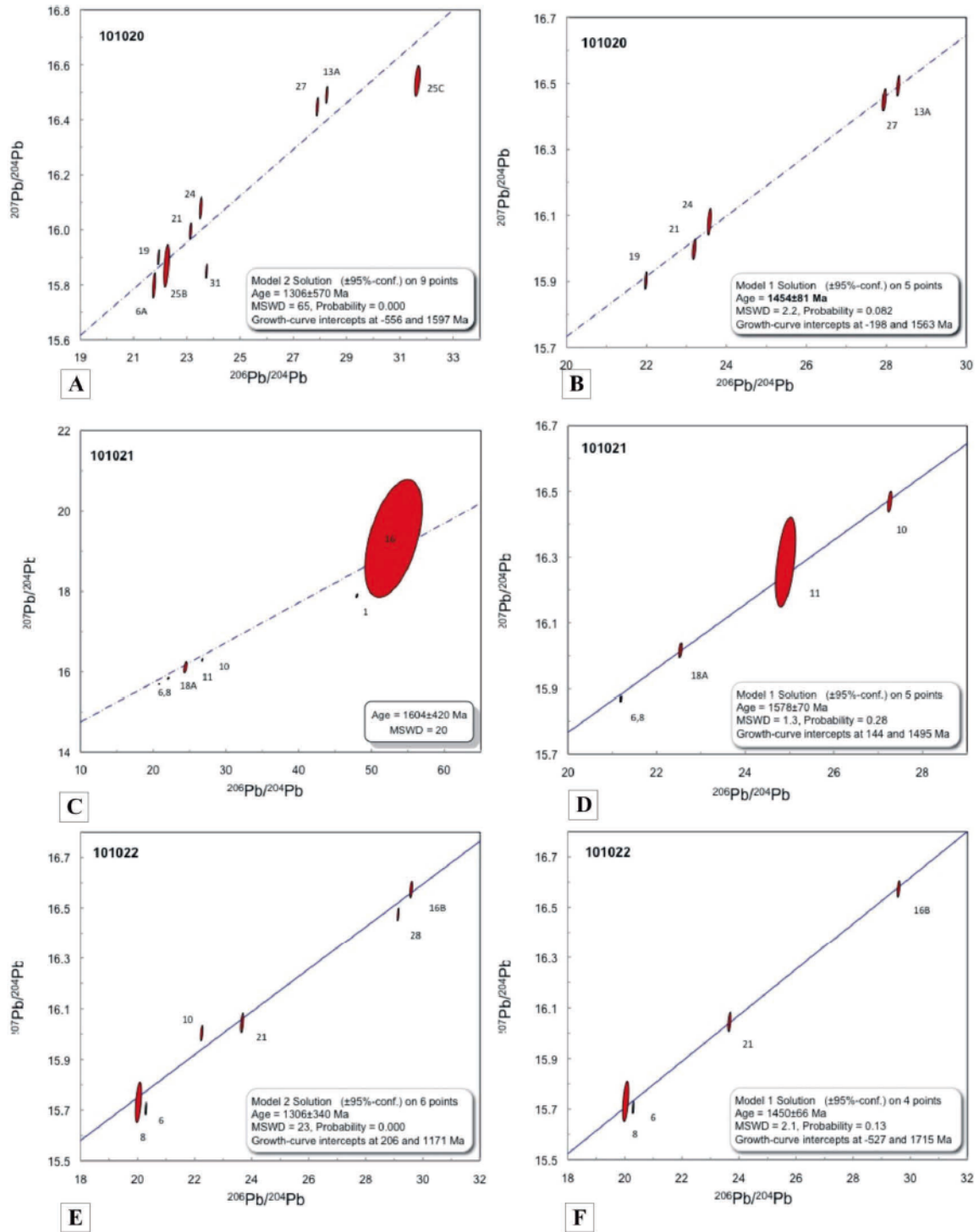


**Figure 5.5.** Pb–Pb diagrams for all the data set (A), (C, E) of the analyzed sections from Polanco Limestones Formation, and selected data points (B), (D, F).

### 5.4.2.2. K-Ar dating

Previous Ar diffusion model placed the onset of sedimentation of the Polanco Limestones Formation to a maximum age of 600 Ma (Aubet et al., 2012). This model considered earlier estimates of the basement, which constrained the maximum depositional age of the Arroyo del Soldado Group to  $633 \pm 8$  Ma. Recent field recognizance by Aubet et al. (2014) show no evidence of these basement rocks underlying the Arroyo del Soldado Group, and therefore these previously considered estimates were discarded. Additionally based on radiometric grounds the age of the Arroyo del Soldado Group was constrained between  $\sim 1,000$  and 650 Ma (Aubet et al., 2014).

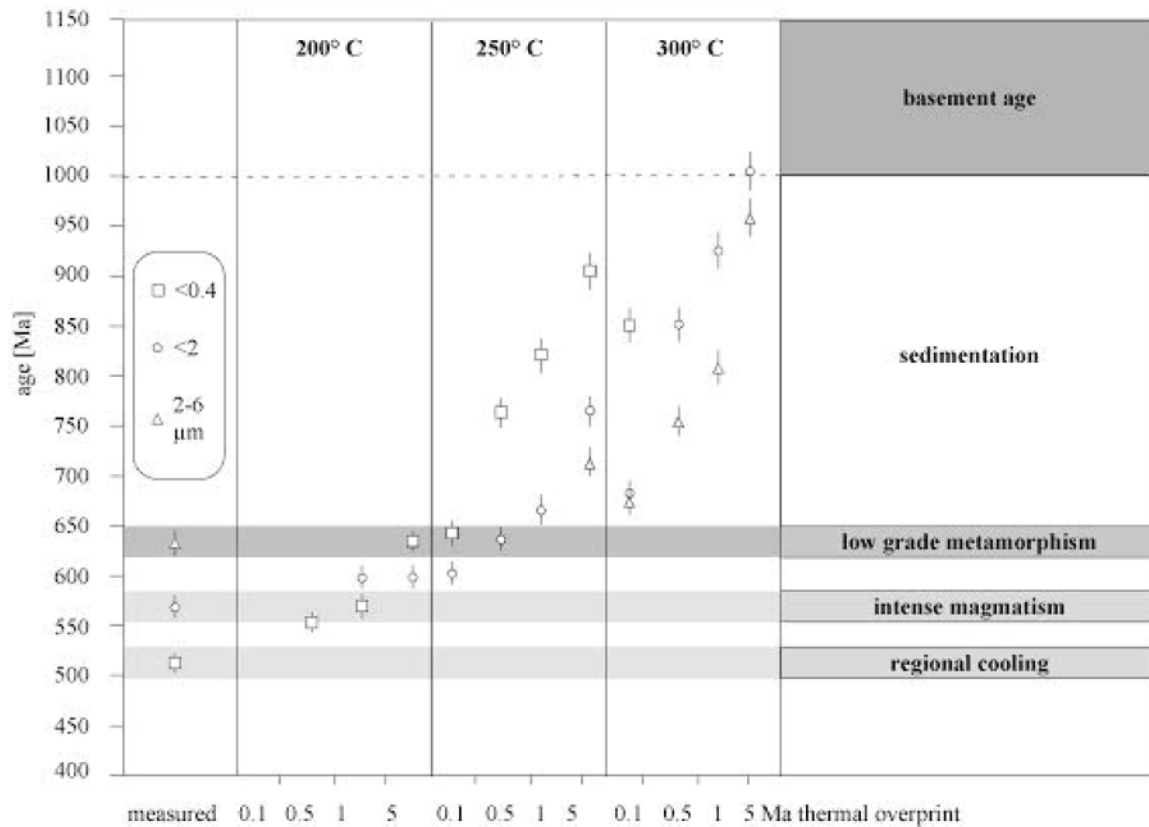


**Figure 5.6.** Summary of the illite age data from the uppermost Yermal Formation.

Considering these new estimates, we present a new Ar diffusion model for shales of the uppermost Yermal Formation to further understand the relative timing of diagenesis in the Yermal Formation and infer the depositional age of the overlying Polanco limestones. Three K-Ar illite ages obtained from the Yermal shales. The <0.4 μm illite fraction yields

the youngest age of  $513.8 \pm 10.4$  Ma. The  $< 2 \mu\text{m}$  illite fraction yields an intermittent age of  $574.7 \pm 11.6$  Ma, whereas the coarse grained  $2\text{-}6 \mu\text{m}$  illite fraction yields the oldest age of  $636.5 \pm 12.8$  Ma (Figure 5.6). Radiogenic  $^{40}\text{Ar}$  ranges from 96.4 to 98.9% indicating negligible atmospheric Ar contamination and reliable analytical conditions for all analyses. The K contents range homogeneously from 4.2 to 4.3%.

## 5.5. Discussion

$\delta^{13}\text{C}_{\text{carb}}$  and  $\delta^{13}\text{C}_{\text{org}}$ , and thereby their fractionation ( $\Delta^{13}\text{C}$ ), can be influenced by several factors such as vital effects and water mass differences, mineralogy and diagenesis, which pose significant challenges to the use of  $\delta^{13}\text{C}$  records as a global correlation tool and to understand their paleoceanographic and paleoatmospheric (e.g.,  $p\text{CO}_2$ ) significance (Saltzman and Thomas, 2012; Knauth and Kennedy, 2009; Sansjofre et al., 2011). In this section, we discuss the syn- and post-depositional factors that could have imprinted the  $^{87}\text{Sr}/^{86}\text{Sr}$  and  $\delta^{13}\text{C}$  signatures of carbonate and organic carbon of the Polanco Limestones Formation and assess their paleoenvironmental implications. Finally, we discuss the age of the unit and potential correlations with other units elsewhere.

### 5.5.1. Assessment of post-depositional alteration on primary C, O and Sr isotope signatures

After deposition the isotopic composition of Sr, C and O in marine carbonates is susceptible to alteration either by diagenetic, metamorphic or meteoric transformations. The potential effects of post-depositional processes on the preservation of marine Sr, C and O isotope records can be evaluated by examination of combined elemental and isotopic trends. In this regard, it is expected that  $\delta^{13}\text{C}$  system be more robust than  $^{87}\text{Sr}/^{86}\text{Sr}$ , which is in turn more robust than  $\delta^{18}\text{O}$  (Banner and Hanson, 1990; Jacobsen and Kaufman, 1999). Previous studies have suggested that  $\delta^{18}\text{O}$ -depletion, a low Sr content, a very high Mn content, a high Mn/Sr ratio, a relationship between Sr/Ca and Mn content and a covariation of  $\delta^{13}\text{C}$  and  $\delta^{18}\text{O}$ , are commonly the result of post-depositional alteration (Brand and Veizer, 1980, 1981; Banner and Hanson, 1990; Jacobsen and Kaufman, 1999; Halverson et al., 2007). In the following, we discuss in detail the

relationship between these alteration indexes and the Sr, C and O isotope signatures from the Polanco Limestones Formation.

### $\delta^{18}\text{O}$

Oxygen-isotopic composition is a sensitive indicator of diagenesis because meteoric and hydrothermal water alteration, even at low degrees of fluid-rock interaction (Banner and Hanson, 1990), commonly results in depletion of  $\delta^{18}\text{O}$  or both  $\delta^{18}\text{O}$  and  $\delta^{13}\text{C}$  in carbonates (Fairchild et al. 1990). Polanco carbonates show a relatively narrow range of  $\delta^{18}\text{O}$  (PDB) values ( $\pm 4\text{‰}$ ) between -4 and -12‰ with an average of -8‰ (Table 5.1). These values are identical to that shown by well-preserved Neoproterozoic carbonates (-8‰), with some variations depending on local depositional conditions (Veizer and Hoefs, 1976; Burdett et al., 1990; Banner and Hanson, 1990; Kah, 2000; Frank and Lyons, 2000; Hoffman and Schrag, 2002; Kasemann et al., 2005). Furthermore, with the exception of three samples, most of our  $\delta^{18}\text{O}$  are below the typical cut-off (-11‰; Kaufman et al., 1993; Kaufman and Knoll, 1995) used to distinguish nearly pristine values, which would suggest that our samples were slightly altered, and thus their carbon isotope compositions would be reflecting original compositions (see below).

### $\delta^{13}\text{C}_{\text{carb}}$

Previous studies have shown that carbon isotope composition is less sensitive to diagenetic alteration than oxygen isotope or trace element (Mn, Sr) composition (Banner and Hanson, 1990; Kaufman et al., 1991; Banner and Kaufman, 1994). Hence, the potential effects of post-depositional process on the preservation of marine carbon isotope records can be evaluated by examining  $\delta^{18}\text{O}$  and trace element data. If sediments react with  $\delta^{13}\text{C}$ -depleted meteoric waters, which are characterized by negative  $\delta^{18}\text{O}$  values, they will acquire  $\delta^{13}\text{C}$ -depleted DIC from the oxidation of terrestrial organic carbon (Vogel, 1993). Likewise, alteration of carbonates by meteoric fluids can produce  $\delta^{13}\text{C}$ -depleted isotope ratios that co-vary with  $\delta^{18}\text{O}$  values (Veizer 1983; Derry et al. 1992; Marshall 1992; Knauth and Kennedy, 2009).  $\delta^{13}\text{C}_{\text{carb}}$  values from the Polanco samples vary between 6 and -3.4‰ (Avge: +1.9‰). The cross-plot of  $\delta^{18}\text{O}$  and the corresponding  $\delta^{13}\text{C}_{\text{carb}}$  (Figure 5.7A) shows that they do not co-vary. This suggests that while the  $\delta^{18}\text{O}$

in these rocks has certainly been overprinted, given fluid-rock exchange and high oxygen concentration of oxygen in water, post-depositional fluid flow did not reset the C-isotopic composition (Veizer, 1983; Marshall, 1992). Furthermore, in contrast to  $\delta^{18}\text{O}$ , explaining how exchange can reset  $\delta^{13}\text{C}_{\text{carb}}$  given the large mass of carbon in carbon sequences is difficult (Derry, 2010). The lack of correlation of  $\delta^{13}\text{C}_{\text{carb}}$  with Mn/Sr (Figure 5.7B) provides further evidence on the robustness of the C-isotope data.

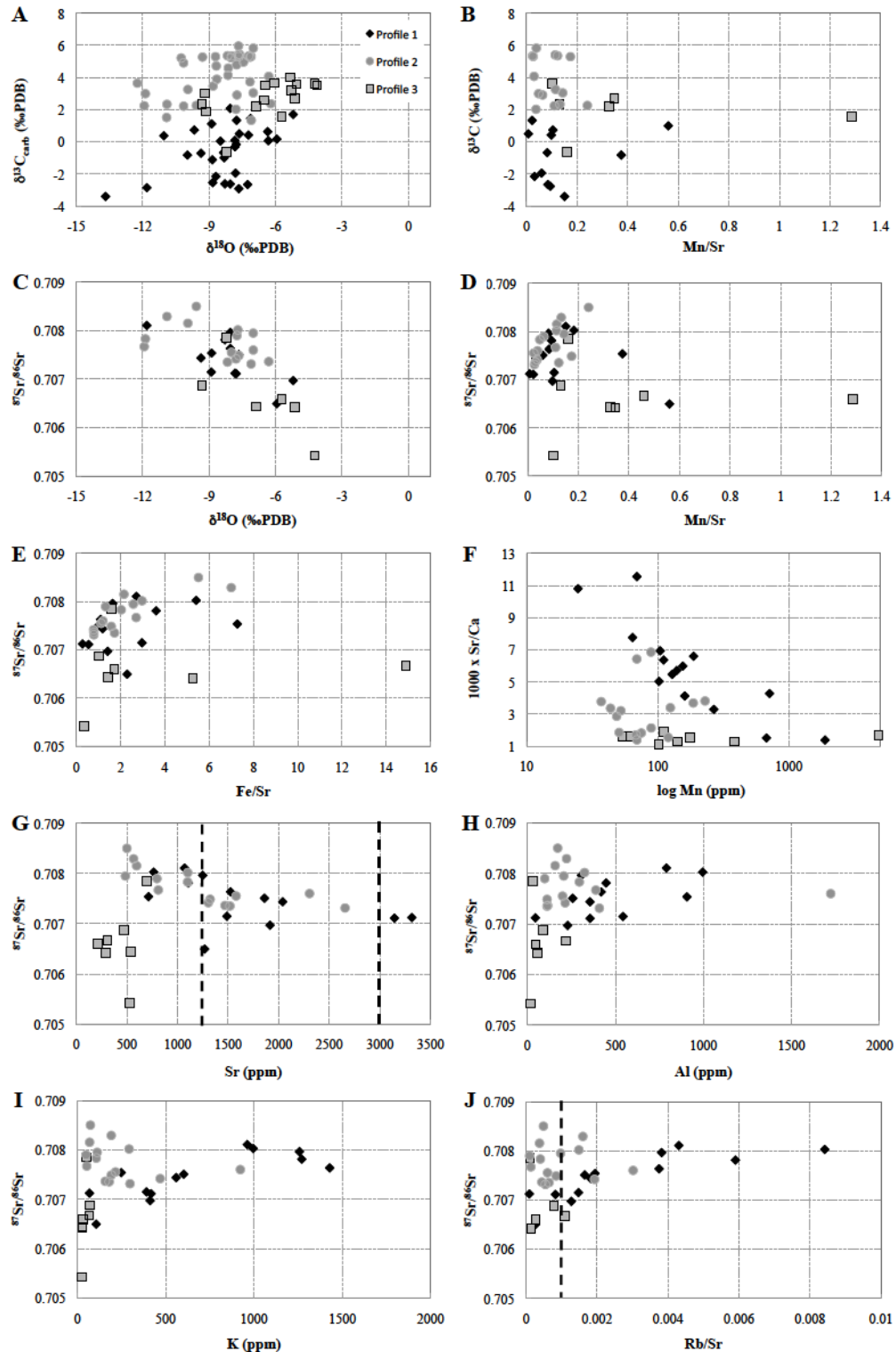


**Figure 5.7.** Scatter diagrams for profiles 1, 2 and 3. (A)  $\delta^{13}\text{C}_{\text{carb}}$  vs.  $\delta^{18}\text{O}$ . (B)  $\delta^{13}\text{C}_{\text{carb}}$  vs. Mn/Sr. (C)  $^{87}\text{Sr}/^{86}\text{Sr}$  vs.  $\delta^{18}\text{O}$ . (D)  $^{87}\text{Sr}/^{86}\text{Sr}$  vs. Mn/Sr. (E)  $^{87}\text{Sr}/^{86}\text{Sr}$  vs. Fe/Sr. (F) Sr/Ca vs. Mn. (G)  $^{87}\text{Sr}/^{86}\text{Sr}$  vs. [Sr]. (H)  $^{87}\text{Sr}/^{86}\text{Sr}$  vs. Al. (I)  $^{87}\text{Sr}/^{86}\text{Sr}$  vs. K. (J)  $^{87}\text{Sr}/^{86}\text{Sr}$  vs. Rb/Sr.

### $\delta^{13}\text{C}_{\text{org}}$

Isotope composition of organic matter may be modified during diagenesis either by bacterial degradation or thermal maturation. Early diagenetic degradation of organic matter can produce a decrease in  $\delta^{13}\text{C}_{\text{org}}$  values between 1 and 2‰ (McArthur et al., 1992; Lehmann et al., 2002; Galimov, 2004). The heavy  $\delta^{13}\text{C}_{\text{org}}$  signature shown by the Polanco carbonates (Avge: -15‰) is therefore very unlikely to have been produced solely by degradation processes. Thermal maturation is a recognized post-depositional process that can alter the  $\delta^{13}\text{C}$  of organic matter (Peters et al., 1981; Simoneit et al., 1981; Hayes et al., 1999). Mobilization of isotopically light organic compounds through thermal maturation results in maximum positive shifts of 2-3‰ (Simoneit et al., 1981; Schidlowski, 1987; Clayton, 1991; Hayes et al., 1999). Larger positive shifts can occur when temperature increases beyond 350°C due to C-isotope exchange with co-existing carbonates, producing C-isotope fractionation between carbonate and organic material ( $\Delta^{13}\text{C}$ ) of less than 10‰ (Schidlowski, 1987). Petrographic analysis of samples from all the three sections studied here shows no evidence indicating temperatures in excess of 300°C. Lower temperature processes are also an unlikely explanation for the small isotopic difference between  $\delta^{13}\text{C}_{\text{org}}$  and  $\delta^{13}\text{C}_{\text{carb}}$  in Polanco because they can only produce minor  $\delta^{13}\text{C}_{\text{org}}$  shifts (<3‰). Furthermore, the occasional preservation of light  $\delta^{13}\text{C}_{\text{org}}$  values (*ca.* -32‰) challenges a pervasive alteration of  $\delta^{13}\text{C}_{\text{org}}$  signatures due to burial or very low metamorphism because, in such scenario, we would expect a near homogenous reset of the  $\delta^{13}\text{C}_{\text{org}}$  values throughout the whole succession, offset by the fractionation imparted by the original signature. This implies that there is another factor that must be considered when explaining the heavy  $\delta^{13}\text{C}_{\text{org}}$  in these carbonates. Such alternative explanation might be provided by low concentrations of atmospheric  $p\text{CO}_2$  (see section 5.5.4 below).

### $^{87}\text{Sr}/^{86}\text{Sr}$

Our samples have Sr-isotope ratios between 0.705423 and 0.708500 (Avge: 0.706962 ± 0.0015385; Table 5.1). Specifically, samples from Profile 1 have a mean ratio of 0.707498 ± 0.000609, Profile 2: 0.707760 ± 0.000740 and Profile 3: 0.707848 ± 0.001239. As stated above, Sr is more prompt to alteration than C isotopes and several

criteria are used to assess the preservation of Sr-isotope ratios in Proterozoic carbonates (e.g., Asmerom et al., 1991; Kaufman et al., 1993; Kaufman and Knoll, 1995; Jacobsen and Kaufman, 1999; Fairchild et al., 2000; Melezhik et al., 2001; Thomas et al., 2004). For example, low  $\delta^{18}\text{O}_{\text{carb}}$  values and their correlation with  $^{87}\text{Sr}/^{86}\text{Sr}$  may indicate exchange with hydrothermal circulating fluids or groundwater more radiogenic than seawater (Derry et al., 1992). In this regard, samples that were measured for Sr-isotope have a limited range of  $\delta^{18}\text{O}$  values ranging from -4 to -12 but with the exception of profile 2 ( $r^2=0.2$ ),  $^{87}\text{Sr}/^{86}\text{Sr}$  values from profiles 1 ( $r^2=0.5$ ) and 3 ( $r^2=0.6$ ) display a moderate negative correlation with  $\delta^{18}\text{O}$  (Figure 5.7C) suggesting post-depositional overprint.

Similar to  $\delta^{13}\text{C}_{\text{carb}}$ , other sensitive indicators of alteration of Sr isotopic values include Mn/Sr and Fe/Sr. The Mn/Sr ratio has proven to be especially useful because Mn (and Fe) generally increases during marine and meteoric diagenesis, and metamorphism and Sr is expelled from carbonates (Brand and Veizer, 1980; Veizer 1983; Derry et al., 1992; Tucker and Wright, 1990; Jacobsen and Kaufman, 1999; Lindsay and Brasier, 2000; Kah, 2000). The maximum Mn/Sr ratio of apparently unaltered samples ranges from 1 to 3 (Derry et al., 1992; 1994; Kaufman et al., 1993; Kaufman and Knoll 1995; Brasier et al., 1996; Montanez et al., 1996; Kennedy et al., 1998; Jacobsen and Kaufman, 1999). Our samples have  $\text{Mn}/\text{Sr}<0.6$  (except one sample) and  $\text{Fe}/\text{Sr}<8$  (except one sample), which conforms with previous inferences of minimal post-depositional alteration. Furthermore, there is no correlation between these ratios and  $^{87}\text{Sr}/^{86}\text{Sr}$  (Figure 5.7D-E).

When plotting Sr/Ca vs. Mn (Figure 5.7F) only Profile 1 shows a moderate negative correlation ( $r^2=0.5$ ). Although high Mn concentrations have been reported in other carbonates that were interpreted as deposited in anoxic or suboxic environments (Shen et al., 2005; Font et al., 2006; Hurtgen et al., 2006; Nédélec et al., 2007; Feng et al., 2010) a drop in the Sr/Ca accompanied by increases in Mn is likely the result of interaction with fresh meteoric waters (Kah, 2000). Even if the three samples containing the highest Mn values (1,000-1,800 ppm) are removed the average concentration is 207 ppm, which is similar to other well-preserved Neoproterozoic carbonates deposited under

oxic conditions (Yoshioka et al., 2003; Frimmel, 2009; Zhao et al., 2009). Therefore, Sr/Ca vs. Mn reveals some alteration in Profile 1.

Although low Sr values are not *a priori* evidence of change in  $^{87}\text{Sr}/^{86}\text{Sr}$  ratio, the Sr content of samples and its correlation with  $^{87}\text{Sr}/^{86}\text{Sr}$  has been also used as an indicator of alteration. Strontium concentrations in carbonate rocks of the Polanco Limestones Formation are typically >500 ppm, however, most of the samples have concentrations >1000 ppm and as high as 3,300 ppm. These elevated Sr strontium content suggests retention of Sr from an original aragonite precursor, with only a minor degree of post-depositional recrystallization. The lowest-Sr values are recorded in profile 3 and can be related to either post-depositional alteration or to an initially low-Sr calcite precursor. As stated above, samples from this profile show a moderate negative correlation between  $^{87}\text{Sr}/^{86}\text{Sr}$  and  $\delta^{18}\text{O}$  ( $r^2=0.6$ ) yet they display the lowest  $^{87}\text{Sr}/^{86}\text{Sr}$  ratios and the highest  $\delta^{18}\text{O}$  values (Table 5.1 and Figure 5.7C), which -at first glance- contradict the idea of post-depositional alteration. Usually post-depositional alteration produces high  $^{87}\text{Sr}/^{86}\text{Sr}$  ratios and low  $\delta^{18}\text{O}$  values, however post-depositional fluids are not always more radiogenic than coeval seawater (Banner and Hanson, 1990; Halverson and Shields, 2012). Furthermore, samples from profile 3 (and one sample from profile 1) do not fit in the coherent diagenetic trajectory defined by profiles 1 and 2 in the  $^{87}\text{Sr}/^{86}\text{Sr}$  vs. [Sr] plot (Figure 5.7G), and thus further supports the interaction with non-radiogenic fluids after deposition that overprinted the original  $^{87}\text{Sr}/^{86}\text{Sr}$ .

Elevated  $^{87}\text{Sr}/^{86}\text{Sr}$  ratios may also result through interaction with detrital silicate particles (Derry et al., 1992). Detrital materials, particularly clay minerals and feldspars can release or exchange Sr with high  $^{87}\text{Sr}/^{86}\text{Sr}$  during mineral recrystallisation due to the decay of  $^{87}\text{Rb}$  to  $^{87}\text{Sr}$  and increase the Sr-isotope ratios in carbonate minerals (Jenkin et al., 2001). Because clays and feldspars also have high Al, K, and Rb contents, by plotting their respective concentrations against  $^{87}\text{Sr}/^{86}\text{Sr}$  ratios we can estimate the influence of detrital components. Samples from Profile 1 show a moderate positive correlation with Al ( $r^2=0.4$ ), K ( $r^2=0.6$ ) and Rb/Sr ( $r^2=0.65$ ) (Figure 5.7H-J), suggesting that detrital contamination is significant in these samples. Conversely, profiles 2 and 3 show no correlation between  $^{87}\text{Sr}/^{86}\text{Sr}$  ratios and Al, K and Rb contents, indicating minimal, if any, influence of clay minerals and feldspar on the  $^{87}\text{Sr}/^{86}\text{Sr}$  ratios (Figure 5.7I-K).

Additionally, a threshold of  $Rb/Sr < 0.001-0.01$  has been suggested to diagnose unaltered and detritus-free samples (Derry et al., 1989; Asmerom et al., 1991; Kaufman et al., 1993). In this sense, the majority of the samples from Profile 1 show the highest  $Rb/Sr$  ratios (0.001-0.01), whereas most of the samples from Profiles 2 and 3 have very low  $Rb/Sr$  ( $< 0.001$ ) (Figure 5.7J). Accordingly, this further supports that detrital components could influence the  $^{87}Sr/^{86}Sr$  ratios of carbonates only in Profile 1.

Consequently, after evaluating the relationship between different alteration indexes and  $^{87}Sr/^{86}Sr$  ratios in our samples we do not consider for our analysis samples from profile 3 and only selected limestones showing the highest Sr concentrations ( $> 2,000$  ppm) and displaying the lowest  $^{87}Sr/^{86}Sr$  ratios ( $< 0.707313$ ) as the least altered samples in profiles 1 and 2. This conservative criterion is the same as in previous works (e.g., Halverson et al., 2007) and tends to minimize radiogenic overprints resulting in imprecise correlations. This implies Sr isotope ratios between 0.707112 and 0.707122 (Avge:  $0.707117 \pm 0.000005$ ) for profile 1 and 0.707313 for profile 2. Likewise, this would imply a primary variation in  $^{87}Sr/^{86}Sr$  by 0.00001 in profiles 1 and a total variation over the whole Polanco section of 0.000201. Because their similar and highest Sr concentrations and lowest  $^{87}Sr/^{86}Sr$  ratios, the two samples from profile 1 are regarded here as the most faithful proxies for original seawater composition.

### 5.5.2. $\delta^{13}C_{carb}$ record of the Polanco Limestones Formation

Classically,  $\delta^{13}C_{carb}$  is interpreted as reflecting the relative fraction of carbon buried as organic matter in marine sediments (Knoll et al., 1986; Des Marais et al., 1992; Kaufman et al., 1997). Positive excursions may be generated by high productivity rates due to higher nutrient influx to the surface ocean or, alternatively, because of an increase in the burial efficiency of organic matter (eg., Bekker and Holland, 2012). In contrast, negative excursions result from either a decrease in primary productivity and/or lower burial efficiency of organic matter in sediments (Kump and Arthur, 1999). In either case, when a change in the isotopic composition of marine dissolved inorganic carbon (DIC) accounts for these excursions, it is expected that the  $\delta^{13}C_{carb}$  record will covary with that of  $\delta^{13}C_{org}$ , offset by the fractionation conveyed by primary production (-20 to -30‰; Hayes et al., 1999). Several carbon isotope excursions recorded in the Neoproterozoic,

however, show no covariance, which suggests that other mechanisms are responsible for these excursions. In this regard, it has been suggested that significant negative  $\delta^{13}\text{C}_{\text{carb}}$  excursions are the result of input and oxidation of massive amounts of  $^{13}\text{C}$ -depleted carbon from sedimentary methane clathrates (Jiang et al., 2003; Bjerrum and Canfield, 2011), labile organic matter (Kaufman et al., 2007), or dissolved organic carbon (Rothman et al., 2003). Based on previously reported  $\delta^{13}\text{C}_{\text{carb}}$  data for the Polanco Limestones Formation, Aubet et al. (2012) suggested that while the basin was demonstratively stratified, as shown by the  $\delta^{13}\text{C}_{\text{carb}}$  gradient between shallow-water and deep-water facies, oxidation of a dissolved organic carbon pool (DOC) pool was not the cause of the negative shift reported in shallower facies.

The occurrence of negative carbon isotope excursions in relatively shallow-water settings as a result of the oxidation of a DOC pool requires the development of a strongly stratified water column and predicts a  $^{13}\text{C}$ -enrichment in carbonates due to high biological productivity in shallow-marine environments and a  $^{13}\text{C}$ -depletion in deep waters by remineralization of photosynthetically produced dissolved organic matter (Knoll et al., 1996; Calver, 2000). Remineralization occurs via a variety of heterotrophic metabolisms, including but not limited to, sulfate reduction and methanogenesis. As a consequence of ocean overturn, large volumes of  $^{13}\text{C}$ -depleted deep-waters are therefore transferred to shallow-water setting generating large negative shifts in  $\delta^{13}\text{C}_{\text{carb}}$  (Rothman et al., 2003). This model has been particularly applied to the Ediacaran Shuram/Wonoka anomaly (~551 Ma) characterized and distinguished from other Neoproterozoic anomalies due to its amplitude ( $\delta^{13}\text{C}_{\text{carb}} < 10\text{‰}$ ) and persistence for several hundred of meters (~700 m) (Le Guerroué et al., 2006; Halverson et al., 2010a,b). Though the origin of this anomaly is still a matter of debate (e.g., Derry, 2010), Aubet et al. (2012) suggested that all these characteristics (i.e., age, amplitude, persistence) are inconsistent with the features shown by the Polanco Limestones Formation. Furthermore, the absence of large DOC pool or its oxidation is readily noticeable when  $\delta^{13}\text{C}_{\text{carb}}$  values of deep-water carbonates are considered (Aubet et al., 2012, their Fig. 6). When compared to values that define the largest negative shallow-water excursion (-3.4‰; Figure 5.3), the deep-water carbonates show even less negative ( $> -3\text{‰}$ ) values, which contrasts with models requiring a large DOC pool. The same holds true if the anaerobic oxidation of

methane, with a  $\delta^{13}\text{C}$  composition between -60 and -90‰ (Kvenvolden, 1995), as a possible source of  $^{12}\text{C}$ -enriched alkalinity is considered. Furthermore, the Polanco carbonates show no evidence of being related to a methane seep environment. In spite of this, stratification of the water column during the deposition of the lower part of the Arroyo del Soldado Group (Yerbal and Polanco Limestones formations) has been previously suggested (Pecoits et al., 2008; Pecoits, 2010; Aubet et al., 2012), which would explain the difference between the positive and slightly negative carbon isotope values of carbonates in shallow and deep water sections, respectively. In modern oceans, DIC of surface waters is enriched in  $\delta^{13}\text{C}$  up to 3‰ relative to deeper waters by the ‘biological pump effect’; i.e., fixation of carbon in the photic zone and delivery of dead organic matter into deeper waters where it is remineralized (Kroopnick, 1985; Berger and Vincent, 1986). In poorly mixed basins, the difference in  $\delta^{13}\text{C}_{\text{DIC}}$  between surface and bottom waters can be even greater (e.g., 7‰ in the Black Sea; Deuser, 1970). The apparent depth gradient in  $\delta^{13}\text{C}_{\text{DIC}}$  between the shallow- and deeper-water carbonates in the Polanco basin is inferred to have been ca. 2-7‰, and therefore comparable to the gradient in modern oceans ( $\leq 3\%$ ) and in stratified basins ( $\leq 7\%$ ).

Negative  $\delta^{13}\text{C}_{\text{carb}}$  excursions may also indicate a decrease in its burial rate, which is either related to low sedimentation or productivity rates (Kump and Arthur, 1999). Low sedimentation rates prevent  $\text{C}_{\text{org}}$  preservation by rapidly burying organic matter below the oxic zone within the sediments. Low productivity, likely induced by low nutrient supply, decreases the flux of organic carbon to the sediments (Derry et al., 1992). Because of the dependence of  $^{87}\text{Sr}/^{86}\text{Sr}$  ratios on the overall erosion rate, the relationship between the Sr record and the isotopic difference between contemporaneous marine carbonate and organic carbon can shed some light on the reasons behind the  $\delta^{13}\text{C}_{\text{carb}}$  fluctuations in the Polanco Limestones Formation. Particularly, the study of the carbon isotopic difference between  $\delta^{13}\text{C}_{\text{carb}}$  and  $\delta^{13}\text{C}_{\text{org}}$  ( $\Delta^{13}\text{C}$ ) can provide important clues on the rates of organic carbon burial and on the concentration of dissolved  $\text{CO}_2$  in the ocean ( $[\text{CO}_2]_{\text{aq}}$ ), which can be related to atmospheric  $p\text{CO}_2$  (Freeman and Hayes, 1992; Hayes et al., 1999; Kump and Arthur, 1999).

### 5.5.3. Fractionation between inorganic and organic carbon

At first glance, a significant stratigraphic variation is observed in the fractionation between inorganic and organic carbon of the Polanco carbonates, ranging from 10 to 35‰ (Figure 5.3). Such fractionation is largely controlled by variations in the  $\delta^{13}\text{C}_{\text{org}}$  record, which displays values between -33 and -7.5‰. If the few samples (five) showing the largest fractionation are removed, then  $\Delta^{13}\text{C}$  values vary from 10 to 24‰ with an average of 15.5‰). Usually, it is assumed that decreasing  $\Delta^{13}\text{C}$  values are a consequence of increasing  $\delta^{13}\text{C}_{\text{org}}$  high productivity rates is the most likely scenario, while the opposite (i.e., decreasing  $\Delta^{13}\text{C}$  not accompanied by increasing  $\delta^{13}\text{C}_{\text{org}}$ ) holds true for low productivity rates and is better explained by higher  $p\text{CO}_2$  (Hayes, 1993). However,  $\Delta^{13}\text{C}$  values can differ from the primary photosynthetic isotope effect ( $\epsilon_p$ ). During photosynthesis, biological fractionation due to enzymatic discrimination against  $^{13}\text{C}$  produces a  $^{13}\text{C}$ -depleted organic carbon relative to the carbon source (Hayes et al., 1999). This fractionation is carried out by RUBISCO (ribulose-1.5 biphosphate carboxylase-oxygenase), which under non- $\text{CO}_2$ -limiting conditions results in a range of  $\delta^{13}\text{C}$  approximately between -29‰ and -21‰ (Lewis et al., 2000). In this regard, several studies have shown that a number of environmental factors (mainly during  $\text{CO}_2$ -limited conditions) affect the isotopic fractionation in different and even within the same species (Rau et al., 1996; Burkhardt et al., 1999; Boller et al., 2011). Additionally, there are a number of factors that contribute to  $\Delta^{13}\text{C}$ , including: 1) diagenesis and metamorphism (e.g., due to thermal maturation; see section 5.5.1 above), 2) organic matter source variation and secondary biological fractionation (i.e., heterotrophy), and 3) the temperature dependent fractionation between DIC and  $\text{CO}_2$  in seawater (Hayes et al., 1999; Kienast et al., 2001).

Previous studies have shown that the sedimentary organic carbon present in carbonate rocks is not always derived from syngenetic sources. Recently, Lee et al. (2013) suggested that the organic matter composition and source inputs vary stratigraphically, reflecting biological community shifts (i.e., mixing of distinct syngenetic sources) in the Ediacaran Shuram Formation, which permits to explain the lack of covariance between  $\delta^{13}\text{C}_{\text{org}}$  and  $\delta^{13}\text{C}_{\text{carb}}$ . Similarly, Johnston et al. (2012) suggested admixtures of terrigenous or migrated organic carbon to explain the lack of

covariance in the C-isotope record of the Cryogenian Trezona anomaly in Namibia. Although these studies have been particularly important to unravel the unusual conditions that caused the two largest  $\delta^{13}\text{C}$  shifts in Earth history (Shuram and Trezona anomalies), and whose origin and timing are highly controversial (e.g., Derry, 2010; Swart and Kennedy, 2012), potential inputs from weathering of fossil detrital carbon sources or migrated non-syngenetic organic matter cannot be ruled out in the Polanco Limestones Formation.

In contrast to the carbon isotope fractionations produced by heterotrophs and temperature, the fractionation associated with photosynthetic production ( $\epsilon_p$ ) of organic matter can be large (from 8 to 18‰; Francois et al., 1993; Bidigare et al., 1997), and thus deserves consideration. Studies on modern marine phytoplankton have shown that  $\epsilon_p$  decreases as growth rates (ratio of cell volume to surface area) increase, or as  $[\text{CO}_2]_{(\text{aq})}$  concentrations decrease (Freeman and Hayes, 1992; Francois et al., 1993; Laws et al., 1995; Bidigare et al., 1997; Popp et al., 1998; Hayes et al., 1999). In the Polanco carbonates, small-scale (few meters) decreasing  $\Delta^{13}\text{C}$  trends are accompanied by increasing  $\delta^{13}\text{C}_{\text{org}}$ . These trends suggest productivity-driven changes during photoautotrophic carbon fixation. As depicted in Figure 5.7, with very few exceptions these positive  $\delta^{13}\text{C}_{\text{org}}$  shifts are associated with positive  $\delta^{13}\text{C}_{\text{carb}}$  excursions and with high nutrient (P) concentrations. The opposite is true for decreasing trends in  $\Delta^{13}\text{C}$  associated with light  $\delta^{13}\text{C}_{\text{org}}$  and  $\delta^{13}\text{C}_{\text{carb}}$  values. Nutrient input may have been driven by the upwelling of nutrient-rich waters or influx from continents. Consistent with the latter are the frequent accompanying increases in Al and Zr concentrations as well as in  $^{87}\text{Sr}/^{86}\text{Sr}$  ratios, which contradict the upwelling source advanced by Frei et al. (2011). The correlation between high nutrient concentrations and low  $\epsilon_p$  values has been linked to high phytoplankton growth rates (Bidigare et al., 1997), and therefore it provides a

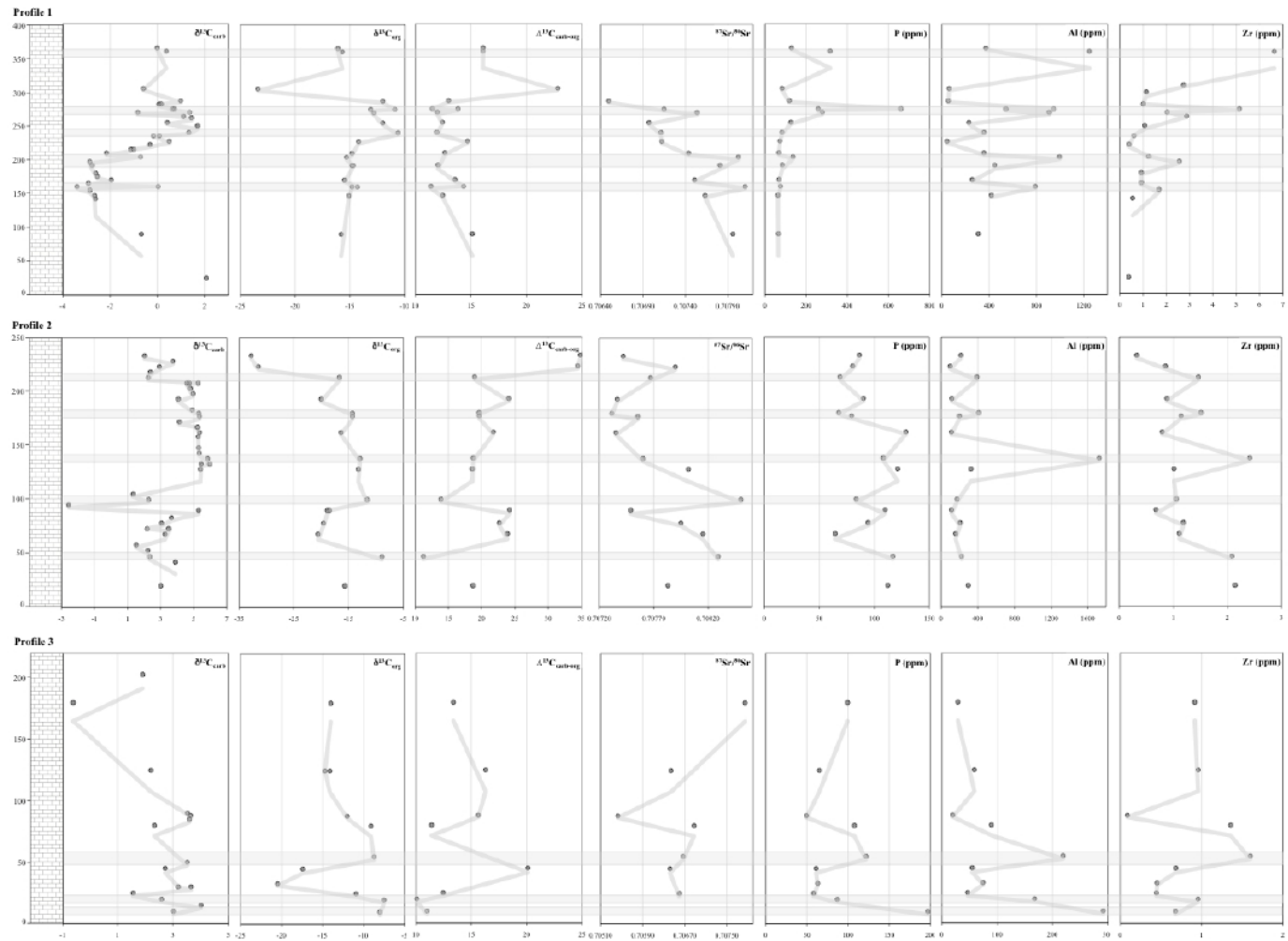


**Figure 5.8.** Profiles of the Polanco Limestones Formation at the Recalde Syncline area with corresponding vertical variations in  $\delta^{13}\text{C}_{\text{carb}}$ ,  $\delta^{13}\text{C}_{\text{org}}$ ,  $\Delta^{13}\text{C}$ ,  $^{87}\text{Sr}/^{86}\text{Sr}$ , P, Al and Zr. Dashed gray areas indicate periods of higher bioproductivity (see text for explanation). Vertical scale in meters.

reasonable explanation for the simultaneous heavy  $\delta^{13}\text{C}_{\text{org}}$  values and high P concentrations found in the Polanco carbonates.

These small-scale fluctuations are superimposed on large-scale variations, which are unrelated to variations in nutrients or lithophile elements. In fact, the  $^{87}\text{Sr}/^{86}\text{Sr}$  ratios drop up-section thereby precluding enhanced burial of organic matter burial as responsible for the positive shifts in  $\delta^{13}\text{C}_{\text{carb}}$ . The larger scale fluctuations are particularly clear in profiles 1 and 2, both of which show an important shift in  $\delta^{13}\text{C}_{\text{carb}}$  records (Figure 5.8). In profile 1, the negative and positive  $\delta^{13}\text{C}_{\text{carb}}$  excursions and the corresponding transition are characterized by a drop in  $\delta^{13}\text{C}_{\text{org}}$  and a rather invariant  $\Delta^{13}\text{C}$  (from 11.4 to 15‰). In profile 2, the most negative  $\delta^{13}\text{C}_{\text{carb}}$  values (< 90m) are accompanied by an increase in  $\Delta^{13}\text{C}$  and an overall decrease in  $\delta^{13}\text{C}_{\text{org}}$ . Up section, between 128 and 208m the slight decrease in consistently positive  $\delta^{13}\text{C}_{\text{carb}}$  values from +5.4 to +4.8‰ is accompanied by increasing  $\Delta^{13}\text{C}$  and decreasing  $\delta^{13}\text{C}_{\text{org}}$ . Therefore, the rather invariant  $\Delta^{13}\text{C}$  in profile 1 suggests a change in the  $[\text{CO}_2]_{\text{aq}}$  while the increasing  $\Delta^{13}\text{C}$  and decreasing  $\delta^{13}\text{C}_{\text{org}}$  indicate a drop in productivity with time for profile 2. In this context, these two sections likely derive from different portions of the basin wherein profile 1 would represent the shallower portion that was more susceptible to changes in  $[\text{CO}_2]_{\text{aq}}$  while signals in section 2 are attenuated by other processes operating in the water column.

Apart from the C-fractionation changes referred above, the consistently low C fractionation throughout the unit is remarkable. Isotopic differences between carbonates and organic carbon are often set between 25 and 30‰ and assumed to be constant. In fact, typical average marine values during the last 800 Ma for  $\Delta^{13}\text{C}$  are in the range of 28-32‰ (Hayes et al., 1999), except for short periods of lower  $\Delta^{13}\text{C}$  such as those in the upper Ordovician and Permo-Triassic boundary linked to a drop in global atmospheric  $p\text{CO}_2$  (Riccardi et al, 2007; Young et al., 2008). The carbon isotope fractionation between organic matter and contemporaneous carbonates depends strongly on the concentration of dissolved  $\text{CO}_2$  in the ocean  $[\text{CO}_2]_{\text{aq}}$ , which can be related to atmospheric  $p\text{CO}_2$  (Kaufman and Xiao, 2003). As stated above,  $\Delta^{13}\text{C}$  values from Polanco show a range largely between 10 and 24‰, with an average value of 15.5‰. Even if we take the best preserved samples (i.e.,  $^{87}\text{Sr}/^{86}\text{Sr} = 0.7071$  and  $[\text{Sr}] > 3,000$  ppm) the  $\Delta^{13}\text{C}$  varies between

12 and 15%. Therefore, assuming no significant postdepositional alteration of the C-isotope signatures (see section 5.1), low  $\epsilon_p$  values in the Polanco carbonates are consistent with a low  $[\text{CO}_2]_{(\text{aq})}$  during their deposition.

#### ***5.5.4. Implications for atmospheric $p\text{CO}_2$***

Three main facies associations were recognized in the Polanco Limestones Formation and interpreted to represent: inner, mid and outer ramp settings (Aubert et al., 2012). The same authors suggested that the scarcity of gravity-induced deposits related to platform margin, the absence of barred restricted marine conditions (e.g., absence of platform-margin buildups), and the gradual transitions between facies suggest deposition on a homoclinal ramp (Read, 1985; Burchette and Wright, 1992). The lack of stromatolites, oolites and distinctive evaporitic textures point to biogenic whitening precipitation as the main mechanism responsible for the formation of these carbonates. According to Riding (2006), the formation of carbonate mud and calcified cyanobacteria was controlled by  $p\text{CO}_2$ , wherein low  $\text{CO}_2$  concentrations led to widespread biogenic whittings caused by planktic cyanobacteria. The reasoning is that low  $\text{CO}_2$  would limit the supply of the DIC that the cyanobacteria require for photosynthesis, and so they would turn to another readily available dissolved source of inorganic carbon:  $\text{HCO}_3^-$ . Cyanobacterial cells pump in bicarbonate and convert it to  $\text{CO}_2$  inside the cell because the C-fixing enzyme RUBISCO only accepts  $\text{CO}_2$ .  $\text{CO}_2$  concentrating mechanisms (CCMs), therefore help to overcome RUBISCO's low affinity for  $\text{CO}_2$  and also depress its oxygenase activity by concentrating  $\text{CO}_2$  at the site of RUBISCO in the cell (e.g., Tortell et al., 2000; Omata et al., 2001; Miyachi et al., 2003; Ogawa and Kaplan, 2003). Cyanobacteria are not known to actively transport  $\text{CO}_2$  through the plasmamembrane, but they transport  $\text{HCO}_3^-$ , concentrating it within the cells at levels up to a thousand times higher than in the external medium (Giordano et al., 2005). Intracellular conversion of  $\text{HCO}_3^-$  to  $\text{CO}_2$  left  $\text{OH}^-$  (Bagder and Price, 2003), which the cells then pumped out, and these abundant hydroxyl ions increased the pH near the cells, triggering  $\text{CaCO}_3$  precipitation – thereby causing whittings. Therefore, biogenic whittings are expected to be especially common and intense at times of globally low  $\text{CO}_2$  levels (when DIC is limited; we refer the reader to Riding (2006) for a more detailed discussion).

The Neoproterozoic is characterized by recurrent glacial events, some of them being global (snowball glaciations), and low CO<sub>2</sub> levels that probably continued into the Ediacaran. In fact, CO<sub>2</sub> drawdown due to enhanced silicate weathering is among the factors inferred to have contributed to glacial events (Hoffman and Schrag, 2002). In contrast, in the Early Cambrian CO<sub>2</sub> levels start to rise quickly, most likely reducing whittings due to the lack of conditions for CCMs (Riding, 2006). In present day cyanobacteria, CCMs are induced when the atmospheric partial pressure of CO<sub>2</sub> falls below ~0.4% (10 PAL) (Badger et al., 2002). It is therefore likely that during the Proterozoic, so long as *p*CO<sub>2</sub> exceeded 10 PAL, cyanobacteria would not have possessed CCMs and would not have developed intense sheath calcification. According to Riding (2006), and consistent with empirical and modelled paleo-atmosphere estimates, crossing of this threshold is indicated in the fossil record by the appearance of calcified sheaths corresponding to *Girvanella* at 750-700 Ma, likely predating the Sturtian glaciation. Prior to Sturtian glaciation, weathering effects could have reduced CO<sub>2</sub> by 0.13% (Donnadieu et al., 2004) and simulations suggest that CO<sub>2</sub> levels may have fallen to 0.0859% (Ridgwell et al., 2003) or even ~0.013% (Hyde et al., 2000). Hence, coeval acquisition of CCMs by planktic cyanobacteria further stimulated whiting production. In contrast to relatively large calcified fossils that resulted from sheath calcification (*Girvanella*), CaCO<sub>3</sub> precipitates associated to planktic cyanobacteria (e.g., *Synechococcus*) are isolated crystals on or adjacent to the cells (Thompson, 2000). Unicellular planktic cyanobacteria are widespread in the open ocean and nearshore environments, forming blooms (Philips et al., 1999). These bloom-forming plankton benefit from efficient CCMs because DIC availability can limit photosynthesis under bloom conditions (Rost et al., 2003). According to Riding (2006), development of CCM was probably slowed by global cooling during glaciations, which in turn favoured diffusive entry of CO<sub>2</sub> into cells. Lower levels of temperature and DIC at this time would have reduced seawater carbonate saturation state, also hindering cyanobacterial calcification. However, during non-glacial periods (e.g., interglacial), global warming and O<sub>2</sub> rise reactivated the development of CCMs (Riding, 2006). In this regard, it was suggested that in a hard-snowball scenario subsequent rapid deglaciation resulted from the buildup of volcanic carbon dioxide during glaciation reaching partial pressures of atmospheric CO<sub>2</sub> from 50 to 250 times

higher than present-day levels (Hoffman and Schrag, 2002). These concentrations would inhibit CCMs, however, a recent study concluded low atmospheric  $p\text{CO}_2$  possibly as low as the current value even during deglaciation periods (Sansjofre et al., 2011).

Preliminary  $\delta^{15}\text{N}$  analyses of the Polanco carbonates suggests that cyanobacteria dominated during phytoplankton blooms. In this regard, the use of nitrogen isotope composition of organic matter is a useful tool to reveal the source from which organic carbon originated either from biological fixation, ammonium assimilation or nitrification, or nitrate denitrification (Cremonese et al., 2013). Polanco carbonates show  $\delta^{15}\text{N}$  values between -0.9 and 4.2 (Avge: +1.8‰). These values are within the range of atmospheric  $\text{N}_2$  fixation by green and purple sulfur photosynthetic bacteria (-4 to -1‰), cyanobacteria (-4 to -1‰) and by assimilation and denitrification in isotopic equilibrium (2 to 6‰) (Cremonese et al., 2013). Significantly, the lowest  $\delta^{15}\text{N}$  value is recorded in carbonates showing high nutrient concentrations and heavy  $\delta^{13}\text{C}_{\text{carb}}$  values, likely indicating  $\text{N}_2$  fixation dominated by cyanobacteria during phytoplankton blooms. In contrast, dolostones show the most positive  $\delta^{15}\text{N}$  value, which would suggest contributions from sulfur bacteria. Therefore, assuming that the overall small  $\epsilon_p$  values in the Polanco carbonates are the result of the  $\text{HCO}_3^-$  utilization by planktic cyanobacteria, the well known positive correlation between  $\epsilon_p$  and  $[1/\text{CO}_{2(\text{aq})}]$  implies that low  $\text{CO}_{2(\text{aq})}$  dominated during sedimentation. Because dissolved bicarbonate is isotopically enriched in  $^{13}\text{C}$  compared to  $\text{CO}_{2(\text{aq})}$  (~10‰ at 15°C; Mook et al., 1974), higher  $\delta^{13}\text{C}$  values of the organic matter would be expected in the case of  $\text{HCO}_3^-$  utilization (Benthien et al., 2002; Rost et al., 2003; Werne and Hollander, 2004). In this context, local changes in nutrient cycling and phytoplankton growth rates would have also imprinted their control on  $^{12}\text{C}$  fractionation.

##### ***5.5.5. Age of the Polanco Limestones Formation and correlation with other units***

Pb-Pb systematic on carbonate samples of the Polanco Limestones Formation yields an age of ca. 1,5 Ga (Figure 5.5). However, there are a number of arguments that would not support this age. Early Mesoproterozoic (>1.3 Ga) to Late Paleoproterozoic (<1.7 Ga) successions are characterized by exceptionally constant  $\delta^{13}\text{C}_{\text{carb}}$  values between -2 and +1‰, which led to this interval to be referred to the dullest time in Earth history (Buick et

al., 1995) and the ‘boring billion’ (Brasier and Lindsay, 1998). These surprisingly constant  $\delta^{13}\text{C}_{\text{carb}}$  values are recorded in sequences from northwestern Australia (Veizer et al., 1992; Buick et al., 1995; Brasier and Lindsay, 1998; Lindsay and Brasier, 2000), northwestern Siberia (Knoll et al., 1995; Bartley et al., 2007; Khabarov and Varaksina, 2011), Russia (Kah et al., 2007; Semikhatov et al., 2009), North America (Hall and Veizer, 1996; Frank et al. 1997; 2003), India (Ray et al., 2003), and North China (Xiao et al., 1997; Li et al., 2003; Chu et al., 2007; Guo et al., 2013; Luo et al., 2014). In contrast,  $\delta^{13}\text{C}_{\text{carb}}$  values from the Polanco samples vary between 6 and -3.4‰, and therefore difficult to explain if an Early Mesoproterozoic age is considered.

On the other hand, Sr isotopic studies on successions between 1.3 and 1.7 Ga yield  $^{87}\text{Sr}/^{86}\text{Sr}$  ratios between 0.70456 and 0.70494, which would suggest the prevalent impact of mantle flux at that time (Pokrovskii and Vinogradov, 1991; Gorokhov et al., 1995; Hall and Vizer, 1996; Ray et al., 2003; Kuznetsov et al., 2008; Semikhatov et al., 2009). Even the lowest  $^{87}\text{Sr}/^{86}\text{Sr}$  ratio (0.705423) of the Polanco Limestones Formation falls well outside of this range and it is more consistent with a Neoproterozoic age.

Significantly, one sample from the Yerbal Formation, which immediately underlies the carbonates of Polanco, showed a late Mesoproterozoic detrital zircon cluster (17%; n=5) between 1,010 and 1,065 Ma (Blanco et al., 2009), indicating that the Polanco Limestones Formation must be younger.

New radiometric and Sr-isotope data reported in this study support previous age estimates for the Polanco Limestones Formation. Based on radiometric grounds, Aubet et al. (2014) suggested that the deposition of the entire Arroyo del Soldado Group occurred between ~1,000 and 650 Ma (Aubet et al., 2014; Aubet et al., 2015). In agreement with these constraints, Polanco carbonates yield a U-Pb isochron age of  $752\pm 95$  Ma (Figure 5.4) and shales of the uppermost Yerbal Formation, which underlies Polanco, show the following K-Ar ages:  $637\pm 13$ ,  $575\pm 12$ , and  $514\pm 10$  Ma (Figure 5.5). While the latter is associated with a cooling event, the former two ages correspond to metamorphic and magmatic events recorded in the area. Significantly, the oldest age ( $637\pm 13$  Ma) constrain the minimum depositional age for the Polanco Limestones Formation. The U-Pb age obtained for the carbonates might imply deposition before the Sturtian glaciation (~715 Ma). In this regard, values as high as 0.7069 and 0.7070 have been found in

pristine carbonates of the Tonian Akademikerbreen Group (Svalvard; Halverson et al., 2007a). The lower Akademikerbreen Group has been correlated with the Little Dal Group (Canada) and Bitter Spring Formation (Australia) wherein all three units record a prominent negative  $\delta^{13}\text{C}_{\text{carb}}$  excursion at  $\sim 800$  Ma (Bitter Spring Stage; Hill et al., 2000; Halverson et al., 2007b). Although the correlation of this negative shift with that of the Polanco Limestones Formation cannot be completely ruled out there are a number of arguments that preclude this correlation. The three units, Akademikerbreen Group, Little Dal Group and Bitter Spring Formation show a very similar match of  $\delta^{13}\text{C}_{\text{carb}}$  within the Bitter Spring stage (Halverson et al., 2007a; b), while no similarities (persistence, amplitude, etc.) are observed when compared to the Polanco Limestones Formation. In spite of the relatively high  $^{87}\text{Sr}/^{86}\text{Sr}$  ratios mentioned above, this interval is characterized by a limited  $^{87}\text{Sr}/^{86}\text{Sr}$  variation from 0.70625 to 0.70660. Furthermore, these values are significantly lower than that commonly associated with the Sturtian glaciation ( $\sim 0.7068$ ; Halverson et al., 2010 and references therein), which likely suggest that Polanco carbonates are even younger than the glacial event. In fact, the best-preserved  $^{87}\text{Sr}/^{86}\text{Sr}$  ratios shown by the Polanco Limestones Formation (0.7071) are in better agreement with those reported for post-glacial limestones of the Cryogenian Period (Halverson et al., 2007; 2010); e.g., Mongolia from 0.7068 to 0.7071 (Shields et al., 1997), Namibia from 0.7068 to 0.7072 (Yoshioka et al., 2003; Halverson et al., 2007), NW Canada to 0.7071 (Kaufman et al., 1997), Australia to 0.7071 (McKirdy et al., 2001), and Scotland to 0.7071 (Thomas et al., 2004). This non-glacial interval ('Late Cryogenian Warm Interval' of Shields et al. (2012)), is characterized by an overall progressive increase in  $\delta^{13}\text{C}_{\text{carb}}$  after the Sturtian ice age culminating in extremely high  $\delta^{13}\text{C}_{\text{carb}}$  values  $\sim 10\text{‰}$  in the upper part to decrease again to an extreme low ( $\sim 18\text{‰}$  negative shift) before the end-Cryogenian (Marinoan) glaciation. Below this large negative excursion, two negative  $\delta^{13}\text{C}_{\text{carb}}$  excursions have been observed at different localities (Halverson et al., 2005; Macdonald et al., 2009a; 2009b).

One of these negative shifts in  $\delta^{13}\text{C}_{\text{carb}}$  is the Trezona anomaly, which after dropping to values of  $-10\text{‰}$  gradually recovers towards positive values before the overlying glacial deposits (McKirdy et al., 2001). This excursion is thought to represent a global signal as it is recorded in carbonate successions on five continents and always

occurs stratigraphically above the +5/+8‰ plateau and below the Marinoan glacial deposits (Narbonne et al., 1994; Kaufman et al., 1997; McKirdy et al., 2001; Hoffman et al., 2002; Xiao et al., 2004; Halverson et al., 2005; Miller, 2008; Rose et al., 2013). The other negative shift in  $\delta^{13}\text{C}_{\text{carb}}$  values is the more recently defined Tayshir anomaly (Macdonald et al., 2009). Although the Tayshir anomaly records a quite prominent negative excursion (-16‰) it has been tentatively correlated with the negative excursion (>-2‰) recorded in the Gruis Formation (Otavi Group) in Namibia, which unfortunately is not observed in the clastic successions of the Cryogenian strata of Canada and Australia (Halverson et al., 2005; Macdonald et al., 2009). Because of the features shown by negative  $\delta^{13}\text{C}_{\text{carb}}$  shift and the generally highly  $^{13}\text{C}$ -enriched carbonates in the Polanco Limestones Formation the correlation with the Gruis excursion is preferred here. This correlation is further supported by similar  $^{87}\text{Sr}/^{86}\text{Sr}$  ratios. As stated above, the best-preserved  $^{87}\text{Sr}/^{86}\text{Sr}$  ratio shown by the Polanco Limestones Formation is 0.7071 while the ratios reported from the Otavi Group between the correlative Sturtian and Marinoan glacial deposits range from 0.7068 and 0.7075 (Halverson et al., 2005).

Based on constraints from the older and younger glacial events, the Gruis excursion is estimated to have occurred between 670 and 660 Ma (Halverson et al., 2005; Macdonald et al., 2009), however, the Cryogenian interglacial period has been shown to be difficult to calibrate. Age constraint suggest that this interval, particularly well expressed in Australia, last about 10 Ma, from 660 to 650 Ma (Zhou et al., 2004; Fanning and Link, 2008). However, recent studies pointed that this interval could start as early as 645 Ma (Kendall et al., 2006; 2009) or at  $680\pm 23$  Ma (Mahan et al., 2010). In a broader view, age constraint for the Sturtian glaciation, at the end of which the interglacial period begun, vary widely, which led to some authors to propose that this glaciation comprised several globally diachronous events or that it was somewhat prolonged. Synglacial ages include the 716.5 Ma for the Rapitan Formation in NW Canada (Macdonald et al., 2010),  $711\pm 4$  Ma age for the Scout Mountain diamictite member of the Pocatello Formation in USA (Fanning and Link, 2004), the  $725\pm 10$  Ma for the Bayisi diamictite in China (Xu et al., 2009), and the  $714\pm 1$  Ma for the Ghubrah Formation of Oman (Bowring et al., 2007; Allen, 2007). With regards to basal post-glacial strata, the reported ages are significantly younger,  $662.4\pm 4$  Ma in Canada (Rooney et al., 2014),  $662.9\pm 4$  Ma in China (Zhou et al.,

2004), 667±5 Ma in USA (Fanning and Link, 2004), and 680±23 Ma in Australia (Mahan et al., 2010). An ash within the Marinoan glacial deposit in Namibia yielded an age of 635.5±0.6 Ma (Hoffmann et al., 2004), while an ash within the Marinoan cap carbonate in South China was dated at 635.2±0.6 Ma (Condon et al., 2005). Therefore, considering the available radiometric and  $^{87}\text{Sr}/^{86}\text{Sr}$  data for the Cryogenian interglacial period and the new data presented herein we suggest that the Polanco Limestones Formation was likely deposited between ~680 and 650 Ma. However, further geochronological work is needed to establish the age of the unit more precisely.

## 5.6. Conclusions

The paired  $\delta^{13}\text{C}_{\text{org}}$  and  $\delta^{13}\text{C}_{\text{carb}}$  trends from the Polanco Limestones Formation of Uruguay record variations in nutrient input from continental runoff and in  $[\text{CO}_2]_{\text{aq}}$  possibly linked to changes in atmospheric  $\text{CO}_2$  levels during the Cryogenian interglacial period. The precipitation of carbonates via biogenic whittings along with the low  $\Delta^{13}\text{C}$  values throughout the entire succession suggests low  $p\text{CO}_2$ .

The interpreted local rises in marine phytoplankton growth rates are coincident with evidence for changes in nutrient input (P), lithophile elements and  $^{87}\text{Sr}/^{86}\text{Sr}$  ratios. These changes are consistent with the notion that enhanced weathering and consequent high nutrient input to the oceans stimulating biological productivity and accelerating carbon flux to the basin floor. These short-lived periods are superimposed on larger-scale fluctuations interpreted in terms of changing  $[\text{CO}_2]_{\text{aq}}$ , and thereby in global  $p\text{CO}_2$ . Additionally, the consistently small  $\Delta^{13}\text{C}$  (Avg: 15.5 ‰) values suggest low atmospheric  $p\text{CO}_2$ , which is further supported by the  $\text{HCO}_3^-$  utilization by planktic cyanobacteria and subsequent precipitation of biogenic whittings.

New U-Pb radiometric data from the Polanco carbonates and reinterpretation of previously reported K-Ar ages on illite yield ages of 752±95 and 637±13 for the diagenesis and peak metamorphic event, respectively. These ages are within previous estimates for the deposition of the unit between ~1,000 and 650 Ma. Based on  $^{87}\text{Sr}/^{86}\text{Sr}$  ratios reported for the Neoproterozoic, the values shown by the Polanco Limestones Formation are in agreement with those reported for other interglacial limestones of the

Cryogenian Period. A preliminary correlation with the negative  $\delta^{13}\text{C}_{\text{carb}}$  excursion recorded in the Gruis Formation (Otavi Group) in Namibia is proposed here.

## 5.7. References

Asmerom, Y., Jacobsen, S. B., Knoll, A. H., Butterfield, N. J., Swett, K., 1991. Strontium isotopic variations of Neoproterozoic seawater: implication for crustal evolution. *Geochim. Cosmochim. Acta*, 5: 2883-2894.

Allen, P. A., 2007, The Huqf Supergroup of Oman: Basin development and context for Neoproterozoic glaciation. *Earth Science Reviews*, 84, 139-185.

Aubet, N.R., Pecoits, E., Bekker, A., Gingras, M., Zwingmann, H., Veroslavsky, G., de Santa Ana, H., Konhauser, K. 2012. Chemostratigraphic constraints on early Ediacaran carbonate ramp dynamics, Río de la Plata craton, Uruguay. *Gonwana Res.*22, 1073-1090.

Aubet, N.R., Pecoits, E., Heaman, I., Veroslavsky, G., Gingras, M., Konhauser, K. 2014. Ediacaran in Uruguay: Facts and controversies. *Journal of South American Earth Sciences* 55, 43-57.

Badger, M.R., Hanson, D.T., Price, G.D., 2002. Evolution and diversity of CO<sub>2</sub> concentrating mechanisms in cyanobacteria. *Functional Plant Biology* 29, 161-173.

Badger, M.R., Price, G.D., 2003. CO<sub>2</sub> concentrating mechanisms in cyanobacteria: molecular components, their diversity and evolution. *J. Exp. Bot.* 54, 609-622.

Banner, J. L. and Kaufman, J., 1994, The isotopic record of ocean chemistry and diagenesis preserved in nonluminescent brachiopods from Mississippian carbonate rocks, Illinois and Missouri. *Geological Society of America Bulletin* 106, 1074-1082.

Banner, J.L., Hanson, G.N., 1990. Calculation of simultaneous isotopic and trace element variations during water-rock interaction with application to carbonate diagenesis. *Geochim. Cosmochim. Acta* 54, 3123-3137.

Banner, J.L., Hanson, G.N., 1990. Calculation of simultaneous isotopic and trace element variations during water-rock interaction with applications to carbonate diagenesis: *Geochim. Cosmochim. Acta* 54, 3123-3137.

- Bartley, J.K., Kah, L.C., McWilliams, J.L., Stagner, A.F., 2007. Carbon isotope chemostratigraphy of the Middle Riphean type section (Avzyan Formation, Southern Urals, Russia): signal recovery in a fold-and-thrust belt. *Chem. Geol.* 237, 211-232.
- Bekker, A., Holland, H.D., 2012. Oxygen overshoot and recovery during the early Paleoproterozoic. *Earth Planet. Sci. Lett.* 317-318, 295-304.
- Benthien, A., Andersen, N., Schulte, S., Muller, P.J., Schneider, R.R., Wefer, G., 2002. Carbon isotopic composition of the C<sub>37:2</sub> alkenone in core top sediments of the South Atlantic Ocean: Effects of CO<sub>2</sub> and nutrient concentrations, *Global Biogeochem. Cycles*, 16, 1012.
- Berger, W.H., Vincent, E. 1986. Deep-sea carbonates: reading the carbon-isotope signal. *Geol Rundsch* 75: 249-269.
- Bian, L., Hinrichs, K.-U., Xie, T., Brassell, S.C., Iversen, N., Fossing, H., Jørgensen, B.B., Hayes, J.M., 2001. Algal and archaeal polyisoprenoids in a recent marine sediment: molecular isotopic evidence for anaerobic oxidation of methane. *Geochem. Geophys. Geosyst.* 2 Paper number 2000GC000112.
- Bidigare, R.R., Flügge, A., Freeman, K.H., Hanson, K.L., Hayes, J.M., Hollander, D., Jasper, J.P., King, L.L., Laws, E.A., Milder, J., Millero, F.J., Pancost, R., Popp, B.N., Steinberg, P.A., Wakeham, S.G., 1997. Consistent fractionation of <sup>13</sup>C in nature and in the laboratory: Growth-rate effects in some haptophyte algae. *Glob Biogeochem Cycl* 11, 279-292
- Bidigare, R.R., Prezelin, B.B., Smith, R.C., 1992. Biooptical models and the problems of scaling, p. 175-212. In: Eds Falkowski, P.G. Primary productivity and biogeochemical cycles in the sea. Plenum.
- Bjerrum, C.J, Canfield, D.E., 2011. Towards a quantitative understanding of the late Neoproterozoic carbon cycle. *Proceedings of the National Academy of Sciences of the United States of America* 108, 5542-5547.
- Boller A. J., Thomas P. J., Cavanaugh C. M., Scott K. M., 2011. Low stable carbon isotope fractionation by coccolithophore RubisCO. *Geochim. Cosmochim. Acta* 75, 7200-7207.

- Bowring, S., Grotzinger, J.P., Condon, D.J., Ramezani, J., Newall, M., Allen, P.A., 2007. Geochronologic constraints on the chronostratigraphic framework of the Neoproterozoic Huqf Supergroup, Sultanate of Oman. *American Journal of Science* 307, 1097-1145.
- Brand, U., Veizer, J. 1980. Chemical diagenesis of a multi component carbonate system: 1. Trace elements. *J. Sed. Petrol* 50, 1219-1236.
- Brasier, M.D., Shields, G., Kuleshov, V.N., Zhegallo, E.A., 1996. Integrated chemo- and biostratigraphic calibration of early animal evolution: Neoproterozoic to early Cambrian, southwest Mongolia. *Geological Magazine* 133, 445-485.
- Brasier, M.D., Lindsay, J.F., 1998. A billion years of environmental stability and the emergence of eukaryotes: new data from Northern Australia. *Geology* 26, 555-558.
- Budd, G. E. 2008. The earliest fossil record of the animals and its significance. *Philosophical Transactions of the Royal Society B*, 363, 1425-1434.
- Buick, R., Des Marais, D.J., Knoll, A.H., 1995. Stable isotopic compositions of carbonates from the Mesoproterozoic Bangemall group, northwestern Australia. *Chem Geol.* 123, 153-171.
- Burchette, T.P., Wright, V.P., 1992. Carbonate ramp depositional systems, *Sedimentary Geol.* 79, 3-57.
- Burdett, J.W., Grotzinger, J.P., Arthur, M.A. 1990. Did major changes in stable isotope compositions of seawater occur? *Geology* 18, 227-230.
- Calver, C., 2000. Isotope stratigraphy of the Ediacaran (Neoproterozoic III) of the Adelaide rift complex, Australia, and the overprint of water column stratification. *Precambrian Res.* 100, 121-150.
- Chu, X.L., Zhang, T.G., Zhang, Q.R., Lyons, T.W., 2007. Sulfur and carbon isotope records from 1700 to 800 Ma carbonates of the Jixian section, northern China: implications for secular isotope variations in Proterozoic seawater and relationships to global supercontinental events. *Geochim. Cosmochim. Acta* 71, 4668-4692.
- Clayton, C.J., 1991. Effect of maturity on carbon isotope ratios of oils and condensates. *Org. Geochem.* 17, 887-899.

Condon, D., Zhu, M., Bowring, S., Wang, W., 2005. U-Pb ages from the Neoproterozoic Doushantuo Formation, China. *Science* 308, 95-98.

Coplen, T.B., Brand, W.A., Gehre, M., Groning, M., Meijer, H.A.J., Toman, B., Verkouteren, R.M., 2006. New guidelines for delta C-13 measurements. *Anal. Chem.* 78, 2439–2441.

Cremonese, L., Shields-Zhou, G., Struck, U. Ling, H. F., Och, L., Chen, X., Li, D., 2013. Marine biogeochemical cycling during the early Cambrian constrained by a nitrogen and organic carbon isotope study of the Xiaotan section, south China. *Precambrian Res.* 225, 148-165.

Derry, L.A., 2010. A burial diagenesis origin for the Ediacaran Shuram-Wonoka carbon. *Earth Planet. Sci. Lett.* 294, 152-162.

Derry, L.A., Kaufman, A.J., Jacobsen, S.B., 1992. Sedimentary cycling and environmental change in the Late Proterozoic: evidence from stable and radiogenic isotopes. *Geochim. Cosmochim. Acta.* 56, 1317-1329.

Des Marais, D. J. 2001. Isotopic evolution of the biochemical carbon cycle during the Precambrian, in *Stable Isotope Geochemistry, Rev. Mineral. Geochem.*, vol. 43, edited by J. W. Valley and D. R. Cole, pp. 556 - 578, Mineral. Soc. of Am., Washington, D. C.

Deuser, W.G. 1970. Isotopic evidence for diminishing supply of available carbon during diatom bloom in the Black Sea. *Nature* 5237, 1069-71.

Donnadieu, Y., Ramstein, G., Fluteau, F., Roche, D., Ganopolski, A. 2004. The impact of atmospheric and oceanic heat transports on the sea-ice-albedo instability during the Neoproterozoic. *Climate Dynamics*, 22, 293-306.

Fairchild, I.J., Marshall, J.D., Bertrand-Sarfati, J. 1990. Stratigraphic shifts in carbon isotopes from Proterozoic stromatolitic carbonates (Mauritania): influences of primary mineralogy and diagenesis. *Amer. J. Sci.* 290-A, 46-79.

Fairchild, I.J., Marshall, J.D., Bertrand-Sarfati, J. 1990. Stratigraphic shifts in carbon isotopes from Proterozoic stromatolitic carbonates (Mauritania): influences of primary mineralogy and diagenesis. *Amer. J. Sci.* 290-A, 46-79.

- Fanning, C.M., Link, P.K., 2004. U-Pb SHRIMP ages of Neoproterozoic (Sturtian) glaciogenic Pocatello Formation, southeastern Idaho. *Geology*, 32, 881-884.
- Fanning, C.M., Link, P.K., 2008. Age constraints for the Sturtian glaciation: data from the Adelaide Geosyncline, South Australia and Pocatello Formation, Idaho, USA. In: Gallagher, S.J., Wallace, M.W. (Eds.), *Neoproterozoic Extreme Climates and the Origin of Early Life*, Selwyn Symposium of the GSA Victoria Division. *Geol. Soc. Aust. Extended Abstr.* 91, 57-62.
- Feng, L.J., Chu, X.L., Huang, J., Zhang, Q.R., Chang, H.J., 2010. Reconstruction of paleo-redox conditions and early sulfur cycling during deposition of the Cryogenian Datangpo Formation in South China, *Gondwana Res.*, 18, 632-637
- Font, E., Nedelec, A., Trindade, R.I.F., Macouin, M., Charrie`re, A. 2006. Chemostratigraphy of the Neoproterozoic Mirassol d'Oeste cap dolostones (Mato Grosso, Brazil): An alternative model for Marinoan cap dolostone formation. *Earth Planet. Sci. Lett.*, 250, 89-103.
- Francois, R., Altabet, M.A., Goericke, R., McCorkle, D.C., Brunet, C., Poisson, A., 1993. Changes in the  $\delta^{13}C$  of surface water particulate organic matter across the subtropical convergence in the S.W. Indian Ocean. *Global Biogeochemical Cycles* 7, 627-644.
- Frank, T.D., Lyons, T.W., Lohmann, K.C., 1997. Isotopic evidence for the paleoenvironmental evolution of the Mesoproterozoic Helena Formation, Belt Supergroup, USA. *Geochim. Cosmochim. Acta* 61, 5023-5041.
- Frank, T.D., Kah, L.C., Lyons, T.W., 2003. Changes in organic matter production and accumulation as a mechanism for isotopic evolution in the Mesoproterozoic ocean. *Geol. Mag.* 140, 397-420.
- Frank, T. D., Lyons, T. W. 2000. The integrity of  $\delta^{18}O$  records in Precambrian carbonates: a Mesoproterozoic case study. In: Eds Grotzinger, J. P., Jame, N. P. *Carbonate sedimentation and diagenesis in the evolving Precambrian world* 315-26. SEPM Special Publication no. 67.
- Freeman, K. H., Hayes, J. M. 1992. Fractionation of carbon isotopes by phytoplankton and estimates of ancient  $CO_2$  levels, *Global Biochemical Cycles*, 6, 185-198.

Frei, R., Gaucher, C., Døssing, L.N., Sial, A.N., 2011. Chromium isotopes in carbonates - A tracer for climate change and for reconstructing the redox state of ancient seawater. *Earth Planet. Sci. Lett.* 312, 114-125.

Frei, R., Gaucher., C., Dossing, L.N., Sial, A.N., 2011. Chromium isotopes in carbonates - A tracer for climate change and for reconstructing the redox state of ancient seawater. *Earth Planet. Sci. Lett.* 312, 114-125.

Frimmel, H.E., 2009. Trace element distribution in Neoproterozoic carbonates as palaeoenvironmental indicator. *Chem. Geol.* 258, 338-353.

Galimov, E.M., 2004. The pattern of  $\delta^{13}\text{C}_{\text{org}}$  versus HI/OI relation in recent sediments as an indicator of geochemical regime in marine basins: comparison of the Black Sea, Kara Sea, and Cariaco Trench. *Chem. Geol.* 204, 287-301.

Gaucher, C., Sial, A.N., Blanco, G., Sprechmann, P. 2004. Chemostratigraphy of the lower Arroyo del Soldado Group (Vendian, Uruguay) and paleoclimatic implications. *Gonwana Res.* 7, 715-730.

Giordano, M., Beardall, J., Raven, J. A., 2005. CO<sub>2</sub> concentrating mechanisms in algae: mechanisms, environmental modulation, and evolution. *Annu. Rev. Plant Biol.* 56, 99-131.

Guo, H., Du, Y.S., Kah, L.C., Huang, J.H., Hu, C.Y., Huang, H., Yu, W.C., 2013. Isotopic composition of organic and inorganic carbon from the Mesoproterozoic Jixian Group, North China: implications for biological and oceanic evolution. *Precambrian Res.* 224, 169-183.

Halverson, G. Maloof, A.C., Schrag, D.P., Dudas, F.O., Hurtgen, M., 2007. Stratigraphy and geochemistry of a ca 800 Ma negative carbon isotope interval in northeastern Svalbard. *Chem. Geol.* 237, 23-45.

Halverson, G.P., Dudas, F.O., Maloof, A.C. and Bowring, S.A., 2007. Evolution of the  $^{87}\text{Sr}/^{86}\text{Sr}$  composition of the Neoproterozoic seawater. *Paleogeography Paleoclimatology Paleocology* 256, 103-129.

Halverson, G.P., Hoffman, P.F., Schrag, D.P., Kaufman, J.A., 2002. A major perturbation of the carbon cycle before the Ghaub glaciation (Neoproterozoic) in Namibia: prelude to snowball earth? *Geophys. Geochem. Geosystems*, 3, 16.

Halverson, G.P., Hurtgen, M.T., Porter, S.M., Collins, A.C., 2010. Neoproterozoic-Cambrian biogeochemical evolution. In: Eds. Gaucher, C., Sial, A.N., Halverson G.P., Frimmel, H., Neoproterozoic-Cambrian tectonics, global change and evolution: a focus on southwestern Gondwana. *Dev. Precambrian Geol.*, 16, 351-356. Elsevier.

Gorokhov, I. M., Semikhatov, M. A., Baskakov, A. V., 1995. Sr Isotopic Composition in Riphean, Vendian, and Lower Cambrian Carbonates from Siberia, *Stratigr. Stratigr. Geol. Correlation* 3 (1), 1-29.

Halverson, G.P., Hurtgen, M.T., Porter, S.M., Collins, A.C., 2010. Neoproterozoic-Cambrian biogeochemical evolution. In: Eds. Gaucher, C., Sial, A.N., Halverson G.P., Frimmel, H., Neoproterozoic-Cambrian tectonics, global change and evolution: a focus on southwestern Gondwana. *Dev. Precambrian Geol.*, 16, 351-356. Elsevier.

Hayes, J.M., 1993. Factors controlling  $\delta^{13}C$  contents of sedimentary compounds: principles and evidence *Mar Geol* 113 111-125.

Hayes, J.M., Strauss, H., Kaufman, A.J. 1999. The abundance of  $\delta^{13}C$  in marine organic matter and isotopic fractionation in the global biogeochemical cycle of carbon during the past 800 Ma. *Chem. Geol.* 161, 103-125.

Hayes, J.M., Strauss, H., Kaufman, A.J., 1999. The abundance of  $\delta^{13}C$  in marine organic matter and isotopic fractionation in the global biogeochemical cycle of carbon during the past 800 Ma. *Chem. Geol.* 161, 103-125.

Hayes, J.M., Strauss, H., Kaufman, A.J., 1999. The abundance of  $\delta^{13}C$  in marine organic matter and isotopic fractionation in the global biogeochemical cycle of carbon during the past 800 Ma. *Chem. Geol.* 161, 103-125.

Heaman, L.M. 1989. The nature of the subcontinental mantle from Sr-Nd-Pb isotopic studies on kimberlitic perovskite. *Earth Planet. Sci. Lett.* 92, 323-334.

Hill, A.C., Arouri, K., Gorjan, P., Walter, M.R., 2000. Geochemistry of marine and nonmarine environments of a Neoproterozoic cratonic carbonate- evaporite: the Bitter

Springs Formation, Central Australia. In: Eds. Grotzinger, J.P., James, N.P., Carbonate Sedimentation and Diagenesis in the Evolving Precambrian World. SEPM Special Publications, 67, 327-344.

Hinrichs, K.U., 2003. Microbial fixation of methane carbon at 2.7 Ga: was an anaerobic mechanism possible? *Geochem. Geophys. Geosyst.* 3 (7). doi:10.1029/2001GC000286.

Hoffman, P.F. & Schrag, D.P., 2000. Snowball Earth. *Scientific American* 282, 68-75.

Hoffmann, K.-H., Condon, D.J., Bowring, S.A., Crowley, J.L., 2004. U-Pb zircon date from the Neoproterozoic Ghaub Formation, Namibia: constraints on Marinoan glaciation. *Geology*, 32, 817-820.

Holmden, C., Creaser, R.A., Muehlenbachs, K., Leslie, S.A., Bergstrom, S.M., 1996. Isotopic and elemental systematics of Sr and Nd in 454 Ma biogenic apatites: implications for paleoseawater studies. *Earth Planet. Sci. Lett.* 142, 425-437.

Hurtgen, M.T., Halverson, G.P., Arthur, M.A., Hoffman, P.F. 2006. Sulfur cycling in the aftermath of a 635-Ma snowball glaciation: Evidence for a synglacial sulfidic deep ocean. *Earth Planet. Sci. Lett.*, 245, 551- 570.

Hyde, W. T., Crowley, T. J., Baum, S. K., Peltier, W.R., 2000. Neoproterozoic "Snowball Earth" simulations with a coupled climate/ice sheet model. *Nature*, 405, 425-430.

Jacobsen, S.B., Kaufman, A.J. 1999. The Sr, C and O isotopic evolution of Neoproterozoic seawater. *Chem. Geol.* 161, 37-57.

Johnston, D.T., Macdonald, F.A., Gill, B.C., Hoffman, P.F., Schrag, D.P., 2012. Uncovering the Neoproterozoic carbon cycle. *Nature*, 483, 320-323.

Kah, L.C., 2000. Preservation of depositional  $\delta^{18}\text{O}$  signatures in Proterozoic dolostones: geochemical constraints on seawater chemistry and early diagenesis. In: Eds. Grotzinger, J.P., James, N.P., Precambrian Carbonates, vol. 65. SEPM, Tulsa, OK, 345-360.

Kah, L.C., Crawford, D.C., Bartley, J.K., Kozlov, V.I., Sergeeva, N.D., Puchkov, V.N., 2007. C-and Sr-isotope chemostratigraphy as a tool for verifying age of Riphean deposits in the Kama-Belaya aulacogen, the east European platform. *Stratigr. Geol. Correl.* 15, 12–29.

- Khabarov, E.M., Varaksina, I.V., 2011. The structure and depositional environments of Mesoproterozoic petroliferous carbonate complexes in the western Siberian craton. *Russ. Geol. Geophys.* 52, 923-944.
- Kasemann, S.A., Hawkesworth, C.J., Prave, A.R., Fallick, A.E., and Pearson, P.N., 2005. Boron and calcium isotope composition in Neoproterozoic carbonate rocks from Namibia: evidence for extreme environmental change. *Earth Planet. Sci. Lett.* 231, 73-86.
- Kaufman, A.J. and Xiao, S., 2003. High CO<sub>2</sub> levels in the Proterozoic atmosphere estimated from analyses of individual microfossils. *Nature* 424, 279-282.
- Kaufman, A.J. Knoll, A.H., 1995. Neoproterozoic variations in the carbon isotopic composition of seawater: Stratigraphic and biogeochemical implications. *Precambrian Res.* 73, 27-49.
- Kaufman, A.J. Xiao, S. 2003. High CO<sub>2</sub> levels in the Proterozoic atmosphere estimated from analyses of individual microfossils. *Nature* 424, 279-282.
- Kaufman, A.J., Corsetti, F.A., Varni, M.A. 2007. The effect of rising atmospheric oxygen on carbon and sulfur isotope anomalies in the Neoproterozoic Johnnie Formation, Death Valley, USA. *Chem. Geol.* 237, 47-63.
- Kaufman, A.J., Hayes, J.M., Knoll, A.H., Germs, G.J.B., 1991. Isotopic compositions of carbonates and organic carbon from upper Proterozoic successions in Namibia: stratigraphic variation and the effects of diagenesis and metamorphism. *Precambrian Res.* 49, 301-327.
- Kaufman, A.J., Jacobsen, S.B., Knoll, A.H., 1993. The Vendian record of Sr and C isotopic variations in seawater: Implications for tectonics and paleoclimate. *Earth Planet. Sci. Lett.* 120, 409-430.
- Kendall, B., Creaser, R.A., Calver, C.R., Raub, T.D., Evans, D.A.D., 2009, Correlation of Sturtian diamictite successions in southern Australia and northwestern Tasmania by Re-Os black shale geochronology and the ambiguity of "Sturtian"- type diamictite-Cap carbonate pairs as chronostratigraphic marker horizons. *Precambrian Research*, 172, 301-310.

- Kendall, B., Creaser, R.A., Selby, D., 2006. Re-Os geochronology of postglacial black shales in Australia: constraints on the timing of “Sturtian” glaciation. *Geology*, 34, 729-732.
- Kennedy, M.J., Runnegar, B., Prave, A.R., Hoffmann, K.H., Arthur, M.A. 1998, Two or four Neoproterozoic glaciations?: *Geology*, v. 26, p. 1059-1063.
- Kienast, M., Calvert, S.E., Pelejero, C., Grimalt, J.O., 2001. A critical review of marine sedimentary  $\delta^{13}\text{C}_{\text{org-pCO}_2}$  estimates: New palaeorecords from the South China Sea and a revisit of other low-latitude  $\delta^{13}\text{C}_{\text{org-pCO}_2}$  records. *Global Biogeochemical Cycles* 15, 113-127.
- Knauth, P.L., Kennedy, M.J. 2009. The late Precambrian greening of the Earth 460, 728-732.
- Knoll, A.H., Hayes, J.M., Kaufman, A.J., Swett, K., Lambert, I.B. 1986. Secular variation in carbon isotope ratios from upper Proterozoic successions of Svalbard and East Greenland. *Nature* 321, 832-837.
- Knoll, A.H., Kaufman, A.J., Semikhatov, M.A., 1995. The carbon-isotopic composition of Proterozoic carbonates: Riphean successions from north-western Siberia (Anabar Massif, Turukhansk Uplift). *Am. J. Sci.* 295, 823-850.
- Knoll, A.H., Walter M.R., Narbonne, G.M., Christie-Blick, N. 2006. The Ediacaran period: a new addition to the geologic time scale. *Lethaia* 39, 13-30.
- Kroopnick, P. M., 1985. The distribution of C-13 of sigma-CO<sub>2</sub> in the world oceans, *Deep-Sea Res.*, 32, 57-84.
- Kump, L.R., Arthur, M.A. 1999. Interpreting carbon-isotope excursions: carbonates and organic matter. *Chem. Geol.* 161, 181-198.
- Kuznetsov, A.B., Ovchinnikova, G.V., Semikhatov, M.A., Gorokhov, I.M., Kaurova, O.K., Krupenin, M.T., Vasileva, I.M., Gorokhovskii, B.M., Maslov, A.V., 2008, The Sr isotopic characterization and Pb-Pb age of carbonate rocks from the Satka formation, the Lower Riphean Burzyan Group of the southern Urals. *Stratigraphy and Geological Correlation*, 16 (2), 120-137.

- Kvenvolden, K.A., 1995. A review of the geochemistry of methane in natural gas hydrate. *Org Geochem* 23: 997-1008.
- Laws, E.A., Popp, B.N., Bidigare, R.R., Kennicutt, M.C., Macko, S.A., 1995. Dependence of phytoplankton carbon isotopic composition on growth rate and [CO<sub>2</sub>]<sub>aq</sub>: theoretical considerations and experimental results. *Geochim. Cosmochimica Acta* 59, 1131-1138.
- Lee, C., Fike, D.A., Love, G.D., Sessions, A.L., Grotzinger, J.P., Summons, R.E., Fischer, W.W., 2013. Carbon isotopes and lipid biomarkers from organic-rich facies of the Shuram Formation, Sultanate of Oman. *Geobiology* 11, 406-19.
- Lehmann M F, Bernasconi S M, Barbieri A, et al. 2002. Preservation of organic matter and alteration of its carbon and nitrogen isotope composition during simulated and in situ early sedimentary diagenesis. *Geochim Cosmochim Acta* 66: 3573-3584
- Lewis, M. A., Weber, D. E., Goodman, L. R., Stanley, R. S., Craven, W. G., Patrick, J. M., Quarles, R. L., Roush, T. H., Macauley, J. M. 2000. Periphyton and sediment bioassessment in north Florida Bay, *Environ. Monit. Assess.*, 65(3), 503-522.
- Li, C., Peng, P.A., Sheng, G.Y., Fu, J.M., Yan, Y.Z., 2003. A molecular and isotopic geochemical study of Meso-to Neoproterozoic (1.73–0.85 Ga) sediments from the Jixian section, Yanshan Basin, North China. *Precambrian Res.* 125, 337-356.
- Lindsay, J.F., Brasier, M.D., 2000. A carbon isotope reference curve for ca. 1700-1575 Ma, McArthur and Mount Isa Basins, Northern Australia. *Precambrian Res.* 99, 271- 308.
- Luo, G., Junium, C. K., Kump, L.R.; Huang, J., Li, C., Feng, Q., Shi, X., Bai, X., and Xie, S., 2014. Shallow stratification prevailed for ~1700 to ~1300 Ma ocean: Evidence from organic carbon isotopes in the North China Craton, *Earth and Planetary Science Letters* 400, 219-232.
- Macdonald, F. A., Schmitz, M. D. et al. 2010. Calibrating the Cryogenian. *Science*, 327, 1241-1243.
- Macdonald, F.A., Jones, D.S. Schrag, D.P., 2009. Stratigraphic and tectonic implications of a newly discovered glacial diamictite-cap carbonate couplet in southwestern Mongolia. *Geology* 37, 123-126.

- Mahan, K.H., Wernicke, B.P., and Jercinovic, M.J., 2010. Th-U-total Pb geochronology of authigenic monazite in the Adelaide rift complex, South Australia, and implications for the age of the type Sturtian and Marinoan glacial deposits. *Earth Planet. Sci. Lett.*, 289, 76-86.
- Marshall, J.D. 1992. Climatic and oceanographic isotopic signals from the carbonate rock record and their preservation. *Geological Magazine*, 129,143-160.
- McArthur, J.M., Burnell, J.A., Hancock, J.M.1992. Sr isotopes at the Cretaceous/Tertiary boundary. *Nature*, 355, 28.
- McCrea, J.M., 1950. On the isotopic chemistry of carbonates and a paleothermometer scale. *J. Chem. Phys.* 5, 48-51.
- McKirdy, D., Burgess, J., Lemon, N., Yu, X., Cooper, A., Gostin, V., Jenkins, R., Both, R., 2001. A chemostratigraphic overview of the late Cryogenian interglacial sequence in the Adelaide Fold-Thrust Belt, South Australia. *Precambrian Res.* 106, 149-186
- Melezhik, V.A., Gorokhov, I.M. Kuznetsov, A.B., Fallick, A.E. 2001. Chemostratigraphy of Neoproterozoic carbonates: implications for 'blind dating'. *Terra Nova.* 13, 1-11.
- Miyachi, S., Iwasaki, I., Shiraiwa, Y., 2003. Historical perspective on microalgal and cyanobacterial acclimation to low- and extremely high-CO<sub>2</sub> conditions. *Photosynth Res* 77, 139-153.
- Montañez, I.P., Banner, J.L., Osleger, D.A., Borg, L.E., Bosserman, P.J. 1996. Integrated Sr isotope variations and sea-level history of Middle to Upper Cambrian platform carbonates: Implications for the evolution of Cambrian seawater <sup>87</sup>Sr/<sup>86</sup>Sr. *Geology.* 24, 917-920.
- Mook, W. G., J. C. Bommerson, J.C., Staverman, W.H., 1974. Carbon isotope fractionation between dissolved bicarbonate and gaseous carbon dioxide. *Earth Plant. Sci. L&t.* 22, 169-176.
- Nedelec, A., Affaton, P., France-Lanord, C., Charriere, A, J. 2007. Sedimentology and chemostratigraphy of the Bwipe Neoproterozoic cap dolostones (Ghana, Volta Basin): A record of microbial activity in a peritidal environment. *Comptes Rendus Geoscience*, 339, 223-239.

- Ogawa, T., Kaplan, A., 2003. Inorganic carbon acquisition systems in cyanobacteria. *Photosynth Res* 77, 105-115.
- Omata T, Gohta S, Takahashi Y, Harano Y, Maeda S-I., 2001. Involvement of a CbbR homolog in low CO<sub>2</sub>-induced activation of the bicarbonate transporter operon in cyanobacteria. *J Bacteriol* 183, 1891-1898.
- Pecoits. E., Gingras, M., Aubet, N., Konhauser, K., 2008. Ediacaran in Uruguay: palaeoclimatic and palaeobiological implications. *Sedimentology*. 55, 689-719.
- Peters, K.E., Rohrback, B.G., Kaplan, I.R., 1981. Carbon and hydrogen stable isotope variations in kerogen during laboratory simulated thermal maturation. *AAPG Bull.* 65, 501-508.
- Phlips, E.J., Badylak, S., Lynch, T.C., 1999. Blooms of the picoplanktonic cyanobacterium *Synechococcus*. Florida Bay, a subtropical inner-shelf lagoon. *Limnology and Oceanography* 44, 1166-1175.
- Pokrovskii, B.G. Vinogradov, V.I., 1991, Strontium, Oxygen and Carbon Isotope Composition in the Upper Precambrian Carbonates from Western Flank of the Anabar Uplift (the Kotuikan River), *Dokl. Akad. Nauk SSSR* 320 (5), 1245-1250.
- Popp, B.N., Laws, E.A., Bidigare, R.R., Dore, J.E., Hanson, K.L., Wakeham, S.G., 1998. Effect of phytoplankton cell geometry on carbon isotopic fractionation. *Geochim. Cosmochim. Acta* 62, 69-77.
- Rau, G. H., Riebesell, U., WolfGladrow, D. 1996. A model of photosynthetic C-13 fractionation by marine phytoplankton based on diffusive molecular CO<sub>2</sub> uptake, *Mar. Ecol-Pog. Ser.*, 133(1--3), 275-285.
- Ray, J.S., Veizer, J., Davis, W.J., 2003, C, O, Sr and Pb isotope systematics of carbonate sequences of the Vindhyan Supergroup, India: age, diagenesis, correlations and implications for global events , *Precambrian Res*, 121, 103-140.
- Read, J.F., 1985. Carbonate platform facies models. *Bull. Am. Assoc. Pet. Geol.*, 69: 1-21.

- Riccardi, A., Kump, L.R., Arthur, M.A., D'Hondt, S., 2007. Carbon isotopic evidence for chemocline upward excursions during the end-Permian event. *Palaeogeogr. Palaeoclimatol. Palaeoecol.* 248, 73-81.
- Ridgwell, A.J., Watson A.J., Maslin, M.A., Kaplan, J.O., 2003. Implications of coral reef buildup for the controls on atmospheric CO<sub>2</sub> since the Last Glacial Maximum. *Paleoceanography*, 18, 1083.
- Riding, R. 2006. Cyanobacterial calcification Cyanobacterial calcification, carbon dioxide concentrating mechanisms, and Proterozoic-Cambrian changes in atmospheric composition. *Geobiology*, 4, 299-316.
- Rose, C.V., Maloof, A.C., Schoene, B., Ewing, R.C., Linnemann, U., Hofmann, M., Cottle, J.M., 2013. The end-Cryogenian glaciation of South Australia. *Geosci. Can.* 40, 256-293.
- Rost, B., Riebesell, U., Burkhardt, S., Sültemeyer, D., 2003. Carbon acquisition of bloom-forming marine phytoplankton. *Limnology and Oceanography* 48, 55-67.
- Rothman, D.H., Hayes, J.M., Summons, R.E., 2003. Dynamics of the Neoproterozoic carbon cycle. *Proc. Nat. Acad. Sci. U.S.A.* 100, 124-129.
- Saltzman, M.R., Thomas, E. 2012. Carbon isotope stratigraphy, *The Geologic Time Scale 2012*. In: Eds. Gradstein, F., Ogg, J., Schmitz, M.D., Ogg, G., 207-232.
- Sansjofre, P., Ader, M., Trindade, R.I.F., Elie, M., Lyons, J., Cartigny, P., Nogueira, A.C.R., 2011. A carbon isotope challenge to the snowball Earth. *Nature* 478, 93-96.
- Sansjofre, P., Ader, M., Trindade, R.I.F., Elie, M., Lyons, J., Cartigny, P., noguerria, A.C.R. 2011. A carbon isotope challenge to the snowball Earth. *Nature* 478, 93-97.
- Schidlowski, M. 1988. A 3,800-million-year isotopic record of life from carbon in sedimentary rocks. *Nature* 333, 313-318.
- Schidlowski, M., (1987) Application of stable carbon isotopes to early biochemical evolution on earth. *Amer. Rev. Earth Planet. Sci.*, v. 15, pp. 47-72
- Schrag, D.P., Berner, R.A., Hoffman, P.F., Halverson, G.P. 2002. On the initiation of a Snowball Earth, *Geochem. Geophys. Geosyst.* 3.

Semikhatova, M.A., Kuznetsov, A. B., Maslov, A. V., Gorokhov, I. M., Ovchinnikova G. V., 2009, Stratotype of the Lower Riphean, the Burzyan Group of the Southern Urals: Lithostratigraphy, Paleontology, Geochronology, Sr- and C-Isotopic Characteristics of its carbonate rocks, *Stratigraphy and Geological Correlation*, 2009, Vol. 17, No. 6, 574-601.

Shen, B., Xiao, S.H., Kaufman, A.J., Bao, H.M., Zhou, C.M, Wang, H.F. 2008. Stratification and mixing of a post-glacial Neoproterozoic ocean: Evidence from carbon and sulfur isotopes in a cap dolostone from northwest China. *Earth Planet. Sci. Lett.*, 265, 209-228

Simoneit, B.R.T., Brenner, S., Peters, K.E., Kaplan, I.R., 1981. Thermal alteration of Cretaceous black shale by diabase intrusions in the Eastern Atlantic: II. Effects on bitumen and kerogen. *Geochim. Cosmochim. Acta* 45, 1581-1602.

Swart, P., Kennedy, M., 2012. Does the global stratigraphic reproducibility of  $\delta^{13}\text{C}$  in Neoproterozoic carbonates require a marine origin? A Pliocene-Pleistocene comparison. *Geology* 40, 87-90.

Thomas, C.W., Graham, C.M., Ellam, R.M., Fallick, A.E. 2004.  $^{87}\text{Sr}/^{86}\text{Sr}$  chemostratigraphy of Neoproterozoic Dalradian limestones of Scotland and Ireland: constraints on depositional ages and time scales. *Journal of the Geological Society*, London 161, 229-242.

Thompson, J.B., 2000. Microbial whittings. In: Eds. Riding, R, Awramik, S.M., *Microbial Sediments*. Springer-Verlag, Berlin, 250-260.

Tortell, P.D., Rau, G.H., Morel, F.M.M., 2000. Inorganic carbon acquisition in coastal Pacific phytoplankton communities. *Limnol. Oceanogr.* 45: 1485-150.

Tucker, M.E., V.P. Wright. 1990. *Carbonate Sedimentology*. Blackwell Scientific Publications, Oxford, 482.

Veizer, J., Clayton, R.N., Hinton, R.W., 1992. Geochemistry of Precambrian carbonates: IV. Early Proterozoic (2.25-0.25 Ga) seawater. *Geochim. Cosmochim. Acta* 56, 875-885.

Veizer J., Hoefs, J. 1976. The nature of  $^{18}\text{O}/^{16}\text{O}$  and  $^{13}\text{C}/^{12}\text{C}$  secular trends in sedimentary carbonate rocks. *Geochim. Cosmochim. Acta* 40, 1387-1395.

Veizer, J. 1983. Chemical diagenesis of carbonates: Theory and application of trace element technique. In: Eds. Arthur, M.A., Anderson, T.F., Kaplan, I.R., Veizer, J., Land, L.S., *Stable Isotopes in Sedimentary Geology*. Society of Economic Paleontologists and Mineralogists Short Course No. 10, Dallas, 3-1 to 3-100.

Veizer, J., 1983. Chemical diagenesis of carbonates: Theory and application of trace element technique. In: Eds. Arthur, M.A., Anderson, T.F., Kaplan, I.R., Veizer, J., Land, L.S., *Stable Isotopes in Sedimentary Geology*. Society of Economic Paleontologists and Mineralogists Short Course No. 10, Dallas, 3-1 to 3-100.

Vogel J.C. 1993. Variability of carbon isotope fractionation during photosynthesis. In: Eds. Ehleringer, J.R., Hall, A.E., Farquhar, G.D., *Stable Isotopes and Plant Carbon-Water Relations* 29-46. Academic Press, San Diego .

Werne, J. P., Hollander, D. J., 2004. Balancing supply and demand: controls on carbon isotope fractionation in the Cariaco Basin (Venezuela) Younger Dryas to present. *Mar. Chem.*, 92, 275- 293.

Xiao, S., Bao, H., Wang, H., Kaufman, A.J., Zhou, C., Li, G., Yuan, X., Ling, H., 2004. The Neoproterozoic Quruqtagh Group in eastern Chinese Tianshan: evidence for a postMarinoan glaciation. *Precambrian Res.* 130, 1-26.

Xiao, S.H., Knoll, A.H., Kaufman, A.J., Yin, L.M., Zhang, Y., 1997. Neoproterozoic fossils in Mesoproterozoic rocks? Chemostratigraphic resolution of a biostratigraphic conundrum from the North China Platform. *Precambrian Res.* 84, 197-220.

Yoshioka, H., Asahara, Y., Tojo, B., Kawakami, S., 2003. Systematic variations in C, O and Sr isotopes and elemental concentrations in Neoproterozoic carbonates in Namibia: implications for a glacial to interglacial transition. *Precambrian Research*, 124, 69-85

Young, S.A., Saltzman, M.R., Bergström, S.M., Leslie, S.A., Xu, C. 2008. Paired  $\delta^{13}\text{C}_{\text{carb}}$  and  $\delta^{13}\text{C}_{\text{org}}$  records of Upper Ordovician (Sandbian-Katian) carbonates in North America and China: Implications for paleoceanographic change. *Palaeogeogr. Palaeoclimatol. Palaeoecol.* 270, 166-178.

Zhao, Y.Y., Zheng, Y.F., Chen, F.K. 2009. Trace element and strontium isotope constraints on sedimentary environment of Ediacaran carbonates in southern Anhui, South China. *Chem. Geol.*, 265, 345-362.

Zhou, C., Tucker, R., Xiao, S., Peng, Z., Yuan, X., Chen, Z., 2004. New constraints on the ages of Neoproterozoic glaciations in south China. *Geology*, 32, 437-440.

## CHAPTER 6: CONCLUSIONS

Despite the Neoproterozoic volcano-sedimentary successions of Uruguay have been the subject of several sedimentologic, chrono-stratigraphic and tectonic interpretation studies, here, it is shown that the stratigraphy, age and tectonic evolution of these units remain uncertain. Extensive fieldwork and radiometric dating, combined with previously published geochronologic and stratigraphic data provide more precise temporal constraints on their depositional age and to establish a more solid framework for the stratigraphic and tectonic evolution of all these units.

Particularly, sedimentological, petrographic, geochemical, geochronological and stable isotopic data were combined to constrain the depositional environment and the age of the Polanco Limestones Formation and to understand the platform dynamics. By comparing chemostratigraphic profiles across the basin (i.e., shallow- vs. deep-water settings), we show that this type of integrated analysis can help to interpret Precambrian carbonate systems, especially those associated with major palaeo-climatic and palaeo-environmental events. The following conclusions can be drawn from this study:

### **6.1. Neoproterozoic of Uruguay**

#### ***6.1.1. Litho- and Chronostratigraphy***

A new litho- and chronostratigraphic framework has been established for the Neoproterozoic of Uruguay. The Ediacaran record consists of the Maldonado Group (Playa Hermosa, Las Ventanas and San Carlos formations), and the Tacuari, Barriga Negra, Rocha and Sierra de Aguirre formations. The Arroyo del Soldado Group (Yerbal, Polanco Limestones and Cerro Espuelitas formations) and the Arroyo de la Pedrera Group (Piedras de Afilas and Cerro Victoria formations) were likely deposited between 700 and 1000 Ma. The best available radiometric age constraints indicate intense magmatic-tectonic activity occurred between 600 and 560 Ma, incompatible with previous models suggesting a stable, Atlantic-type passive margin on this portion of southwestern Gondwana.

### ***6.1.2. Geochronology***

The mixed siliciclastic-carbonate Arroyo del Soldado Group, which includes the Polanco Limestones Formation, was deposited during the Tonian-Cryogenian, between ~1,000 and 650 Ma, in a passive continental margin developed along the southeastern margin of the Nico Pérez Terrane. In contrast, the deposition of the siliciclastic and volcanoclastic Playa Hermosa, Las Ventanas, San Carlos and Barriga Negra formations occurred during the upper Ediacaran (<585 Ma) in small fault-bounded basins developed over the Nico Pérez, Edén and Cuchilla Dionisio terranes.

### ***6.1.3. Palaeogeography and Tectonic Evolution***

Far from being a definite model, our results suggest that the present-day terrane configuration took place in a relatively short (~100 Ma long) period of time between ~650 and 560 Ma. In this regard, the Edén and Nico Pérez terranes likely accreted at ~650-620 Ma (Edén Accretionary Event), followed by their accretion to the Piedra Alta Terrane at ~620-600 Ma (Piedra Alta Accretionary Event), and culminating with the accretion of the Cuchilla Dionisio Terrane at ~600-560 Ma (Cuchilla Dionisio Accretionary Event).

Based on the distinct stratigraphy, geology, U-Pb zircon ages and Nd isotopes, a new terrane, named Edén Terrane, is now defined. As for the above-mentioned terranes, the boundaries between this block and the adjacent terranes are highly tectonized, with large-scale ductile shear zones implying that the geodynamic history of the Ediacaran is dominated by oblique movements with episodes of emplacement of granite complexes during transpressional and posterior extensional events.

## **6.2. Polanco Limestones Formation**

### ***6.2.1. Sedimentology and Diagenesis***

Facies analyses indicate that the Polanco Limestones Formation was deposited on a storm-dominated homoclinal ramp, where inner-, mid- and outer-ramp facies associations were recognized and described. Inner ramp facies association is characterized by coarsening- and thickening-upward regressive cycles of calcarenites representing upper, middle and lower shoreface environments deposited above the mean fair-weather wave

base in well-oxygenated waters. Mid-ramp facies association consists of thinly-bedded calcisiltite and dolosiltite with hummocky and swaley cross-stratified calcarenites and thin massive or parallel-stratified calcarenite beds. Outer ramp deposits comprise limestone and dolostone rhythmites and bedded dolostones deposited below the mean storm wave-base and under anoxic conditions.

Petrographic observations permits the recognition of two major stages affecting carbonates and their relative chronology: (1) depositional and early diagenetic phases (micritic to microsparitic dolostones and limestones), and (2) late diagenetic phases (blocky and fracture-filling cements).

Petrographic, textural and diverse geochemical proxies used here suggest that most of the studied samples did not experience significant post-depositional alteration of the carbon isotope composition and thus, these carbonates record near-primary seawater signature. Accordingly, the carbonates can be used for chemostratigraphic comparisons. In contrast, Sr isotope compositions are more variable, reflecting the effects of diagenesis and probable exchange with clay minerals or simply changes in relative riverine input. In this regard, carbonates from the South Isla Patrulla and Recalde sections are suitable for Sr chemostratigraphy whereas those from the Los Tapes section should be excluded.

### ***6.2.2. Carbon and strontium isotope records***

The paired  $\delta^{13}\text{C}_{\text{org}}$  and  $\delta^{13}\text{C}_{\text{carb}}$  trends from the Polanco Limestones Formation of Uruguay record variations in nutrient input from continental runoff and in  $[\text{CO}_2]_{\text{aq}}$  possibly linked to changes in atmospheric  $\text{CO}_2$  levels during the Cryogenian interglacial period. The precipitation of carbonates via biogenic whittings along with the low  $\Delta^{13}\text{C}$  values throughout the entire succession suggests low  $p\text{CO}_2$ .

The interpreted local rises in marine phytoplankton growth rates are coincident with evidence for changes in nutrient input (P), lithophile elements and  $^{87}\text{Sr}/^{86}\text{Sr}$  ratios. These changes are consistent with the notion that enhanced weathering and consequent high nutrient input to the oceans stimulating biological productivity and accelerating carbon flux to the basin floor. These short-lived periods are superimposed on larger-scale fluctuations interpreted in terms of changing  $[\text{CO}_2]_{\text{aq}}$ , and thereby in global  $p\text{CO}_2$ . Additionally, the consistently small  $\Delta^{13}\text{C}$  (Avg: 15.5 ‰) values suggest low atmospheric

$p\text{CO}_2$ , which is further supported by the  $\text{HCO}_3^-$  utilization by planktic cyanobacteria and subsequent precipitation of biogenic whittings.

The  $\delta^{13}\text{C}_{\text{carb}}$  gradient between relatively shallow-water (non-storm dominated) and deep-water facies can be explained by the ‘photic pump’ effect. When compared with the modern ocean gradient, the slightly larger  $\delta^{13}\text{C}_{\text{carb}}$  gradient found in the Polanco Limestones Formation may result from either higher primary productivity at that time, or most likely, a more prominent stratification of the water column.

### **6.2.3. Age**

New U-Pb radiometric data from the Polanco carbonates and K-Ar ages on illite of the uppermost Yermal Formation yield ages of  $752\pm 95$  and  $637\pm 13$  for the diagenesis and peak metamorphic event, respectively. These ages fit with independent estimates (detrital zircon ages) for the deposition of the unit between  $\sim 1,000$  and  $650$  Ma. Based on  $^{87}\text{Sr}/^{86}\text{Sr}$  ratios reported for the Neoproterozoic, the values shown by the Polanco Limestones Formation are in agreement with those reported for other interglacial limestones of the Cryogenian Period. A preliminary correlation with the negative  $\delta^{13}\text{C}_{\text{carb}}$  excursion recorded in the Gruis Formation (Otavi Group) in Namibia is proposed here.

### **6.3. FUTURE WORK**

Chemostratigraphic studies based on Sr and C isotopes have proven extremely useful at facilitating correlation over large distances, unraveling the palaeo-oceanographic conditions during deposition and establishing age constraints. This study has provided substantial advances in the understanding of the stratigraphy, sedimentology, age and environmental significance of the C-isotope record of the Polanco Limestones Formation. Unfortunately, chemostratigraphic studies present complications that arise from local biological, diagenetic and physico-chemical factors on individual  $\delta^{13}\text{C}$  records that can mask the global signal. Because of the importance of the Polanco Limestones Formation in the context of the global-scale geochemical, climatic and biotic events that signed the Neoproterozoic, and to better assess the global versus local contribution in the  $\delta^{13}\text{C}$  record I suggest that future studies should be oriented to perform:

- Lipid biomarker analyses in order to assess the potentially diverse C-sources. In this study, it has been assumed that the organic matter was formed within the basin and was contemporaneous with carbonate minerals; however, sedimentary organic carbon present in carbonate rocks is not always derived from syngenetic sources. As such, variations in organic matter composition may reflect biological community shifts (e.g., seasonality), admixtures of terrigenous or migrated (non-syngenetic) organic carbon, which impart specific  $\delta^{13}\text{C}_{\text{org}}$  signatures. The identification of different biomarkers and compound-specific isotopic measurements of individual lipids will allow to identify sources and variations of organic carbon and help to better understand the C record.
- Lithium isotopic composition of carbonates to determine concentration and variation of  $p\text{CO}_2$ . The Polanco Limestones Formation was deposited during the Cryogenian interglacial period, which is thought to be characterized by high  $p\text{CO}_2$  (greenhouse) that caused enhanced weathering of the glacially eroded landscape, increased alkalinity, and ultimately carbonate precipitation. Surprisingly, the consistently small  $\Delta^{13}\text{C}$  values of the Polanco carbonates suggest low atmospheric  $p\text{CO}_2$ . Lithium isotopes are tracers of silicate weathering and their composition along with the C-isotope record will contribute to understanding the atmospheric  $p\text{CO}_2$  during this crucial period.
- Neodymium isotopes as a proxy for past ocean circulation, hydrothermal inputs and continental weathering regimes. Both, continental and hydrothermal sources have been proposed to the Polanco Limestones Formation. Accordingly, a systematic Nd isotope study, in combination with Lu and C isotopes, is critical for examining links between nutrient input –either from land or hydrothermal vents-, bioproductivity shifts, and ultimately global climate change.
- Further geochronological constraints on the deposition of the Polanco Limestones Formation. Although a new age was established for the unit in this study, new radiometric ages are necessary in order to integrate geological and geochemical

data in a more robust geochronological framework, and therefore improve our understanding of the biotic and environmental events during the Neoproterozoic. In the absence of volcanic rocks, diagenetic minerals such as monazite and xenotime can be targeted for dating. Future radiometric dating will allow to firmly establish a consistent litho- and chronostratigraphic framework; particularly, when attempting regional and global correlations, and inferences on global palaeoenvironmental and palaeobiological events.

## REFERENCES

- Adams, C.J., Miller, H., Aceñolaza, F.G., Toselli, A.J., Griffin, W.L. 2011. The Pacific Gondwana margin in the late Neoproterozoic-early Paleozoic: Detrital zircon U–Pb ages from metasediments in northwest Argentina reveal their maximum age, provenance and tectonic setting. *Gondw. Res.* 19, 71-83.
- Allen, P. A., 2007, The Huqf Supergroup of Oman: Basin development and context for Neoproterozoic glaciation. *Earth Science Reviews*, 84, 139-185.
- Almeida, R.P., Janikian, L., Fragoso-Cesar, A.R., Fambrini, G.L., 2010. The Ediacaran to Cambrian rift system of southeastern South America: tectonic implications. *Jour. Geol.* 118, 145-161.
- Amthor, J.E., Grotzinger, J.P., Schröder, S., Bowring, S.A., Ramezani, J., Martin, M.W. Matter, A., 2003. Extinction of Cloudina and Namacalathus at the Precambrian-Cambrian boundary in Oman. *Geol. Soc. Am. Bull.* 31, 431-434.
- Asmerom, Y., Jacobsen, S. B., Knoll, A. H., Butterfield, N. J., Swett, K., 1991. Strontium isotopic variations of Neoproterozoic seawater: implication for crustal evolution. *Geochim. Cosmochim. Acta*, 5: 2883-2894.
- Aubet, N., Pecoits, E., Bekker, A., Gingras, M.K., Zwingmann, H., Veroslavsky, G., de Santa Ana, H., Konhauser, K.O., 2012. Chemostratigraphic constraints on early Ediacaran carbonate ramp dynamics, Río de la Plata craton, Uruguay. *Gondw. Res.* 22, 1073-1090.
- Aubet, N., Pecoits, E., Bekker, A., Gingras, M.K., Zwingmann, H., Veroslavsky, G., de Santa Ana, H., Konhauser, K.O., 2013. Reply to Comment by C. Gaucher et al. on “Chemostratigraphic constraints on early Ediacaran carbonate ramp dynamics, Río de la Plata craton, Uruguay”. *Gondw. Res.* 23, 1186-1188.
- Aubet, N., Pecoits, E., Heaman, L., Veroslavsky, G., Gingras, M., Konhauser, K. 2014. Ediacaran in Uruguay: facts and controversies. *Journal of South American Earth Sciences* 55, 43-57.

Aubert, N., Pecoits, E., Heaman, L., Veroslavsky, G., Konhauser, K.O., In review. U-Pb detrital zircon ages from some Neoproterozoic successions of Uruguay: provenance, stratigraphy and tectonic evolution.

Azmy, K., Kaufman, A.J. Misi, A., Oliveira, T.F., 2006. Isotope stratigraphy of the Lapa Formation, São Francisco Basin, Brazil: implications for Late Neoproterozoic glacial events in South America. *Precambrian Research* 149, 231-248.

Baadsgard, H., 1987. Rb-Sr and K-Ca isotope systematics in minerals from potassium horizons in the Prairie Evaporite Formation, Saskatchewan, Canada. *Chemical Geology* 66, 1-15.

Badger, M.R., Hanson, D.T., Price, G.D., 2002. Evolution and diversity of CO<sub>2</sub> concentrating mechanisms in cyanobacteria. *Functional Plant Biology* 29, 161-173.

Badger, M.R., Price, G.D., 2003. CO<sub>2</sub> concentrating mechanisms in cyanobacteria: molecular components, their diversity and evolution. *J. Exp. Bot.* 54, 609-622.

Banner, J.L., Hanson, G.N., 1990. Calculation of simultaneous isotopic and trace element variations during water-rock interaction with application to carbonate diagenesis. *Geochim. Cosmochim. Acta* 54, 3123-3137.

Banner, J. L. and Kaufman, J., 1994, The isotopic record of ocean chemistry and diagenesis preserved in nonluminescent brachiopods from Mississippian carbonate rocks, Illinois and Missouri. *Geological Society of America Bulletin* 106, 1074-1082.

Bartley, J.K., Kah, L.C., McWilliams, J.L., Stagner, A.F., 2007. Carbon isotope chemostratigraphy of the Middle Riphean type section (Avzyan Formation, Southern Urals, Russia): signal recovery in a fold-and-thrust belt. *Chem. Geol.* 237, 211-232.

Basei, M., Siga, Jr.O., Masquelin, H., Harara, O., Reis Neto, J. and Preciozzi, F., 2000. The Dom Feliciano Belt of Brazil and Uruguay and its foreland domain, the Río de la Plata Craton. In: Cordani, U., Milani, E., Thomaz F.A., Campos, D. (Eds.), *Tectonic evolution of South America*, pp. 311-334.

Basei, M.A.S., Frimmel, H.E., Nutman, A.P., Preciozzi, F., Jacob, J., 2005. The connection between the Neoproterozoic Dom Feliciano (Brazil/Uruguay) and Gariep (Namibia/South Africa) orogenic belts. *Prec. Res.* 139, 139-221.

- Basei, M.A.S., Frimmel, H.E., Nutman, A.P., Preciozzi, F., 2008. West Gondwana amalgamation based on detrital zircon ages from Neoproterozoic Ribeira and Dom Feliciano belts of South America and comparison with coeval sequences from SW Africa. In: Pankhurst RJ, Trouw RAJ, de Brito Neves BB, De Wit MJ (Eds.) West Gondwana: Pre-Cenozoic Correlations Across the South Atlantic Region vol 294. Geological Society, London, special publications, pp 239-256.
- Basei, M.A.S., Peel, E., Sanchez-Bettucci, L., Preciozzi, F., Nutman, A.P., 2011. The basement of the Punta del Este Terrane (Uruguay): an African Mesoproterozoic fragment at the eastern border of the South American Rio de la Plata craton. *Int. J. Earth Sci. (Geol Rundsch)* 100, 289-304.
- Bau, M., Dulski, P., 1996. Distribution of yttrium and rare-earth elements in the Penge and Kuruman iron-formations, Transvaal Supergroup, South Africa. *Precambrian Research* 79, 37-55.
- Bekker, A., Holland, H.D., 2012. Oxygen overshoot and recovery during the early Paleoproterozoic. *Earth Planet. Sci. Lett.* 317-318, 295-304.
- Bekker, A., Sial, A.N., Karhu, J.A., Ferrerira, V.P., Noce, C.M., Kaufman, A.J., Romano, A.W., Pimentel, M.M., 2003. Chemostratigraphy of carbonates from the Minas Supergroup, Quadrilátero Ferrífero (Iron Quadrangle), Brazil: A stratigraphic record of early Proterozoic atmospheric, biogeochemical and climatic change. *American Journal of Science* 303, 865-904.
- Bekker, A., Karhu, J.A., Kaufman, A.J., 2006. Carbon isotope record for the onset of the Lomagundi carbon isotope excursion in the Great Lakes area, North America. *Precambrian Research* 148, 145-180.
- Benthien, A., Andersen, N., Schulte, S., Muller, P.J., Schneider, R.R., Wefer, G., 2002. Carbon isotopic composition of the C<sub>37:2</sub> alkenone in core top sediments of the South Atlantic Ocean: Effects of CO<sub>2</sub> and nutrient concentrations, *Global Biogeochem. Cycles*, 16, 1012.
- Berger, W.H., Vincent. E. 1986. Deep-sea carbonates: reading the carbon-isotope signal. *Geol Rundsch* 75: 249-269.

- Bian, L., Hinrichs, K.-U., Xie, T., Brassell, S.C., Iversen, N., Fossing, H., Jørgensen, B.B., Hayes, J.M., 2001. Algal and archaeal polyisoprenoids in a recent marine sediment: molecular isotopic evidence for anaerobic oxidation of methane. *Geochem. Geophys. Geosyst.* 2 Paper number 2000GC000112.
- Bidigare, R.R., Flügge, A., Freeman, K.H., Hanson, K.L., Hayes, J.M., Hollander, D., Jasper, J.P., King, L.L., Laws, E.A., Milder, J., Millero, F.J., Pancost, R., Popp, B.N., Steinberg, P.A., Wakeham, S.G., 1997. Consistent fractionation of  $^{13}\text{C}$  in nature and in the laboratory: Growth-rate effects in some haptophyte algae. *Glob Biogeochem Cycl* 11, 279-292
- Bidigare, R.R., Prezelin, B.B., Smith, R.C., 1992. Biooptical models and the problems of scaling, p. 175-212. In: Eds Falkowski, P.G. Primary productivity and biogeochemical cycles in the sea. Plenum.
- Bjerrum, C.J., Canfield, D.E., 2011. Towards a quantitative understanding of the late Neoproterozoic carbon cycle. *Proceedings of the National Academy of Sciences of the United States of America* 108, 5542-5547.
- Blanco, G., Gaucher, C., 2005. Estratigrafía, paleontología y edad de la Formación Las Ventanas (Neoproterozoico, Uruguay). *Lat. Am. J. Sedimentol. Basin Anal.* 12, 109-124
- Blanco, G., Rajesh, H.M., Gaucher, C., Germs, G.J.B., Chemale Jr., F., 2009. Provenance of the Arroyo del Soldado Group (Ediacaran to Cambrian, Uruguay): Implications for the paleogeographic evolution of southwestern Gondwana. *Prec. Res.* 171, 57-73.
- Boller A. J., Thomas P. J., Cavanaugh C. M., Scott K. M., 2011. Low stable carbon isotope fractionation by coccolithophore RubisCO. *Geochim. Cosmochim. Acta* 75, 7200-7207.
- Bonhomme, M., Thuizat, G.R., Pinault, Y., Clauer, N., Wendling, R., Winkler, R., 1975. Méthode de datation potassium-argon. *Appareillage et Technique*, Strasbourg, 53.
- Borba, A.W., Mizusaki, A.M.P., 2003. Santa Bárbara Formation (Caçapava do Sul, southern Brazil): depositional sequences and evolution of an Early Paleozoic post-collisional basin. *J. South Am. Earth Sci.* 16, 365-380.

Bossi, J., 1966. Geología del Uruguay. Departamento de Publicaciones de la Universidad de la República, Montevideo.

Bossi, J., Campal, N., 1992. Magmatismo y tectónica transcurrente durante el Paleozoico Inferior en Uruguay. In: Gutiérrez-Marco, J.G., Saavedra, J., Rabano, I. (Eds.), Paleozoico Inferior de Iberoamérica. Universidad de Extremadura, Mérida, pp. 343-356.

Bossi, J., Campal, N., Civetta, L., Demarchi, G., Girardi, V.A.V., Mazzucchelli, M., Negrini, L., Rivalenti, G., Fragoso Cesar, A.R.S., Sinigoi, S., Teixeira, W., Piccirillo, E.M., Molesini, M. 1993. Early Proterozoic dike swarms from Western Uruguay: geochemistry, Sr-Nd isotopes and petrogenesis. *Chem. Geol.* 106, 263-277.

Bossi, J., Cingolani, C., Llambías, E., Varela, R., Campal, N., 1993. Características del magmatismo post-orogénico finibrasiliano en el Uruguay: formaciones Sierra de Ríos y Sierra de Ánimas. *Rev. Brasil. Geocien.* 23, 282-288.

Bossi, J., Ferrando, L., Montaña, J., Campal, N., Morales, H., Gancio, F., Schipilov, A., Piñeyro, D., Sprechmann, P., 1998. Carta Geológica del Uruguay. Escala 1:500.000. Versión digital. Geoeditores, Montevideo.

Bossi, J., Ferrando, L., 2001. Carta Geológica del Uruguay, Escala 1:500.000. Versión 2.0 Digital, Facultad de Agronomía, Montevideo.

Bossi, J., Campal, N., Hartmann, L.A., Schipilov, A. 2001. Predevoniano en el Uruguay; terrenos y SHRIMP II. Actas XI Cong. Latinoam. Geol. Montevideo. CD-ROM version.

Bossi, J., Cingolani, C., 2009. Extension and general evolution of the Rio de la Plata Craton. In: Gaucher C, Sial AN, Halverson GP, Frimmel HE (Eds.) Neoproterozoic-Cambrian tectonics, global change and evolution: a focus on southwestern Gondwana. *Developments in Precambrian Geology*, vol 16, Elsevier, pp 73-85.

Bosworth, W., Huchon, P., McClay, K., 2005. The Red Sea and Gulf of Aden Basins. *J. Afr. Earth Sci.* 43, 334-378.

Bowring, S., Grotzinger, J.P., Condon, D.J., Ramezani, J., Newall, M., Allen, P.A., 2007. Geochronologic constraints on the chronostratigraphic framework of the Neoproterozoic Huqf Supergroup, Sultanate of Oman. *American Journal of Science* 307, 1097-1145.

- Bowring, S., Myrow, P., Landing, E., Ramezani, J., Grotzinger, J., 2003. Geochronological constraints on terminal Neoproterozoic events and the rise of metazoans. *Geophys. Res. Abstracts* 5, 219.
- Brand, U., Veizer, J. 1980. Chemical diagenesis of a multi component carbonate system: 1. Trace elements. *J. Sed. Petrol* 50, 1219-1236.
- Brasier, M.D., Lindsay, J.F., 1998. A billion years of environmental stability and the emergence of eukaryotes: new data from Northern Australia. *Geology* 26, 555-558.
- Brasier, M.D., Shields, G., Kuleshov, V.N., Zhegallo, E.A., 1996. Integrated chemo- and biostratigraphic calibration of early animal evolution: Neoproterozoic to early Cambrian, southwest Mongolia. *Geological Magazine* 133, 445-485.
- Bristow, T.F., Kennedy, M.J., 2008. Carbon isotope excursions and the oxidant budget of the Ediacaran atmosphere and ocean. *Geology* 36, 863-866.
- Brito Neves, B.B., Campos Neto, M.C., Fuck, R.A., 1999. From Rodinia to Western Gondwana: an approach to the Brasiliano-Pan African cycle and orogenic collage. *Episodes* 22, 155-166.
- Budd, G. E. 2008. The earliest fossil record of the animals and its significance. *Philosophical Transactions of the Royal Society B*, 363, 1425-1434.
- Buick, R., Des Marais, D.J., Knoll, A.H., 1995. Stable isotopic compositions of carbonates from the Mesoproterozoic Bangemall group, northwestern Australia. *Chem Geol.* 123, 153-171.
- Burchette, T.P., Wright, V.P., 1992. Carbonate ramp depositional systems, *Sedimentary Geol.* 79, 3-57.
- Burdett, J.W., Grotzinger, J.P., Arthur, M.A. 1990. Did major changes in stable isotope compositions of seawater occur? *Geology* 18, 227-230.
- Calver, C., 2000. Isotope stratigraphy of the Ediacaran (Neoproterozoic III) of the Adelaide rift complex, Australia, and the overprint of water column stratification. *Precambrian Res.* 100, 121-150.

Campal, N., Schipilov, A., 1998. Evolución paleogeográfica del nudo tectónico de puntas del Arroyo Mansavillagra durante el proceso de formación del Supercontinente Gondwana (1500 a 500 Ma). Volumen 2, Ciclo Grenvilliano. Fac. de Agronomía-CONICYT, Montevideo.

Campal, N., Schipilov, A., 1995. The Illescas bluish quartz rapakivi granite (Uruguay-South America): some geological features. In: Symp. Rapakivi Granites and Related Rocks, Belem, Brazil, p. 18.

Campal, N., Schipilov, A., 2005. La Formación Cerros de Aguirre: evidencias de magmatismo Vendiano en el Uruguay. *Lat. Amer. J. Sedimentol. Basin Anal.* 12, 161-174.

Canfield, D.E., Poulton, S.W., Knoll, A.H., Narbonne, G.M., Ross, G., Goldberg, T., Strauss, H., 2008. Ferruginous Conditions Dominated Later Neoproterozoic Deep-Water Chemistry. *Science* 321, 949-952.

Canfield, D.E., Poulton, S.W., Narbonne, G.M., 2007. Late-Neoproterozoic Deep-Ocean Oxygenation and the Rise of Animal Life. *Science* 315, 92-95.

Chu, X.L., Zhang, T.G., Zhang, Q.R., Lyons, T.W., 2007. Sulfur and carbon isotope records from 1700 to 800 Ma carbonates of the Jixian section, northern China: implications for secular isotope variations in Proterozoic seawater and relationships to global supercontinental events. *Geochim. Cosmochim. Acta* 71, 4668-4692.

Cingolani, C.A., Hartmann, L.A., Santos, J.O.S., McNaughton, N.J., 2012. U-Pb SHRIMP dating of zircons from the Buenos Aires Complex of the Tandilia Belt, Rio de la Plata Craton, Argentina. *Actas del XV Congreso Geológico Argentino*. El Calafate.

Clauer, N., Chaudhuri, S., 1995. *Clays in crustal environments: isotope dating and tracing*, Springer, Berlin.

Clayton, C.J., 1991. Effect of maturity on carbon isotope ratios of oils and condensates. *Org. Geochem.* 17, 887-899.

Condon, D., Zhu, M., Bowring, S., Wang, W., 2005. U-Pb ages from the Neoproterozoic Doushantuo Formation, China. *Science* 308, 95-98.

Coplen, T.B., Brand, W.A., Gehre, M., Groning, M., Meijer, H.A.J., Toman, B., Verkouteren, R.M., 2006. New guidelines for delta C-13 measurements. *Anal. Chem.* 78, 2439-2441.

Cordani, U.G., Sato, K., Teixeira, W., Tassinari, C.C.G., and Basei, M.A.S., 2000. Crustal evolution of the South American platform. In: Cordani, U.G., Milani, E.J., Thomaz-Filho, A., and Campos, D.A. (Eds.), *Tectonic evolution of South America*, pp. 19-40.

Cordani, U.G., Teixeira, W., D'Agrella-Filho, M.S., Trindade, R.I. 2009. The position of the Amazonian craton in supercontinents. *Gondw. Res.* 15, 396-407.

Cordani, U.G., Teixeira, W., Tassinari, C.C.G., Coutinho, J.M.V., Ruiz, A.S., 2010. The Rio Apa Craton in Mato Grosso do Sul (Brazil) and northern Paraguay: Geochronological evolution, correlations and tectonic implications for Rodinia and Gondwana. *A. Jour. Sci.* 310, 981-1023.

Cozzi, A., Allen, P.A., Grotzinger, J.P., 2004. Understanding carbonate ramp dynamics using  $\delta^{13}C$  profiles: examples from the Neoproterozoic Buah Formation of Oman. *Terra Nova* 16, 62-67.

Crank, J., 1975. *The Mathematics of Diffusion*, second ed. Oxford University Press, Oxford.

Cremonese, L., Shields-Zhou, G., Struck, U. Ling, H. F., Och, L., Chen, X., Li, D., 2013. Marine biogeochemical cycling during the early Cambrian constrained by a nitrogen and organic carbon isotope study of the Xiaotan section, south China. *Precambrian Res.* 225, 148-165.

Dalrymple, G.B., Lanphere, M.A, 1969. *Potassium-argon dating: principles, techniques and applications to geochronology*, W.H. Freeman, San Francisco.

DePaolo, D.J., Wasserburg, G.J., 1976. Nd isotopic variations and petrogenetic models. *Geophys. Res. Lett.* 3, 249-252.

Derry, L.A., 2010. A burial diagenesis origin for the Ediacaran Shuram-Wonoka carbon. *Earth Planet. Sci. Lett.* 294, 152-162.

Derry, L.A., Kaufman, A.J., Jacobsen, S.B., 1992. Sedimentary cycling and environmental change in the Late Proterozoic: evidence from stable and radiogenic isotopes. *Geochim. Cosmochim. Acta.* 56, 1317-1329.

Derry, L.A., Keto, L.S., Jacobsen, S.B., Knoll, A.H., Swett, K., 1989. Strontium isotopic variations in Upper Proterozoic carbonates from Svalbard and East Greenland. *Geochimica et Cosmochimica Acta* 53, 2331-2339.

Des Marais, D. J. 2001. Isotopic evolution of the biochemical carbon cycle during the Precambrian, in *Stable Isotope Geochemistry*, Rev. Mineral. Geochem., vol. 43, edited by J. W. Valley and D. R. Cole, pp. 556 - 578, Mineral. Soc. of Am., Washington, D. C.

Deuser W.G., 1970. Carbon-13 in Black Sea Waters and Implications for the Origin of Hydrogen Sulfide. *Science* 168, 1575-1577.

Deuser, W.G. 1970. Isotopic evidence for diminishing supply of available carbon during diatom bloom in the Black Sea. *Nature* 5237, 1069-71.

Donnadieu, Y., Ramstein, G., Fluteau, F., Roche, D., Ganopolski, A. 2004. The impact of atmospheric and oceanic heat transports on the sea-ice-albedo instability during the Neoproterozoic. *Climate Dynamics*, 22, 293-306.

Dott Jr, R.H., 1983. Episodic sedimentation; how normal is average? How rare is rare? Does it matter? *Journal of Sedimentary Research* 53, 5-23.

Dott Jr, R.H., Bourgeois, J., 1982. Hummocky stratification: significance of its variable bedding sequences. *GSA Bulletin* 93, 663-680.

Elizalde, G., 1979. Carta Geológica de la Costa. Conservación y Mejora de Playas. Ministerio de Transporte y Obras Públicas, Programa de las Naciones Unidas para el Desarrollo – UNESCO, Montevideo. pp. 101-235.

Escayola, M.P., Pimentel, M.M., Armstrong, R., 2007. Neoproterozoic backarc basin: sensitive high-resolution ion microprobe U-Pb and Sm-Nd isotopic evidence from the Eastern Pampean Ranges, Argentina. *Geology* 35, 495-498.

- Fairchild, I.J., Marshall, J.D., Bertrand-Sarfati, J. 1990. Stratigraphic shifts in carbon isotopes from Proterozoic stromatolitic carbonates (Mauritania): influences of primary mineralogy and diagenesis. *Amer. J. Sci.* 290-A, 46-79.
- Fambrini, G.L., Fragoso-Cesar, A.R.S., Almeida, R.P., Riccomini, C., 2005. A Formação Barriga Negra (Ediacarano do Uruguai): caracterização estratigráfica e correlação com unidades do Estado do Rio Grande do Sul, Brasil. *Rev. Brasil. Geoc.* 35, 515-524.
- Fanning, C.M., Link, P.K., 2004. U-Pb SHRIMP ages of Neoproterozoic (Sturtian) glaciogenic Pocatello Formation, southeastern Idaho. *Geology*, 32, 881-884.
- Fanning, C.M., Link, P.K., 2008. Age constraints for the Sturtian glaciation: data from the Adelaide Geosyncline, South Australia and Pocatello Formation, Idaho, USA. In: Gallagher, S.J., Wallace, M.W. (Eds.), *Neoproterozoic Extreme Climates and the Origin of Early Life*, Selwyn Symposium of the GSA Victoria Division. *Geol. Soc. Aust. Extended Abstr.* 91, 57-62.
- Fantin, M., 2003. *Geología de la Sierra de Aguirre, Departamento de Rocha, Uruguay*. Trabajo Final de la Licenciatura, Universidad de Buenos Aires, 92 pp.
- Favre, P., Stampfli, G.M., 1992. From rifting to passive margin: the examples of the Red Sea, Central Atlantic and Alpine Tethys. *Tectonophysics* 215, 69-97.
- Feng, L.J., Chu, X.L., Huang, J., Zhang, Q.R., Chang, H.J., 2010. Reconstruction of paleo-redox conditions and early sulfur cycling during deposition of the Cryogenian Datangpo Formation in South China, *Gondwana Res.*, 18, 632-637
- Fernades, L.A.D. Tommasi, A., Porcher, C.C., 1992. Deformation patterns in the southern Brazilian branch of the Dom Feliciano Belt: A reappraisal. *Jour. South Amer. Earth Sci.* 5, 77-96.
- Fernandes, L.A.D., Koester, E., 1999. The Neoproterozoic Dorsal de Canguçu strike-slip shear zone: its nature and role in the tectonic evolution of southern Brazil. *J. Afr. Earth Sci.* 29, 3-24.
- Fike, D.A., Grotzinger, J.P., Pratt, L.M., Summons, R.E., 2006. Oxidation of the Ediacaran ocean. *Nature* 444, 744-747.

- Font, E., Nedelec, A., Trindade, R.I.F., Macouin, M., Charrie`re, A. 2006. Chemostratigraphy of the Neoproterozoic Mirassol d'Oeste cap dolostones (Mato Grosso, Brazil): An alternative model for Marinoan cap dolostone formation. *Earth Planet. Sci. Lett.*, 250, 89-103.
- Fragoso-Cesar, A.R.S., 1980. O Cratón do Rio de la Plata e o Cinturão Dom Feliciano no Escudo Uruguaio-Sul-Rio-Grandense. *Soc. Bras. Geol.* 5, 2879-2892.
- Fragoso-Cesar, A.R.S., Machado, R.Y., Gómez Rifas, C., 1987. Observações sobre o Cinturão Dom Feliciano no Escudo Uruguaio e correlações com o Escudo do Rio Grande do Sul. In: III Symposium Sul-Brasileiro de Geologia, Curitiba, Brasil, Vol. 2, pp. 791-809.
- Francois, R., Altabet, M.A., Goericke, R., McCorkle, D.C., Brunet, C., Poisson, A., 1993. Changes in the  $\delta^{13}C$  of surface water particulate organic matter across the subtropical convergence in the S.W. Indian Ocean. *Global Biogeochemical Cycles* 7, 627-644.
- Frank, T. D., Lyons, T. W. 2000. The integrity of  $\delta^{18}O$  records in Precambrian carbonates: a Mesoproterozoic case study. In: Eds Grotzinger, J. P., Jame, N. P. Carbonate sedimentation and diagenesis in the evolving Precambrian world) 315-26. SEPM Special Publication no. 67.
- Frank, T.D., Kah, L.C., Lyons, T.W., 2003. Changes in organic matter production and accumulation as a mechanism for isotopic evolution in the Mesoproterozoic ocean. *Geol. Mag.* 140, 397-420.
- Frank, T.D., Lyons, T.W., Lohmann, K.C., 1997. Isotopic evidence for the paleoenvironmental evolution of the Mesoproterozoic Helena Formation, Belt Supergroup, USA. *Geochim. Cosmochim. Acta* 61, 5023-5041.
- Freeman, K. H., Hayes, J. M. 1992. Fractionation of carbon isotopes by phytoplankton and estimates of ancient CO<sub>2</sub> levels, *Global Biochemical Cycles*, 6, 185-198.
- Frei, R., Gaucher, C., Canfield, D.E., Poulton, S.W. 2009. Fluctuations in Precambrian atmospheric oxygenation recorded by chromium isotopes. *Nature* 461, 250-253.

- Frei, R., Gaucher, C., Døssing, L.N., Sial, A.N., 2011. Chromium isotopes in carbonates - A tracer for climate change and for reconstructing the redox state of ancient seawater. *Earth Planet. Sci. Lett.* 312, 114-125.
- Frei, R., Gaucher, C., Stolper, D., Canfield, D.E., 2013. Fluctuations in late Neoproterozoic atmospheric oxidation - Cr isotope chemostratigraphy and iron speciation of the late Ediacaran lower Arroyo del Soldado Group (Uruguay). *Gondw. Res.* 23, 797-811.
- Frimmel, H.E., 2009. Trace element distribution in Neoproterozoic carbonates as palaeoenvironmental indicator. *Chem. Geol.* 258, 338-353.
- Fuck, R.A., Brito Neves, B.B., Schobbenhaus, C., 2008. Rodinia descendants in South America. *Prec. Res.* 160, 108-126.
- Galimov, E.M., 2004. The pattern of  $\delta^{13}C_{org}$  versus HI/OI relation in recent sediments as an indicator of geochemical regime in marine basins: comparison of the Black Sea, Kara Sea, and Cariaco Trench. *Chem. Geol.* 204, 287-301.
- Gastal, M.C.P., Lafon, J.M., Hartmann, L.A., Koester, E., 2005. Sm-Nd isotope compositions as a proxy for magmatic processes during the Neoproterozoic of southern Brazilian shield. *J. South Am. Earth Sci.* 18, 255-276.
- Gaucher, C., 2000. Sedimentology, paleontology and stratigraphy of the Arroyo del Soldado Group (Vendian to Cambrian, Uruguay). *Beringeria* 26, 1-120.
- Gaucher, C., Sprechmann, P., Schipilov, A., 1996. Upper and Middle Proterozoic fossiliferous sedimentary sequences of the Nico Pérez Terrane of Uruguay: Lithostratigraphic units, paleontology, depositional environments and correlations. *N. Jb. Geol. Paläontol. Abh.* 199, 339-367.
- Gaucher, C., Sprechmann, P., Montaña, J., 1998. New advances in the geology and paleontology of the Vendian to Cambrian Arroyo del soldado Group of the Nico Perez Tarrane of Uruguay. *N. Jb. Geol. Paläont. Mh.* 2, 106-118.
- Gaucher, C., Boggiani, P., Sprechmann, P., Sial, A.N., Fairchild, T., 2003. Integrated correlation of the Vendian to Cambrian Arroyo del Soldado and Corumbá Groups

(Uruguay and Brazil): paleogeographic, paleoclimatic and paleobiologic implications. *Prec. Res.* 120, 241-278.

Gaucher, C., Chiglino, L., Pecoits, E., 2004. Southernmost exposures of the Arroyo del Soldado Group (Vendian to Cambrian, Uruguay): palaeogeographic implications for the amalgamation of W-Gondwana. *Gondw. Res.* 3, 701-714.

Gaucher, C., Sial, A.N., Blanco, G., Sprechmann, P., 2004. Chemostratigraphy of the lower Arroyo del Soldado Group (Vendian, Uruguay) and paleoclimatic implications. *Gondw. Res.* 7, 715-730.

Gaucher, C., Blanco, G., Chiglino, L., Poiré, D., Germs, G.J.B., 2008. Acritarchs of the Las Ventanas Formation (Ediacaran, Uruguay): Implications for the timing of coeval rifting and glacial events in western Gondwana. *Gondw. Res.* 13, 488-501.

Gaucher, C., Sial, A.N., Poiré, D., Gómez-Peral, L., Ferreira, V.P., Pimentel, M.M., 2009. Chemostratigraphy. In: Gaucher, C., Sial, A.N., Halverson, G.P. and Frimmel, H.E. (Eds.), Neoproterozoic-Cambrian tectonics, global change and evolution: a focus on southwestern Gondwana. *Developments in Precambrian Geology* 16, Elsevier, Amsterdam, 115-122.

Gaucher, C., Poiré, D., 2009. Biostratigraphy. Neoproterozoic-Cambrian evolution of the Río de la Plata Palaeocontinent. In: Gaucher, C., Sial, A.N., Halverson, G.P., Frimmel, H.E. (Eds.), Neoproterozoic-Cambrian tectonics, global change and evolution: a focus on southwestern Gondwana. *Develop. Prec. Geol.* 16, 103-114.

Gaucher, C., Frei, R., Chemale, Jr.F., Frei, D., Bossi, J., Martínez, G., Chiglino, L., Cernuschi, F., 2011. Mesoproterozoic evolution of the Rio de la Plata Craton in Uruguay: at the heart of Rodinia? *Int. J. Earth Sci. (Geol Rundsch)* 100, 273-288.

Gaucher, C., Poiré, D.G., Bossi, J., Bettucci S.L., Beri, A. 2013. Comment on "Bilaterian Burrows and Grazing Behavior at >585 Million Years Ago". *Science* 339, 906.

Germs, G.J.B., 1972. New shelly fossils from Nama Group, South West Africa. *American Journal of Science* 272, 752-761.

Geyer, G. 2005. The Fish River Subgroup in Namibia: stratigraphy, depositional environments and the Proterozoic-Cambrian boundary problem revisited. *Geol. Mag.*, 142, 465-498.

Giordano, M., Beardall, J., Raven, J. A., 2005. CO<sub>2</sub> concentrating mechanisms in algae: mechanisms, environmental modulation, and evolution. *Annu. Rev. Plant Biol.* 56, 99-131.

Goldstein, S.J., Jacobsen, S.B., 1988. Nd and Sr isotopic systematics of river water suspended material: implications for crustal evolution. *Earth and Planetary Science Letters* 87, 249-265.

Goldstein, S.L., O’Nions, R.K., Hamilton, P.J., 1984. A Sm-Nd isotopic study of atmospheric dusts and particulates from major river systems. *Earth Planet. Sci. Lett.* 70, 221-236.

Goñi, J.C., Hoffstetter, R., 1964. Uruguay. In: Hoffstetter, R. (Ed.) *Lexique stratigraphique international*. Centre National de la Recherche Scientifique, Paris, France, Fascicule 9a, pp. 1-202.

Gorokhov, I. M., Semikhatov, M. A., Baskakov, A. V., 1995. Sr Isotopic Composition in Riphean, Vendian, and Lower Cambrian Carbonates from Siberia, *Stratigr. Stratigr. Geol. Correlation* 3 (1), 1-29.

Gradstein, F. J., Ogg, A., Smith, A., 2004. *Geologic Time Scale*, Cambridge University Press, Cambridge.

Gradstein, F.M., Ogg, J.G., Schmitz, M., Ogg, G., 2012. *Geological Time Scale*. Cambridge University Press, Cambridge, pp. 413-435.

Grey, K., Calver, C.R., 2007. Correlating the Ediacaran of Australia. *Geol. Soc. London, Spec. Pub.* 286, 115-135.

Gross, A.O.M.S., Droop, G.T.R., Porcher, C.C., Fernandes, L.A.D., 2009. Petrology and thermobarometry of mafic granulites and migmatites from the Chafalote Metamorphic Suite: new insights into the Neoproterozoic P-T evolution of the Uruguayan-Sul-Rio-Grandense Shield. *Prec. Res.* 170, 157-174.

Grotzinger, J.P., Bowring, S.A., Saylor, B.Z., Kaufman, A.J., 1995. Biostratigraphic and geochronologic constraints on early animal evolution. *Science* 270, 598-604.

Guo, H., Du, Y.S., Kah, L.C., Huang, J.H., Hu, C.Y., Huang, H., Yu, W.C., 2013. Isotopic composition of organic and inorganic carbon from the Mesoproterozoic Jixian Group, North China: implications for biological and oceanic evolution. *Precambrian Res.* 224, 169-183.

Halls, H.C., Campal, N., Davis, D.W., Bossi, J., 2001. Magnetic studies and U–Pb geochronology of the Uruguayan dyke swarm, Río de la Plata craton, Uruguay: paleomagnetic and economic implications. *J. South A. Earth Sci.* 14, 349-361.

Halverson, G.P., Hoffman, P.F., Schrag, D.P., Kaufman, J.A., 2002. A major perturbation of the carbon cycle before the Ghaub glaciation (Neoproterozoic) in Namibia: prelude to snowball earth? *Geophys. Geochem. Geosystems*, 3, 16.

Halverson, G.P., Hoffman, P.F., Schrag, D.P., Maloof, A.C., Rice, A.H.N., 2005. Toward a Neoproterozoic composite carbon-isotope record. *Geological Society of America Bulletin* 117, 1181-1207.

Halverson, G. Maloof, A.C., Schrag, D.P., Dudas, F.O., Hurtgen, M., 2007. Stratigraphy and geochemistry of a ca 800 Ma negative carbon isotope interval in northeastern Svalbard. *Chem. Geol.* 237, 23-45.

Halverson, G.P., Dudas, F.O., Maloof, A.C. and Bowring, S.A., 2007. Evolution of the  $^{87}\text{Sr}/^{86}\text{Sr}$  composition of the Neoproterozoic seawater. *Paleogeography Paleoclimatology Paleoecology* 256, 103-129.

Halverson, G.P., Hurtgen, M.T., Porter, S.M., Collins, A.C., 2010. Neoproterozoic-Cambrian biogeochemical evolution. In: Gaucher, C., Sial, A.N., Halverson, G.P. and Frimmel, H.E. (Eds.), *Neoproterozoic-Cambrian tectonics, global change and evolution: a focus on southwestern Gondwana. Developments in Precambrian Geology* 16, Elsevier, Amsterdam, 351-356.

Halverson, G.P., Hurtgen, M.T., Porter, S.M., Collins, A.C., 2010. Neoproterozoic-Cambrian biogeochemical evolution. In: Eds. Gaucher, C., Sial, A.N., Halverson G.P.,

Frimmel, H., Neoproterozoic-Cambrian tectonics, global change and evolution: a focus on southwestern Gondwana. *Dev. Precambrian Geol.*, 16, 351-356. Elsevier.

Hart, B.S., Plint, A.G., 1989. Gravelly shoreface deposits: a comparison of modern and ancient sequences. *Sedimentology* 36, 551-557.

Hartmann, L.A., Campal, N., Santos, J.O.S., McNaughton, N.J., Bossi, J., Schipilov, A., Lafon, J.-M., 2001. Archean crust in the Rio de la Plata Craton, Uruguay-SHRIMP U-Pb zircon reconnaissance geochronology. *J. South Am. Earth Sci.* 14, 557-570.

Hartmann, L.A., Philipp, R.P., Liu, D., Wan, Y., Wang, Y., Santos, J.O., Vasconcellos, M.A.Z., 2004. Paleoproterozoic magmatic provenance of detrital zircons, Porongos Complex Quartzites, Southern Brazilian Shield. *International Geology Review*, 46, 127-157.

Hartmann, L.A., Piñeyro, D., Bossi, J., Leite, J.A.D., Mcnaughton, N.J., 2000. Zircon U-Pb SHRIMP dating of Paleoproterozoic Isla Mala granitic magmatism in the Rio de la Plata Craton, Uruguay. *J. South A. Earth Sci.* 13, 105-113.

Hartmann, L.A., Santos, J.O., Bossi, J., Campal, N., Schipilov, A., Mac Naughton, N. J., 2002. Zircon and titanite U-Pb SHRIMP geochronology of Neoproterozoic felsic magmatism on the eastern border of the Río de la Plata Craton, Uruguay. *J. South Am. Earth Sci.* 15, 229-236.

Hasui Y., Cameiro C. dal R., Coimbra A.M., 1975. The Ribera Folded Belt. *Rev. Bras. Geoc.* 5, 257-266.

Hayes, J.M, 1993. Factors controlling  $\delta^{13}C$  contents of sedimentary compounds: principles and evidence *Mar Geol* 113 111-125.

Hayes, J.M., Strauss, H., Kaufman, A.J. 1999. The abundance of  $\delta^{13}C$  in marine organic matter and isotopic fractionation in the global biogeochemical cycle of carbon during the past 800 Ma. *Chem. Geol.* 161, 103-125.

Heaman, L.M. 1989. The nature of the subcontinental mantle from Sr-Nd-Pb isotopic studies on kimberlitic perovskite. *Earth Planet. Sci. Lett.* 92, 323-334.

- Hill, A.C., Arouri, K., Gorjan, P., Walter, M.R., 2000. Geochemistry of marine and nonmarine environments of a Neoproterozoic cratonic carbonate- evaporite: the Bitter Springs Formation, Central Australia. In: Eds. Grotzinger, J.P., James, N.P., Carbonate Sedimentation and Diagenesis in the Evolving Precambrian World. SEPM Special Publications, 67, 327-344.
- Hinrichs, K.U., 2003. Microbial fixation of methane carbon at 2.7 Ga: was an anaerobic mechanism possible? *Geochem. Geophys. Geosyst.* 3 (7). doi:10.1029/ 2001GC000286.
- Hoffman, P.F. & Schrag, D.P., 2000. Snowball Earth. *Scientific American* 282, 68-75.
- Hoffmann, K.-H., Condon, D.J., Bowring, S.A., Crowley, J.L., 2004. U-Pb zircon date from the Neoproterozoic Ghaub Formation, Namibia: constraints on Marinoan glaciation. *Geology*, 32, 817-820.
- Holmden, C., Creaser, R.A., Muehlenbachs, K., Leslie, S.A., Bergstrom, S.M., 1996. Isotopic and elemental systematics of Sr and Nd in 454 Ma biogenic apatites: implications for paleoseawater studies. *Earth Planet. Sci. Lett.* 142, 425-437.
- Horodyski, R.J., Knauth, L.P., 1994. Life on Land in the Precambrian. *Science* 263, 494-498.
- Hua, H., Chen, Z., Yuan, X., Zhang, L. and Xiao, S., 2005. Skeletogenesis and asexual reproduction in the earliest biomineralizing animal Cloudina. *Geology* 33, 277-280.
- Huon, S., Cornee, J.J., Pique, A., Rais, N., Clauer, N., Liewig, N., Zayane, R., 1993. Mise en évidence au Maroc d'événements thermiques d'âge triasico-liasique à l'ouverture de l'Atlantique. *Bulletin de la Société Géologique de France* 164, 165-176.
- Hurtgen, M.T., Halverson, G.P., Arthur, M.A., Hoffman, P.F. 2006. Sulfur cycling in the aftermath of a 635-Ma snowball glaciation: Evidence for a synglacial sulfidic deep ocean. *Earth Planet. Sci. Lett.*, 245, 551- 570.
- Hyde, W. T., Crowley, T. J., Baum, S. K., Peltier, W.R., 2000. Neoproterozoic "Snowball Earth" simulations with a coupled climate/ice sheet model. *Nature*, 405, 425-430.
- Ishikawa, T., Ueno, Y., Komiya, T., Sawaki, Y., Han, J., Shu, D., Li, Y., Maruyama, S., Yoshida, N., 2008, Carbon isotope chemostratigraphy of a Precambrian/Cambrian

boundary section in the Three Gorge area, South China: Prominent global-scale isotope excursions just before the Cambrian Explosion. *Gondwana Research* 14, 193-208.

Jacobsen, S.B., Kaufman, A.J. 1999. The Sr, C and O isotopic evolution of Neoproterozoic seawater. *Chem. Geol.* 161, 37-57.

Jaffey, A.H., Flynn, K.F., Glendenin, L.E., Bentley, W.C., Essling, A. M., 1971. Precision measurement of half-lives and specific of <sup>235</sup>U and <sup>238</sup>U. *Phys. Rev. C*4, 1889-1906.

Janikian, L., Almeida, R.P., Fragoso-Cesar, A.R.S., Souza Martins, V.T., Dantas, E.L., Tohver, E., McReath, I., D'Agrella-Filho, M.S., 2012. Ages (U–Pb SHRIMP and LA ICPMS) and stratigraphic evolution of the Neoproterozoic volcano-sedimentary successions from the extensional Camaquã Basin, Southern Brazil. *Gondw. Res.* 21, 466-482.

Javaux, E.J., Knoll, A.H., Walter, M.R., 2001. Morphological and ecological complexity in early eukaryotic ecosystems. *Nature* 412, 66-69.

Javaux, E.J., Knoll, A.H., Walter, M.R., 2004. TEM evidence for eukaryotic diversity in mid-Proterozoic oceans. *Geobiology* 2, 121-132.

Jiang, G., Kaufman, A. J., Christie-Blick, N., Zhang, S., Wu, H., 2007. Carbon isotope variability across the Ediacaran Yangtze platform in South China: Implications for a large surface-to-deep ocean gradient. *Earth and Planetary Science Letters* 261, 303-320.

Jiang, G., Kennedy, M.J., Christie-Blick, N., 2003. Stable isotopic evidence for methane seeps in Neoproterozoic postglacial cap carbonates. *Nature* 426, 822-826.

Jiang, G., Shi, X., Zhang, S., Wang, Y., Xiao, S. 2011. Stratigraphy and paleogeography of the Ediacaran Doushantuo Formation (ca. 635-551 Ma) in South China. *Gondw. Res.* 19, 831-849.

Johansson, A., 2014. From Rodinia to Gondwana with ‘SAMBA’ model – A distant view from Baltica towards Amazonia and beyond. *Prec. Res.* 244, 226-235.

Johnston, D.T., Macdonald, F.A., Gill, B.C., Hoffman, P.F., Schrag, D.P., 2012. Uncovering the Neoproterozoic carbon cycle. *Nature*, 483, 320-323.

Johnston, D.T., Poulton, S.W., Goldberg, T., Sergeev, V.N., Podkovyrov, V., Vorob'eva, N.G., Bekker, A., Knoll, A.H., 2012. Late Ediacaran redox stability and metazoan evolution. *Earth Planet. Sci. Lett.*, 335-336, 25-35.

Kah, L.C., 2000. Preservation of depositional  $\delta^{18}\text{O}$  signatures in Proterozoic dolostones: geochemical constraints on seawater chemistry and early diagenesis. In: Eds. Grotzinger, J.P., James, N.P., *Precambrian Carbonates*, vol. 65. SEPM, Tulsa, OK, 345-360.

Kah, L.C., Crawford, D.C., Bartley, J.K., Kozlov, V.I., Sergeeva, N.D., Puchkov, V.N., 2007. C- and Sr-isotope chemostratigraphy as a tool for verifying age of Riphean deposits in the Kama-Belaya aulacogen, the east European platform. *Stratigr. Geol. Correl.* 15, 12–29.

Kasemann, S.A., Hawkesworth, C.J., Prave, A.R., Fallick, A.E., and Pearson, P.N., 2005. Boron and calcium isotope composition in Neoproterozoic carbonate rocks from Namibia: evidence for extreme environmental change. *Earth Planet. Sci. Lett.* 231, 73-86.

Kaufman, A.J. and Xiao, S., 2003. High  $\text{CO}_2$  levels in the Proterozoic atmosphere estimated from analyses of individual microfossils. *Nature* 424, 279-282.

Kaufman, A.J., Knoll, A.H., 1995. Neoproterozoic variations in the carbon isotopic composition of seawater: Stratigraphic and biogeochemical implications. *Precambrian Res.* 73, 27-49.

Kaufman, A.J., Xiao, S., 2003. High  $\text{CO}_2$  levels in the Proterozoic atmosphere estimated from analyses of individual microfossils. *Nature* 424, 279-282.

Kaufman, A.J., Corsetti, F.A., Varni, M.A., 2007. The effect of rising atmospheric oxygen on carbon and sulfur isotope anomalies in the Neoproterozoic Johnnie Formation, Death Valley, USA. *Chem. Geol.* 237, 47-63.

Kaufman, A.J., Hayes, J.M., Knoll, A.H., Germs, G.J.B., 1991. Isotopic compositions of carbonates and organic carbon from upper Proterozoic successions in Namibia: stratigraphic variation and the effects of diagenesis and metamorphism. *Precambrian Res.* 49, 301-327.

Kaufman, A.J., Jacobsen, S.B., Knoll, A.H., 1993. The Vendian record of Sr and C isotopic variations in seawater: Implications for tectonics and paleoclimate. *Earth Planet. Sci. Lett.* 120, 409-430.

Kaufman, A.J., Knoll, A.H., Narbonne, G.M., 1997. Isotopes, ice ages, and terminal Proterozoic Earth history. *Proceedings of the National Academy of Science U.S.A.* 94, 6600-6605.

Kawashita, K., Gaucher, C., Sprechmann, P., Teixeira, W., Victória, R., 1999. Preliminary chemostratigraphic insights on carbonate rocks from Nico Pérez Terrane (Uruguay), In: *Actas II South American Symposium on Isotope Geology*, Córdoba, Argentina, pp. 399-402.

Kawashita, K., Gaucher, C., Sprechmann, P., Teixeira, W., Victória, R., 1999. Preliminary chemostratigraphic insights on carbonate rocks from Nico Pérez Terrane (Uruguay), In: *Actas II South American Symposium on Isotope Geology*, Córdoba, pp. 399-402.

Kendall, B., Creaser, R.A., Calver, C.R., Raub, T.D., Evans, D.A.D., 2009, Correlation of Sturtian diamictite successions in southern Australia and northwestern Tasmania by Re-Os black shale geochronology and the ambiguity of “Sturtian”- type diamictite-Cap carbonate pairs as chronostratigraphic marker horizons. *Precambrian Research*, 172, 301-310.

Kendall, B., Creaser, R.A., Selby, D., 2006. Re-Os geochronology of postglacial black shales in Australia: constraints on the timing of “Sturtian” glaciation. *Geology*, 34, 729-732.

Kennedy, M.J., Runnegar, B., Prave, A.R., Hoffmann, K.H., Arthur, M.A. 1998, Two or four Neoproterozoic glaciations?: *Geology*, v. 26, p. 1059-1063.

Khabarov, E.M., Varaksina, I.V., 2011. The structure and depositional environments of Mesoproterozoic petroliferous carbonate complexes in the western Siberian craton. *Russ. Geol. Geophys.* 52, 923-944.

Kienast, M., Calvert, S.E., Pelejero, C., Grimalt, J.O., 2001. A critical review of marine sedimentary  $\delta^{13}\text{C}_{\text{org-pCO}_2}$  estimates: New palaeorecords from the South China Sea and

a revisit of other low-latitude  $\delta^{13}\text{C}_{\text{org}}$ -pCO<sub>2</sub> records. *Global Biogeochemical Cycles* 15, 113-127.

Knauth, L.P., Martin, J.K., 2009. The late Precambrian greening of the Earth. *Nature* 460, 728-732.

Knoll, A.H., Walter, M.R., Narbonne, G.M., Christie-Blick, N., 2004. A new Period for the geologic time scale. *Science* 3005, 621-622.

Knoll, A.H., Hayes, J.M., Kaufman, A.J., Swett, K., Lambert, I.B., 1986. Secular variation in carbon isotope ratios from Upper Proterozoic successions of Svalbard and East Greenland. *Nature* 321, 832-838.

Knoll, A.H., Kaufman, A.J., Semikhatov, M.A., 1995. The carbon-isotopic composition of Proterozoic carbonates: Riphean successions from north-western Siberia (Anabar Massif, Turukhansk Uplift). *Am. J. Sci.* 295, 823-850.

Knoll, A.H., Walter M.R., Narbonne, G.M., Christie-Blick, N. 2006. The Ediacaran period: a new addition to the geologic time scale. *Lethaia* 39, 13-30.

Knoll, A.H., Walter, M.R., 1992. Latest Proterozoic stratigraphy and Earth history. *Nature* 356, 673-678.

Konopásek, J., Košler, J., Sláma, J., Janoušek, V. 2014. Timing and sources of pre-collisional Neoproterozoic sedimentation along the SW margin of the Congo Craton (Kaoko Belt, NW Namibia). *Gondw. Res.* 26, 386-401.

Kröner, A., Cordani, U., 2003. African, southern Indian and South American cratons were not part of the Rodinia supercontinent: evidence from field relationships and geochronology. *Tectonophysics* 375, 325-352.

Kroopnick, P.M., 1985. The distribution of  $^{13}\text{C}$  of  $\Sigma\text{CO}_2$  in the world oceans. *Deep-Sea Research* 32, 57-84.

Kump, L.R., Arthur, M.A. 1999. Interpreting carbon-isotope excursions: carbonates and organic matter. *Chem. Geol.* 161, 181-198.

Kuznetsov, A.B., Ovchinnikova, G.V., Semikhatov, M.A., Gorokhov, I.M., Kaurova, O.K., Krupenin, M.T., Vasileva, I.M., Gorokhovskii, B.M., Maslov, A.V., 2008, The Sr

isotopic characterization and Pb-Pb age of carbonate rocks from the Satka formation, the Lower Riphean Burzyan Group of the southern Urals. *Stratigraphy and Geological Correlation*, 16 (2), 120-137.

Kvenvolden, K.A., 1995. A review of the geochemistry of methane in natural gas hydrate. *Org Geochem* 23: 997-1008.

Laws, E.A., Popp, B.N., Bidigare, R.R., Kennicutt, M.C., Macko, S.A., 1995. Dependence of phytoplankton carbon isotopic composition on growth rate and [CO<sub>2</sub>]<sub>aq</sub>: theoretical considerations and experimental results. *Geochim. Cosmochimica Acta* 59, 1131-1138.

Le Guerroué, E., 2010. Duration and synchronicity of the largest negative carbon isotope excursion on Earth: The Shuram/Wonoka anomaly. *Comptes Rendus Geosc.* 342, 204-214.

Le Guerroué, E., Allen, P.A., Cozzi, A., Etienne, J.L., Fanning, C., 2006. 50 Myr recovery from the largest negative c excursion in the Ediacaran ocean. *Terra Nova* 18, 147-153.

Lee, C., Fike, D.A., Love, G.D., Sessions, A.L., Grotzinger, J.P., Summons, R.E., Fischer, W.W., 2013. Carbon isotopes and lipid biomarkers from organic-rich facies of the Shuram Formation, Sultanate of Oman. *Geobiology* 11, 406-19.

Lehmann M F, Bernasconi S M, Barbieri A, et al. 2002. Preservation of organic matter and alteration of its carbon and nitrogen isotope composition during simulated and in situ early sedimentary diagenesis. *Geochim Cosmochim Acta* 66: 3573-3584

Leite, J.A.D., Hartmann, L.A., McNaughton, N.J., Chemale F.Jr., 1998. SHRIMP U-Pb Zircon geochronology of Neoproterozoic juvenile and crustal-reworked terranes in southernmost Brazil. *Int. Geol. Rev.* 40, 688-705.

Lenz, C., Fernandes, L.A.D., McNaughton, N.J., Porcher, C.C., and Masquelin, H., 2011. Magmatic and metamorphic U-Pb SHRIMP ages in zircons for the Cerro Bori Orthogneisses, Dom Feliciano Belt in Uruguay. *Prec. Research* 185, 149-163.

- Lewis, M. A., Weber, D. E., Goodman, L. R., Stanley, R. S., Craven, W. G., Patrick, J. M., Quarles, R. L., Roush, T. H., Macauley, J. M. 2000. Periphyton and sediment bioassessment in north Florida Bay, *Environ. Monit. Assess.*, 65(3), 503-522.
- Li, C., Peng, P.A., Sheng, G.Y., Fu, J.M., Yan, Y.Z., 2003. A molecular and isotopic geochemical study of Meso-to Neoproterozoic (1.73–0.85 Ga) sediments from the Jixian section, Yanshan Basin, North China. *Precambrian Res.* 125, 337-356.
- Li, Z.X., Bogdanova, S.V., Collins, A.S., Davidson, A., De Waele, B., Ernst, R.E., Fitzsimons, I.C.W., Fuck, R.A., Gladkochub, D.P., Jacobs, J., Karlstrom, K.E., Lu, S., Natapov, L.M., Pease, V., Pisarevsky, S.A., Thrane, K., Vernikovsky, V., 2008. Assembly, configuration, and break-up history of Rodinia: a synthesis. *Prec. Res.* 160, 179-210.
- Liew, T.C., Hofmann, A.W., 1988. Precambrian crustal components, plutonic associations, plate environment of the Hercynian Fold Belt of Central Europe: indications from a Nd and Sr isotopic study. *Contr. Miner. Petr.* 98, 129-138.
- Liewig, N., Clauer, N., Sommer, F., 1987. Rb-Sr and K-Ar dating of clay diagenesis in Jurassic sandstone oil reservoirs, North Sea. *AAPG Bulletin* 71, 1467-1474.
- Lindsay, J.F., Brasier, M.D., 2000. A carbon isotope reference curve for ca. 1700-1575 Ma, McArthur and Mount Isa Basins, Northern Australia. *Precambrian Res.* 99, 271- 308.
- Longerich, H.P., Jenner, G.A., Fryer, B.J., Jackson, S.E., 1990. Inductively coupled plasma-mass spectrometric analysis of geological samples; a critical evaluation based on case studies. *Chemical Geology* 83, 105-118.
- Ludwig K.R., 2008. *Isoplot version 3.7, User's Manual*, Berkeley Geochronology Center Special Publication 4.
- Luo, G., Junium, C. K., Kump, L.R.; Huang, J., Li, C., Feng, Q., Shi, X., Bai, X., and Xie, S., 2014. Shallow stratification prevailed for ~1700 to ~1300 Ma ocean: Evidence from organic carbon isotopes in the North China Craton, *Earth and Planetary Science Letters* 400, 219-232.
- Lyons, T., Reinhard, C., Planavsky, N., 2014. The rise of oxygen in Earth's early ocean and atmosphere. *Nature*, 506, 307-315.

- Macdonald, F. A., Schmitz, M. D. et al. 2010. Calibrating the Cryogenian. *Science*, 327, 1241-1243.
- Macdonald, F.A., Jones, D.S. Schrag, D.P., 2009. Stratigraphic and tectonic implications of a newly discovered glacial diamictite-cap carbonate couplet in southwestern Mongolia. *Geology* 37, 123-126.
- Mahan, K.H., Wernicke, B.P., and Jercinovic, M.J., 2010. Th-U-total Pb geochronology of authigenic monazite in the Adelaide rift complex, South Australia, and implications for the age of the type Sturtian and Marinoan glacial deposits. *Earth Planet. Sci. Lett.*, 289, 76-86.
- Mallmann, G., Chemale Jr.F., Avila, J.N., Kawashita, K., Armstrong, R., 2007. Isotope geochemistry and geochronology of the Nico Perez Terrane, Río de La Plata Craton, Uruguay. *Gondw. Res.* 12, 489-508.
- Marshall, J.D. 1992. Climatic and oceanographic isotopic signals from the carbonate rock record and their preservation. *Geological Magazine*, 129,143-160.
- Martin, M.W., Grahdankin, D.V., Bowring, S.A., Evans, D.A.D., Fedonkin, M.A., Kirschvink, J.L., 2000. Age of Neoproterozoic bilaterian body and trace fossils, White Sea, Russia: Implications for metazoan evolution. *Science* 288, 841-845.
- Maruyama, S., Santosh, M., 2008. Models on Snowball Earth and Cambrian explosion: A synopsis. *Gondwana Research* 14, 22-32.
- Masquelin, H., 1990. Análisis estructural de las zonas de cizalla en las migmatitas de Punta del Este-Uruguay. *Acta Geol. Leopold.* 30, 139-158.
- Masquelin, H., Tabó, M., 1988. Carta Geologica del Uruguay, Escala 1/100.000, Hoja Carape, E-26. DINAMIGE-UdelaR, Montevideo, pp. 11.
- Masquelin, H., Pías, J., 1989. Carta geológica de las Hojas San Carlos - Punta del Este, escala 1:100.000. DINAMIGE, Montevideo.
- Masquelin, H., Sánchez-Bettucci, L., 1993. Propuesta de evolución tectono-sedimentaria para la fosa tardi-brasiliana en la región de Piriápolis, Uruguay. *Rev. Brasil. Geocienc.* 23, 313-322.

- Masquelin, H., 2004. El Complejo Cerro Olivo, Sureste de Uruguay: una revisión estratigráfica y tectónica. In: IV Congreso Uruguayo de Geología Actas CD-ROM version. Montevideo, Uruguay.
- Masquelin, H., Fernandes, L.A.D., Lenz, C., Porcher, C.C., McNaughton, N.J., 2011. The Cerro Olivo Complex: a pre-collisional Neoproterozoic magmatic arc in Eastern Uruguay. *Int. Geol. Rev.* 54, 1161-1183.
- Mazzuchelli, M., Rivalenti, G., Piccirillo, E.M., Girardi, V.A.V., Civetta, L., Petrini, R., 1995. Petrology of the Proterozoic mafic dyke swarms of Uruguay and constraints on their mantle source composition. *Prec. Res.* 74, 177-194.
- McArthur, J.M., Burnell, J.A., Hancock, J.M. 1992. Sr isotopes at the Cretaceous/Tertiary boundary. *Nature*, 355, 28.
- McCall, G.J.H., 2006. The Vendian (Ediacaran) in the geological record: Enigmas in geology's prelude to the Cambrian explosion. *Earth Sci. Rev.* 77, 1-229.
- McCrea, J.M., 1950. On the isotopic chemistry of carbonates and a paleothermometer scale. *J. Chem. Phys.* 5, 48-51.
- McDougall, I., Harrison T.M., 1999. *Geochronology and Thermochronology by the  $^{40}\text{Ar}/^{39}\text{Ar}$  method*, second ed. Oxford University Press, Oxford.
- McDougall, I., Roksandic, Z., 1974. Total fusion  $^{40}\text{Ar}/^{39}\text{Ar}$  ages using HIFAR reactor. *Journal of the Geological Society of Australia* 21, 81-89.
- McFadden, K.A., Huang, J., Chu, X., Jiang, G., Kaufman, A.J., Zhou, C., Yuan, X., Xiao, S., 2008. Pulsed oxidation and biological evolution in Ediacaran Doushantuo Formation. *Proceedings of the National Academy of Science U.S.A.* 105, 3197-3202.
- McKirdy, D., Burgess, J., Lemon, N., Yu, X., Cooper, A., Gostin, V., Jenkins, R., Both, R., 2001. A chemostratigraphic overview of the late Cryogenian interglacial sequence in the Adelaide Fold-Thrust Belt, South Australia. *Precambrian Res.* 106, 149-186
- Meert, J.G., Lieberman, B.S., 2008. The Neoproterozoic assembly of Gondwana and its relationship to the Ediacaran-Cambrian radiation. *Gondwana Research* 14, 5-21.

Melezhik, V.A., Gorokhov, I.M., Kuznetsov, A.B., Fallick, A.E. 2001. Chemostratigraphy of Neoproterozoic carbonates: implications for 'blind dating'. *Terra Nova*. 13, 1-11.

Melezhik, V.A., Gorokhov, I.M., Kuznetsov, A.B., Fallick, A.E., 2001. Chemostratigraphy of Neoproterozoic carbonates: implications for 'blind dating'. *Terra Nova* 13, 1-11.

Midot, D., 1984. Etude geologique et diagnostic metallogénique pour l'exploration du secteur de Minas (Uruguay). Diplome de Docteur de 3e Cycle. Université Pierre et Marie Curie, Paris.

Miyachi, S., Iwasaki, I., Shiraiwa, Y., 2003. Historical perspective on microalgal and cyanobacterial acclimation to low- and extremely high-CO<sub>2</sub> conditions. *Photosynth Res* 77, 139-153.

Montaña, J., Sprechmann, P., 1993. Calizas estromatolíticas y oolíticas y definición de la Formación Arroyo de la Pedrera (?Vendiano, Uruguay). *Rev. Brasil. Geocienc.* 23, 306-312.

Montañez, I.P., Banner, J.L., Osleger, D.A., Borg, L.E., Bosserman, P.J., 1996. Integrated Sr isotope variations and sea-level history of Middle to Upper Cambrian platform carbonates: Implications for the evolution of Cambrian seawater <sup>87</sup>Sr/<sup>86</sup>Sr. *Geology* 24, 917-920.

Mook, W. G., J. C. Bommerson, J.C., Staverman, W.H., 1974. Carbon isotope fractionation between dissolved bicarbonate and gaseous carbon dioxide. *Earth Plant. Sci. L&t.* 22, 169-176.

Narbonne, G.M., 2005. The Ediacara biota: Neoproterozoic origin of animals and their ecosystems. *Annu. Rev. Earth Planet. Sci.* 33, 421-42.

Narbonne, G.M., Xiao, S., Gehling, J.G., Shields-Zhou, G.A., 2012. The Ediacaran Period. In: Gradstein, F.M., Ogg, J.G., Schmitz, M., Ogg, G. (Eds.), *Geological Time Scale 2012*. Cambridge University Press, Cambridge, pp. 413-435.

Nedelec, A., Affaton, P., France-Lanord, C., Charriere, A, J. 2007. Sedimentology and chemostratigraphy of the Bwipe Neoproterozoic cap dolostones (Ghana, Volta Basin): A

record of microbial activity in a peritidal environment. *Comptes Rendus Geoscience*, 339, 223-239.

O'Brien, S.J., King, A.F., 2005. Late Neoproterozoic (Ediacaran) stratigraphy of Avalon Zone sedimentary rocks, Bonavista Peninsula, Newfoundland. Newfoundland and Labrador Department of Natural Resources, Geological Survey, Report 05-1, pp. 101-113.

Ogawa, T., Kaplan, A., 2003. Inorganic carbon acquisition systems in cyanobacteria. *Photosynth Res* 77, 105-115.

Ohno, T., Komiya, T., Ueno, Y., Hirata, T. Maruyama, S., 2008. Determination of  $^{88}\text{Sr}/^{86}\text{Sr}$  mass-dependent isotopic fractionation and radiogenic isotope variation of  $^{88}\text{Sr}/^{86}\text{Sr}$  in the Neoproterozoic Doushantuo Formation. *Gondwana Research* 14, 126-133.

Omata T, Gohta S, Takahashi Y, Harano Y, Maeda S-I., 2001. Involvement of a CbbR homolog in low  $\text{CO}_2$ -induced activation of the bicarbonate transporter operon in cyanobacteria. *J Bacteriol* 183, 1891-1898.

O'Neil, J.R., Epstein, S., 1966. A method for oxygen isotope analysis of milligram quantities of water and some of its applications. *Journal of Geophysical Research* 71, 4955-4961.

Oyhantçabal, P. Heimann, A., Miranda, S., 2001. An evaluation of strain in the syntectonic Solís de Mataojo Granitic Complex, Uruguay. *J. Struct. Geol.* 23, 807-817.

Oyhantçabal, P., 2005. The Sierra Ballena Shear zone: kinematics, timing and its significance for the geotectonic evolution of southeast Uruguay. *Georg-August Universität zu Göttingen, Göttingen*, pp. 139.

Oyhantçabal, P., Siegesmund, S., Wemmer, K., 2011. The Río de la Plata Craton: a review of units, boundaries, ages and isotopic signature. *Int. J. Earth Sci.* 100, 201-220.

Oyhantçabal, P., Siegesmund, S., Wemmer, K., Frei, R., Layer, P., 2007. Post-collisional transition from calc-alkaline to alkaline magmatism during transcurrent deformation in the southernmost Dom Feliciano Belt (Braziliano-Pan-African, Uruguay). *Lithos* 98, 141-159.

Oyhantçabal, P., Siegesmund, S., Wemmer, K., Presnyakov, S., Layer, P., 2009. Geochronological constraints on the evolution of the southern Dom Feliciano Belt (Uruguay). *J. Geol. Soc.* 166, 1075-1084.

Oyhantçabal, P., Wagner-Eimer, M., Wemmer, K., Schulz, B., Frei, R., Siegesmund, S., 2012. Paleo- and Neoproterozoic magmatic and tectonometamorphic evolution of the Isla Cristalina de Rivera (Nico Pérez Terrane, Uruguay). *Int. J. Earth Sci. (Geol. Rundsch.)*,

Palmer, M.R., Edmond, J.M., 1989. The strontium isotope budget of the modern ocean. *Earth and Planetary Science Letters* 92, 11-26.

Pankhurst, R.J., Ramos, A., Linares, E., 2003. Antiquity of the Rio de la Plata Craton in Tandilia, southern Buenos Aires province, Argentina. *J. South Am. Earth Sci.* 16, 5-13.

Pazos P., Tófaló, R., Sánchez-Bettucci, L., 2003. The record of the Varanger Glaciation at the Rio de la Plata Craton, Vendian-Cambrian of Uruguay. *Gondw. Res.* 6, 65-77.

Pazos, P., Sánchez Bettucci, L., Loureiro, J. 2008. The Neoproterozoic glacial record in the Río de la Plata Craton: a critical reappraisal. *Geol. Soc. London, Spec. Pub.*, 294, 343-364.

Pecoits, E., 2002. Análisis faciológico y aspectos geológicos de la Formación Las Ventanas; un nuevo enfoque. In: Pecoits, E. and Masquelin, H. (Eds.), *II Taller Sobre la Estratigrafía del Precámbrico del Uruguay*. pp. 34-36. Facultad de Ciencias, Montevideo, Uruguay.

Pecoits, E., 2003a. Sedimentología y consideraciones estratigráficas de la Formación Las Ventanas en su área tipo, departamento de Maldonado, Uruguay. In: Pecoits, E. (Ed.), *Estratigrafía del Precámbrico del Uruguay*. *Rev. Soc. Uruguay. Geol. Spec. Publ.* 1, 124-140.

Pecoits, E., 2003b. Age and preliminary correlation of the Las Ventanas Formation and Bom Jardim-Cerro do Bugio allogroups (Vendian, Uruguay and Brazil). In: Frimmel, H.E (Ed.), *III International Colloquium Vendian-Cambrian of W-Gondwana, Programme and Extended Abstracts*, pp. 32-34. Cape Town, South Africa.

Pecoits, E., Aubet, N., Oyhantçabal, P., Sánchez Bettucci, L., 2004. Estratigrafía de sucesiones sedimentarias y volcanosedimentarias Neoproterozoicas del Uruguay. *Rev. Soc. Uruguay. Geol.* 11, 18-27.

Pecoits, E., Oyhantçabal, P., 2004. Geotectonic evolution of Uruguay during the Neoproterozoic-Cambrian. In: I Symposium on Neoproterozoic-Early Paleozoic events in SW-Gondwana. Extended Abstracts, IGCP Project 478, pp. 43-45, Brazil.

Pecoits, E., Gingras, M., Aubet, N., Konhauser, K., 2008. Ediacaran in Uruguay: palaeoclimatic and palaeobiological implications. *Sedimentology* 55, 689-719.

Pecoits, E., 2010. Ediacaran iron formations and carbonates of Uruguay: palaeoceanographic, palaeoclimatic and palaeobiologic implications. Ph.D. thesis, University of Alberta.

Pecoits, E., Aubet, N.R., Gingras, M.K., Poulton, S.W., Bekker, A., Veroslavsky, G., Konhauser, K.O., 2011. An Ediacaran iron formation: New evidence for ferruginous late Neoproterozoic seawater. *Precambrian Research*, in press. (doi:10.1016/j.precamres.2011.10.002).

Pecoits, E., Gingras, M.K., Konhauser, K.O., 2011. Las Ventanas and San Carlos formations, Maldonado Group, Uruguay. *Geological Society, London, Memoirs* 36, 555-564.

Pecoits, E., Konhauser, K.O., Aubet, N.R., Heaman, L.M., Veroslavsky, G., Stern, R.A., Gingras, M.K., 2012. Bilaterian burrows and grazing behavior at >585 Million years ago. *Science* 336, 1693-1696.

Peel, E., Preciozzi, F., 2006. Geochronologic synthesis of the Piedra Alta Terrane, Uruguay. V South American Symposium on Isotope Geology. Punta del Este, Uruguay, pp. 234-237.

Pelechaty, S.M., 1998. Integrated chronostratigraphy of the Vendian system of Siberia: implications for a global stratigraphy. *Journal of the Geological Society of London* 155, 957-973.

- Peters, K.E., Rohrback, B.G., Kaplan, I.R., 1981. Carbon and hydrogen stable isotope variations in kerogen during laboratory simulated thermal maturation. AAPG Bull. 65, 501-508.
- Phlips, E.J., Badylak, S., Lynch, T.C., 1999. Blooms of the picoplanktonic cyanobacterium *Synechococcus*. Florida Bay, a subtropical inner-shelf lagoon. *Limnology and Oceanography* 44, 1166-1175.
- Plint, A.G., 2011. Wave- and storm-dominated shoreline and shallow marine systems. In: Dalrymple, R.W. and James, N.P., (Eds.), *Facies Models*, 4th Edition, Geological Association of Canada, 167-200.
- Poiré, D.G., González, P.D., Canalicchio, J. M. Repetto, F.G., Canessa, N.D., 2005. Estratigrafía del Grupo Mina Verdún, Proterozoico de Minas, Uruguay. *Latin Am. J. Sediment. Basin Anal.* 12, 125-143.
- Pokrovskii, B.G. Vinogradov, V.I., 1991, Strontium, Oxygen and Carbon Isotope Composition in the Upper Precambrian Carbonates from Western Flank of the Anabar Uplift (the Kotuikan River), *Dokl. Akad. Nauk SSSR* 320 (5), 1245-1250.
- Popp, B.N., Laws, E.A., Bidigare, R.R., Dore, J.E., Hanson, K.L., Wakeham, S.G., 1998. Effect of phytoplankton cell geometry on carbon isotopic fractionation. *Geochim. Cosmochim. Acta* 62, 69-77.
- Porcher, C.C., McNaughton, N.J., Leite, J.A.D., Hartmann, L.A., Fernandes, L.A.D., 1999. Idade Shrimp em zircão: vulcanismo ácido do Complexo Metamórfico Porongos. In: *Simpósio sobre Vulcanismo e Ambientes Associados. Abstracts*, Gramado, 110.
- Preciozzi, F., 1988. Carta geológica del Uruguay, Hoja F-23 Pirarajá, Escala 1:100.000. Memoria explicativa. DINAMIGE-UdelaR, Montevideo, pp. 15.
- Preciozzi, F., Spoturno, J., Heinzen, W., Rossi, P., 1988. Carta Geológica del Uruguay a escala 1:500.000. Memoria explicativa. DINAMIGE, Montevideo, pp. 90.
- Preciozzi, F., Pena, S., Masquelin, E., Pías, J., Tabó, F., 1989. Memoria explicativa del fotoplano Piriápolis. DINAMIGE-UdelaR, Montevideo, pp. 11.

Preciozzi, F., Masquelin, H., Sánchez Bettucci, L., 1993. Geología de la Porción Sur del Cinturón Cuchilla de Dionisio. In: I Simp. Int. Neoproterozoico - Cámbrico de la Cuenca del Plata), Guía de Excursiones, La Paloma, pp. 1-39.

Preciozzi, F., Basei, M.A.S., Masquelin, H., 1999a. New geochronological data from the Piedra Alta Terrane (Rio de La Plata Craton). In: II South American Symposium on Isotope Geology, Córdoba, pp. 341-343.

Preciozzi, F., Masquelin, H., Basei, M.A.S., 1999b. The Namaqua/Grenville terrane of eastern Uruguay. In: Proceedings of the II South American Symposium on Isotope Geology, Actas, Córdoba (Argentina), pp. 338-340.

Preciozzi, F., Peel, E., Muzio, R., Ledesma, J.J. and Guerequiz, R., 2001. Dom Feliciano Belt and Punta del Este Terrane: Geochronological features. III South Amer. Symp. Isotope Geol. Pucón, Chile.

Preciozzi, F., Peel, E., 2005. El cinturón Dom Feliciano y sus relaciones con el craton del Río de la Plata y el Terreno Punta del Este - geología y geocronología. Informe Final, Proyecto Conicyt-FCE #6009.

Ramos, V.A., 2010. The Grenville-age basement of the Andes. *J. South A. Earth Sci.* 29, 77-91.

Ramos, V.A., Vujovich, G., Martino, R., Otamendi, J. 2010. Pampia: a large cratonic block missing in the Rodinia supercontinent. *Jour. Geod.* 50, 243-255.

Ramos, V.A., Vujovich, G.I., 1993. The Pampia Craton within Western Gondwanaland. In: Ortega-Gutierrez, F., Coney, P., Centeno-García, E., Gomez-Caballero, A. (Eds.), Proceedings of The First Circum-Pacific and Circum-Atlantic Terrane Conference. Mexico, pp. 113-116.

Rapela, C.W., Pankhurst, R.J., Casquet, C., Baldo, E., Saavedra, J., Galindo, C., Fanning, C.M., 1998. The Pampean Orogeny of the southern proto-Andes: evidence for Cambrian continental collision in the Sierras de Cordoba. In: Pankhurst, R.J., Rapela, C.W. (Eds.), The proto-Andean Margin of Gondwana, vol. 142. Geological Society, London, Sp. Pub, pp. 181-217.

Rapela, C.W., Pankhurst, R.J., Casquet, C., Baldo, E., Saavedra, J., Galindo, C., Fanning, C.M., 2007. The Pampean Orogeny of the southern proto-Andes: Cambrian continental collision in the Sierras de Cordoba. *Earth Sci. Rev.* 142, 181-217.

Rapela, C.W., Fanning, C.M., Casquet, C., Pankhurst, R.J., Spalletti, L., Poiré, D., Baldo, E.G., 2011. The Rio de la Plata craton and the adjoining Pan-African/brasiliano terranes: Their origins and incorporation into south-west Gondwana. *Gondw Research* in press.

Rapela, C.W., Pankhurst, R.J., Casquet, C., Baldo, E., Galindo, C., Fanning, C.M., Dahlquist, J.M., 2010. The Western Sierras Pampeanas: protracted Grenville-age history (1330-1030 Ma) of intra-oceanic arcs, subduction-accretion at continental-edge and AMCG intraplate magmatism. *J. South A. Earth Sci.* 29, 105-127.

Rau, G. H., Riebesell, U., WolfGladrow, D. 1996. A model of photosynthetic C-13 fractionation by marine phytoplankton based on diffusive molecular CO<sub>2</sub> uptake, *Mar. Ecol-Pog. Ser.*, 133(1-3), 275-285.

Ray, J.S., Veizer, J., Davis, W.J., 2003, C, O, Sr and Pb isotope systematics of carbonate sequences of the Vindhyan Supergroup, India: age, diagenesis, correlations and implications for global events, *Precambrian Res*, 121, 103-140.

Read, J.F., 1985. Carbonate platform facies models. *Bull. Am. Assoc. Pet. Geol.*, 69: 1-21.

Riccardi, A., Kump, L.R., Arthur, M.A., D'Hondt, S., 2007. Carbon isotopic evidence for chemocline upward excursions during the end-Permian event. *Palaeogeogr. Palaeoclimatol. Palaeoecol.* 248, 73-81.

Ridgwell, A.J., Watson A.J., Maslin, M.A., Kaplan, J.O., 2003. Implications of coral reef buildup for the controls on atmospheric CO<sub>2</sub> since the Last Glacial Maximum. *Paleoceanography*, 18, 1083.

Riding, R. 2006. Cyanobacterial calcification Cyanobacterial calcification, carbon dioxide concentrating mechanisms, and Proterozoic-Cambrian changes in atmospheric composition. *Geobiology*, 4, 299-316.

Rivalenti, G., Mazzucchelli, M., Molesini, M., Petrini, R., Girardi, V.A.V., Bossi, J., Campal, N., 1995. Petrology of Late Proterozoic mafic dikes in the Nico Perez region, central Uruguay. *Mineral. Petrol.* 55, 239-263.

Rivers, T., 1997. Lithotectonic elements of the Grenville Province: review and tectonic implications. *Prec. Res.* 86, 117-154.

Rose, C.V., Maloof, A.C., Schoene, B., Ewing, R.C., Linnemann, U., Hofmann, M., Cottle, J.M., 2013. The end-Cryogenian glaciation of South Australia. *Geosci. Can.* 40, 256-293.

Rost, B., Riebesell, U., Burkhardt, S., Sültemeyer, D., 2003. Carbon acquisition of bloom-forming marine phytoplankton. *Limnology and Oceanography* 48, 55-67.

Rothman, D.H., Hayes, J.M., Summons, R.E., 2003. Dynamics of the Neoproterozoic carbon cycle. *Proc. Nat. Acad. Sci. U.S.A.* 100, 124-129.

Ruf, M., Elmar Link, E., Pross, J., Aigner, T., 2005. A multi-proxy study of deeper-water carbonates (Upper Jurassic, southern Germany): combining sedimentology, chemostratigraphy and palynofacies. *Facies* 51, 327-349.

Saalmann, K., Gerdes, A., Lahaye, Y., Hartmann, L.A., Remus, M.V.D., Läufer, A., 2011. Multiple accretion at the eastern margin of the Río de la Plata craton: the prolonged Brasiliano orogeny in southernmost Brazil. *Int. J. Earth Sci. (Geol. Rundsch)* 100, 355-378.

Saltzman, M.R., Thomas, E., 2012. Carbon isotope stratigraphy, *The Geologic Time Scale 2012*. In: Eds. Gradstein, F., Ogg, J., Schmitz, M.D., Ogg, G., 207-232.

Sambridge, M.S., Compston, W., 1994. Mixture modelling of multi-component data sets with application to ion-probe zircon ages: *Earth Planet. Sci. Lett.* 128, 373-390.

Sánchez Bettucci, L., Linares, E., 1996. Primeras edades en basaltos del Complejo Sierra de las Ánimas, Uruguay. In: XIII Congreso Geológico Argentino y III Congreso de Exploración de Hidrocarburos, Actas I pp. 399-404. La Plata.

Sánchez-Bettucci, L., 1998. Evolución tectónica del cinturón Dom Feliciano en la región Minas-Piriapolis, Uruguay. Ph.D. Thesis. Universidad de Buenos Aires, Argentina.

Sánchez-Bettucci, L., Ramos, V.A., 1999. Aspectos geológicos de las rocas metavolcanicas y metasedimentarias del Grupo Lavallega, sudeste de Uruguay. *Rev. Bras. Geoc.* 29, 557-570.

Sánchez-Bettucci, L., Preciozzi, F., Basei, M.A.S., Oyhantçabal, P., Peel, E., Loureiro, J., 2003. Campanero Unit: A Probable Paleoproterozoic Basement and its Correlation to other Units of Southeastern Uruguay. IV South Amer. Symp. Isotope Geol. Salvador, Brazil.

Sánchez Bettucci, L., Koukharsky, M., Pazos, P.J., Stareczek, S., 2009. Neoproterozoic subaqueous extrusive-intrusive rocks in the Playa Hermosa Formation in Uruguay: Regional and stratigraphic significance. *Gondw. Res.* 16, 134-144.

Sánchez Bettucci, L., Masquelin, E., Peel, E., Oyhantçabal, P., Muzio, R., Ledesma, J.J., Preciozzi, F., 2010. Comment on “Provenance of the Arroyo del Soldado Group (Ediacaran to Cambrian, Uruguay): implications for the palaeogeographic evolution of southwestern Gondwana”. *Prec. Res.* 180, 328-333.

Sansjofre, P., Ader, M., Trindade, R.I.F., Elie, M., Lyons, J., Cartigny, P., nogueria, A.C.R. 2011. A carbon isotope challenge to the snowball Earth. *Nature* 478, 93-97.

Santos, J.O.S., Hartmann, L.A., Bossi, J., Campal, N., Schipilov, A., Piñeyro, D., McNaughton, N.J., 2003. Duration of the Transamazonian and its correlation within South America based on U-Pb SHRIMP geochronology of the La Plata Craton, Uruguay. *Int. Geol. Rev.* 45, 27-48.

Sawaki, Y., Ohno, T., Fukushi, Y., Komiya, T., Ishikawa, T., Hirata, T., Maruyama, S., 2008. Sr isotope excursion across the Precambrian–Cambrian boundary in the Three Gorges area, South China. *Gondwana Research* 14, 134-147.

Sawaki, Y., Ohno, T., Tahata, M., Komiya, T., Hirata, T., Maruyama, S., Windley, B.F., Han, J., Shu, D. Li, Y., 2010. The Ediacaran radiogenic Sr isotope excursion in the Doushantuo Formation in the Three Gorges area, South China. *Precambrian Research* 176, 46-64.

Saylor, B.Z., Kaufman, A.J., Grotzinger, J.P., Urban, F., 1998. A composite reference section for terminal Proterozoic strata of southern Namibia. *J. Sed. Res.* 68, 1223-1235.

- Saylor, B.Z., Kaufman, A.J., Grotzinger, J.P., Urban, F., 1998. A composite reference section for terminal Proterozoic strata of southern Namibia. *Journal of Sedimentary Research* 68, 1223-1235.
- Schidlowski, M., 1987. Application of stable carbon isotopes to early biochemical evolution on earth. *Amer. Rev. Earth Planet. Sci.*, 15, 47-72.
- Schidlowski, M. 1988. A 3,800-million-year isotopic record of life from carbon in sedimentary rocks. *Nature* 333, 313-318.
- Schrag, D.P., Berner, R.A., Hoffman, P.F., Halverson, G.P. 2002. On the initiation of a Snowball Earth, *Geochem. Geophys. Geosyst.* 3.
- Seguret, M., Moussine-Pouchkaine, A., Gabaglia, G.R., Bouchette, F., 2001. Storm deposits and storm-related coarse carbonate breccias on a pelagic outer shelf (south-east basin France). *Sedimentology* 48, 231-254.
- Semikhatova, M.A., Kuznetsov, A. B., Maslov, A. V., Gorokhov, I. M., Ovchinnikova G. V., 2009, Stratotype of the Lower Riphean, the Burzyan Group of the Southern Urals: Lithostratigraphy, Paleontology, Geochronology, Sr- and C-Isotopic Characteristics of its carbonate rocks, *Stratigraphy and Geological Correlation*, 2009, Vol. 17, No. 6, 574-601.
- Shen, B., Xiao, S.H., Kaufman, A.J., Bao, H.M., Zhou, C.M, Wang, H.F. 2008. Stratification and mixing of a post-glacial Neoproterozoic ocean: Evidence from carbon and sulfur isotopes in a cap dolostone from northwest China. *Earth Planet. Sci. Lett.*, 265, 209-228.
- Shen, Y., Zhang, T., Hoffman, P. F., 2008. On the coevolution of Ediacaran oceans and animals. *Proceedings of the National Academy of Science U.S.A.* 105, 7376-7381.
- Shields, G., Veizer, J., 2002. Precambrian marine carbonate isotope database: version 1.1. *Geochemistry, Geophysics, Geosystems* 3.
- Shields, G.A., 2007. A normalized seawater strontium isotope curve: possible implications for Neoproterozoic–Cambrian weathering rates and the further oxygenation of the Earth. *Earth* 2, 35-42.

- Shields-Zhou, G.A., Hill, A.C., Macgabhann, B.A., The Cryogenian Period. In: Gradstein, F.M., Ogg, J.G., Schmitz, M., Ogg, G. (Eds.), *Geological Time Scale 2012*. Cambridge University Press, Cambridge, 393-411.
- Simoneit, B.R.T., Brenner, S., Peters, K.E., Kaplan, I.R., 1981. Thermal alteration of Cretaceous black shale by diabase intrusions in the Eastern Atlantic: II. Effects on bitumen and kerogen. *Geochim. Cosmochim. Acta* 45, 1581-1602.
- Simonetti, A., Heaman, L.M., Chacko, T., Banerjee, N.R., 2006. In situ petrographic thin section U-Pb dating of zircon, monazite, and titanite using laser ablation-MC-ICP-MS. *Int. Jour. Mass. Spectrom.* 253, 87-97.
- Simonetti, A., Heaman, L.M., Hartlaub, R.P., Creaser, R.A., MacHattie, T.G., Bohm, C., 2005. U-Pb zircon dating by laser ablation-MC-ICP-MS using a new multiple ion counting Faraday collector array. *J. Anal. Atom. Spectrom.* 20, 677-686.
- Spagnuolo, C.M., Rapalini, A.E., Astini, R.A., 2012. Assembly of Pampia to the SW Gondwana margin: a case of strike-slip docking? *Gondw. Res.* 2-3, 406-421.
- Spoturno, J., Loureiro, J., Oyhançabal, P., Pascale, A., 2012. Mapa Geologico y de Recursos Minerales del Departamento de Maldonado a Escala 1/100 000. DINAMIGE-Facultad de Ciencias.
- Sprechmann, P., Gaucher, C., Blanco, G., Montaña, J., 2004. Stromatolitic and trace fossils community of the Cerro Victoria Formation, Arroyo del Soldado Group (Lowermost Cambrian, Uruguay). *Gondw. Res.* 7, 753-766.
- Steiger, R. H., Jäger, E., 1977. Subcommittee on Geochronology: convention on the use of decay constants in geo-and cosmochronology. *Earth and Planetary Science Letters* 36, 359-362.
- Summons, R.E. Hayes, J.M., 1992. Principles of molecular and isotopic biogeochemistry. In: Schopf, J.W., Klein, C. (Eds.), *The Proterozoic Biosphere: A multidisciplinary study*, Cambridge, UK, Cambridge University Press, 83-93.
- Swanson-Hysell, N.L., Rose, C.V., Calmet, C.C., Halverson, G.P., Hurtgen, M.T., Maloof, A.C., 2010. Cryogenian glaciation and the onset of carbon-isotope decoupling. *Science* 328, 608-611.

Swart, P., Kennedy, M., 2012. Does the global stratigraphic reproducibility of  $\delta^{13}\text{C}$  in Neoproterozoic carbonates require a marine origin? A Pliocene-Pleistocene comparison. *Geology* 40, 87-90.

Teixeira, W., Renne, P., Bossi, J., Campal, N., D'Agrella, F., 1999.  $^{40}\text{Ar}/^{39}\text{Ar}$  and Rb/Sr geochronology of the Uruguayan dike swarm, Río de la Plata Craton and implications for Proterozoic intraplate activity in western Gondwana. *Prec. Res.* 93, 153-180.

Thomas, C.W., Graham, C.M., Ellam, R.M., Fallick, A.E. 2004.  $^{87}\text{Sr}/^{86}\text{Sr}$  chemostratigraphy of Neoproterozoic Dalradian limestones of Scotland and Ireland: constraints on depositional ages and time scales. *Journal of the Geological Society, London* 161, 229-242.

Thomas, W.A., Astini, R.A., Mueller, P.A., Gehrels, G.E., Wooden, J.L., 2004. Transfer of the Argentine Precordillera terrane from Laurentia: constraints from detrital-zircon geochronology. *Geology* 32, 965-968.

Thompson, J.B., 2000. Microbial whittings. In: Eds. Riding, R., Awramik, S.M., *Microbial Sediments*. Springer-Verlag, Berlin, 250-260.

Tohver, E., D'Agrella-Filho, M.S., Trindade, R.I.F., 2006. Paleomagnetic record of Africa and South America for the 1200–500 Ma interval, and evaluation of Rodinia and Gondwana assemblies. *Prec. Res.* 147, 193-222.

Tortell, P.D., Rau, G.H., Morel, F.M.M., 2000. Inorganic carbon acquisition in coastal Pacific phytoplankton communities. *Limnol. Oceanogr.* 45: 1485-150.

Tucker, M.E., V.P. Wright. 1990. *Carbonate Sedimentology*. Blackwell Scientific Publications, Oxford, 482.

Umpierre, M., 1966. Edades de las lavas Mezoicas del Uruguay. In: Bossi, J., *Geología del Uruguay*. Departamento de Publicaciones de la Universidad de la República. Montevideo. Uruguay.

Umpierre, M., Halpern, M., 1971. Edades Sr-Rb del Sur de la República Oriental del Uruguay. *Rev. Asoc. Geol. Arg.* 26, 133-155.

- Umpierre, M., Halpern, M., 1971. Edades Sr-Rb del Sur de la República Oriental del Uruguay. *Revista de la Asociación Geológica Argentina* 26, 133-155.
- Vasconcelos, C., McKenzie, J.A., 1997. Microbial mediation of modern dolomite precipitation and diagenesis under anoxic conditions (Lagoa Vermelha, Rio de Janeiro, Brazil). *Journal of Sedimentary Research* 67, 378-390.
- Veizer J., Hoefs, J. 1976. The nature of  $^{18}\text{O}/^{16}\text{O}$  and  $^{13}\text{C}/^{12}\text{C}$  secular trends in sedimentary carbonate rocks. *Geochim. Cosmochim. Acta* 40, 1387-1395.
- Veizer, J. 1983. Chemical diagenesis of carbonates: Theory and application of trace element technique. In: Eds. Arthur, M.A., Anderson, T.F., Kaplan, I.R., Veizer, J., Land, L.S., *Stable Isotopes in Sedimentary Geology*. Society of Economic Paleontologists and Mineralogists Short Course No. 10, Dallas, 3-1 to 3-100.
- Veizer, J., Clayton, R.N., Hinton, R.W., 1992. Geochemistry of Precambrian carbonates: IV. Early Paleoproterozoic (2.25-0.25 Ga) seawater. *Geochim. Cosmochim. Acta* 56, 875-885.
- Verdecchia, S.O., Casquet, C., Baldo, E.G., Pankhurst, R.J., Rapela, C.W., Fanning, M., Galindo, C., 2011. Mid- to Late Cambrian docking of the Rio de la Plata craton to southwestern Gondwana: age constraints from U-Pb SHRIMP detrital zircon ages from Sierras de Ambato and Velasco (Sierras Pampeanas, Argentina). *Jour. Geol. Soc.* 168, 1061-1071.
- Verdel, Ch., Wernicke, B.P., Bowring, S.A., 2011. The Shuram and subsequent Ediacaran carbon isotope excursions from southwest Laurentia, and implications for environmental stability during the metazoan radiation *GSA Bulletin* 123, 1539-1559.
- Veroslavsky, G., de Santa Ana, H., Daners, G., 2006. Tacuarí Formation (Nov. Nom.): Lithostratigraphy, facies, environment, age and geological significance (Cerro Largo-Uruguay). *Rev. Soc. Uru. Geol.* 13, 23-35.
- Vogel J.C. 1993. Variability of carbon isotope fractionation during photosynthesis. In: Eds. Ehleringer, J.R., Hall, A.E., Farquhar, G.D., *Stable Isotopes and Plant Carbon-Water Relations* 29-46. Academic Press, San Diego.

- Walter, M.R., Veevers, J.J., Calver, C.R., Gorjan, P., Hill, A.C., 2000. Dating the 840–544 Ma Neoproterozoic interval by isotopes of strontium, carbon, and sulfur in seawater, and some interpretative models. *Precambrian Research* 100, 371-433.
- Werne, J. P., Hollander, D. J., 2004. Balancing supply and demand: controls on carbon isotope fractionation in the Cariaco Basin (Venezuela) Younger Dryas to present. *Mar. Chem.*, 92, 275- 293.
- Wijbrans, J. R., McDougall I., 1986.  $^{40}\text{Ar}/^{39}\text{Ar}$  dating of white micas from an alpine high-pressure metamorphic belt on Naxos. *Contributions to Mineralogy and Petrology* 93, 187-194.
- Xiao, S., Bao, H., Wang, H., Kaufman, A.J., Zhou, C., Li, G., Yuan, X., Ling, H., 2004. The Neoproterozoic Quruqtagh Group in eastern Chinese Tianshan: evidence for a postMarinoan glaciation. *Precambrian Res.* 130, 1-26.
- Xiao, S.H., Knoll, A.H., Kaufman, A.J., Yin, L.M., Zhang, Y., 1997. Neoproterozoic fossils in Mesoproterozoic rocks? Chemostratigraphic resolution of a biostratigraphic conundrum from the North China Platform. *Precambrian Res.* 84, 197-220.
- Yoshioka, H., Asahara, Y., Tojo, B., Kawakami, S., 2003. Systematic variations in C, O and Sr isotopes and elemental concentrations in Neoproterozoic carbonates in Namibia: implications for a glacial to interglacial transition. *Precambrian Research*, 124, 69-85
- Young, S.A., Saltzman, M.R., Bergström, S.M., Leslie, S.A., Xu, C. 2008. Paired  $\delta^{13}\text{C}_{\text{carb}}$  and  $\delta^{13}\text{C}_{\text{org}}$  records of Upper Ordovician (Sandbian-Katian) carbonates in North America and China: Implications for paleoceanographic change. *Palaeogeogr. Palaeoclimatol. Palaeoecol.* 270, 166-178.
- Zhao, Y.Y., Zheng, Y.F., Chen, F.K. 2009. Trace element and strontium isotope constraints on sedimentary environment of Ediacaran carbonates in southern Anhui, South China. *Chem. Geol.*, 265, 345-362.
- Zhou, C., Tucker, R., Xiao, S., Peng, Z., Yuan, X., Chen, Z., 2004. New constraints on the ages of Neoproterozoic glaciations in south China. *Geology*, 32, 437-440.

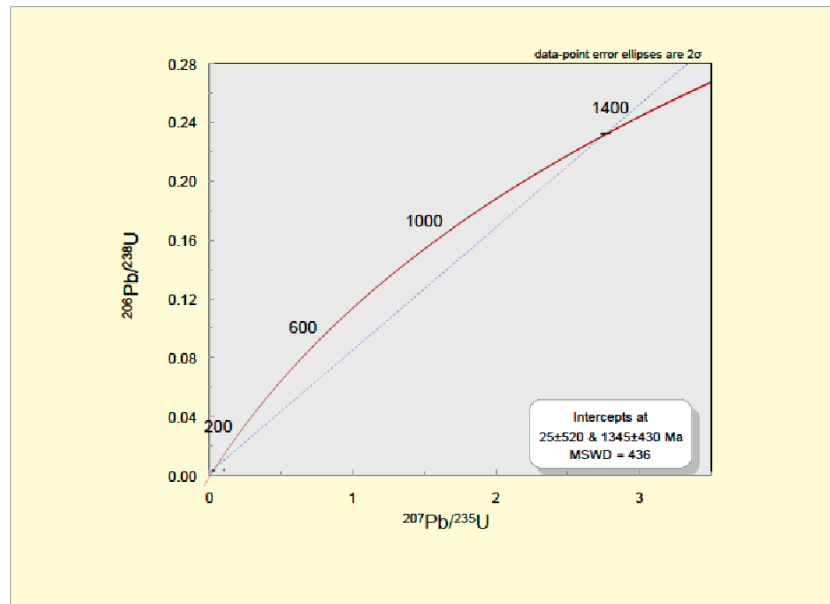
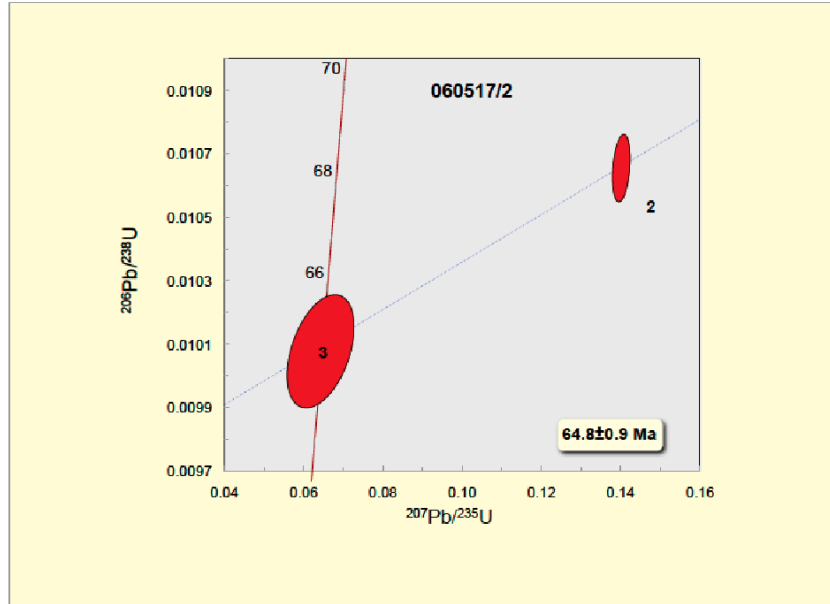
Zimmermann, U., 2011. Comment on “Provenance of the Arroyo del Soldado Group (Ediacaran to Cambrian, Uruguay): Implications for the palaeogeographic evolution of southwestern Gondwana”. *Prec. Res.* 186, 233-236.

Zwingmann, H., Yamada, K., Tagami, T., 2010. Timing of brittle faulting within the Nojima fault zone, Japan. *Chemical Geology* 275, 176-185.

# APPENDIX 1: SUPPLEMENTARY INFORMATION FOR CHAPTER 2

U-Pb Zircon Results for Sample 060517/2.

Description	Weight (µg)	U (ppm)	Th (ppm)	Pb (ppm)	Th/U	TCPb (pg)	Pb <sup>17</sup> /Pb <sup>206</sup>	<sup>206</sup> Pb/ <sup>238</sup> U	<sup>207</sup> Pb/ <sup>235</sup> U	2σ	<sup>206</sup> Pb/ <sup>238</sup> U	2σ	P	Model Ages (Ma)				
														<sup>206</sup> Pb/ <sup>238</sup> U	2σ	<sup>207</sup> Pb/ <sup>235</sup> U	2σ	%Disc
1 single large tan	3.2	141	127	48	0.90	27	4.84	264	2.7764	0.0280	0.23335	0.00050	0.481	1352.0	2.8	1349.2	7.5	-0.6
2 6 equant 3:1	4.2	359	203	7	0.58	11	1.58	108	0.1408	0.0019	0.01086	0.00008	0.281	88.4	0.5	133.8	1.8	98.1
3 6 elongate clear	1.8	310	153	4	0.48	1.0	2.81	188	0.0665	0.0068	0.01010	0.00014	0.428	64.8	0.0	64.4	6.5	-16.0



APPENDIX 2: SUPPLEMENTARY INFORMATION FOR CHAPTER 3

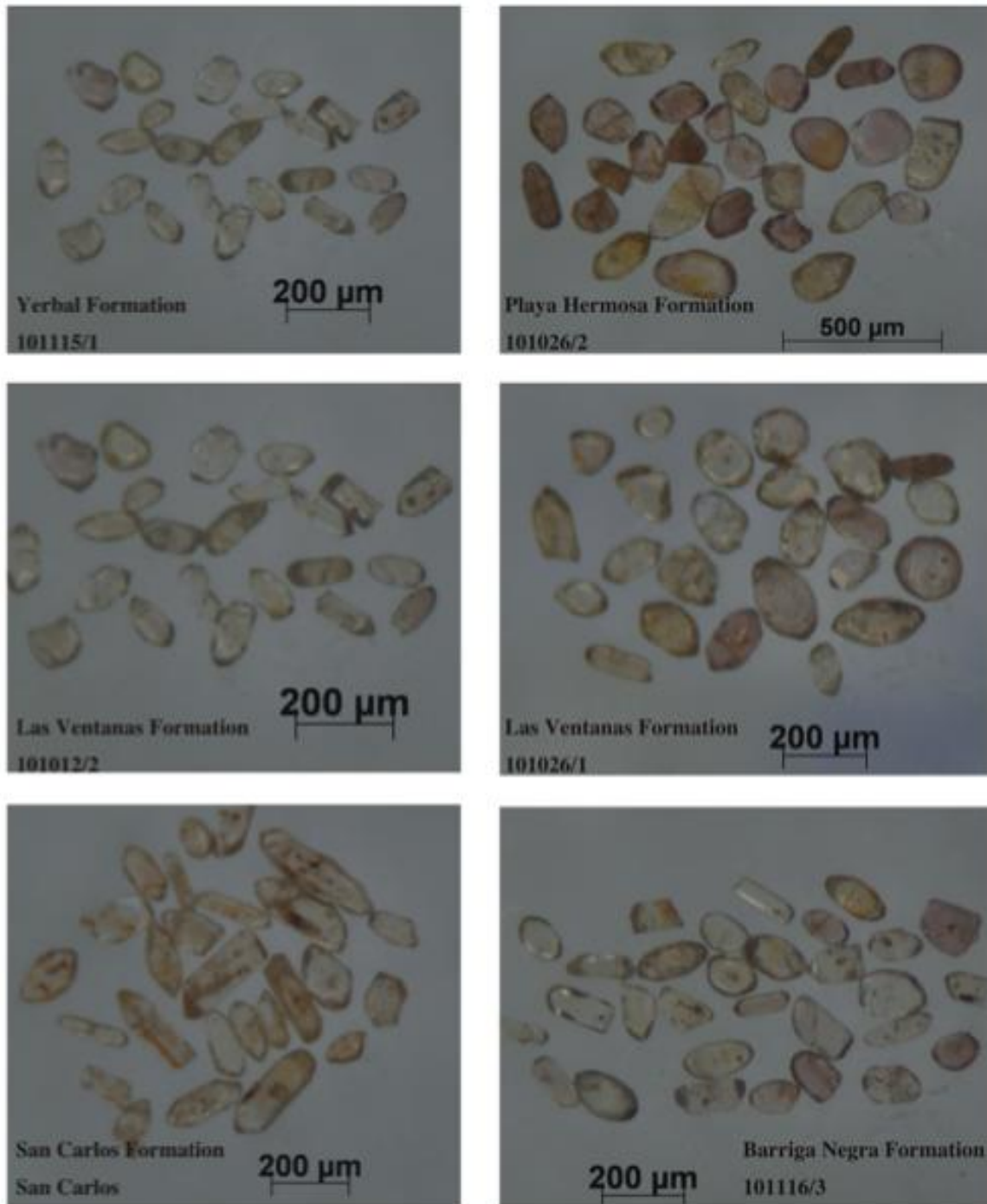


**Figure A.2.1.** A selection of representative detrital zircon grains from each sample analyzed in this study.

sample name	$^{206}\text{Pb}$ (cps)		$^{207}\text{Pb}/^{235}\text{U}$		$^{206}\text{Pb}/^{238}\text{U}$		$\rho$	$^{207}\text{Pb}/^{235}\text{U}$		$^{206}\text{Pb}/^{238}\text{U}$		$^{207}\text{Pb}/^{235}\text{U}$		$^{206}\text{Pb}/^{238}\text{U}$	
	cp	err	2 $\sigma$	err	2 $\sigma$	err		age (Ma)	error (Ma)						
1011151-1	61549	0	0.23108	0.00132	17.65985	0.63137	0.55427	0.01956	0.987	3060	9	2971	34	2843	81
1011151-2	431154	0	0.23228	0.00117	18.32881	0.60657	0.57230	0.01872	0.988	3068	8	3007	31	2917	76
1011151-3	870411	0	0.22973	0.00108	18.24123	0.62656	0.57588	0.01959	0.991	3050	8	3003	33	2932	80
1011151-4	734130	0	0.22802	0.00104	18.28121	0.68060	0.58147	0.02148	0.992	3038	7	3005	35	2955	87
1011151-5	1053916	0	0.22682	0.00106	18.88642	0.75168	0.60391	0.02387	0.993	3030	7	3036	38	3046	95
1011151-6	1481060	12	0.13053	0.00087	6.81932	0.19430	0.35702	0.00992	0.976	2209	11	2080	25	1960	47
1011151-7	385382	0	0.20408	0.00103	15.21947	0.56664	0.54089	0.01995	0.991	2859	8	2829	35	2787	83
1011151-8	355007	0	0.12491	0.00053	5.91435	0.21202	0.34341	0.01219	0.990	2027	9	1963	31	1903	58
1011151-9	292102	0	0.13760	0.00063	7.17102	0.27709	0.37797	0.01450	0.993	2197	8	2133	34	2067	67
1011151-10	724524	0	0.21293	0.00106	14.30467	0.45137	0.48725	0.01518	0.988	2928	8	2770	30	2559	65
1011151-11	1088557	43	0.13719	0.00069	7.43947	0.22624	0.39329	0.01180	0.986	2192	9	2166	27	2138	54
1011151-12	712892	46	0.22526	0.00104	17.74276	0.58904	0.57638	0.01895	0.990	3004	7	2976	31	2934	77
1011151-13	440229	32	0.22520	0.00103	17.58591	0.65182	0.57145	0.02102	0.992	3004	7	2967	35	2914	86
1011151-14	391590	45	0.22717	0.00110	17.65269	0.58289	0.56359	0.01941	0.989	3032	8	2971	31	2881	75
1011151-15	720778	63	0.22956	0.00106	18.57949	0.59814	0.58700	0.01870	0.990	3049	7	3020	31	2977	76
1011151-16	475274	40	0.22018	0.00109	18.40553	0.72876	0.58247	0.02289	0.993	3046	8	3011	37	2959	93
1011151-17	1095098	33	0.21469	0.00129	16.81027	0.58885	0.56788	0.01960	0.985	2941	10	2924	33	2899	80
1011151-18	280046	29	0.13782	0.00068	7.39133	0.20172	0.38895	0.01044	0.983	2200	9	2160	24	2118	48
1011151-19	253192	39	0.13889	0.00072	7.36694	0.26020	0.38468	0.01344	0.989	2213	9	2157	31	2098	62
1011151-20	812531	14	0.24738	0.00274	22.18918	0.85730	0.65055	0.02408	0.958	3168	17	3192	37	3230	93
1011151-21	762928	0	0.23030	0.00115	17.97745	0.62638	0.56614	0.01952	0.990	3058	8	2983	33	2892	80
1011151-22	772625	0	0.21197	0.00097	16.19637	0.67560	0.55417	0.02296	0.994	2921	7	2888	39	2842	95
1011151-23	796126	0	0.22914	0.00102	18.71930	0.51586	0.59250	0.01611	0.987	3046	7	3027	26	3000	65
1011151-24	816938	0	0.21313	0.00097	16.46202	0.59280	0.58020	0.02001	0.992	2929	7	2904	34	2867	82
1011151-26	137693	0	0.13839	0.00073	7.27371	0.26073	0.38119	0.01352	0.989	2207	9	2146	32	2082	63
1011151-27	348294	0	0.23044	0.00115	17.93075	0.64347	0.59433	0.02006	0.990	3055	8	2986	34	2885	82
1011151-30	1173150	0	0.18066	0.00083	13.43118	0.50643	0.54654	0.01912	0.991	2748	8	2711	31	2651	61
1011151-31	268055	2	0.13803	0.00065	7.39712	0.23076	0.38888	0.01199	0.989	2203	8	2161	28	2117	55
1011151-31	1099466	0	0.22403	0.00109	17.31069	0.59920	0.56071	0.01921	0.990	3010	8	2953	33	2870	79
1011151-32	200772	0	0.22714	0.00108	17.93137	0.70694	0.57256	0.02241	0.993	3032	8	2986	37	2918	91
1011151-33	1491633	2	0.22456	0.00105	17.32801	0.66675	0.55958	0.02138	0.993	3014	7	2953	36	2865	88
1011151-34	240456	0	0.25238	0.00131	20.78734	0.66290	0.59738	0.01880	0.987	3200	8	3129	30	3019	75
1011151-35	336122	30	0.20581	0.00388	13.95397	0.66153	0.49174	0.02139	0.918	2873	30	2747	44	2578	92
1011151-36	410455	2	0.13883	0.00068	7.27034	0.23828	0.37982	0.01231	0.989	2213	8	2145	29	2075	57
1011151-37	253418	9	0.22782	0.00108	17.52841	0.63816	0.55803	0.02014	0.991	3037	8	2964	34	2858	83
1011151-38	701080	11	0.26192	0.00188	22.52362	0.88185	0.62639	0.02401	0.983	3258	11	3207	37	3125	95
1011151-39	360974	5	0.13839	0.00067	7.32041	0.25219	0.38363	0.01309	0.990	2207	8	2151	30	2093	61
1011151-40	538821	0	0.22996	0.00105	17.82881	0.61268	0.56230	0.01915	0.991	3052	7	2981	33	2876	79
1011151-41	311625	0	0.21837	0.00107	15.79864	0.57660	0.52834	0.01911	0.991	2958	8	2865	34	2734	80
1011151-42	730728	0	0.22739	0.00104	17.80688	0.61829	0.56157	0.01955	0.991	3034	7	2968	33	2878	80
1011151-43	1003090	0	0.14444	0.00071	8.38648	0.31369	0.42111	0.01562	0.991	2281	8	2274	33	2260	70
1011151-44	1198591	0	0.21020	0.00096	15.83988	0.53291	0.54654	0.01822	0.991	2967	7	2867	32	2811	75
1011151-45	2573743	0	0.21380	0.00106	16.31164	0.63968	0.55333	0.02152	0.992	2955	8	2895	37	2839	89
1011151-46	589707	0	0.18235	0.00085	12.53501	0.48289	0.49956	0.01907	0.993	2674	8	2645	36	2608	82
1011151-47	1119009	3	0.22911	0.00276	17.76134	0.78079	0.56225	0.02377	0.982	3046	19	2977	41	2876	97
1011151-48	589490	0	0.22031	0.00109	18.01885	0.56876	0.56991	0.01779	0.989	3047	8	2991	30	2907	73
1011151-49	1404532	0	0.25183	0.00126	21.77120	0.62317	0.67071	0.01767	0.985	3196	8	3174	27	3138	70
1011151-50	383048	0	0.21445	0.00102	15.92384	0.55069	0.53854	0.01845	0.991	2939	8	2872	33	2777	77
1011151-51	1593921	0	0.22365	0.00103	16.99137	0.64209	0.55102	0.02067	0.993	3007	7	2994	36	2820	85
1011151-52	94190	0	0.19782	0.00269	4.65947	0.49901	0.17083	0.01815	0.992	2808	22	1760	86	1017	99
1011151-53	513681	0	0.22976	0.00103	17.38314	0.50292	0.54872	0.01568	0.988	3050	7	2956	27	2826	65
1011151-54	309572	0	0.13817	0.00065	7.15961	0.21342	0.37581	0.01106	0.987	2204	8	2131	26	2057	52
1011151-55	1236651	0	0.13765	0.00070	7.31092	0.29679	0.38523	0.01551	0.992	2198	9	2150	36	2101	72
1011151-57	1555043	0	0.20987	0.00103	15.67265	0.52560	0.54162	0.01797	0.989	2905	8	2857	32	2790	75
1011151-58	390392	0	0.22806	0.00108	18.14888	0.72956	0.57465	0.02294	0.993	3045	8	2998	38	2927	93
1011151-59	1257133	0	0.20808	0.00100	15.33533	0.60128	0.53452	0.02080	0.992	2891	8	2836	37	2760	87
1011151-60	1758643	0	0.21077	0.00096	15.59857	0.52644	0.53676	0.01791	0.991	2911	7	2853	32	2770	75
1011151-62	215113	0	0.13932	0.00068	7.26878	0.25776	0.37798	0.01213	0.989	2219	8	2144	28	2067	57
1011151-63	2414397	0	0.22750	0.00117	17.66714	0.82073	0.56323	0.01957	0.989	3035	8	2973	33	2880	80
1011151-64	819978	0	0.22082	0.00104	17.90998	0.54063	0.56501	0.01687	0.989	3051	7	2985	30	2887	69
1011151-65	1826517	0	0.22725	0.00105	17.55534	0.60792	0.56666	0.01922	0.991	3033	7	2977	32	2894	79
1011151-66	1581972	0	0.25533	0.00128	21.79141	0.64354	0.61898	0.02376	0.992	3218	8	3174	37	3106	94
1011151-67	621078	13	0.13989	0.00105	7.42548	0.26371	0.38497	0.01336	0.977	2226	13	2164	31	2099	62
1011151-68	563919	0	0.13774	0.00069	7.39006	0.27107	0.38913	0.01414	0.991	2199	9	2160	32	2119	65
1011151-69	383989	0	0.20710	0.00150	15.52482	0.59022	0.54368	0.02020	0.982	2883	12	2848	36	2799	84
1011151-70	324394	0	0.13874	0.00073	7.49511	0.28320	0.39182	0.01466	0.990	2212	9	2172	33	2131	68
1011151-71	776147	65	0.13967	0.00084	7.41832	0.30477	0.38523	0.01565	0.989	2223	10	2163	36	2101	72
1011151-72	384073	33	0.13944	0.00069	7.28864	0.25122	0.37807	0.01293	0.990	2220	8	2145	30	2067	60
1011151-73	593132	51	0.13897	0.00068	7.30917	0.25088	0.38145	0.01396	0.990	2214	8	2150	30	2083	60
1011151-75	310208	46	0.22798	0.00111	17.03405	0.62973	0.54195	0.01988	0.991	3038	8	2937	35	2792	83
1011151-77	1162862	12	0.13829	0.00068	7.10773	0.23989	0.37277	0.01245	0.988	2206	9	2125	30	2042	58
1011151-78	550299	100	0.14011	0.00077	7.02676	0.22909	0								

sample name	<sup>206</sup> Pb (cpa)	<sup>207</sup> Pb (cpa)	<sup>206</sup> Pb/ <sup>207</sup> Pb	1 σ	<sup>206</sup> Pb/ <sup>238</sup> U	1 σ	<sup>207</sup> Pb/ <sup>235</sup> U	1 σ	ρ	<sup>206</sup> Pb/ <sup>207</sup> Pb ± 1 σ	age (Ma)	error (Ma)	<sup>207</sup> Pb/ <sup>235</sup> U ± 1 σ	age (Ma)	error (Ma)	<sup>206</sup> Pb/ <sup>238</sup> U ± 1 σ	age (Ma)	error (Ma)	discordance
101026-1	124627	37	0.13300	0.00186	6.97562	0.73719	0.38067	0.03987	0.991	2137	34	2108	90	2079	184	3.1			
101026-2	608114	20	0.13377	0.00189	7.29812	0.79478	0.39568	0.04280	0.993	2148	23	2149	93	2149	93	2149	195	-0.1	
101026-3	174855	14	0.12671	0.00182	6.60246	0.63952	0.37793	0.03639	0.991	2053	22	2060	82	2060	82	2060	168	-0.8	
101026-4	112391	20	0.12887	0.00173	6.45440	0.73181	0.36045	0.04050	0.993	2083	23	2033	94	1994	191	5.5			
101026-5	364469	27	0.13322	0.00186	7.10105	0.69138	0.38953	0.03761	0.992	2138	22	2134	83	2124	83	2124	172	0.4	
101026-6	180773	15	0.13143	0.00188	6.41654	0.63968	0.35412	0.03501	0.992	2117	22	2035	84	1954	165	8.9			
101026-7	197314	16	0.12848	0.00181	6.49119	0.60746	0.36643	0.03390	0.989	2077	25	2045	79	2013	158	3.6			
101026-8	64186	7	0.05824	0.00181	0.76377	0.07188	0.09512	0.00845	0.944	539	67	576	41	586	50	-9.1			
101026-9	449108	815	0.14742	0.00270	2.70398	0.35385	0.13303	0.01724	0.990	2316	31	1330	93	805	97	69.2			
101026-10	276739	15	0.12716	0.00182	6.50820	0.60338	0.37121	0.03403	0.990	2059	22	2047	78	2035	158	1.4			
101026-11	208697	58	0.14129	0.00303	7.53977	0.79344	0.38703	0.03987	0.979	2243	37	2178	90	2109	183	7.0			
101026-12	241891	10	0.12058	0.00140	4.44904	0.42412	0.30475	0.02877	0.990	1730	24	1722	76	1715	141	1.0			
101026-13	275536	9	0.12924	0.00164	6.74442	0.65056	0.37848	0.03619	0.991	2088	22	2078	82	2069	167	1.0			
101026-14	94672	286	0.10044	0.00726	0.89885	0.11058	0.06490	0.00646	0.809	1632	129	651	57	405	39	77.5			
101026-15	188202	12	0.12898	0.00172	6.71594	0.63663	0.37768	0.03544	0.990	2084	23	2075	81	2065	164	1.1			
101026-16	202879	67	0.12810	0.00184	6.00911	0.65180	0.34025	0.03551	0.993	2072	22	1977	88	1888	169	10.2			
101026-17	274251	103	0.13053	0.00165	6.22915	0.60242	0.34512	0.03319	0.991	2105	22	2009	81	1916	157	10.4			
101026-18	74073	79	0.06102	0.00113	0.75953	0.07606	0.09028	0.00888	0.983	640	39	574	43	574	52	13.5			
101026-19	398699	117	0.12836	0.00182	7.23730	1.10766	0.41100	0.06237	0.997	2076	22	2146	128	2219	279	-8.2			
101026-20	643668	221	0.13342	0.00173	6.59887	0.72790	0.35870	0.03929	0.993	2144	23	2059	93	1976	184	9.1			
101026-21	251117	73	0.13500	0.00174	7.13983	0.75395	0.38359	0.04020	0.993	2164	23	2129	90	2093	185	3.8			
101026-22	177573	92	0.13114	0.00187	6.74944	0.64588	0.37529	0.03540	0.991	2113	23	2079	81	2045	164	3.8			
101026-23	48888	104	0.06053	0.00128	0.77167	0.07358	0.09246	0.00859	0.755	623	45	581	41	570	51	8.8			
101026-24	72201	97	0.13835	0.00181	7.54631	0.74178	0.39408	0.03854	0.991	2207	23	2177	85	2146	176	3.2			
101026-25	152523	91	0.13433	0.00175	6.91246	0.65523	0.37325	0.03559	0.991	2155	23	2100	82	2045	165	6.0			
101026-26	137441	140	0.11530	0.00153	3.48372	0.35035	0.21914	0.02184	0.991	1885	24	1524	76	1277	114	35.5			
101026-27	111439	154	0.06120	0.00088	0.78450	0.07313	0.09297	0.00856	0.888	646	30	588	41	573	50	11.8			
101026-28	115241	160	0.13299	0.00181	6.55614	0.61753	0.35755	0.03332	0.990	2138	24	2053	80	1971	156	9.1			
101026-29	608343	186	0.12837	0.00188	6.28417	0.71411	0.35505	0.04008	0.993	2076	23	2016	95	1959	188	6.5			
101026-30	398232	194	0.13350	0.00173	6.46384	0.63521	0.35312	0.03311	0.991	2144	22	2041	83	1940	161	11.0			
101026-31	287442	203	0.06165	0.00124	0.85896	0.08775	0.10187	0.01012	0.980	662	43	633	47	623	59	5.8			
101026-32	485712	238	0.13027	0.00166	7.08889	0.71056	0.39467	0.03924	0.992	2102	22	2123	85	2144	179	-2.4			
101026-33	693349	269	0.12446	0.00172	5.12356	0.52355	0.29856	0.03023	0.991	2021	24	1840	83	1684	148	18.9			
101026-34	537071	237	0.13079	0.00167	6.45654	0.68334	0.35803	0.03761	0.993	2109	22	2040	89	1973	176	7.5			
101026-35	215881	185	0.13153	0.00166	6.90913	0.68897	0.36809	0.03788	0.992	2119	22	2100	85	2081	174	2.1			
101026-36	121	121	0.12621	0.00166	6.54511	0.66621	0.35424	0.03526	0.992	2062	22	2006	76	1922	148	5.5			
101026-37	285314	186	0.12843	0.00163	6.17016	0.56011	0.34044	0.03132	0.990	2077	22	2007	76	1927	148	8.3			
101026-38	183090	171	0.12869	0.00163	6.27851	0.62485	0.35394	0.03483	0.992	2080	22	2015	84	1953	164	7.1			
101026-39	235361	189	0.13202	0.00187	6.65033	0.65751	0.36534	0.03582	0.992	2125	22	2066	84	2007	167	6.4			
101026-40	194095	242	0.13211	0.00168	7.07928	0.64724	0.36863	0.03519	0.990	2126	22	2121	78	2116	161	0.5			
101026-41	196238	255	0.13337	0.00171	6.77733	0.66924	0.36854	0.03608	0.992	2143	22	2083	84	2033	168	6.5			
101026-42	125244	283	0.13439	0.00169	6.63721	0.58349	0.34923	0.03111	0.990	2089	24	1993	85	1712	152	23.4			
101026-43	506995	200	0.11836	0.00166	3.78252	0.39480	0.23178	0.02397	0.991	1932	25	1589	81	1484	124	33.7			
101026-44	92569	188	0.06107	0.00084	0.82766	0.08144	0.09830	0.00955	0.888	642	36	612	44	604	56	6.1			
101026-45	443405	220	0.13196	0.00169	6.51744	0.74169	0.35821	0.04051	0.994	2134	22	2048	96	1974	189	8.2			
101026-46	78934	165	0.05974	0.00082	0.78126	0.07053	0.09486	0.00846	0.888	594	39	586	39	586	39	1.7			
101026-47	512625	132	0.12728	0.00170	6.02099	0.54750	0.34310	0.03006	0.989	2060	21	1979	76	1902	146	8.9			
101026-48	252877	91	0.13009	0.00165	6.77855	0.62301	0.37790	0.03440	0.990	2099	22	2083	78	2066	159	1.8			
101026-49	445440	609	0.13580	0.00348	0.10349	0.50966	0.46322	0.02500	0.990	2174	69	2121	83	2062	163	32.3			
101026-50	652376	590	0.13428	0.00276	5.83730	0.81534	0.31528	0.04356	0.989	2155	35	1952	114	1767	210	20.6			
101026-51	584217	63	0.13088	0.00187	6.60140	0.60068	0.36582	0.03296	0.990	2110	22	2060	77	2010	154	5.5			
101026-52	372495	77	0.13479	0.00171	6.97296	0.66015	0.37519	0.03520	0.991	2161	22	2108	81	2054	163	5.8			
101026-53	167101	71	0.13769	0.00164	6.54523	0.63789	0.37176	0.03592	0.991	2066	22	2052	82	2038	167	1.6			
101026-54	263029	61	0.12857	0.00185	6.43814	0.60449	0.36519	0.03378	0.991	2078	22	2037	79	1997	158	4.5			
101026-55	327895	69	0.13090	0.00177	6.11995	0.58996	0.34322	0.03239	0.990	2089	24	1993	81	1902	155	10.3			
101026-56	219369	54	0.12693	0.00163	6.54859	0.62302	0.36554	0.03442	0.991	2097	22	2052	80	2008	160	4.9			
101026-57	262398	70	0.13250	0.00175	6.08002	0.60488	0.33281	0.03381	0.991	2131	23	1987	83	1852	157	11.1			
101026-58	148577	65	0.13300	0.00172	6.41192	0.62160	0.34965	0.03359	0.991	2138	22	2034	82	1933	158	15.1			
101026-59	246990	46	0.12782	0.00161	6.40168	0.59946	0.36324	0.03370	0.991	2048	22	2032	79	1997	157	4.0			
101026-60	107298	77	0.06444	0.00228	0.81498	0.08306	0.09173	0.03900	0.841	756	73	605	47	586	53	26.2			
101026-61	461572	64	0.13247	0.00157	5.54831	0.56179	0.32362	0.03253	0.992	2025	22	1908	84	1803	157	13.6			
101026-62	877964	140	0.13734	0.00159	6.43317	0.40989	0.36640	0.03443	0.991	2082	22	2037	80	2013	160	2.8			
101026-63	443370	142	0.13178	0.00166	6.71215	0.60105	0.36941	0.03275	0.990	2122	22	2074	76	2027	152	5.3			
101026-64	262894	113	0.13179	0.00166	6.98436	0.67740	0.38437	0.03696	0.992	2122	22	2109	83	2097	170	1			

sample name	<sup>206</sup> Pb (cps)	<sup>207</sup> Pb (cps)	<sup>206</sup> Pb/ <sup>207</sup> Pb	2 σ	<sup>207</sup> Pb/ <sup>235</sup> U	2 σ	<sup>206</sup> Pb/ <sup>238</sup> U	2 σ	ρ	age (Ma)	error (Ma)	<sup>207</sup> Pb/ <sup>235</sup> U	2 σ	<sup>206</sup> Pb/ <sup>238</sup> U	2 σ	<sup>206</sup> Pb/ <sup>238</sup> U	2 σ	discordance
101012-2-1	61610	24	0.06146	0.00164	0.82590	0.05124	0.09746	0.00946	0.003	655	56	611	28	599	32	8.9		
101012-2-2	60708	33	0.10757	0.00271	4.32597	0.25536	0.29106	0.01557	0.004	1759	45	1698	48	1690	77	7.0		
101012-2-3	71596	32	0.06009	0.00155	0.79328	0.04477	0.08814	0.00490	0.008	1067	55	557	26	545	26	10.7		
101012-2-4	119083	57	0.07569	0.00441	1.53299	0.21151	0.14684	0.01837	0.007	1187	113	943	81	883	100	20.0		
101012-2-5	596611	356	0.12965	0.00260	5.19085	0.33774	0.29039	0.01708	0.004	2089	48	1851	54	1643	85	24.3		
101012-2-5B	203065	90	0.08099	0.00680	1.39997	0.20754	0.12537	0.01532	0.024	1321	157	889	84	761	87	39.9		
101012-2-6	64044	129	0.06190	0.00165	0.82365	0.05739	0.09651	0.00621	0.024	671	56	610	31	594	36	12.0		
101012-2-6B	148669	109	0.05940	0.00153	0.78055	0.04908	0.09531	0.00533	0.008	582	55	586	27	587	31	-0.9		
101012-2-7	292006	131	0.15341	0.00440	8.69973	0.36587	0.41134	0.02401	0.007	2384	48	2307	58	2231	109	8.1		
101012-2-8	743389	149	0.18095	0.00447	12.26255	0.71081	0.49150	0.02578	0.005	2662	40	2625	53	2577	110	3.8		
101012-2-9	1043157	339	0.18333	0.00458	12.25538	0.79824	0.48751	0.02930	0.023	2674	41	2634	59	2560	126	5.2		
101012-2-10	280810	20	0.12653	0.00113	6.51180	0.37797	0.37324	0.01961	0.005	2050	43	2047	50	2045	91	0.3		
101012-2-10B	308106	16	0.12661	0.00112	6.43436	0.38839	0.36860	0.02030	0.013	2051	43	2037	52	2033	95	1.6		
101012-2-11	305532	31	0.09148	0.00227	3.13501	0.18977	0.24856	0.01373	0.012	1457	46	1441	46	1431	70	2.0		
101012-2-12	172962	85	0.05971	0.00150	0.77867	0.05110	0.09458	0.00573	0.023	593	54	585	29	583	34	1.9		
101012-2-12B	289183	57	0.05992	0.00149	0.80444	0.05595	0.09737	0.00633	0.024	601	53	599	31	599	37	0.3		
101012-2-13	86358	104	0.05894	0.00154	0.76728	0.04412	0.09402	0.00485	0.002	561	56	576	25	579	29	-3.4		
101012-2-14	208232	118	0.18170	0.00449	12.60008	0.72848	0.50294	0.02629	0.004	2668	40	2650	53	2626	113	1.9		
101012-2-15	650351	111	0.13371	0.00337	6.64763	0.40210	0.36059	0.01983	0.009	2147	43	2066	52	1985	93	8.8		
101012-2-16	61408	107	0.05979	0.00153	0.80208	0.04607	0.09737	0.00500	0.005	596	55	598	26	599	29	-0.5		
101012-2-16B	76039	96	0.05983	0.00154	0.79642	0.04590	0.09654	0.00497	0.004	598	55	595	26	594	29	0.6		
101012-2-17	187258	219	0.07054	0.00263	0.92082	0.06130	0.09548	0.00520	0.026	944	74	667	32	588	31	39.5		
101012-2-18	81175	98	0.06095	0.00174	0.82085	0.04821	0.09768	0.00563	0.015	607	60	609	27	601	29	6.8		
101012-2-19	64497	107	0.06105	0.00233	0.81580	0.05341	0.09891	0.00511	0.013	641	80	606	29	596	30	7.1		
101012-2-20	443255	148	0.13478	0.00335	7.16407	0.41111	0.38551	0.01994	0.002	2161	43	2132	50	2102	92	3.3		
101012-2-21	109991	121	0.06061	0.00155	0.78753	0.04722	0.09424	0.00518	0.010	625	54	590	27	581	30	7.5		
101012-2-22	243467	215	0.06603	0.00176	0.91054	0.05844	0.10003	0.00584	0.010	807	55	657	31	615	34	25.0		
101012-2-23	56087	131	0.06128	0.00184	0.83405	0.05013	0.09871	0.00514	0.005	649	63	618	27	607	30	6.8		
101012-2-23B	79396	132	0.06002	0.00157	0.82630	0.04918	0.09886	0.00530	0.000	626	55	612	27	608	31	3.0		
101012-2-24	89471	173	0.05706	0.00186	0.80277	0.04877	0.10243	0.00524	0.005	494	70	600	27	629	31	-2.8		
101012-2-24B	59571	142	0.06583	0.00150	0.79424	0.04660	0.10103	0.00533	0.002	475	58	594	26	625	31	-8.1		
101012-2-25	390766	59	0.13041	0.00348	4.89966	0.32146	0.27251	0.01633	0.013	2103	46	1802	54	1554	82	29.4		
101012-2-25B	206399	279	0.12988	0.00322	6.33131	0.35859	0.34807	0.01807	0.002	2086	43	2009	49	1925	86	9.4		
101012-2-26	330614	154	0.13504	0.00336	7.88190	0.47320	0.43332	0.02313	0.010	2165	43	2218	53	2276	104	-6.1		
101012-2-26B	260072	216	0.13566	0.00336	7.86019	0.45482	0.42023	0.02197	0.004	2172	43	2215	51	2262	99	-4.9		
101012-2-27	562920	218	0.17876	0.00444	12.54277	0.74986	0.50888	0.02767	0.009	2641	41	2646	55	2652	117	-0.5		
101012-2-28	290779	209	0.12423	0.00218	6.46629	0.38968	0.37343	0.02429	0.005	2042	44	2065	49	2065	69	2.8		
101012-2-29	199272	187	0.16467	0.00682	11.44783	0.87876	0.50419	0.03259	0.042	2504	68	2560	69	2632	138	-6.2		
101012-2-30	493205	244	0.12771	0.00317	7.16906	0.44659	0.40712	0.02326	0.017	2067	43	2133	54	2202	106	-7.7		
101012-2-31	570318	351	0.19041	0.00491	11.76982	0.66544	0.44830	0.02256	0.000	2746	43	2586	52	2388	100	15.6		
101012-2-31B	594421	310	0.23588	0.00585	20.03783	1.12783	0.61010	0.03113	0.008	3092	39	3095	53	3094	123	-0.1		
101012-2-32	53734	256	0.05897	0.00166	0.82705	0.05130	0.10171	0.00562	0.002	566	60	612	28	624	33	-10.8		
101012-2-33	63335	271	0.06328	0.00206	0.86791	0.06305	0.09948	0.00540	0.017	718	89	634	34	611	32	15.5		
101012-2-34	107662	249	0.06400	0.00167	0.89486	0.05966	0.10441	0.00510	0.017	742	54	649	31	623	36	16.8		
101012-2-34	912516	458	0.13964	0.00351	7.53648	0.43604	0.39145	0.02040	0.001	2223	43	2177	51	2130	94	4.9		
101012-2-35	347422	189	0.15405	0.00393	9.06091	0.58114	0.42659	0.02510	0.018	2391	43	2344	57	2280	113	5.0		
101012-2-36	92574	160	0.06103	0.00179	0.81842	0.04987	0.09726	0.00516	0.016	640	62	607	27	598	30	6.9		
101012-2-37	459076	105	0.16822	0.00417	9.73234	0.58385	0.41960	0.02387	0.010	2540	41	2410	54	2359	103	13.1		
101012-2-38	80705	117	0.05683	0.00154	0.79935	0.04509	0.09777	0.00486	0.017	466	59	574	25	601	29	-30.4		
101012-2-39	249666	385	0.13796	0.00399	7.88312	0.82358	0.41442	0.04055	0.016	2202	74	2218	63	2235	164	-1.6		
101012-2-40	121030	102	0.06218	0.00204	0.83916	0.05922	0.09738	0.00511	0.005	680	49	619	32	602	34	12.1		
101012-2-41	90386	59	0.06143	0.00154	0.81206	0.04698	0.09587	0.00500	0.001	654	53	604	26	590	29	10.3		
101012-2-42	244723	121	0.06425	0.00170	0.87072	0.04912	0.09820	0.00490	0.003	750	55	636	26	604	29	20.3		
101012-2-43	211197	92	0.13062	0.00324	7.11706	0.45768	0.39516	0.02223	0.015	2106	43	2126	53	2147	102	-2.3		
101012-2-44	620220	144	0.17495	0.00432	11.21367	0.71080	0.46488	0.02714	0.021	2606	41	2541	57	2461	118	6.7		
101012-2-45	161801	130	0.12976	0.00321	6.40531	0.41038	0.33801	0.02116	0.022	2095	43	2033	55	1973	100	6.8		
101012-2-46	1507429	49	0.11729	0.00295	4.86662	0.28920	0.30089	0.02020	0.006	1916	45	1796	46	1696	80	13.0		
101012-2-47	311729	457	0.19580	0.00321	7.85829	0.61206	0.38294	0.02139	0.043	2792	43	2189	70	1806	107	47.8		
101012-2-48	405895	214	0.13738	0.00339	7.58831	0.45555	0.40002	0.02192	0.012	2184	42	2183	52	2172	100	1.2		
101012-2-49	254061	273	0.06295	0.00184	0.87159	0.05651	0.10041	0.00581	0.003	707	61	636	30	617	34	13.3		
101012-2-50	57932	171	0.06491	0.00180	0.88309	0.05427	0.09877	0.00541	0.002	771	57	643	29	607	32	22.3		
101012-2-51	51580	196	0.06517	0.00182	0.83551	0.06458	0.09299	0.00670	0.016	780	58	617	35	573	39	20.7		
101012-2-52	535498	182	0.13099	0.00331	6.88842	0.38826	0.33140	0.01922	0.004	2111	44	2097	49	2083	89	1.6		
101012-2-53	387757	178	0.13683	0.00338	7.38977	0.44801	0.39170	0.02168	0.013	2187	42	2160	63	2131	100	3.9		
101012-2-54	191767	192	0.10728	0.00266	4.42616	0.25547	0.29923	0.01559	0.008	1754	45	1717	47	1688	77	4.3		
101012-2-55	180517	260	0.06558	0.00249	0.84805	0.05387	0.09674	0.00483	0.017	728	81	634	29	595	28	19.1		
101012-2-56	128436	280	0.18856	0.00468	13.34500	0.80798	0.51407	0.03200	0.020									



sample name	<sup>206</sup> Pb (cps)	<sup>207</sup> Pb (cps)	<sup>207</sup> Pb/ <sup>206</sup> Pb	2 σ	<sup>207</sup> Pb/ <sup>238</sup> U	2 σ	<sup>206</sup> Pb/ <sup>238</sup> U	2 σ	ρ	age (Ma)	error (Ma)	age (Ma)	error (Ma)	age (Ma)	error (Ma)	discordance
SAN CARLOS-1	24799	103	0.06086	0.00057	0.73243	0.02054	0.08728	0.00231	0.943	634	20	558	12	539	14	15.6
SAN CARLOS-1B	37572	338	0.09734	0.01347	1.18954	0.16914	0.08914	0.00259	0.206	1574	259	793	75	550	15	67.8
SAN CARLOS-2	33681	148	0.06093	0.00063	0.75511	0.02247	0.09011	0.00251	0.937	637	22	574	13	556	13	13.3
SAN CARLOS-3	131419	125	0.06309	0.00034	0.94076	0.03674	0.10814	0.00418	0.990	711	12	799	19	862	24	7.3
SAN CARLOS-4	121529	132	0.06072	0.00033	0.74605	0.01958	0.08911	0.00229	0.979	629	11	566	11	550	14	13.1
SAN CARLOS-5	326573	165	0.08044	0.00035	2.07399	0.06238	0.18699	0.00556	0.990	1208	8	1140	20	1105	30	9.3
SAN CARLOS-6	175319	127	0.07731	0.00039	1.89554	0.05182	0.17784	0.00478	0.983	1129	10	1080	18	1055	26	7.1
SAN CARLOS-6B	372650	186	0.07903	0.00030	1.97883	0.04263	0.18160	0.00385	0.984	1173	8	1108	14	1076	21	9.0
SAN CARLOS-7	234595	187	0.11784	0.00067	5.18914	0.12439	0.31938	0.00743	0.971	1924	10	1851	20	1787	36	8.2
SAN CARLOS-7B	303789	150	0.11467	0.00094	5.47286	0.17774	0.34614	0.01116	0.993	1875	7	1896	28	1916	53	2.6
SAN CARLOS-8	32420	169	0.06051	0.00068	0.75917	0.02170	0.09100	0.00259	0.919	622	24	574	12	561	14	10.1
SAN CARLOS-9	271059	388	0.08390	0.00440	1.55258	0.09312	0.13423	0.00391	0.485	1290	99	952	36	812	23	39.4
SAN CARLOS-10	83380	306	0.07954	0.00393	1.01030	0.05649	0.09213	0.00241	0.468	1186	95	709	28	588	14	54.4
SAN CARLOS-11	285425	175	0.08504	0.00326	2.32391	0.19659	0.19896	0.01481	0.833	1316	75	1222	58	1170	79	14.2
SAN CARLOS-12	811234	671	0.10273	0.00236	3.60600	0.11944	0.25419	0.00608	0.721	1674	42	1550	26	1460	31	14.3
SAN CARLOS-13	294929	2498	0.15919	0.00954	2.79157	0.18928	0.12719	0.00404	0.469	2447	98	1353	49	772	23	72.5
SAN CARLOS-14	696348	8124	0.23176	0.01744	3.53114	0.33752	0.11113	0.00645	0.611	3064	115	1339	73	679	37	81.7
SAN CARLOS-15	101866	165	0.06016	0.00039	0.75827	0.02446	0.09141	0.00289	0.980	609	57	574	14	564	17	7.8
SAN CARLOS-15B	125235	192	0.05994	0.00033	0.74552	0.02089	0.08996	0.00248	0.981	601	12	564	12	555	15	8.0
SAN CARLOS-16	100331	181	0.06384	0.00020	0.88028	0.02494	0.10001	0.00280	0.987	738	10	641	13	614	16	11.4
SAN CARLOS-17	240119	2950	0.20266	0.03338	2.39898	0.38175	0.08231	0.00170	0.125	2848	246	1212	111	510	10	85.2
SAN CARLOS-18	130089	437	0.08986	0.00573	1.51224	0.10641	0.12206	0.00363	0.422	1423	117	935	42	742	21	50.6
SAN CARLOS-19	32169	231	0.06159	0.00056	0.73396	0.01812	0.08643	0.00198	0.929	660	19	559	11	534	12	19.8
SAN CARLOS-20	19746	192	0.06189	0.00099	0.72211	0.01975	0.08462	0.00188	0.810	670	34	552	12	524	11	22.8
SAN CARLOS-21	177195	475	0.07694	0.00482	1.04344	0.07052	0.09836	0.00249	0.375	1120	120	726	34	605	15	48.1
SAN CARLOS-22	307239	237	0.11285	0.00081	4.65893	0.13280	0.25992	0.00206	0.968	1846	13	1760	24	1888	41	9.7
SAN CARLOS-23	93949	213	0.06134	0.00032	0.73796	0.02584	0.10447	0.00226	0.984	700	11	554	12	541	17	11.5
SAN CARLOS-24	241834	522	0.08044	0.00206	1.26709	0.06081	0.11425	0.00464	0.846	1208	50	831	27	697	27	44.6
SAN CARLOS-24B	402874	6489	0.27488	0.00936	3.47732	0.14798	0.09175	0.00234	0.600	3334	52	1522	33	566	14	86.5
SAN CARLOS-25	214453	222	0.06142	0.00027	0.85454	0.02390	0.10091	0.00279	0.988	654	9	627	13	620	16	5.5
SAN CARLOS-26	100982	195	0.05993	0.00034	0.74701	0.02051	0.09040	0.00317	0.987	601	12	566	15	558	19	7.5
SAN CARLOS-26B	91250	226	0.06107	0.00106	0.75313	0.03211	0.08944	0.00348	0.913	642	37	570	18	552	21	14.5
SAN CARLOS-27	317196	231	0.08062	0.00033	2.20623	0.05358	0.19830	0.00475	0.985	1212	8	1182	17	1166	25	42.2
SAN CARLOS-28	184136	243	0.06532	0.00058	0.75708	0.02118	0.09103	0.00248	0.974	615	14	572	12	502	15	9.1
SAN CARLOS-29	98949	217	0.06134	0.00032	0.73796	0.02584	0.10447	0.00226	0.984	700	11	554	12	541	17	11.5
SAN CARLOS-30	159911	245	0.06744	0.00035	1.08818	0.02596	0.12042	0.00275	0.974	830	11	757	12	733	16	11.3
SAN CARLOS-31	195291	284	0.06550	0.00031	1.16192	0.03670	0.12673	0.00396	0.989	822	10	783	17	769	23	6.8
SAN CARLOS-32	167114	285	0.06627	0.00031	1.16742	0.03663	0.12776	0.00396	0.989	815	10	785	17	775	23	5.2
SAN CARLOS-33	96725	261	0.06599	0.00042	1.12726	0.03107	0.12390	0.00333	0.974	808	13	766	15	753	19	7.0
SAN CARLOS-34	134127	291	0.06252	0.00031	0.90657	0.02044	0.10517	0.00231	0.976	692	11	655	11	645	13	7.2
SAN CARLOS-35	103438	277	0.05993	0.00033	0.75211	0.02347	0.09102	0.00280	0.984	601	12	569	14	562	16	6.8
SAN CARLOS-36	200633	253	0.06351	0.00023	0.78227	0.02162	0.10447	0.00226	0.984	700	11	554	12	541	17	11.5
SAN CARLOS-37	306370	419	0.08577	0.00122	2.22626	0.07723	0.11825	0.00596	0.912	1333	27	1189	24	1112	32	18.1
SAN CARLOS-38	217903	269	0.08176	0.00030	2.28911	0.06641	0.20307	0.00602	0.992	1240	7	1209	21	1192	33	4.2
SAN CARLOS-39	276239	397	0.06961	0.00362	1.21105	0.05334	0.12618	0.00289	0.519	917	76	806	24	766	16	28.9
SAN CARLOS-40	104372	246	0.08030	0.00152	2.07365	0.09172	0.18746	0.00748	0.903	1204	37	1141	30	1108	40	8.8
SAN CARLOS-41	129796	408	0.07044	0.00342	1.00821	0.05942	0.10381	0.00346	0.566	941	96	708	30	637	20	34.0
SAN CARLOS-42	206912	276	0.06252	0.00030	0.90686	0.02807	0.10520	0.00322	0.988	692	10	655	15	645	19	7.2
SAN CARLOS-43	163371	452	0.07366	0.00044	0.99983	0.02696	0.09805	0.00259	0.975	1032	12	702	14	603	15	45.5
SAN CARLOS-44	226313	313	0.06618	0.00028	1.15293	0.02747	0.12653	0.00407	0.992	812	9	779	18	767	23	5.9
SAN CARLOS-45	122104	1101	0.10073	0.00235	2.22626	0.28947	0.08839	0.00316	0.153	1658	377	813	123	545	19	69.5
SAN CARLOS-46	308707	355	0.13301	0.00078	6.66005	0.14160	0.36316	0.00742	0.961	2138	10	2067	19	1997	35	7.7
SAN CARLOS-47	204067	377	0.06504	0.00027	0.76814	0.02609	0.09203	0.00310	0.991	623	10	579	15	568	18	9.3
SAN CARLOS-48	497063	10095	0.28906	0.05978	4.53314	0.94633	0.11374	0.00325	0.137	3413	289	1737	160	694	19	83.7
SAN CARLOS-48B	270445	521	0.07354	0.00125	1.25288	0.04090	0.12357	0.00344	0.854	1029	34	825	18	751	20	28.6
SAN CARLOS-49	243927	1472	0.11934	0.01617	1.91903	0.27004	0.11662	0.00443	0.270	1846	224	1088	90	711	26	66.9
SAN CARLOS-50	248376	385	0.08441	0.00035	2.47895	0.07893	0.13300	0.00673	0.991	1302	8	1266	23	1245	36	4.8
SAN CARLOS-51	118406	513	0.06591	0.00040	0.80814	0.02743	0.10956	0.00305	0.979	739	13	644	15	618	18	17.3
SAN CARLOS-52	128851	517	0.06891	0.00050	1.16200	0.03738	0.12330	0.00383	0.974	806	15	783	17	744	22	18.0
SAN CARLOS-53	69592	481	0.06097	0.00045	0.74888	0.02884	0.08909	0.00337	0.982	638	16	568	17	550	20	14.4
SAN CARLOS-54	347409	450	0.13329	0.00116	6.05821	0.15344	0.32964	0.00784	0.939	2142	15	1984	22	1837	38	16.6
SAN CARLOS-55	329465	2698	0.09795	0.02561	1.31876	0.34859	0.09765	0.00376	0.146	1585	423	854	142	601	22	65.0
SAN CARLOS-56	92592	465	0.06524	0.00029	0.77013	0.03178	0.08562	0.00185	0.524	782	72	580	18	530	11	33.6
SAN CARLOS-57	131032	441	0.06058	0.00030	0.72964	0.01957	0.08738	0.00230	0.983	624	11	556	11	540	14	14.0
SAN CARLOS-57B	175447	732	0.08121	0.00867	0.95952	0.10908	0.08487	0.00162	0.176	1227	196	678	52	525	10	59.5
SAN CARLOS-58	193263	442	0.06606	0.00024	0.74004	0.01972	0.08937	0.00235	0.988	606	9	562	11	552	14	9.1
SAN CARLOS-59	182339	734	0.09566	0.01149	1.42043	0.18091	0.10669	0.00422	0.311	1559	211	898	73	853	25	61.0
SAN CARLOS-60	117173	401	0.06165	0.00035	0.80333	0.02140	0.09451	0.00246	0.977	602	12	599	12	582	14	12.6
SAN CARLOS-61	46132	409	0.06377	0.00336	0.79518	0.05082	0.09044	0.00328	0.567	734	108	594	28	558	19	25.0
SAN CARLOS-62	83523	368	0.06715	0.00043	1.16429	0.04320	0.12575	0.00490	0.985	842	13	784	20	764	26	9.9
SAN CARLOS-63	56234	381	0.06113	0.00052	0.74157	0.01854	0.08798	0.00207	0.940							

sample name	<sup>206</sup> Pb (cps)	<sup>208</sup> Pb (cps)	<sup>207</sup> Pb/ <sup>206</sup> Pb	2 σ	<sup>207</sup> Pb/ <sup>235</sup> U	2 σ	<sup>206</sup> Pb/ <sup>238</sup> U	2 σ	ρ	age (Ma)	error (Ma)	age (Ma)	error (Ma)	age (Ma)	error (Ma)	discordance
101116-3-1	20712	110	0.06205	0.00142	0.82182	0.05483	0.06905	0.06602	0.940	676	48	609	30	591	35	13.1
101116-3-1B	28294	210	0.07470	0.00230	1.02489	0.06757	0.09951	0.00578	0.383	1060	61	716	33	677	34	44.3
101116-3-2	31561	155	0.06196	0.00095	0.72966	0.07875	0.09265	0.00550	0.969	641	55	585	27	571	31	11.4
101116-3-2B	36461	156	0.06902	0.00136	0.76883	0.04758	0.09268	0.00532	0.959	636	44	589	27	577	31	9.7
101116-3-3	56421	168	0.06204	0.00166	0.86422	0.05730	0.09959	0.00606	0.918	706	55	621	31	612	35	14.0
101116-3-4	23630	179	0.06752	0.00147	0.89632	0.05651	0.06638	0.00570	0.938	854	45	650	30	593	33	32.0
101116-3-4B	46901	203	0.06545	0.00212	0.85514	0.06392	0.06477	0.00638	0.901	789	67	627	34	584	37	27.2
101116-3-5	70785	216	0.13522	0.00163	0.69750	0.48234	0.37478	0.06438	0.983	2167	21	2110	57	2052	113	6.2
101116-3-6	162389	217	0.12472	0.00149	0.54379	0.32341	0.31622	0.01842	0.980	2025	21	1891	50	1771	90	14.3
101116-3-6B	227505	229	0.12783	0.00145	0.63144	0.43884	0.35754	0.02572	0.988	2068	20	2018	62	1970	121	5.5
101116-3-7	119072	230	0.10723	0.00148	0.39727	0.42482	0.32572	0.02387	0.985	2057	20	2032	57	2007	112	1.8
101116-3-8	407414	326	0.28466	0.00333	24.24952	1.63765	0.61718	0.04105	0.985	3390	18	3278	64	3099	162	10.8
101116-3-9	96180	259	0.15396	0.00206	9.32294	0.55468	0.43917	0.02546	0.974	2390	23	2370	53	2347	103	2.2
101116-3-10	234063	7	0.18208	0.00208	12.65829	0.69453	0.50421	0.02706	0.978	2672	19	2655	50	2632	115	1.8
101116-3-11	156208	0	0.12825	0.00145	6.53584	0.38585	0.36962	0.02142	0.982	2074	20	2051	51	2028	100	2.6
101116-3-12	463840	5	0.17319	0.00200	11.39838	0.67439	0.47736	0.00770	0.981	2589	19	2556	54	2516	120	3.4
101116-3-13	165197	1	0.18240	0.00213	12.14881	0.67977	0.48207	0.02844	0.978	2675	19	2616	51	2541	114	6.1
101116-3-14	271608	18	0.12604	0.00184	6.40492	0.36357	0.34863	0.02002	0.966	2644	26	2622	49	2623	95	11.2
101116-3-15	512778	0	0.21807	0.00327	16.28821	0.91450	0.54173	0.02931	0.964	2966	24	2894	52	2791	121	7.3
101116-3-16	445947	0	0.12374	0.00151	6.03134	0.34669	0.33551	0.01985	0.977	2011	22	1990	40	1951	94	3.4
101116-3-17	397917	0	0.17712	0.00214	12.49730	0.72440	0.51173	0.02901	0.978	2626	20	2643	53	2684	123	-1.8
101116-3-18	172321	1	0.18217	0.00206	12.17544	0.70764	0.48474	0.02784	0.981	2673	19	2618	53	2548	119	5.6
101116-3-20	38064	0	0.06922	0.00136	0.80577	0.04957	0.09705	0.00562	0.941	611	44	600	27	597	33	2.5
101116-3-21	107430	0	0.05967	0.00075	0.78227	0.04333	0.09508	0.00513	0.974	592	27	587	24	586	30	11.1
101116-3-22	118625	153	0.12923	0.00148	6.04828	0.36317	0.34863	0.02002	0.966	2644	26	2622	49	2623	95	11.2
101116-3-24	50796	0	0.05982	0.00084	0.81426	0.04626	0.09872	0.00544	0.969	597	30	605	26	607	32	-1.7
101116-3-25	52333	0	0.06368	0.00218	0.87909	0.05946	0.10012	0.00570	0.957	731	71	640	31	615	33	16.6
101116-3-26	372584	22	0.13218	0.00160	6.65648	0.38297	0.36524	0.02055	0.978	2127	21	2067	50	2007	96	6.6
101116-3-27	133520	629	0.13645	0.01895	2.00207	0.31310	0.10641	0.00591	0.355	2183	234	1116	101	652	34	73.6
101116-3-28	39238	0	0.06530	0.00101	0.88949	0.04888	0.09879	0.00521	0.960	784	32	648	26	607	30	23.6
101116-3-29	44765	0	0.05826	0.00082	0.72580	0.04312	0.09619	0.00520	0.968	539	30	581	34	592	30	-0.3
101116-3-30	21528	0	0.07341	0.00198	0.10049	0.09089	0.10169	0.02018	0.968	718	32	718	32	718	32	0.0
101116-3-31	500837	128	0.21587	0.00243	15.70197	0.97447	0.52754	0.03220	0.983	2950	18	2859	58	2731	134	9.1
101116-3-31B	393167	170	0.18907	0.00245	12.86908	0.79588	0.47124	0.02856	0.980	2810	20	2670	57	2499	134	13.8
101116-3-32	255497	178	0.17360	0.00214	11.24793	0.61407	0.46992	0.02499	0.974	2593	20	2544	50	2483	109	5.1
101116-3-32B	212357	168	0.17368	0.00203	11.34086	0.65273	0.47358	0.02669	0.979	2593	19	2552	52	2499	116	4.4
101116-3-33	255521	388	0.14730	0.00365	8.03274	0.59025	0.39551	0.02526	0.932	2315	42	2235	60	2148	116	8.4
101116-3-34	171622	236	0.12499	0.00144	6.09305	0.46159	0.35309	0.02647	0.988	2029	20	1988	64	1948	125	4.5
101116-3-35	161116	235	0.17370	0.00165	6.16533	0.47124	0.35191	0.02878	0.983	2810	23	2670	57	2499	134	6.0
101116-3-36	251894	239	0.19812	0.00203	11.43704	0.69619	0.47099	0.02815	0.982	2617	19	2559	55	2488	122	5.0
101116-3-37	125831	225	0.13158	0.00161	6.65295	0.36574	0.34670	0.01995	0.975	2119	21	2066	47	2014	92	5.8
101116-3-38	547703	678	0.17466	0.00277	10.53833	0.78171	0.43759	0.02171	0.977	2803	26	2483	67	2340	141	12.0
101116-3-39	64053	207	0.13126	0.00169	6.48079	0.44119	0.35808	0.02394	0.982	2115	22	2043	58	1973	113	7.8
101116-3-40	184648	182	0.18138	0.00206	12.02082	0.70048	0.48067	0.02747	0.981	2666	19	2606	53	2530	119	6.1
101116-3-41	216093	202	0.18173	0.00207	12.53064	0.70531	0.50040	0.02756	0.979	2689	19	2646	52	2616	117	2.4
101116-3-42	206816	256	0.09462	0.00119	3.42941	0.20146	0.26217	0.01574	0.981	1321	22	1189	45	1201	77	1.4
101116-3-43	336511	281	0.13973	0.00171	6.09090	0.38917	0.34663	0.02040	0.963	2084	22	1989	53	1869	103	8.0
101116-3-43B	336511	793	0.14471	0.00332	6.60284	0.48190	0.33093	0.02283	0.949	2284	30	2060	62	1843	110	22.2
101116-3-44	131037	271	0.12463	0.00147	6.12494	0.34422	0.35643	0.01899	0.976	2024	21	1994	47	1965	90	3.3
101116-3-45	45778	281	0.06392	0.00159	0.85203	0.06250	0.09687	0.00607	0.940	739	52	626	34	595	39	20.4
101116-3-46	74566	309	0.05987	0.00074	0.74023	0.04202	0.08968	0.00497	0.976	599	27	563	24	554	29	7.9
101116-3-47	71672	370	0.07045	0.00170	0.92250	0.05236	0.09497	0.00522	0.915	941	49	684	29	585	31	39.6
101116-3-48	39379	315	0.06383	0.00204	0.81397	0.05133	0.09238	0.00503	0.962	736	66	604	30	570	30	23.6
101116-3-49	49739	304	0.06146	0.00125	0.80186	0.05999	0.09545	0.00604	0.952	656	58	589	30	552	30	19.6
101116-3-50	43239	356	0.06260	0.00100	0.78951	0.04616	0.09148	0.00514	0.962	695	34	591	26	564	30	19.6
101116-3-51	57023	20	0.06034	0.00100	0.78349	0.04702	0.09417	0.00543	0.961	616	35	587	26	580	32	6.1
101116-3-52	143658	25	0.12620	0.00145	6.20695	0.39099	0.35670	0.02209	0.983	2046	20	2005	54	1907	104	4.5
101116-3-53	133095	25	0.12490	0.00148	6.16188	0.37868	0.35779	0.02158	0.981	2027	21	1999	52	1972	102	3.2
101116-3-54	148228	4	0.13613	0.00163	6.98315	0.39737	0.37205	0.02070	0.978	2179	21	2109	49	2039	97	7.5
101116-3-55	399236	1	0.17006	0.00223	10.45750	0.61590	0.44598	0.02561	0.975	2558	22	2476	55	2377	113	8.4
101116-3-56	31509	10	0.12995	0.00156	6.05115	0.36915	0.34670	0.01995	0.978	2046	20	2014	48	1978	92	13.5
101116-3-57	319189	1	0.12625	0.00146	6.25177	0.34935	0.33915	0.01964	0.978	2046	20	2012	48	1978	92	13.5
101116-3-58	251887	0	0.12866	0.00148	6.30820	0.43590	0.35560	0.02423	0.986	2080	20	2020	50	1991	114	6.6
101116-3-59	428372	0	0.29752	0.00335	25.99156	1.56732	0.63359	0.03753	0.982	3457	17	3346	57	3164	146	10.7
101116-3-60	50054	2	0.06792	0.00172	0.83746	0.05445	0.08942	0.00536	0.921	866	52	618	30	552	32	37.8
101116-3-61	30079	0	0.06014	0.00112	0.77662	0.04654	0.09366	0.00534	0.951	609	40	584	26	577	31	5.4
101116-3-62	39971	2	0.06076	0.00095	0.72508	0.04673	0.08661	0.00541	0.970	631	33	552	27	534	32	16.0
101116-3-64	38473	3	0.06268	0.00116	0.86100	0.04673	0.08661	0.00541	0.970	631	33	552	27	534	32	16.0
101116-3-65	34443	13	0.06945	0.00148	0.99415	0.06209	0.09442	0.006								

sample name	<sup>238</sup> Pb (ppm)	<sup>235</sup> Pb (ppm)	<sup>232</sup> Th/ <sup>238</sup> Pb	2 σ	<sup>207</sup> Pb/ <sup>235</sup> U	2 σ	<sup>206</sup> Pb/ <sup>238</sup> U	2 σ	ρ	ρ*	age (Ma)	error (Ma)	<sup>206</sup> Pb/ <sup>238</sup> U	2 σ	<sup>206</sup> Pb/ <sup>238</sup> U	2 σ	discordance
<b>Session 1 (Sample 1011151)</b>																	
GJ1-32-1	351674	3	0.06053	0.00034	0.82306	0.02763	0.00946	0.00236	0.986	0.001	626	12	610	13	603	19	3.3
GJ1-32-2	323459	0	0.06033	0.00032	0.81366	0.02393	0.00973	0.00207	0.986	0.001	623	11	603	14	600	18	4.0
GJ1-32-3	331647	0	0.06023	0.00030	0.80689	0.02600	0.00970	0.00209	0.986	0.001	612	11	602	14	600	17	2.1
GJ1-32-4	331900	0	0.06013	0.00033	0.80669	0.02477	0.00970	0.00204	0.986	0.001	608	12	601	14	598	17	1.6
GJ1-32-5	323562	0	0.06003	0.00031	0.81120	0.02426	0.00980	0.00209	0.985	0.001	603	11	603	14	603	17	0.3
GJ1-32-6	290889	87	0.06048	0.00031	0.81789	0.02246	0.00988	0.00205	0.982	0.030	621	11	607	12	603	16	3.0
GJ1-32-7	272897	0	0.06033	0.00039	0.80236	0.02479	0.00946	0.00202	0.978	0.000	615	14	598	14	594	17	3.7
GJ1-32-8	344631	0	0.06036	0.00033	0.80533	0.02482	0.00975	0.00204	0.984	0.000	617	12	600	14	595	17	3.6
GJ1-32-9	271912	0	0.06099	0.00033	0.79206	0.02337	0.00928	0.00203	0.982	0.000	637	12	592	13	581	16	9.2
GJ1-32-10	282492	0	0.06060	0.00033	0.79830	0.02399	0.00937	0.00206	0.981	0.000	623	12	596	13	588	16	6.1
GJ1-32-11	273323	0	0.06070	0.00032	0.79945	0.02321	0.00944	0.00207	0.980	0.000	629	14	591	14	582	17	7.8
GJ1-32-12	273378	0	0.06073	0.00034	0.77773	0.02453	0.00938	0.00208	0.984	0.000	630	12	584	14	573	17	9.5
OG1-1	2112161	0	0.20939	0.00139	29.20878	1.02231	0.17179	0.02943	0.991	0.000	2469	7	2460	24	2460	24	-1.2
OG1-2	1908832	222	0.20953	0.00137	28.76746	1.01717	0.16537	0.02882	0.991	0.012	2477	7	2374	23	2236	25	8.1
OG1-3	1635726	0	0.20966	0.00142	27.68746	1.49560	0.16745	0.03640	0.996	0.000	2454	7	2408	22	2331	130	4.6
OG1-4	1374365	76	0.20834	0.00201	23.53631	1.01156	0.15222	0.02511	0.987	0.005	2408	11	2349	41	2098	101	15.0
OG1-5	1247372	66	0.20914	0.00141	28.71239	0.96336	0.06822	0.02213	0.990	0.000	2466	7	2444	22	2406	87	2.2
OG1-6	1291589	111	0.20921	0.00137	29.39381	0.99329	0.10566	0.02323	0.991	0.000	2471	7	2461	23	2442	20	1.1
<b>Session 2 (Sample 1010262)</b>																	
GJ1-32-1	82348	72	0.03141	0.00185	0.77630	0.04331	0.00986	0.00488	0.862	0.087	333	61	283	23	296	27	-11.9
GJ1-32-2	79081	75	0.03937	0.00132	0.79702	0.05701	0.00976	0.00636	0.947	0.102	381	59	359	23	397	37	-3.3
GJ1-32-3	78113	60	0.03746	0.00134	0.72115	0.03793	0.00301	0.00411	0.856	0.144	501	49	519	22	563	24	-8.4
GJ1-32-4	93348	135	0.06091	0.00063	0.79012	0.04129	0.00948	0.00482	0.980	0.135	656	22	591	23	580	28	9.3
GJ1-32-5	103573	135	0.06142	0.00103	0.79208	0.04384	0.00934	0.00492	0.931	0.130	654	36	592	23	576	29	12.4
GJ1-32-6	109589	238	0.06095	0.00095	0.73205	0.03194	0.00946	0.00491	0.984	0.222	649	34	557	26	557	28	12.4
GJ1-32-7	115430	119	0.06103	0.00070	0.73215	0.03313	0.00973	0.00508	0.965	0.106	640	24	561	19	542	25	16.0
GJ1-32-8	99343	131	0.06192	0.00142	0.74713	0.04900	0.00871	0.00338	0.937	0.132	671	48	567	28	541	32	20.3
GJ1-32-9	99427	27	0.06008	0.00063	0.74718	0.02302	0.00920	0.00547	0.970	0.039	609	22	567	19	557	23	8.6
GJ1-32-10	134667	121	0.06067	0.00067	0.80671	0.04108	0.00944	0.00579	0.988	0.083	627	24	601	23	594	28	1.6
GJ1-32-11	160041	184	0.05850	0.00062	0.75877	0.04436	0.00947	0.00541	0.983	0.115	540	23	573	25	580	32	-5.9
GJ1-32-12	16327	177	0.03282	0.00084	0.77282	0.02717	0.00826	0.00218	0.978	0.107	701	26	581	27	579	33	2.2
OG1-1	6072	122	0.20903	0.00132	29.33148	1.02124	0.16948	0.02811	0.991	0.000	2472	14	2326	23	2460	24	-0.4
OG1-2	27824	54	0.20936	0.00139	27.86856	1.15701	0.07518	0.02711	0.988	0.109	2467	13	2414	23	2326	141	3.2
OG1-3	394571	9	0.20887	0.00169	29.43092	1.38397	0.17420	0.03787	0.986	0.002	2464	14	2468	21	2474	141	-0.4
OG1-4	335338	127	0.20934	0.00247	27.69030	1.18700	0.07047	0.02813	0.978	0.038	2468	14	2408	41	2308	106	2.9
OG1-5	493267	232	0.20936	0.00169	28.67800	1.20916	0.09016	0.02902	0.982	0.022	2469	9	2427	14	2425	146	1.4
OG1-6	385550	230	0.20940	0.00238	28.45397	1.30467	0.09348	0.03136	0.982	0.060	2477	13	2435	44	2397	118	2.3
OG1-7	600806	141	0.20924	0.00234	28.38933	1.19204	0.09149	0.02843	0.979	0.024	2456	13	2431	40	2388	107	2.5
OG1-8	1102621	197	0.20912	0.00234	29.49333	1.38081	0.17996	0.03314	0.983	0.018	2455	13	2470	45	2406	125	-1.3
OG1-9	446693	124	0.20905	0.00215	28.44621	1.14624	0.09544	0.03184	0.980	0.020	2459	14	2427	41	2464	116	4.8
OG1-10	784444	214	0.20902	0.00234	28.34843	1.15356	0.09684	0.03782	0.988	0.027	2439	13	2428	33	2409	142	1.1
OG1-12	630716	140	0.20924	0.00234	29.08116	1.19822	0.10978	0.02880	0.978	0.023	2456	13	2456	40	2437	107	0.0
<b>Session 3 (Sample 1010122)</b>																	
GJ1-32-1	105722	53	0.06081	0.00132	0.79418	0.04906	0.00971	0.00479	0.973	0.033	633	60	594	26	583	26	8.1
GJ1-32-2	93798	63	0.03970	0.00048	0.80218	0.03963	0.00978	0.00473	0.986	0.069	593	17	599	22	600	28	-1.3
GJ1-32-3	99216	163	0.03784	0.00051	0.80794	0.03998	0.10311	0.00493	0.986	0.162	524	19	601	22	602	29	-19.7
GJ1-32-4	98799	110	0.03923	0.00037	0.84646	0.03917	0.00946	0.00473	0.986	0.023	562	17	584	23	582	27	1.9
GJ1-32-5	77239	24	0.06003	0.00091	0.79082	0.04111	0.00931	0.00473	0.977	0.031	601	32	592	23	588	28	3.0
GJ1-32-6	79138	44	0.03200	0.00020	0.77299	0.04331	0.00931	0.00483	0.974	0.031	567	28	581	23	585	27	-3.7
OG1-1	251596	152	0.20976	0.00174	27.99638	1.33521	0.07963	0.03339	0.993	0.061	2464	9	2419	47	2343	127	4.5
OG1-2	262189	156	0.20903	0.00172	28.03346	1.31838	0.07018	0.03318	0.993	0.059	2463	9	2427	46	2419	126	0.8
OG1-3	228034	51	0.20972	0.00170	28.79643	1.43772	0.10387	0.03491	0.999	0.023	2433	9	2447	46	2433	131	0.7
OG1-4	299658	46	0.20939	0.00157	27.50833	1.36211	0.09293	0.03322	0.988	0.015	2466	19	2402	47	2394	125	0.5
OG1-5	273288	141	0.20909	0.00169	29.78474	1.43532	0.10684	0.03517	0.993	0.023	2468	9	2427	47	2408	126	1.4
OG1-6	248308	51	0.20907	0.00168	29.60405	1.43463	0.10323	0.03481	0.983	0.013	2455	9	2474	47	2396	159	-1.9
OG1-7	204633	73	0.20944	0.00174	29.45493	1.33211	0.11532	0.03333	0.992	0.038	2462	9	2469	45	2480	124	-0.7
OG1-8	233328	7	0.20964	0.00171	28.68180	1.39860	0.09856	0.03376	0.993	0.003	2463	9	2443	47	2408	127	2.1
OG1-9	191619	58	0.20961	0.00179	29.58915	1.53701	0.12189	0.03721	0.993	0.030	2458	9	2473	29	2500	138	-1.6
<b>Session 4 (Sample 1010261)</b>																	
GJ1-32-1	133106	171	0.03704	0.00140	0.71911	0.03325	0.00944	0.00388	0.866	0.128	493	53	550	21	564	23	-15.0
GJ1-32-2	133763	164	0.03754	0.00138	0.88971	0.03951	0.00820	0.00478	0.919	0.121	512	48	538	23	540	27	-6.7
GJ1-32-3	136	156	0.03693	0.00137	0.88389	0.03913	0.00813	0.00478	0.919	0.123	489	42	528	19	517	21	-10.6
GJ1-32-4	132438	143	0.03634	0.00130	0.89487	0.03996	0.										

<b>Sample #</b>	<b>Lithostratigraphic Unit</b>	<b>Rock Type</b>	<b>Coordinates</b>
101115/1	Yerbal Formation	Coarse sandstone	33°58'15" S 54°57'28" W
101026/2	Playa Hermosa Formation	Pebbly sandstone	34°51'16" S 55°18'09" W
101012/2	Las Ventanas Formation	Pebbly sandstone	34°38'32" S 55°16'33" W
101012/1	Las Ventanas Formation	Pebbly sandstone	34°22'20" S 55°16'40" W
San Carlos	San Carlos Formation	Pebbly sandstone	34°50'07" S 54°53'03" W
101116/3	Barriga Negra Formation	Coarse sandstone	33°49'58" S 54°57'06" W

**Table A.2.8.** Sample locations.

### APPENDIX 3: SUPPLEMENTARY INFORMATION FOR CHAPTER 4

The following are the supplementary materials related to this article.

**Figure 1.** (A) Post-Archean-Australian-Shale (PAAS) normalized REY diagram. (B) Binary plot of Ce/Ce\* vs. Pr/Pr\*.

**Table 1.** K-Ar age dating standards.

**Table 2.** XRD results.

**Table 3.** K-Ar data from the uppermost Yerbal Formation (sample #101025/1).

**Table 4.** Argon diffusion calculations.

**Table 5.** Recalculated K-Ar ages.

#### A.3. Supplementary analytical methods.

The sample was gently disaggregated using a repetitive freezing and heating technique to avoid artificial reduction of rock components with K-bearing minerals such as micas or K-feldspars (Liewig et al., 1987). Grain size fractions  $<2$  and  $2-6 \mu\text{m}$  were separated in distilled water according to Stoke's law and a  $<0.4 \mu\text{m}$  was separated using a high-speed centrifuge. Clay mineralogy and polytypes were characterized by X-ray Diffraction (XRD). The mineralogy of the size fractions was determined by XRD on air-dried (N) and glycolated samples. Diffractograms of the samples were obtained and analysed with a Philips automated EPD 1700 X-ray diffractometer using  $\text{CuK}\alpha$  radiation and 40 KV/30 mA. The samples were scanned over the range  $2\theta = 2-35^\circ$  at  $0.015^\circ 2\theta/\text{sec}$ . XRD limits for K-feldspars are around 3% and contamination phases cannot be detected below this value. For clay polytype investigations the samples were lightly pressed into shallow stainless steel holders for X-ray diffraction analysis. Oriented samples were prepared by dispersing approximately 40 mg of material using ultrasonic agitation in approximately 5 ml of deionised water. The slurries were deposited under suction onto  $0.22 \mu\text{m}$  Duropore<sup>®</sup> filter membranes then saturated with magnesium twice using 1M  $\text{MgCl}_2$ . The films were washed 5 times with deionised water then five drops of glycerol added and gently spread over the entire clay surface. The samples remained on the vacuum manifold until all traces of liquid glycerol was gone. The oriented samples were placed onto

absorbent paper towels to remove excess of glycerol on the backs of the samples before mounting onto 25 mm aluminum discs with double sided tape. XRD patterns were recorded with a PANalytical X'Pert Pro microprocessor-controlled diffractometer using Fe filtered Co Ka radiation, 0.25° divergence slit, 0.50° anti-scatter slit and X'Celerator fast Si strip detector. The diffraction patterns were recorded in steps of 0.016° 2 $\theta$  with a 1 second counting time per step, and logged to data files on a PC for analysis using HighScore Plus and CSIRO XPLOTT software. The K-Ar dating technique follows methods described in detail elsewhere (Dalrymple and Lanphere, 1969; Faure, 1986). Potassium content was determined by atomic absorption using Caesium for ionization suppression. Two sample aliquots of approximately 100 mg were dissolved with HF and HNO<sub>3</sub>. The samples, once in solution were diluted to 0.3 to 1.5 ppm K for the atomic absorption analysis. The pooled error of duplicate K determination on all samples and standards is better than 2%. Conventional K-Ar isotopic determinations were performed using a procedure similar to that described by Bonhomme et al. (1975). Samples were pre-heated under vacuum at 80°C for several hours to reduce the amount of atmospheric Ar adsorbed onto the mineral surfaces during sample handling. Argon was extracted from the separated mineral fractions by fusing samples within a vacuum line serviced by an on-line <sup>38</sup>Ar spike pipette. The isotopic composition of the spiked Ar was measured with an on-line VG3600 mass spectrometer using a Faraday cup. The <sup>38</sup>Ar spike was calibrated against biotite GA1550 (McDougall and Roksandic, 1974). After fusion of the sample in a low blank Heine resistance furnace, the released gases were subjected to a two-stage purification procedure with a CuO getter for the first step and two Ti getters for the second step. Blanks for the extraction line and mass spectrometer were systematically determined and the mass discrimination factor was determined periodically by airshots. Normally 15 mg of sample material was required for Argon analyses. During the course of the study 2 standards and 2 airshot values were measured. The K-Ar dating standard and airshot results are summarised in Supplementary Table 1. The error for Argon analyses is below 1% and the <sup>40</sup>Ar/<sup>36</sup>Ar value for airshots averaged 294.28 ± 0.29. The KAr ages were calculated using <sup>40</sup>K abundance and decay constants recommended by Steiger and Jäger (1977). The age uncertainties take into account the errors during sample

weighing,  $^{38}\text{Ar}/^{36}\text{Ar}$  and  $^{40}\text{Ar}/^{38}\text{Ar}$  measurements and K analysis. K-Ar age errors are within 2 sigma uncertainty.